Saskatchewan
Energy and Mines

Saskatchewan
Geological Survey

Miscellaneous Report 2001-4.1

Summary of Investigations 2001, Volume 1, Saskatchewan Geological Survey

Printed under the authority of the
Minister of Energy and Mines

Although the Department of Energy and Mines has exercised all reasonable care in the compilation, interpretation, and production of this report, it is not possible to ensure total accuracy, and all persons who rely on the information contained herein do so at their own risk. The Department of Energy and Mines and the Government of Saskatchewan do not accept liability for any errors, omissions or inaccuracies that may be included in, or derived from, this report.

Cover:
Left: Photomicrograph of dolomitized skeletal micrite from the Mississippian Madison Formation in southwestern Saskatchewan (Fargo Decalta 6-27-3-26W3 well, 1391.7 m). The specimen is from the 10 m thick dolomitized zone that immediately underlies the sub-Mesozoic unconformity. Dolomitization and solution of skeletal remains have given the rocks in this zone good reservoir characteristics with pore volumes as high as 27% and permeabilities up to several hundred millidarcies. The oil visible in the pores of this rock has a gravity of about 12° API (see Kent and Kreis, this volume). The rectangular skeletal fragment in the middle of the field is about 3 mm long.
(Photograph by D.M. Kent)
Right: A selection of conodonts from the Upper Ordovician of Saskatchewan (see Nowlan and Haidl, this volume).
(Images supplied by G.S. Nowlan)

Additional copies of this report may be obtained by contacting:

Saskatchewan Energy and Mines
Communications Branch
2101 Scarth Street, 3rd floor
Regina, SK S4P 3V7
(306) 787-2528
FAX: (306) 787-2527
E-mail: enquiry@sem.gov.sk.ca

Editors:
J.E. Christopher
C.F. Gilboy
F.M. Haidl
L.K. Kreis

Production Editor:
C.L. Brown

ISSN 0228 5657
Printed by PrintWest Communications

Foreword

This third issue of the Summary of Investigations, Volume 1, is published at an exciting time on two fronts for geoscience research in Saskatchewan.

Firstly, on March 13, 2001, the Honourable Maynard Sonntag, Minister of Energy and Mines, announced that annual spending on geoscience research would be increased by $920,000: $500,000 will be spent on southern geoscience and $420,000 for northern geoscience. This funding demonstrates Saskatchewan's recognition of the importance of geoscience in the development of the province's energy and mineral resources. This recognition mirrors the Cooperative Geological Mapping Strategies which outline Saskatchewan's and Canada's needs and priorities for geosciences. Included in its economic and technical goals are:

1) to increase investment in energy and mineral exploration;
2) to stimulate new discoveries;
3) to reverse the decline of reserves in mature areas;
4) to help ensure sustainable development;
5) to fill important gaps in subsurface and surface geological map coverage of Canada by mapping areas previously unmapped or not previously surveyed at a satisfactory scale, by incorporating advances in geoscience and by repeating geophysical surveys to modern standards;
6) to enhance our geoscience expertise and its practical applications; and
7) to widely disseminate the results to clients, especially in the minerals, energy, and government sectors in an easily accessible form.

The discovery of new reserves in relatively mature, but by no means exhausted, basins (such as the Williston and Western Canada Sedimentary basins) is a particularly strong challenge faced by industry. The Saskatchewan government recognizes the need to support industry by gathering, interpreting, and making available high-quality geoscience data to help enable companies to develop new exploration models, strategies, and targets. In this way, new discoveries will be made, resulting in many benefits to the people of Saskatchewan.

Saskatchewan Energy and Mines, in co-operation with Saskatchewan industry and its research partners in Natural Resources Canada and the Universities of Saskatchewan and Regina, will determine what research needs to be conducted and prioritize it. Saskatchewan Energy and Mines is in the process of arranging consultation to address these questions. The department requests your input into this process.

Another geoscience research initiative being launched in 2000-2001 is linked to the International Energy Agency Weyburn CO_2 Monitoring and Storage Project. The study area extends about 100 km around the Weyburn Field and is linked to PanCanadian Resources' CO_2 flood. The Geoscience Framework component of the project is one of six task areas designed to assess the capacity of a carbonate oil reservoir to store CO_2 over time. It brings together researchers from Saskatchewan Energy and Mines, the Universities of Saskatchewan, Regina and Alberta, PanCanadian Resources, and other agencies. In 2001, the Geoscience Framework will receive some $358,000 of project funding to enhance our understanding of the relationships between sedimentation, diagenesis, salt dissolution, tectonics, and fluid flow pathways and barriers of the entire sedimentary section from the contact of Precambrian crystalline basement with Cambrian sediments to the present-day surface.

This Summary volume contains 15 papers describing current research in Saskatchewan's subsurface. I invite you to read them, and trust that you will find them both interesting and useful.

George Patterson
Executive Director
Exploration and Geological Services

April 2001

Contents

page

Foreword iii

Contents iv

A. Contributed Papers

Preliminary Results of Isotopic Geochemistry of Ordovician Red River Carbonates, Subsurface of Southeastern Saskatchewan: Implication for Process of Dolomitization and Diagenetic Modification of Dolomites ..... *Hairuo Qing, Donald Kent, and Stephen Bend* 3

Reservoir Characterization of Burrow-mottled Carbonates: The Yeoman Formation of Southern Saskatchewan – Preliminary Report ..... *Rozalia Pak, S. George Pemberton, and Murray K. Gingras* 10

Biostratigraphy and Paleoecology of Late Ordovician Conodonts from a Composite Section in the Subsurface of Saskatchewan ..... *Godfrey S. Nowlan and F.M. Haidl* 14

O and C Isotopes of the Middle Devonian Lower Winnipegosis, Brightholme and Ratner Carbonates, Elk Point Basin, Southeastern Saskatchewan ..... *Hairuo Qing, Katherine M. Bergman, and Orrin Cameron* 32

Carbonate/Evaporite Deposits of the Shell Lake Marker Bed, Middle Devonian Elk Point Basin, Rocanville, Saskatchewan ..... *Arden K.A. Marsh, Katherine M. Bergman, and Jisuo Jin* 37

Mississippian Madison Formation Low-gravity Oilfields in Southwestern Saskatchewan: Examples of Unconformity Diagenesis Controlling Reservoir Quality ..... *D.M. Kent and L.K. Kreis* 46

Onlap within the Mississippian Midale Beds of Southeastern Saskatchewan ..... *J.H. Lake* 56

Investigating CO_2 Storage Potential of Carbonate Rocks during Tertiary Recovery from a Billion Barrel Oil Field, Weyburn, Saskatchewan: Part 1 – the Geoscience Framework (IEA Weyburn CO_2 Monitoring and Storage Project) ..... *C.F. Gilboy, F.M. Haidl, L.K. Kreis, and O.G. Burrowes* 61

Investigating CO_2 Storage Potential of Carbonate Rocks during Tertiary Recovery from a Billion Barrel Oil Field, Weyburn, Saskatchewan: Part 2 – Reservoir Geology (IEA Weyburn CO_2 Monitoring and Storage Project) ..... *G. Burrowes* 64

Paleomagnetic Indications for a Late Paleozoic Age for Part of the Watrous Formation, Williston Basin, Southern Saskatchewan ..... *Randolph J. Enkin, Judith Baker, and K.G. Osadetz* 72

Isotopic Data (Sr, S, and O) from Anhydrites in the Northern Williston Basin, and Pennsylvanian Ages for the Watrous and Amaranth Formations of Saskatchewan and Manitoba ..... *R.E. Denison, H.R. Krouse, and T.P. Poulton* 77

The Lower Cretaceous Mannville Meadow Lake Basin and its Temporal Counterparts, West-central Saskatchewan ..... *J.E. Christopher* 94

Lithofacies Architecture of the Upper Cretaceous Belle Fourche Formation, Saskatchewan, Alberta, and Montana – Its Relationship to Sites of Shallow Biogenic Gas Production ..... *J.L. Ridgley and C.F. Gilboy* 106

Stratigraphic Position of a Late Cretaceous (Cenomanian) Bonebed, East-central Saskatchewan ..... *Stephen L. Cumbaa and Harold N. Bryant* 121

Timing of Gas Generation in the Cretaceous Milk River Formation, Southeastern Alberta and Southwestern Saskatchewan – Evidence from Authigenic Carbonates ..... *Neil S. Fishman, Jennie L. Ridgley, and Donald L. Hall* 125

B. Appendices

Acknowledgments 139

Organization Chart 140

Staff List ..... inside back cover

102-06699/

A. Contributed Papers

Preliminary Results of Isotopic Geochemistry of Ordovician Red River Carbonates, Subsurface of Southeastern Saskatchewan: Implication for Process of Dolomitization and Diagenetic Modification of Dolomites

Hairuo Qing [1], Donald Kent [2], and Stephen Bend [1]

Qing, H., Kent, D., and Bend, S. (2001): Preliminary results of isotopic geochemistry of Ordovician Red River carbonates, subsurface of southeastern Saskatchewan: Implication for process of dolomitization and diagenetic modification of dolomites; *in* Summary of Investigations 2001, Volume 1, Saskatchewan Geological Survey, Sask. Energy Mines, Misc. Rep. 2001-4.1.

1. Introduction

The discovery of prolific Ordovician Red River reservoirs in 1995 in southeastern Saskatchewan was the catalyst for extensive exploration activity which has resulted in the discovery of more than 15 new Red River pools (Haidl *et al.*, 2000) (Figure 1). Cumulative oil production reached 2.29 x 10^6 m^3 (14.4 x 10^6 bbls) in June 2000, primarily from the upper part of the Yeoman Formation with minor contribution from the lower part of the Lake Alma Member of the Herald Formation (Figure 2). The best yields of Ordovician Red River production to date have been from dolostone reservoirs indicating that dolomitization has played a major role in forming reservoir quality porosity (Kent, 1999; Kreis and Kent, 2000). Understanding the processes of dolomitization, including sources of dolomitizing fluids and timing of dolomitization is, therefore, crucial for the prediction of the connectivity, spatial distribution, and heterogeneity of dolomite reservoirs. This information, in turn, is important to locate new frontier exploration targets and/or to design and implement effective enhanced oil recovery (EOR) techniques in these reservoirs.

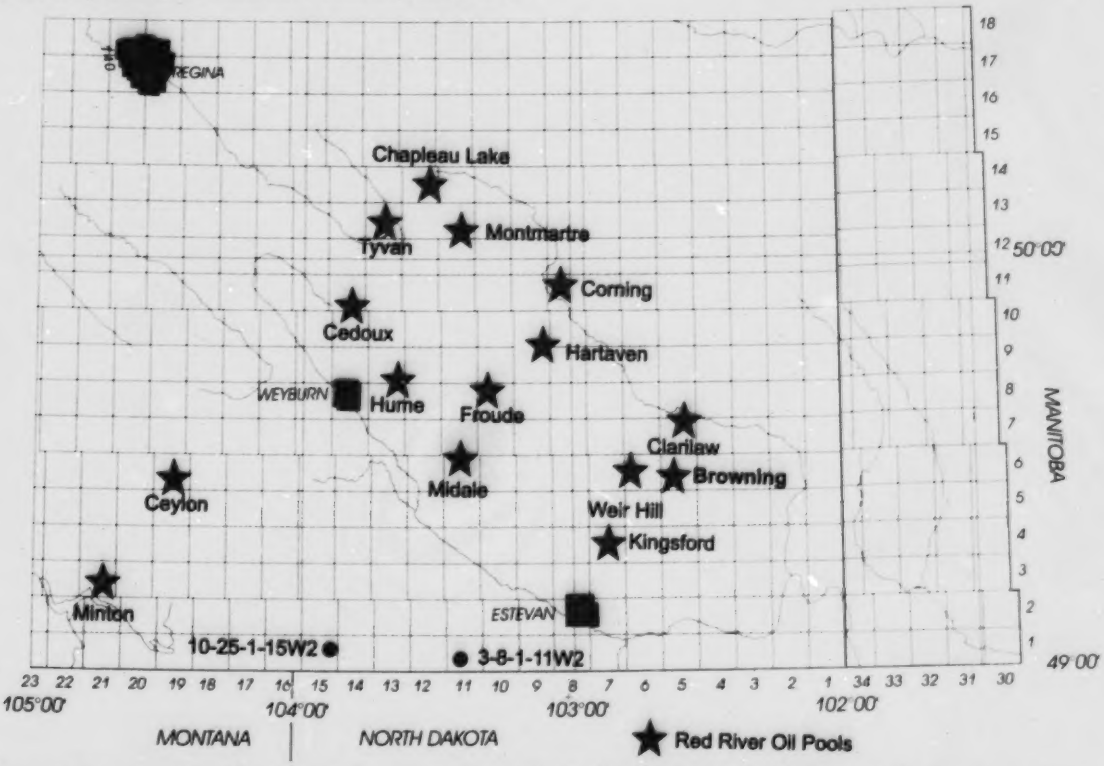

Figure 1 - Location of the Home Dome Torquay S 3-8-1-11W2 and Home K-Tel Hoffer 10-25-1-15W2 wells, and major Ordovician Red River oil pools in southeastern Saskatchewan (modified after Kreis and Kent, 2000).

[1] Department of Geology, University of Regina, Regina, SK S4S 0A2.
[2] D.M. Kent Consulting Geologist Ltd., 86 Metcalfe Road, Regina, SK S4V 0H8.

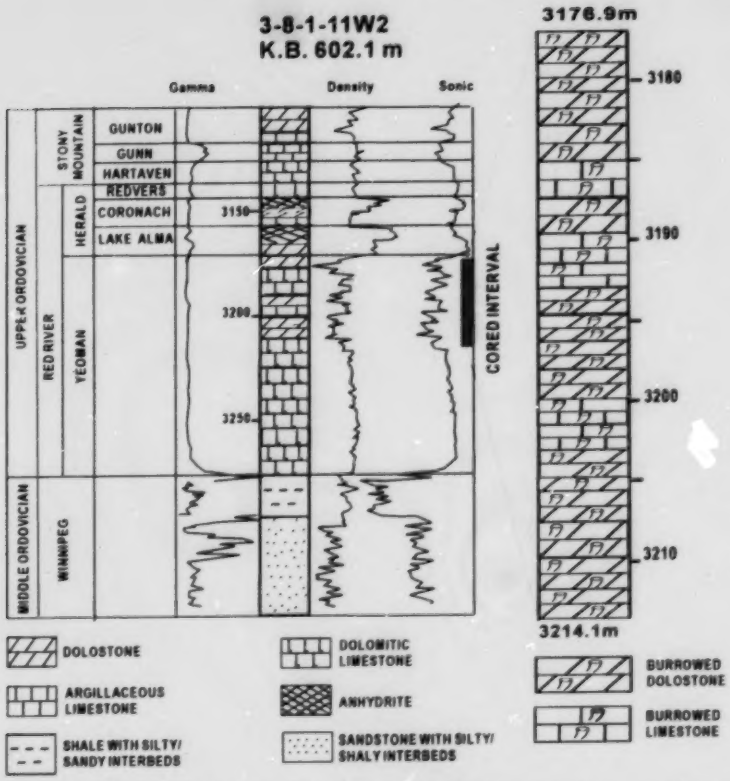

Figure 2 - The general stratigraphy of Ordovician Red River carbonates with summary of lithology of cores from the Home Dome Torquay S 3-8-1-11W2 well.

Dolomitization patterns in Red River carbonates are complex. In the Yeoman Formation, there are dolomitized *Thalassinoides* burrows with the host matrix preserved as limestones, dolomitized *Thalassinoides* burrows, as well as host matrix resulting in complete dolostones (Figure 3), minor saddle dolomite precipitated as cement in vugs and fractures (Figure 3), and limestone sections where both (*Thalassinoides*) burrows and host matrix escaped dolomitization. Dolomite in the Lake Alma Member of the Herald Formation is either non-porous cryptocrystalline dolomudstone or finely crystalline porous dolomudstone.

Several models have been proposed for dolomitization (e.g. Kendall, 1976, 1977, 1984; Longman *et al.* 1983, 1984; Fox, 1993; Longman and Haidl, 1996; Zenger, 1996a, 1996b; Kissling 1997; Canter, 1998; Kent, 1999; Kreis and Kent, 2000). These models were based mainly on petrography with little supporting geochemical data except for Fox (1993) and Zenger (1996a, 1996b). In this summary, we report preliminary results on the petrography and geochemistry of Red River dolostones and their implication to processes of dolomitization and diagenetic modification of isotopic signatures of dolomites.

2. Petrography and Isotopic Geochemistry

Twenty-one samples were analyzed for $\delta^{18}O$ and $\delta^{13}C$ and nine samples were measured for $^{87}Sr/^{86}Sr$. Most of these samples were collected from the Ordovician Red River carbonates from the Home Dome Torquay S 3-8-1-11W2 well in the subsurface of southeastern Saskatchewan (Figure 1). This well was selected for the investigation because its Red River cores contain a complete suite of diagenetic products, including saddle dolomite cements, one of the primary targets for this study. The core from the 3-8-1-11W2 well penetrated the uppermost Yeoman Formation over the interval from 3176.9 to 3214.1 m (Figure 2). The Yeoman Formation is characterized by *Thalassinoides* burrows in a matrix of packstones, wackestones, or mudstones. Two types of replacement dolomite were identified in the cored intervals: i) in *Thalassinoides* burrows, and ii) in the host matrix. Small amounts of saddle dolomite cements were also identified. Isotopic data from the Lake Alma Member of the Herald Formation in the Home K-Tel Hoffer 10-25-1-15W2 well (Figure 1) were also obtained to provide a comparison between rocks from different depositional settings.

a) Replacement Dolomite in *Thalassinoides* Burrows

Based on our observation of core samples from 3-8-1-11W2, the width of the burrows ranges from 0.5 cm to 2 cm, most commonly being about 1 cm. These burrows have irregular edges (walls) that separate burrow-infill sediments from matrix host. The sediment infill in *Thalassinoides* burrows is normally grey, with a darker tone than that of the host matrix (Figure 3). These burrows are filled with carbonate sediments with fewer grains and/or skeletal fragments than in the host rock matrix. Much smaller (0.2 to 0.3 cm in diameter) and darker coloured burrows, interpreted as a "second-stage" worm burrows by Kendall (1976, 1977), commonly occur inside the *Thalassinoides* burrows (Figure 3). Locally, these smaller burrows may also extend directly into the matrix. In the cored section in 3-8-1-11W2, all the

Thalassinoides burrows are preferentially dolomitized, and, based on visual observation, have lower porosity and permeability than the host matrix. The $\delta^{18}O$ value for seven samples collected from *Thalassinoides* burrows varies from -5.9 to -7.8 ‰ PDB (avg. -6.7 ‰ PDB) and the $\delta^{13}C$ value ranges from 0.1 to 0.7 ‰ PDB (avg. 0.33 ‰ PDB) (Figure 4). The $^{87}Sr/^{86}Sr$ ratios of three samples vary from 0.7084 to 0.7088 (avg. 0.7086) (Figure 5).

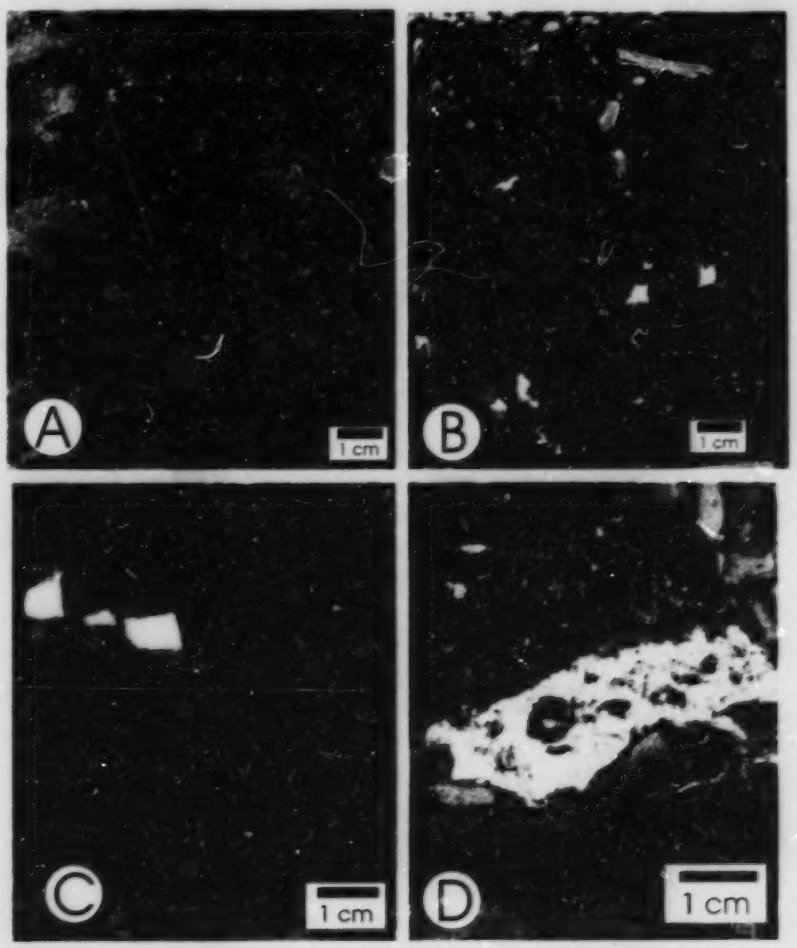

Figure 3 - Core photographs from 3-8-1-11W2.
A) Thalassinoides burrow with irregular edges (walls) that separate burrow infill sediments from matrix host. The sediment in the burrows normally has a darker tone than the host matrix. Note much smaller (0.2 to 0.3 cm diameter) and darker coloured burrows within many of the Thalassinoides burrows. Locally, these smaller burrows may also extend directly into the matrix. They have been interpreted as "second-stage" worm burrows by Kendall (1976, 1977); 3191.6 m.
B) Note white saddle dolomite which occurs as cement in vugs that are preferentially distributed in Thalassinoides and "second-stage" burrows. Some of these vugs have geopetal structure with saddle dolomite precipitated as cement in the upper part of the vugs; 3190.7 m.
C) Saddle dolomite precipitated as cement in the geopetal structure in square- or rectangular-shaped vugs. These vugs occur preferentially in Thalassinoides burrows.
D) Saddle dolomite cement in a large, irregularly shaped vug that has probably been solution enlarged in a pre-existing Thalassinoides burrow.

b) Replacement Dolomite in Matrix Carbonates

The matrix carbonate of the upper Yeoman Formation is light brown, with generally lighter colour than carbonates that fill *Thalassinoides* burrows. It consists mainly of skeletal packstones and wackestones, but in places, due to local variation of grain components, is made up of grainstones or mudstones. Compared with the carbonate-fill in *Thalassinoides* burrows, the matrix carbonate generally contains coarser grains and more abundant skeletal fragments. In most of the cored section in 3-8-1-11W2, the matrix carbonates are dolomitized. Some intervals, however, especially in the middle upper section of core (Figure 2), contain matrix carbonates preserved as limestones. Based on visual observation, the matrix dolomites are much more porous and permeable than *Thalassinoides* burrow infills. The $\delta^{18}O$ value for seven matrix dolomite samples varies from -6.6 to -8.1 ‰ PDB (avg. -7.4 ‰ PDB) and the $\delta^{13}C$ value ranges from 0.7 to -0.4 ‰ PDB (avg. 0.16 ‰ PDB) (Figure 4). The $^{87}Sr/^{86}Sr$ ratios of three samples vary from 0.7085 to 0.7087 (avg. 0.7086) (Figure 5).

c) Saddle Dolomite Cement

Minor amounts of saddle dolomite were observed in the upper part of the Yeomen Formation. Saddle dolomite is white in colour. It occurs as cement in vugs and fractures; in places it preferentially fills vugs in *Thalassinoides* burrows (Figures 3B to 3D). Saddle dolomite was also precipitated as cement in the upper part of geopetal structures (Figures 3B and 3C). The lower part of geopetal structures is filled with brown dolomite sand probably formed by local dissolution of host rock through invasion of hydrothermal fluids during burial. The vugs filled with saddle dolomites are generally irregular, square, or rectangular in shape and 0.5 to 1.5 cm in diameter (Figure 3). The $\delta^{18}O$ value for five saddle dolomites varies from -10.2 to -11.1 ‰ PDB (avg. -10.7 ‰ PDB) and

the $\delta^{13}C$ value ranges from 0.9 to -0.2 ‰ PDB (avg. 0.2 ‰ PDB) (Figure 4). The $^{87}Sr/^{86}Sr$ ratios of three samples vary from 0.7082 to 0.7097 (avg. 0.7088) (Figure 5).

3. Interpretation

Because seawater shows secular variation in oxygen, carbon, and strontium isotopic composition through geologic time (e.g. Burke *et al.*, 1982; Veizer *et al.*, 1997), it is critical to establish the isotopic signatures for Late Ordovician seawater before interpreting isotopic data from the Red River dolomites.

a) Isotopic Signatures of Late Ordovician Seawater

Red River carbonates were deposited in an epeiric sea from Edenian to Richmondian time during the Late Ordovician Period (Elias *et al.*, 1988). The $\delta^{18}O$ and $\delta^{13}C$ values of marine calcite precipitated from Late Ordovician seawater were estimated to be in a range from -6 to -4 ‰ PDB and -1 to 1 ‰ PDB respectively (Figure 4), based on the analyses of pristine Maysvillian brachiopod shells from Ohio (Qing and Veizer, 1994). Major *et al.* (1992) suggested that the oxygen isotopic fractionation between calcite and dolomite varies from 1.5 to 3.5 ‰ PDB. Taking a mean of 2.5 ‰ as the fractionation between dolomite and calcite, primary isotopic signatures of dolomites precipitated from normal Late Ordovician seawater should have $\delta^{18}O$ values from -3.5 to -1.5 ‰ PDB (Figure 4). Dolomites formed by slightly evaporated Late Ordovician seawater prior to gypsum precipitation should have $\delta^{18}O$ values slightly higher than -1.5 ‰ PDB. Qing *et al.* (1998) proposed that $^{87}Sr/^{86}Sr$ ratios of Late Ordovician seawater range from 0.7078 to 0.7082, based on their analyses of brachiopod shells, marine cements, and conodonts. Dolomites that formed by normal Late Ordovician seawater should, therefore, have $^{87}Sr/^{86}Sr$ ratios from 0.7078 to 0.7082 (Figure 5).

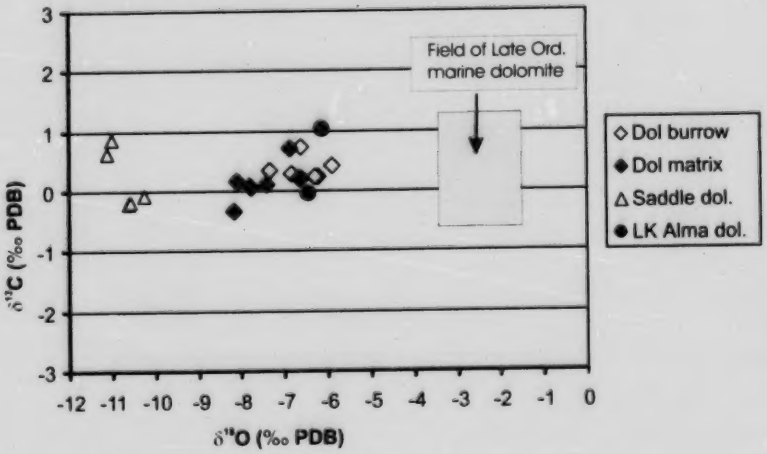

Figure 4 - Cross plot of δ^{18} and $\delta^{13}C$ values for Red River carbonates.

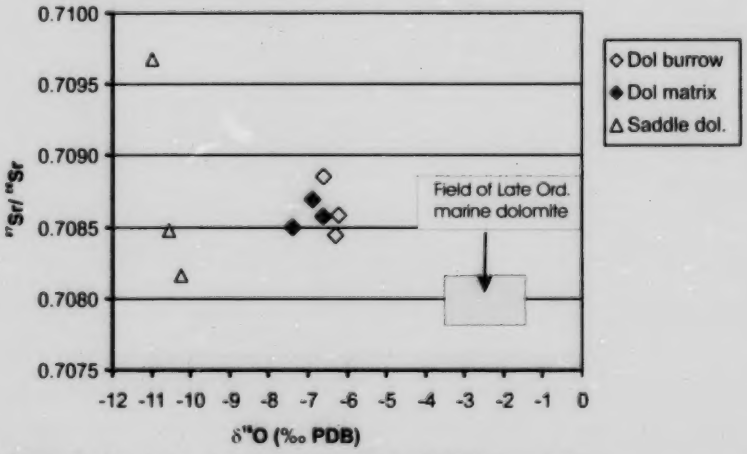

Figure 5 - Cross plot of $\delta^{18}O$ and $^{87}Sr/^{86}Sr$ for Red River carbonates.

b) Dolomitized *Thalassinoides* Burrow Infills

The oxygen isotopes of dolomitized *Thalassinoides* burrow infills (-5.9 to -7.8 ‰ PDB) are much lower than the estimated $\delta^{18}O$ values of dolomites precipitated from normal Late Ordovician seawater (-3.5 to -1.5 ‰ PDB) (Figure 4); and the $^{87}Sr/^{86}Sr$ ratios (0.7084 to 0.7088) are much higher compared to the expected values of Late Ordovician seawater dolomites (0.7078 to 0.7082) (Figure 5). Based on petrographic evidence, Kendall (1976, 1977, 1984) suggested that burrow infills were dolomitized either by reflux evaporitic brines during precipitation of the Lake Alma anhydrite, or during the neomorphism of high-magnesium calcite. In either case, dolomitization of burrow-infill sediments should have occurred early by fluids derived from Late Ordovician seawater and those dolomites should have isotopic signatures of Late Ordovician seawater. The low $\delta^{18}O$ values and high $^{87}Sr/^{86}Sr$ ratios of dolomitized burrow infills relative to the expected values of Late Ordovician seawater dolomites can, therefore, be interpreted as a result of modification or resetting by later diagenetic fluids during burial.

c) Matrix Dolomite

The oxygen isotopes of matrix dolomite (avg. -7.4 ‰ PDB) are lower and the $^{87}Sr/^{86}Sr$ ratios are higher than the estimated values for Late Ordovician marine dolomite (Figure 4). The $\delta^{18}O$ values of matrix dolomites are also lower than those of dolomitized burrows (avg. -6.7 ‰ PDB) sampled from the same specimen, but their $^{87}Sr/^{86}Sr$ ratios are similar (Figure 5). The matrix dolomite has been interpreted to be a later generation formed during burial (Longman *et al.*, 1983; Kendall, 1976, 1977,1984; Kent, 1999; Kreis and Kent, 2000). The low $\delta^{18}O$ value of matrix dolomites (-6.6 to -8.1 ‰ PDB) could be attributed to dolomitization at higher temperatures during burial. Kendall (1977, 1984) suggested that Middle Devonian brines could be the source of dolomitizing fluids for the matrix dolomite. The $^{87}Sr/^{86}Sr$ ratios of Middle Devonian seawater were in the range from 0.7078 to 0.7081 (Burke *et al.*, 1982). The dolomites in the Winnipegosis reef complexes from Dawson Bay, Manitoba, which were interpreted to be dolomitized by Middle Devonian seawater, have an $^{87}Sr/^{86}Sr$ ratio of 0.7080, within the range of the estimated Middle Devonian seawater (Mountjoy *et al.*, 1992). The Red River matrix dolomites, however, have $^{87}Sr/^{86}Sr$ ratios (0.7085 to 0.7087) higher than estimated Middle Devonian seawater. Three possible sources that could account for the observed $^{87}Sr/^{86}Sr$ ratios include:

1) Late Silurian seawater ($^{87}Sr/^{86}Sr$ ratio from 0.7085 to 0.7088) that fluxed through Red River carbonates; or
2) formation waters expelled from Winnipeg or Deadwood sediments, i.e. modified Middle Ordovician (pre-Llandeilo) to Cambrian seawater with $^{87}Sr/^{86}Sr$ ratios from 0.7085 to 0.7090 that migrated up to Red River carbonates; or
3) marine and modified marine fluids that have been in contact with crystalline basement and moved up along fault and fracture systems as hydrothermal fluids due to "thermal convection" (c.f. Aulstead and Spencer, 1985; Wendte *et al.*, 1998).

Further investigation is underway to pinpoint the source of dolomitizing fluids.

d) Saddle Dolomite Cement

The amount of saddle dolomite cements found in the upper part of the Yeomen Formation is much less than that reported in the Alberta Basin (e.g. Aulstead and Spencer, 1985; Machel and Anderson, 1989; Qing and Mountjoy, 1989, 1994; Machel *et al.*, 1996). The scarcity of saddle dolomite cement in the Williston Basin is probably due to its much more tranquil tectonic setting compared with that in the Alberta Basin. The low $\delta^{18}O$ value of saddle dolomites (-10.2 to -11.1 ‰ PDB) and the high $^{87}Sr/^{86}Sr$ ratios (0.7082 to 0.7097) (Figures 4 and 5) suggest the possible influence of hydrothermal fluids (c.f. Kreis and Kent, 2000) in the region.

e) Lake Alma Dolomudstones

In this study, oxygen and carbon isotopes of two samples of finely crystalline dolomudstones from the Lake Alma Member in the 10-25-1-15W2 well were also analyzed. The samples are from the unit immediately below the anhydrite of the Lake Alma Evaporite. These dolomudstones of the Lake Alma Member are thought to have been deposited from penesaline brines prior to precipitation of the Lake Alma anhydrite. The proximity of the dolomite to anhydrite is presumed to have contributed to their texture (finely crystalline with lamination) and to the dramatic decrease (absence) of normal marine fossils. The $\delta^{18}O$ values of the Lake Alma dolomites (-6.1 to -6.4 ‰ PDB) are similar to dolomitized burrow infills, but much lower than the estimated $\delta^{18}O$ values of dolomites from normal and/or evaporitic Late Ordovician seawater (-3.5 to -1.5 ‰ PDB) (Figure 4). This suggests that original isotopic signatures of Lake Alma dolomites, similar to those of dolomitized *Thalassinoides* burrow infills, have also been reset during later diagenetic modification.

4. Conclusions

The Late Ordovician Yeoman Formation is characterized by burrow-mottled (*Thalassinoides*) packstones, wackestones, and mudstones that have been subjected to a variable degree of dolomitization interpreted to have occurred in several stages.

The $\delta^{18}O$ values of dolomitized *Thalassinoides* burrow infills (-5.9 to -7.8 ‰ PDB) are lower than the estimated $\delta^{18}O$ values of dolomites precipitated from normal Late Ordovician seawater (-3.5 to -1.5 ‰ PDB) and the $^{87}Sr/^{86}Sr$ ratios (0.7084 to 0.7088) are much higher compared to the expected values of Late Ordovician seawater dolomites (0.7078 to 0.7082). If these burrow infills were dolomitized early by Late Ordovician seawater, their original isotopic signatures must have been modified or reset by later diagenetic fluids during burial.

The $\delta^{18}O$ values of matrix dolomite (-6.6 to -8.1 ‰ PDB; avg. -7.4 ‰ PDB) are lower than the estimated values, and the $^{87}Sr/^{86}Sr$ ratios (0.7085 to 0.7087) are higher than those expected for Late Ordovician marine dolomite. If matrix dolomitization occurred during burial, the low $\delta^{18}O$ values could be due to associated temperature increase. The high $^{87}Sr/^{86}Sr$ ratios suggest that dolomitizing fluids were Late Silurian seawater, formation waters expelled from Winnipeg or Deadwood sediments, or hydrothermal fluids associated with "thermal convection".

Minor amounts of saddle dolomite cement are present in the Red River carbonates in the Williston Basin. The low $\delta^{18}O$ value of saddle dolomites (-10.2 to -11.1 ‰ PDB) and the high $^{87}Sr/^{86}Sr$ ratios (0.7082 to 0.7097) suggest the possible influence of hydrothermal fluids in the region.

5. Acknowledgments

The study is funded by Petroleum Technology Centre (PTRC) in Regina, Wascana Energy Inc. (Calgary), and NSERC. Isotope analyses were performed at the University of Saskatchewan courtesy of Dr. Chris Holmden. The Saskatchewan Energy and Mines (SEM) Subsurface Geological Laboratory provided access to the cores. Ruth Bezys (Manitoba Energy and Mines) is thanked for guiding H. Qing to the Tyndall Stone quarries. Discussions with and support from Dale Leckie (Wascana), Fran Haidl (SEM), and Kim Kreis (SEM) throughout this project are greatly appreciated.

6. References

Aulstead, K.L. and Spencer, R.J. (1985): Diagenesis of the Keg River Formation, northeastern Alberta: Fluid inclusion evidence; Bull. Can. Petrol. Geol., v33, p167-183.

Burke, W.H., Denison, R.E., Hetherington, E.A., Koepnick, R.B., Nelson, H.F. and Otto, J.B. (1982): Variation of seawater $^{87}Sr/^{86}Sr$ throughout Phanerozoic time; Geol., v10, p516-519.

Canter K.L. (1998): Facies, cyclostratigraphic and secondary diagenetic controls on reservoir distribution, Ordovician Red River Formation, Midale Field, southern Saskatchewan; *in* Kreis, L.K. (ed.), Eighth International Williston Basin Symposium, Core Workshop Volume, Regina, October 1998, Saskatchewan, North Dakota, and Montana Geological Societies, p41-65.

Elias, R.J., Nowlan, G.S., and Bolton, T.E. (1988): Paleontology of the type section, Fort Garry Member, Red River Formation (Upper Ordovician), southern Manitoba; *in* Wohlberg, D.L. (ed.), Contributions to Paleozoic paleontology in honor of Rousseau H. Flower; New Mexico Bur. Mines Miner. Resour., Mem. 44, p341-359.

Fox, J.S. (1993): Depositional and diagenetic controls on porosity evolution in the "C" Zone, Red River Formation (Upper Ordovician), Divide County, North Dakota; unpubl. M.A. thesis, Univ. N. Dakota, 311p.

Haidl, F.M., Kreis, L.K., Miles, W., Nickel, E., and Ware, M.J. (2000): Relationships between Phanerozoic sedimentation, erosion, hydrocarbon accumulations and basement tectonics: Examples from Lower Paleozoic strata in southeastern Saskatchewan; GeoCanada 2000, Calgary, May 2000, Conference CD, ext. abstr. #933.

Kendall, A.C. (1976): The Ordovician carbonate succession (Bighorn Group) of southeastern Saskatchewan; Sask. Miner. Resour., Rep. 180, 185p.

_____ (1977): Origin of dolomite mottling in Ordovician limestones from Saskatchewan and Manitoba; Bull. Can. Petrol. Geol., v25, p480-504.

_____ (1984): Origin and geometry of Red River dolomite reservoirs, western Williston Basin: Discussion; Amer. Assoc. Petrol. Geol. Bull., v68, p776-779.

Kent, D.M. (1999): Geology of Ordovician Winnipeg and Red River rocks, southeast Saskatchewan; Depositional environments and reservoir potential of Lower and Middle Paleozoic rocks in Saskatchewan; Can. Soc. Petrol. Geol., Short Course G-4, Calgary, p1-37.

Kissling, D.L. (1997): Rethinking the configurations of Red River reservoirs; Fifth International Williston Basin Horizontal Well Workshop; Saskatchewan Energy and Mines and North Dakota Geological Survey, Regina.

Kreis, L.K. and Kent, D.M. (2000): Basement controls on Red River sedimentation and hydrocarbon production in southeastern Saskatchewan; *in* Summary of Investigations 2000, Volume 1, Saskatchewan Geological Survey, Sask. Energy Mines, Misc. Rep. 2000-4.1, p21-42.

Longman, M.W., Fertal, T.G., and Glennie, J.S. (1983): Origin and geometry of Red River dolomite reservoirs, western Williston Basin; Amer. Assoc. Petrol. Geol. Bull., v67, p744-771.

Longman, M.W., Fertal, T.G., and Glennie, J.S. (1984): Origin and geometry of Red River dolomite reservoirs, western Williston Basin: Reply; Amer. Assoc. Petrol. Geol. Bull., v68, p780-784.

Longman, M.W. and Haidl, F.M. (1996): Cyclic deposition and development of porous dolomites in the Upper Ordovician Red River Formation, Williston Basin; *in* Longman, M.W. and Sonnenfeld, M.D. (eds.); Paleozoic Systems of the Rocky Mountain Region; Rocky Mtn. Sec., SEPM, p29-46.

Machel, H.G. and Anderson, J.H. (1989): Pervasive subsurface dolomitization of the Nisku Formation in central Alberta. J. Sed. Petrol., v59, 891-911.

Machel, H.G., Cavell, P.A., and Patey, K.S. (1996): Isotopic evidence for carbonate cementation and recrystallization, and for tectonic expulsion of fluids into the Western Canada Sedimentary Basin; Geol. Soc. Amer. Bull., v108, p1108-1119.

Major, R.P., Lloyd, R.M., and Lucia, F.J. (1992): Oxygen isotope composition of Holocene dolomite formed in a humid hypersaline setting; Geol., v20, p586-588.

Mountjoy, E., Qing, H., and McNutt, R. (1992): Sr isotopic composition of Devonian dolomites,

Western Canada Sedimentary Basin: Significance as sources of dolomitizing fluids; App. Geochem., v7, p57-75.

Qing, H. and Mountjoy, E. (1989): Multistage dolomitization in Rainbow buildups, Middle Devonian Keg River Formation, Alberta, Canada; J. Sed. Petrol., v59, p114-126.

_____ (1994): Formation of coarsely crystalline, hydrothermal dolomite reservoirs in the Presqu'ile barrier, Western Canada Sedimentary Basin; Amer. Assoc. Petrol. Geol. Bull., v78, p55-77.

Qing, H. and Veizer, J. (1994): Oxygen and carbon isotopes of the Ordovician articulate brachiopods: Implication for the isotopic composition of Ordovician seawater; Geochim. Cosmochim. Acta, v58, p4429-4442.

Qing, H., Barnes, C.R., Buhl, D., and Veizer, J. (1998): The Sr isotopic composition of Ordovician and Silurian brachiopods and conodonts: Relationships to geological events and implications for coeval seawater; Geochim. Cosmochim. Acta, v62, no10, p1721-1733.

Veizer, J., Bruckschen, P., Pawellek, F., Diener, A., Podlaha, O.G., Carden, A.F.G., Jasper, T., Korte, C., Strauss, H., Azmy, K., and Ala, D. (1997): Oxygen isotope evolution of Phanerozoic seawater; Palaeogeog., Palaeoclim., Palaeoecol., v132, p159-172.

Wendte, J. Qing, H., Dravis, J.J., Moore, S.L.O., Stasiuk, L.D., and Ward, G. (1998): High-temperature saline (thermoflux) dolomitization of Devonian Swan Hills platform and bank carbonates, Wild River area, west-central Alberta; Bull. Can. Petrol. Geol., v46, p210-265.

Zenger, D.H. (1996a): Dolomitization patterns in widespread "Bighorn facies" (Upper Ordovician), Western Craton, USA; Carbonates and Evaporites, v11, p219-225.

_____ (1996b): Dolomitization of the "C" zone, Red River Formation (Upper Ordovician) in deep core, Williston Basin, Richland County, eastern Montana; Contributions to Geology, Univ. Wyoming, v31, no1, p57-75.

Reservoir Characterization of Burrow-mottled Carbonates: The Yeoman Formation of Southern Saskatchewan – Preliminary Report

Rozalia Pak [1], S. George Pemberton [1], and Murray K. Gingras [2]

Pak, R., Pemberton, S.G., and Gingras, M.K. (2001): Reservoir characterization of burrow-mottled carbonates: The Yeoman Formation of southern Saskatchewan – preliminary report; *in* Summary of Investigations 2001, Volume 1, Saskatchewan Geological Survey, Sask. Energy Mines, Misc. Rep. 2001-4.1.

1. Introduction

Previous studies have examined the reservoir heterogeneity caused by burrowing and burrow-related diagenetic fabrics in the Devonian Wabamun Formation, the Triassic Sag River Formation, the Cretaceous Schauaiba Formation, and the Jurassic Arab-D Formation. The Lower Red River Formation of southern Saskatchewan, otherwise known as the Yeoman Formation, also has a complex diagenetic history which is closely related to the burrows and borings found within the formation. Since the discovery of Berkley et al Midale 4-2-7-11W2 in 1995, over 65 665 m^3 of oil have been produced from the Midale Pool alone (Haidl *et al.*, 2000). The abundance of recent wells drilled penetrating the Red River Formation provides an excellent opportunity to examine in greater depth the relationship between reservoir quality and burrow-related diagenetic fabrics. In some zones, dolomitization of burrows and aureoles around burrows has created valuable porous and permeable zones (Zimmer, 1997). In others, dolomitization, silicification, and anhydrite precipitation have destroyed valuable reservoirs. An understanding of reservoir configuration is crucial for modeling fluid flow, and for setting up secondary and tertiary recovery schemes.

a) Background

The Ordovician Yeoman or the Burrowed 'C' Interval of the Red River Formation was deposited in a shallow epicontinental sea which straddled the equator at that time. The uppermost unit of the Yeoman Formation is the subsurface equivalent of the well-known dolomite-mottled Tyndall Limestone. Dolomite occurs preferentially in and around burrow fills in the Tyndall Limestone. The diagenetic history of subsurface strata is similar, but more complex, with some zones completely dolomitized and others greatly affected by pressure solution. The diagenetic fabrics have either produced or destroyed reservoir zones in the Yeoman Formation.

In order for fluid flow through heterogeneous media to be effectively modeled, the spatial distribution of porosity and permeability must be understood. An accurate model of these static properties must be established. Conduits such as fractures may control most of the fluid flow pattern. The fossil burrows of infauna also create small-scale heterogeneities and may cause substantial variability in porosity and permeability. Where burrows and associated diagenetic features act as flow conduits, the flow system becomes more difficult to model. Reserve calculations can greatly be reduced or increased when burrow networks have different porosity values than the matrix.

Kreis and Kent (2000) found that the basement structures affected sedimentation patterns in the Red River Formation. Burrow fabrics are sensitive to the depositional environment, and changes in sedimentation rate, salinity, and current. Subsequently, the burrow-related diagenetic fabrics also vary with original sedimentary fabrics. Kent (pers. comm., 2000) found that the burrow patterns varied from the crest to the flanks of basement structures. Although it has been recognized that burrows greatly affect the diagenetic history, there is a paucity of literature describing the ichnology of the Yeoman Formation.

The variability in dolomitization is high even within a single oil pool. It is therefore not surprising that, to date, no agreement has been made concerning what processes are responsible for the dolomitization of the Red River Formation. Seepage-reflux dolomitization, as described by Longman *et al.* (1983), has been most widely applied. Such a model, however, has not been universally accepted (Kendall, 1984). Recent studies have begun to look more closely at small-scale diagenetic models (Gingras, 2001; Zenger, 1996). It has been suggested that the dolomitization may be intricately linked to the burrow networks, and that micro-chemical environments created in the burrow systems facilitate dolomite formation. Dolomitization associated with the burrow networks is inferred to be syndepositional or early diagenetic.

b) Study Area

A representative number of wells will be examined from each of the following pools: the Midale area, located between Townships 6 and 7 and Ranges 10W2 to 12W2; the Tyvan area located in Township 13 and

[1] University of Alberta, Department of Earth and Atmospheric Sciences, Earth Sciences Building, Edmonton, AB T6G 2E3.
[2] University of New Brunswick, Department of Geology, P.O. Box 4400, Fredericton, NB E3B 5A3.

Range 13W2; and the Ceylon area between Townships 5 to 7 and Ranges 17W2 to 21W2. The study will compare these three oil pools, in order to determine how the burrow fabrics have affected diagenesis. Permeability data will show whether the diagenesis has created or destroyed permeable zones.

2. Preliminary Results

Twenty-two wells have been logged to date (Table 1), and several have been sampled. Some samples were taken for preparing thin sections, others for examining the burrow fabrics more closely. The first objective of this project has been to classify the burrow fabrics and determine which burrow-related fabrics are primary and which are the effects of later diagenesis. Kendall (1976, 1977) argued against the possibility that the mottles formed as diagenetic haloes around smaller diameter burrows. He believed the mottles to be *Thalassinoides*-like burrows, and the smaller burrows (*Planolites* and *Chondrites*) to be the product of later re-burrowing. This view has been the more popular one (e.g. Haidl *et al.*, 1997; Canter, 1998). Kissling (1999, p1184) suggested that these traces may be dwelling burrows built by filter-feeders and that "burrow mottles may represent the coherent walls of the small burrows, maintained by secretion or physical packing of excreta." Carroll (1979) preferred the interpretation that the mottles are diagenetic. Recently Gingras (2001) has revisited the possibility that the mottles are in fact diagenetic haloes of dolomite which radiate outwards from a central causative burrow. Examination of the above wells has suggested that both scenarios may simultaneously exist in the Yeoman Formation. Some zones of the Yeoman Formation are very similar to the Tyndall Limestone. The mottles do not have sharp walls and all have causative burrows (Figure 1). These mottle types have been found to contain the trace fossils *Planolites*, *Chondrites*, *Paleophycus*, and *Skolithos*. Not all burrows have diagenetic haloes, nor do all the mottles form around one specific type of burrow. No relationship has yet been observed between the distribution of mottle- vs. non-mottle-bounded burrows and the appearance of the contained burrow.

Other mottles have sharp walls, and appear to fill all criteria necessary to be classified as *Thalassinoides* (Figure 2). Further detailed examination and petrographic work are necessary to confirm this.

Variability in burrow fabrics becomes more complex upon closer inspection, and often a freshly polished surface is required for the recognition of burrows. Criteria for differentiating *Thalassinoides* and

Table 1 - List of logged cores.

Well Name	Location	Logged Interval (m)	
PCP Weyburn	21/B6-20-6-13W2	2620.0	2648.0
Berkley et al Hume N	41/7-2-9-13W2	2441.0	2447.7
Shell Yeoman	1/6-32-8-16W2	2451.8	2494.0
Berkley et al Midale	21/7-2-7-11W2	2578.0	2597.0
Berkley et al Midale	1/8-3-7-11W2	2579.0	2604.7
Berkley et al Midale	11/7-3-7-11W2	2562.5	2617.2
Berkley et al Midale	21/16-3-7-11W2	2570.0	2591.4
Berkley et al Midale	1/12-2-7-11W2	2543.0	2603.6
Berkley et al Midale	31/11-35-6-11W2/A	2582.0	2610.5
Berkley et al Midale	31/11-34-6-11W2	2568.0	2604.0
Berkley et al Midale	41/2-10-7-11W2	2560.8	2599.0
Rigel Upton Midale	11/9A-28-6-11W2	2590.6	2621.0
Tri Link Tyvan	41/7-17-13-13W2	2152.0	2170.0
Tri Link Tyvan	21/8-17-13-13W2	2143.0	2179.0
Tri Link Tyvan	11/10-17-13-13W2	2152.0	2173.8
Tri Link Tyvan	1/10-28-13-13W2	2160.0	2178.0
Tri Link Tyvan	11/2-29-13-13W2	2147.0	2169.0
Northrock Rich Ceylon	42/11-12-6-20W2	2682.0	2694.1
Husky Ceylon	11/5-8-6-19W2	2704.0	2740.0
Husky Ceylon	41/6-5-6-19W2	2714.9	2749.5
Saskoil Ceylon	1/10-18-5-19W2	2758.5	2774.0
Husky Ceylon	41/10-18-5-20W2	2771.0	2789.0

Figure 1 - Dolomitic haloes around** Paleophycus **and** Chondrites **burrows; Tri Link Tyvan 21/8-17-13-13W2, 2170.9 m.

Figure 2 -** Chondrites **within re-burrowed** Thalassinoides(?)**; Husky Ceylon 11/5-8-6-19W2, 2719.2 m.

diagenetic haloes will have to be established and tested.

Some interesting traces have been observed in the Yeoman Formation. One of these is the trace fossil *Trychophycus*, which is the large, shallow U-shaped trilobite burrow (Figure 3). These burrows often appear to be lithoclasts. The fill of these burrows is dolomitized, even when the matrix is calcareous. Slightly different fossils are contained in these burrows and their walls are lined with organics. These burrows were only observed in the lowermost undolomitized parts of the core. Burrow diameter ranges from 1 to 8 cm.

3. Future Work

The recognition and classification of burrow types in the Yeoman Formation require further work. General criteria such as the nature of burrow fills and linings commonly cannot be applied. Many burrows have been hollowed out by dissolution, sometimes resulting in vuggy porosity (Figure 4). The same type of difficulties have been encountered in separating primary fabrics from secondary fabrics in carbonate sediments.

Thin sections will be prepared and examined in order to facilitate the differentiation of burrow and diagenetic fabrics. Once this has been completed an attempt will be made to subdivide the Yeoman Formation into ichnofacies. The diagenetic overprints that have affected the various ichnofacies in these three oil pools will be tabulated and compared. The final part of this project will entail describing spatial porosity and permeability configuration. Data will be obtained by taking spot permeability measurements using a Pressure Decay Profile Permeameter. This will provide us with valuable data on the reservoir variability within the Yeoman Formation.

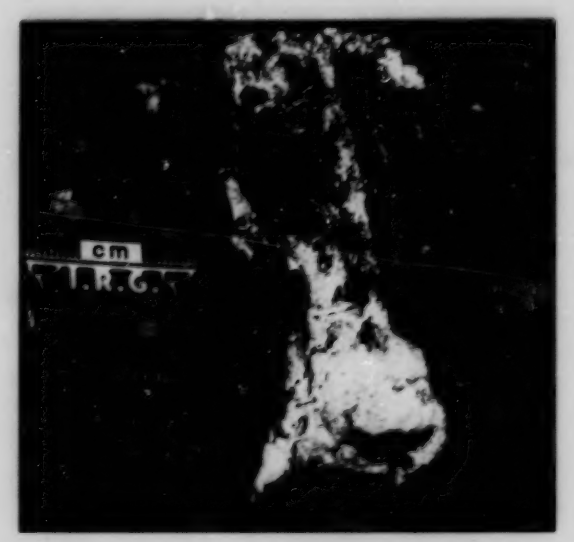

Figure 3** - Trychophycus **burrow; Berkley et al Midale 11/7-3-7-11W2, 2613.4 m.

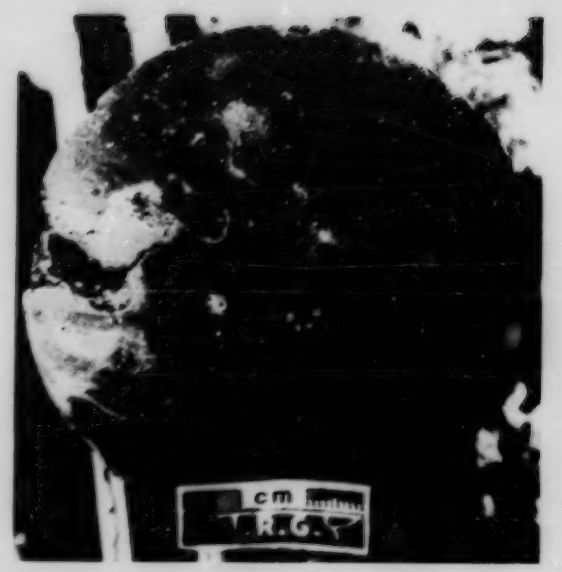

Figure 4 - Vuggy porosity; Berkley et al Midale 1/8-3-7-11W2, 2593.9 m.

4. Acknowledgments

We would like to thank all the staff at the Saskatchewan Energy and Mines Subsurface Geological Laboratory for their kindness and generous assistance. We would also like to thank Husky Oil Operation Limited for funding this project and especially Andre Laflamme for his insightful advice in starting up this project.

5. References

Canter, K.L. (1998): Facies, cyclostratigraphy and secondary diagenetic controls on reservoir distribution, Ordovician Red River Formation, Midale Field, southern Saskatchewan; Eighth International Williston Basin Symposium, Core Workshop Volume, p41-66.

Carroll, W.K. (1979): Depositional environments and paragenetic porosity controls, Upper Red River Formation, North Dakota; N. Dakota Geol. Surv., Report of Investigation 66, 51p.

Gingras, M.K. (2001): Applications in ichnology and sedimentology; unpubl. Ph.D. thesis, Univ. Alberta.

Haidl, F.M., Kreis, L.K., Miles, M., Nickel, E., and Ware, M.J. (2000): Relationship between Phanerozoic sedimentation, erosion, hydrocarbon accumulations and basement tectonics: Examples

from the Lower Paleozoic strata in southeastern Saskatchewan; GeoCanada 2000, Calgary, May 2000, Conference CD, ext. abstr. #933.

Haidl, F.M., Longman, M.W., Pratt, B.R., and Bernstein, L.M. (1997): Variations in lithofacies in Upper Ordovician Herald and Yeoman formations (Red River), North Dakota and southern Saskatchewan; Can. Soc. Petrol. Geol.–Soc. Econ. Paleont. Mineral. Joint Convention, Core Conference, p5-40.

Kendall, A.C. (1976): The Ordovician Carbonate Succession (Bighorn Group) of Southeastern Saskatchewan; Sask. Dep. Miner. Resour., Rep. 180, 186p.

_____ (1977): Origin of dolomite mottling in Ordovician limestones from Saskatchewan and Manitoba; Bull. Can. Petrol. Geol., v25, p480-504.

_____ (1984): Origin and geometry of Red River dolomite reservoirs, western Williston Basin: Discussion; Amer. Assoc. Petrol. Geol. Bull., v68, p776-779.

Kissling, D.L. (1999): Life and death roles of Red River *Thalassinoides*; Amer. Assoc. Petrol. Geol. Bull., v83, p1184.

Kreis, L.K. and Kent, D.M. (2000): Basement controls on Red River sedimentation and hydrocarbon production in southeastern Saskatchewan; *in* Summary of Investigations 2000, Volume 1, Saskatchewan Geological Survey, Sask. Energy Mines, Misc. Rep. 2000-4.1, p21-42.

Longman, M.W., Fertal, T.G., and Glennie, J.S. (1983): Origin and geometry of Red River dolomite reservoirs, western Williston Basin; Amer. Assoc. Petrol. Geol. Bull., v67, p744-771.

Zenger, D.H. (1996): Dolomitization of the "C" Zone, Red River Formation (Upper Ordovician) in a deep core, Williston Basin, Richland County, eastern Montana; Contributions to Geology, Univ. Wyoming, Vol. 31, p57-75.

Zimmer, P. (1997): Dolomitization in the Yeoman Member, Red River Formation, Minton Pool, south central Saskatchewan: Timing, distribution and controls; unpubl. B.Sc. thesis, Univ. Regina, 52p.

Biostratigraphy and Paleoecology of Late Ordovician Conodonts from a Composite Section in the Subsurface of Saskatchewan [1]

Godfrey S. Nowlan [2] and F.M. Haidl

Nowlan, G.S. and Haidl, F.M. (2001): Biostratigraphy and paleoecology of Late Ordovician conodonts from a composite section in the subsurface of Saskatchewan; *in* Summary of Investigations 2001, Volume 1, Saskatchewan Geological Survey, Sask. Energy Mines, Misc. Rep. 2001-4.1.

1. Introduction

This paper reports on the biostratigraphy and paleoecology of conodonts recovered from Upper Ordovician strata in four wells in southeastern Saskatchewan (Figure 1). The cored intervals from these wells represent a composite section through the Yeoman, Herald, and Stony Mountain formations (Figure 2). Sixty-six samples have yielded more than 5000 conodont elements assignable to a variety of species. Despite the generally small size of the samples (average 408 grams), more than 95% of the samples have produced conodonts, although many samples produce very few specimens.

Previous work on Upper Ordovician conodont biostratigraphy in the subsurface of Saskatchewan has focused on the Ordovician-Silurian boundary interval (Norford *et al.*, 1998; Nowlan and Haidl, 1999). An analysis of conodonts in the Late Ordovician of Alberta has been submitted for publication (Nowlan, in review). A paper on the paleontology of the Fort Garry Member of the Red River Formation in Manitoba (Elias *et al.*, 1988) is the only other published record of conodonts in this interval in the Canadian part of the Williston Basin.

2. Stratigraphy

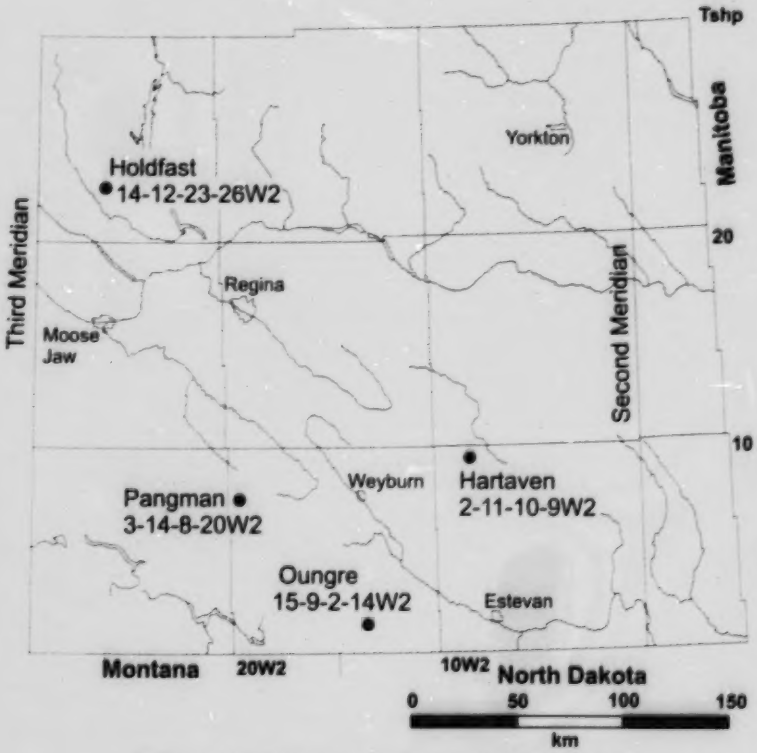

Figure 1 - Location map of wells sampled for this study.

Middle to Upper Ordovician strata in the study area comprise a basal clastic unit (Winnipeg Formation) and an overlying sequence characterized by repetition of carbonate and evaporite lithologies (Yeoman, Herald, Stony Mountain, and Stonewall formations) (Figure 2).

a) Winnipeg Formation

A time gap between the Winnipeg and Yeoman formations is generally implied, but no biostratigraphic data to support this are available from Saskatchewan. The earliest report on conodonts from the Winnipeg Formation was that of Furnish *et al.* (1936) which demonstrated its Middle Ordovician age, and that it is therefore much younger than the underlying Deadwood Formation. Later reports on conodonts from the Winnipeg Formation include those of Amsden and Miller (1942) in Wyoming, Carlson (1960) in North Dakota, and Oberg (1966) from the outcrop belt in Manitoba. More recently, the Icebox and Roughlock members

[1] Geological Survey of Canada Contribution No. 2000292.
[2] Geological Survey of Canada, 3303 - 33rd Street NW, Calgary, AB T2L 2A7.

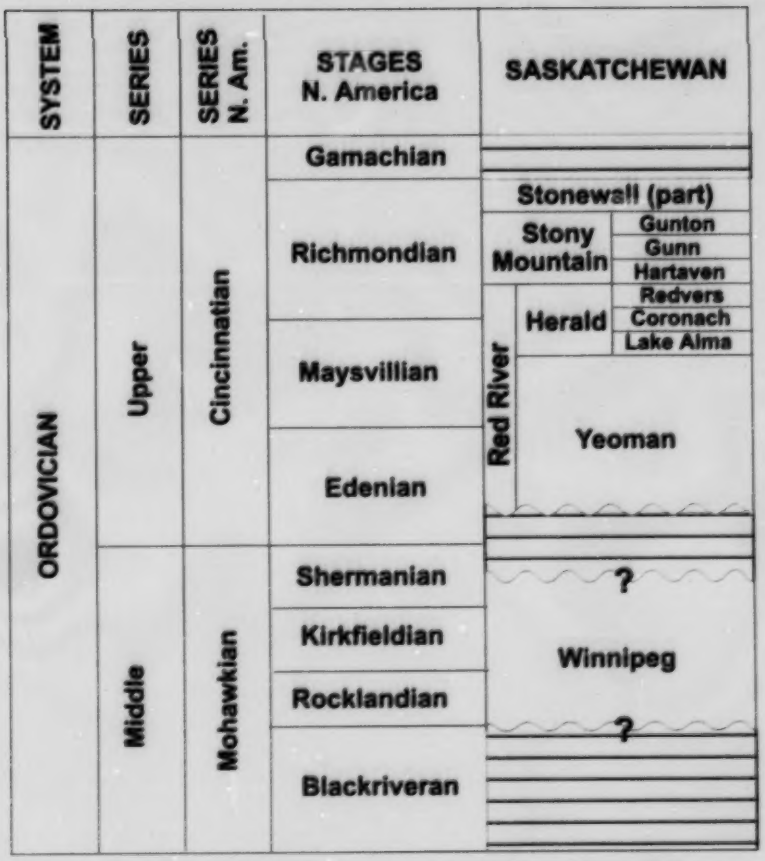

Figure 2 - Correlation of Saskatchewan strata with Middle and Upper Ordovician stages.

of the Winnipeg Formation in South Dakota have been shown to be Rocklandian to Kirkfieldian, and Kirkfieldian to earliest Shermanian in age respectively (Sweet, 1982). However, data for North Dakota as reported by Kessler (1991) may indicate that the Red River is in depositional continuity with the Winnipeg in southern North Dakota and that, therefore, the Roughlock in northern North Dakota may be Edenian. The rocks in the upper part of the Winnipeg Formation in the few Saskatchewan cores of the Yeoman/Winnipeg boundary zone examined to date are not suitable for acid digestion and so no samples were taken for conodont analyses. However, the question of a hiatus between the Winnipeg and Yeoman needs to be addressed, especially in the southeastern corner of Saskatchewan where Kreis (2000) has indicated the presence of the Roughlock Member.

b) Red River (Yeoman and Herald Formations)

The stratigraphic nomenclature established for Red River strata in southeastern Saskatchewan reflects the interpretation that the repetition of carbonate and evaporite strata represents three brining-upward cycles. The Yeoman Formation and the lower Herald (Lake Alma Member) form the oldest cycle, and the upper Herald relates to the middle (Coronach Member) and youngest (Redvers Unit) cycles (Kendall, 1976). New core and geophysical log data from the more than 300 wells drilled into the Red River since 1976 suggest a more complex depositional history than the current stratigraphic breakdown implies (Pratt *et al.*, 1996; Haidl *et al.*, 1997; Kreis and Kent, 2000). However, further work is required to establish a detailed sequence stratigraphic framework for Ordovician and Silurian strata in the Williston Basin before formal stratigraphic nomenclature can be revised.

Yeoman Formation

The Yeoman Formation is composed primarily of burrow-mottled fossiliferous lime mudstones and wackestones which have been dolomitized to varying degrees. The burrows which give a mottled appearance to the rocks are large *Thalassinoides*-like structures within which are small cylindrical burrows (*Planolites, Chondrites, Paleophycus, Skolithos)* (Kendall, 1976, 1977; Pratt *et al.*, 1996; Canter, 1998; Kissling, 1999; Pak *et al.*, this volume). Other trace fossils include *Trychophycus* (Pak *et al.*, this volume). Tabulate corals and solitary and colonial rugose corals, cephalopods, brachiopods, bryozoans, echinoderms, stromatoporoids, and gastropods are the most commonly observed macrofossils in core (Brindle, 1960; Kendall, 1976; Pratt *et al.*, 1996; Haidl *et al.*, 1997). Conodonts from this formation in Saskatchewan have not been reported before, although Sweet (1979) has detailed them from equivalent strata in Wyoming and South Dakota. The micro-alga *Gloeocapsomorpha prisca*, of probable cyanobacterial origin (Stasiuk, 1991; Stasiuk *et al.*, 1993), is the primary component of organic-rich kerogenites (kukersites) which are preserved as thin but widespread layers in the upper one-third of the Yeoman.

Herald/Yeoman Contact

The contact between the Yeoman and the overlying Herald (Lake Alma Member) is difficult to pick both in core and on geophysical logs. In core, strata between the burrow-mottled rocks typical of the Yeoman and

the laminated to thinly bedded dolostones which characterize the lower Lake Alma are variable in lithology. This thin (<1 m to 8 m) transitional unit is composed of variably dolomitized, poorly mottled, irregularly bedded lime mudstones with texturally variable fossiliferous, peloidal and/or coated grain layers (Kendall, 1976; Longman and Haidl, 1996; Pratt *et al.*, 1996, Haidl *et al.*, 1997; Kissling, 1997; Kreis and Kent, 2000). An 8 m thick reefal sequence in the LVR et al Steelman 7-28-4-4W2 well includes a stromatoporoid dolorudstone and a microbial doloboundstone (Pratt *et al.*, 1996; Haidl *et al.*, 1997). At the two wells of this study in which this contact is cored (15-9-2-14W2 and 14-12-23-26W2), the "transitional unit" is placed in the Yeoman Formation; i.e. the Herald/Yeoman contact is placed at the base of the lowermost laminated dolomudstone bed. Other workers interpret the "transitional unit" as the lowermost unit of the Lake Alma Member of the Herald Formation (e.g. Kreis and Kent, 2000).

Herald Formation

Conodonts have not been reported previously from this unit in Saskatchewan. However conodonts from the Bighorn Group in Wyoming (Stone and Furnish, 1959; Sweet, 1979) are at least partially equivalent. Conodonts have also been reported from the Fort Garry Member of the Red River Formation in the outcrop belt of Manitoba (Elias *et al.*, 1988), a probable equivalent of the Herald Formation. The conodonts indicate a Richmondian age, at least for the upper part of the Fort Garry Member.

Lake Alma Member

The Lake Alma Member comprises laminated to bedded, commonly slightly argillaceous, dolomudstones and calcareous dolomudstones. Interbedded with the dolomudstones in some wells, including the Cal-Stan Holdfast 14-12-23-26W2 well in this study, are beds of burrow-mottled and/or fossiliferous dolostone. In the extreme eastern part of Saskatchewan (Range 2W2 and eastward), beds of coated grain dolostone, which may have originated as oolitic grainstones, are interbedded with the laminated dolomudstones (Kent, 1960; Kendall, 1976; Haidl *et al.*, 1997; Kent and Haidl, 1999; Kreis and Kent, 2000).

The Lake Alma anhydrite, the upper unit of the Lake Alma Member, is composed of nodular, bedded, and laminated anhydrite with interbeds of dolomudstone (commonly anhydritic). This is the most widespread of the Lower Paleozoic evaporite units. It extends from the basin centre in North Dakota to as far north as Township 33, as far west as Range 10W3 and into Manitoba to the east (Kent, 1960; Kendall, 1976; Norford *et al.*, 1994; Longman and Haidl, 1996).

Coronach Member

Where fully developed (as in the 15-9-2-14W2 and 2-11-10-9W2 cores), the Coronach Member comprises: 1) a basal, slightly argillaceous dolomudstone, locally with scattered quartz grains; 2) a fossiliferous, commonly burrowed, wackestone or dolowackestone; 3) slightly argillaceous laminated dolomudstones (locally lime mudstones); and 4) the Coronach anhydrite (Kendall, 1976). The basin-centred anhydrite unit is thinner and less widespread than the Lake Alma anhydrite, extending north only to Township 11 in south-central Saskatchewan.

Redvers Unit

The Redvers unit is composed of a basal argillaceous dolomudstone bed and an upper laminated dolomudstone or lime mudstone. This unit is mapped with confidence only where an argillaceous marker bed separates it from the overlying Stony Mountain carbonates on geophysical logs.

Stony Mountain Formation

Ethington and Furnish (1960) recovered Richmondian conodonts from two Stony Mountain samples in the type area north of Winnipeg, Manitoba. A more detailed assessment of conodonts from equivalent strata in the United States has been provided by Sweet (1979).

In all but the extreme western and northwestern parts of the study area, where it is undifferentiated, the Stony Mountain Formation is subdivided into (O-Y): 1) the Hartaven Member of slightly argillaceous to argillaceous fossiliferous lime mudstones and wackestones; 2) the Gunn Member of fossiliferous very argillaceous limestones with interbeds of variably dolomitized lime mudstones; and 3) the Gunton Member of primarily nodular, commonly unfossiliferous, dolomudstones, overlain by laminated dolomudstones and a capping anhydrite.

3. Conodont Biostratigraphy and Paleoecology

The distribution of conodont species in each of the wells is discussed below. A reference for the biostratigraphic subdivisions mentioned in the text is shown as Figure 2. Tables 1 to 4 show the numerical distribution of species in samples from the wells and Figures 3 to 5 show relative abundance curves for genera in each of the wells, except Imperial Pangman for which there is little data. Selected specimens of most of the species reported in Tables 1 to 4 are illustrated in Figures 6 and 7.

Imperial Pangman 3-14-8-20W2

From Imperial Pangman 3-14-8-20W2, four samples were taken from the lowest 16 ft (4.9 m) of the

Table 1 - Numerical distribution of conodont species by sample depth in feet and GSC locality number in the Pangman well.

Imperial Pangman 3-14-8-20W2

	Yeoman				
	8470.1(C-257739)	8464.2 (C-257740)	8459.0 (C-257741)	8454.0 (C-257742)	
Belodina sp.	0	1	0	0	
Panderodus gibber	0	0	0	1	
Panderodus gracilis	0	17	0	8	
Pseudobelodina? dispansa	0	0	0	1	
Pseudobelodina vulgaris vulgaris	0	1	0	0	
Total:	**0**	**19**	**0**	**10**	**29**
Mass (grams):	300	393	300	285	1278

Yeoman Formation. No rock suitable for acid digestion was found in the Winnipeg Formation. The distribution of conodonts recovered is shown in Table 1. The 29 specimens are mainly assignable to species of the widespread and long-ranging genus *Panderodus*. One specimen of *Pseudobelodina vulgaris vulgaris* at 8464.2 ft (2579.9 m) indicates a Late Ordovician, mid-Edenian or younger age for the lower part of the Yeoman Formation. This interpretation is based on the range of this species as defined primarily by Sweet (1979, 1984).

Cal-Stan Holdfast 14-12-23-26W2

From Cal-Stan Holdfast 14-12-23-26W2 16 samples from 130 ft (39.6 m) of the Yeoman Formation and six from the lower 44 ft (13.4 m) of the Herald Formation were analyzed (Figure 3).

Biostratigraphy

The distribution of conodonts is shown in Table 2. Samples from the lower part of the core in the Yeoman Formation (below the 5759.1 ft; 1755.4 m) level, GSC loc. C-322670) yielded few conodonts and thus no biostratigraphic interpretations are made for the interval 5759.1 ft. to 5805.4 ft (1755.4 m to1769.5 m).

The first appearance of *Culumbodina penna* Sweet, which is indicative of Middle Edenian to Middle Maysvillian age, occurs at 5743.6 ft (1750.6 m) (GSC loc. C-322668) and additional specimens occur up to 5714.0 ft (1741.6 m) (GSC loc. C-322664), well within the upper part of the Yeoman.

The upper samples in the well are dominated by specimens of *Aphelognathus* aff. *A. divergens* Sweet. This species is similar to specimens described by Sweet (1979) as *A. divergens* but also shares some characteristics with the older species *A. shoshonensis* Sweet. Although Sweet (1979) indicated that these species did not have overlapping ranges, he suggested that they may be part of a lineage. The faunas in this interval and those of a similar interval in the Oungre well (upper Yeoman–lower Herald) appear to be transitional between the two species, or their ranges overlap. Although the age of upper Yeoman to lower Herald remains uncertain, it is at least Middle Maysvillian, as indicated by *Culumbodina penna* lower in the section, or possibly younger.

This *Aphelognathus* species is associated with an abundance of simple cones lacking biostratigraphic significance, but two species, *Parabelodina denticulata* Sweet and *Parabelodina* cf. *P. adenticulata*, seem to occur within the upper Yeoman–lower Herald interval and may have future biostratigraphic utility. Such specimens were identified as *Parabelodina denticulata* at 10,019.0 ft (3053.8 m) (GSC loc. C-257708) in the Lake Alma Member of the Herald Formation in the Oungre 15-9-2-14W2 well. In the Holdfast well, they occur at 5661.8 ft (1725.7 m) and 5682.5 ft (1732.0 m) (GSC locs. C-322658 and C-322660) in beds of the upper Yeoman and the middle of the Lake Alma Member (Table 2 and Figure 3).

Paleoecology

The fact that the distribution of Ordovician conodont genera and species are affected by facies distribution was first recognized by Seddon and Sweet (1971). They attributed the patterns they had recognized to a pelagic habit in conodonts. This was challenged by Barnes and Fåhraeus (1975) who suggested that most Ordovician conodont genera were benthic or nektobenthic, living at or near the bottom of the water column. In both studies the distribution of conodont genera was related to facies distribution.

A study specific to Upper Ordovician biofacies was completed by Sweet and Bergström (1984) in which they recognized six conodont biofacies for the Edenian-Maysvillian of North America.

Their biofacies are modified herein to reflect local faunas and other biofacies work on the Late Ordovician by Nowlan and Barnes (1981). The biofacies for the Late Ordovician, in order from shallowest to deepest, are based on conodont genera believed to be benthic or nektobenthic:
1) *Rhipidognathus* biofacies, 2) *Oulodus-Aphelognathus* biofacies, 3) *Plectodina* biofacies, 4) *Phragmodus* biofacies, and 5) *Amorphognathus* biofacies. The genera *Panderodus* and *Drepanoistodus* and many of the other simple cone genera such as *Belodina* and *Pseudobelodina* are believed to be pelagic.

The relative abundance of significant genera from the Holdfast well is summarized in Figure 3. Although all samples are reported, the value of those with only a few specimens should be discounted. The lower part of this well (5767 to 5805.4 ft; 1757.8 to 1769.5 m) yields few conodonts and most are specimens of *Panderodus*. Thus, there are no paleoecological indicators except a

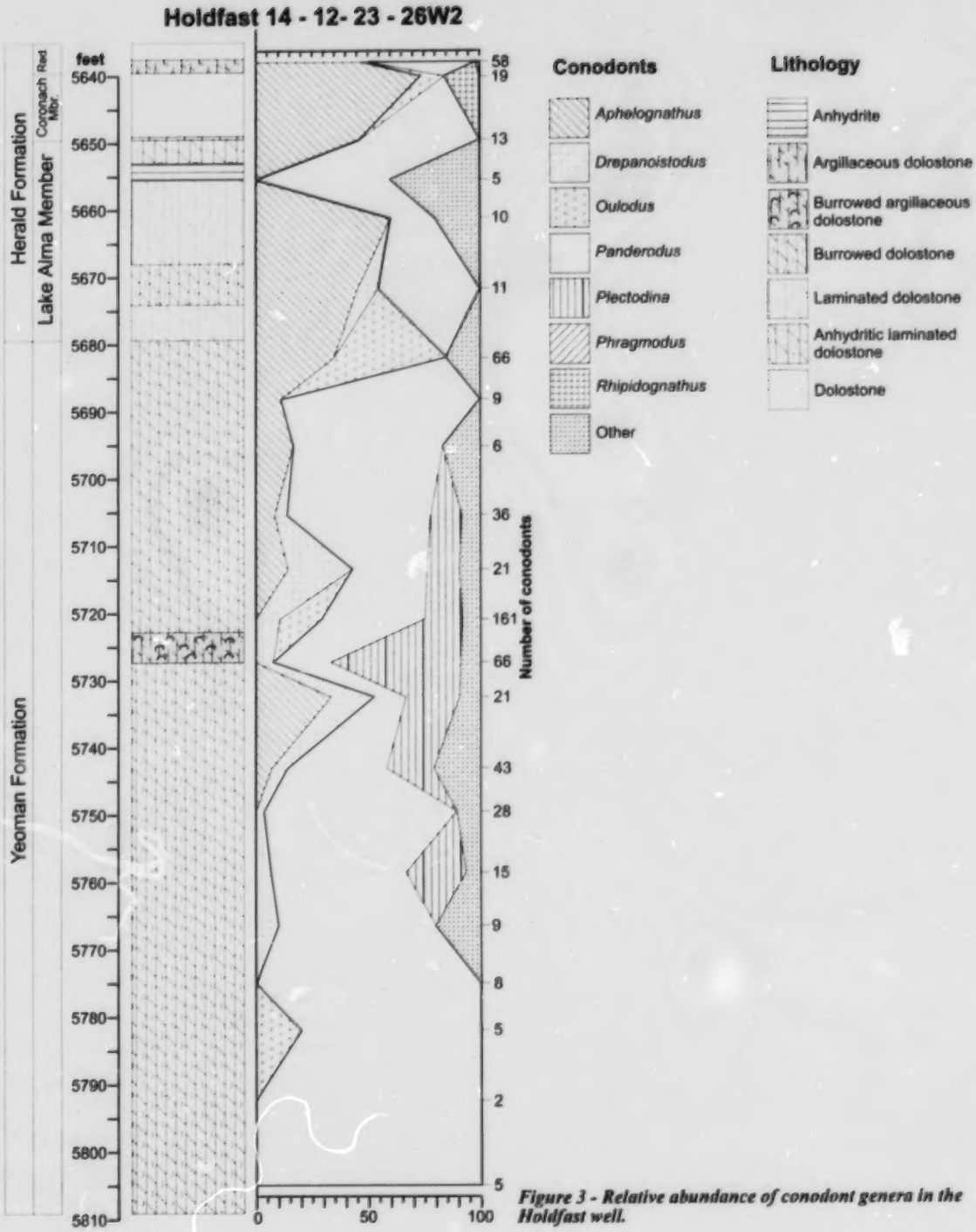

Figure 3 - Relative abundance of conodont genera in the Holdfast well.

Cal-Stan Holdfast 14-12-23-26W2

	Yeoman																Herald						
	5805.4 (C-322675)	5792.8 (C-322674)	5782.5 (C-322673)	5775.5 (C-322672)	5767.0 (C-322671)	5759.1 (C-322670)	5750.0 (C-322669)	5743.6 (C-322668)	5733.0 (C-322667)	5727.8 (C-322666)	5721.4 (C-322665)	5714.0 (C-322664)	5706.0 (C-322663)	5695.7 (C-322662)	5688.7 (C-322661)	5682.5 (C-322660)	5672.3 (C-322659)	5661.8 (C-322658)	5656.0 (C-322657)	5650.1 (C-322656)	5640.6 (C-322655)	5638.5 (C-322654)	
Aphelognathus aff *A. divergens*	0	0	0	0	0	0	0	0	0	0	0	0	0	0	0	23	5	6	0	6	14	27	
Aphelognathus sp.	0	0	0	0	0	0	0	3	7	0	0	3	3	1	1	0	0	0	0	0	0	0	
Belodina confluens	0	0	0	0	1	1	0	4	1	2	2	0	0	0	0	0	0	0	0	0	0	0	
Culumbodina occidentalis	0	0	0	0	0	0	0	1	0	0	0	0	0	0	0	0	0	0	0	0	0	0	
Culumbodina pinna	0	0	0	0	0	0	0	1	0	0	0	1	0	0	0	0	0	0	0	0	0	0	
Drepanoistodus suberectus	0	0	0	0	1	1	1	3	4	5	17	6	2	0	0	0	1	0	0	0	0	2	
Oulodus ulrichi	0	0	0	0	0	0	0	0	0	0	30	0	0	0	0	0	0	0	0	0	0	0	
Oulodus? sp.	0	0	1	0	0	0	0	0	0	0	0	0	0	0	0	0	0	0	0	0	0	0	
Panderodus bergstroemi	0	0	0	0	1	0	2	2	0	0	0	1	0	0	0	0	0	0	0	0	0	0	
Panderodus cf. *P. bergstroemi*	0	0	0	0	0	0	0	0	0	0	0	0	0	0	0	0	0	0	0	7	0	0	
Panderodus gibber	0	0	0	0	1	0	1	0	0	0	4	0	3	0	1	4	0	0	0	0	0	2	
Panderodus gracilis	5	2	4	8	5	9	21	17	2	17	70	6	20	4	6	29	5	2	3	0	2	22	
Panderodus panderi	0	0	0	0	0	0	0	0	1	0	0	0	0	0	1	0	0	0	0	0	0	4	
Panderodus serratus	0	0	0	0	0	0	0	0	0	0	0	0	0	0	0	0	0	0	0	0	0	0	
Parabelodina denticulata	0	0	0	0	0	0	0	0	0	0	0	0	0	0	0	6	0	0	0	0	0	0	
Parabelodina cf. *P. denticulata*	0	0	0	0	0	0	0	0	0	0	0	0	0	0	0	1	0	2	0	0	0	0	
Plegagnathus nelsoni	0	0	0	0	0	0	0	0	0	0	0	0	0	0	0	0	0	0	0	0	0	1	
Plectodina aculeatoides	0	0	0	0	0	0	0	9	5	38	27	0	0	0	0	0	0	0	0	0	0	0	
Plectodina florida	0	0	0	0	0	0	0	0	0	0	0	0	5	0	0	0	0	0	0	0	0	0	
Plectodina sp.	0	0	0	0	0	4	0	0	0	0	0	3	0	0	0	0	0	0	0	0	0	0	
Pseudobelodina inclinata	0	0	0	0	0	0	0	0	0	0	0	0	1	0	0	3	0	0	0	0	0	0	
Pseudobelodina vulgaris vulgaris	0	0	0	0	0	0	0	0	1	3	6	0	2	0	0	0	0	0	0	0	0	0	
Pseudobelodina? *dispansa*	0	0	0	0	0	0	2	1	0	1	4	1	0	0	0	0	0	0	2	0	0	0	
Pseudooneotodus mitratus	0	0	0	0	0	0	1	1	0	0	0	0	0	0	0	0	0	0	0	0	0	0	
Rhipidognathus symmetricus	0	0	0	0	0	0	0	0	0	0	0	0	0	0	0	0	0	0	0	0	3	0	
Walliserodus sp.	0	0	0	0	0	0	0	1	0	0	1	0	0	1	0	0	0	0	0	0	0	0	
Total:	**5**	**2**	**5**	**8**	**9**	**16**	**28**	**43**	**21**	**68**	**161**	**21**	**36**	**6**	**9**	**68**	**11**	**10**	**5**	**13**	**19**	**58**	**617**
Mass (grams):	595	535	665	378	578	314	436	624	430	393	402	521	442	418	650	552	496	440	608	489	501	453	10920

Table 2 - Numerical distribution of conodont species by sample depth in feet and GSC locality number in the Holdfast well.

few specimens of the genus *Oulodus* indicating relatively shallow conditions.

Deepening of the basin is indicated by the appearance of *Plectodina* at 5759.1 ft (1755.4 m) and the genus is well represented through to the 5706 ft (1739.2 m) level. However, clear indications of sea-level oscillations are recognized by the presence of shallower water biofacies represented by *Aphelognathus* at 5733 ft (1747.4 m) and 5743.6 ft (1750.6 m). Abundant *Oulodus* mixed with *Plectodina* at 5721.4 ft (1743.9 m) may suggest an intermediate water depth. An argillaceous dolostone bed at 5727.8 ft (1745.8 m) produced the greatest abundance of *Plectodina*, suggesting an increase in water depth. Samples from adjacent beds are also abundant in conodonts.

The remainder of the section appears to represent shallower water deposition with *Aphelognathus* and *Oulodus* dominating the fauna throughout the 5638.5 to 5695.7 ft (1718.6 to 1736.0 m) interval. Abundance is low and specimens of *Aphelognathus* are excluded close to an evaporite unit within the Lake Alma Member. An extremely shallow episode is recorded by *Rhipidognathus* at 5640.6 ft (1719.3 m) within the uppermost part of the Coronach Member of the Herald Formation.

No indications of deep water biofacies were found in this well.

CDR Shell FPC Oungre 15-9-2-14W2

The core from CDR Shell FPC Oungre 15-9-2-14W2 brackets the upper Yeoman, Herald, and lowermost Stony Mountain formations. Nine samples were taken from the uppermost 63 ft (19.2 m) of the Yeoman Formation, ten samples from the Herald Formation (104 ft, 31.7 m thick) and three from the lower 13 ft (3.96 m) of the Stony Mountain Formation (Figure 4).

Biostratigraphy

The distribution of conodont species is shown in Table 3. The lowest six samples (10,040.5 to 10,089.0 ft; 3060.3 to 3075.1 m) yield specimens probably assignable to *Aphelognathus* but the specimens are so fragmentary or the preserved apparatuses are too incomplete for specific identification. These samples also include specimens of *Oulodus*? sp. and *Pseudobelodina vulgaris vulgaris*, the latter supplying a minimum age of mid-Edenian for the interval as at Pangman. Good specimens of *Plectodina aculeatoides*, a species that ranges from mid-Edenian to mid-Richmondian, were collected at 10,052.5 ft (3064.0 m) and 10,061.5 ft (3066.7 m).

A single specimen assignable to *Culumbodina* occurs at 10,040.5 ft (3060.3 m) which suggests an age no younger than mid-Maysvillian. This places an upper age limit on this lower part of the Yeoman at the Oungre well.

The next highest biostratigraphically significant form, *Aphelognathus* aff. *A. divergens*, occurs at 10,028.3 ft (3056.6 m) in the upper part of the Yeoman Formation. This form is most similar to *A. divergens* reported by Sweet (1979, 1984) to be restricted to the Richmondian Stage of the Upper Ordovician, but the M elements are more similar to those of *A. shoshonensis*, a somewhat older species. These specimens appear just a few feet above mid-Maysvillian conodonts, and thus may be transitional between Maysvillian *A. shonshonensis* and Richmondian *A. divergens* and suggest a Late Maysvillian age. This is similar to the situation noted at the Holdfast well.

Samples higher in the Yeoman Formation and from the lower part of the Herald Formation are conodont poor. Specimens of *Panderodus bergstroemi*, a mid-Maysvillian or younger species, occur at 10,019.0 ft (3053.8 m) but the interval from 9937.5 ft (3029.0 m) to 10,006.55 ft (3050.0 m) is virtually barren except for specimens of the long-ranging *Panderodus*.

Aphelognathus re-appears at 9927.5 ft (3025.9 m), together with a single specimen of *Rhipidognathus*, a paleoecologically significant form, representing extremely shallow conditions. Unfortunately the specimens of *Aphelognathus* are not particularly well preserved and cannot be firmly identified as *A. divergens* which is the species expected in the Herald Formation based on correlation with the Fort Garry Member in Manitoba. Additional collections are required to sort out the evolution of *Aphelognathus* in this part of Saskatchewan.

A diverse fauna appears at the base of the Harthaven Member of the Stony Mountain Formation. It includes the biostratigraphically diagnostic *Amorphognathus ordovicicus* known from late Maysvillian to Gamachian strata around the world, and abundant specimens of *Phragmodus undatus* and a variety of other taxa. Higher samples in the Stony Mountain Formation yield a markedly similar fauna.

Paleoecology

The numerically dominant taxon throughout the Yeoman and Herald formations is the probably pelagic, simple cone conodont *Panderodus*. The shallow water *Oulodus-Aphelognathus* biofacies (10,070.2 to 10,089.0 ft; 3069.4 to 3075.1 m) characterizes the lower part of the Yeoman Formation in the Oungre well. Slight deepening is indicated by the succeeding *Plectodina* biofacies (10,032.2 to 10,061.5 ft; 3057.8 to 3066.7 m) and a return to the shallower water in the uppermost Yeoman at 10,028.3 ft (3056.6 m) is coincident with a change from mottled dolostone to bioclastic dolostone.

Conodonts are generally rare in the Herald Formation; in part, this may reflect proximity of several samples to anhydrite beds. From the available evidence, the Herald appears to have been deposited in shallow water inhabited mainly by pelagic forms, but also periodically by the *Oulodus-Aphelognathus* biofacies.

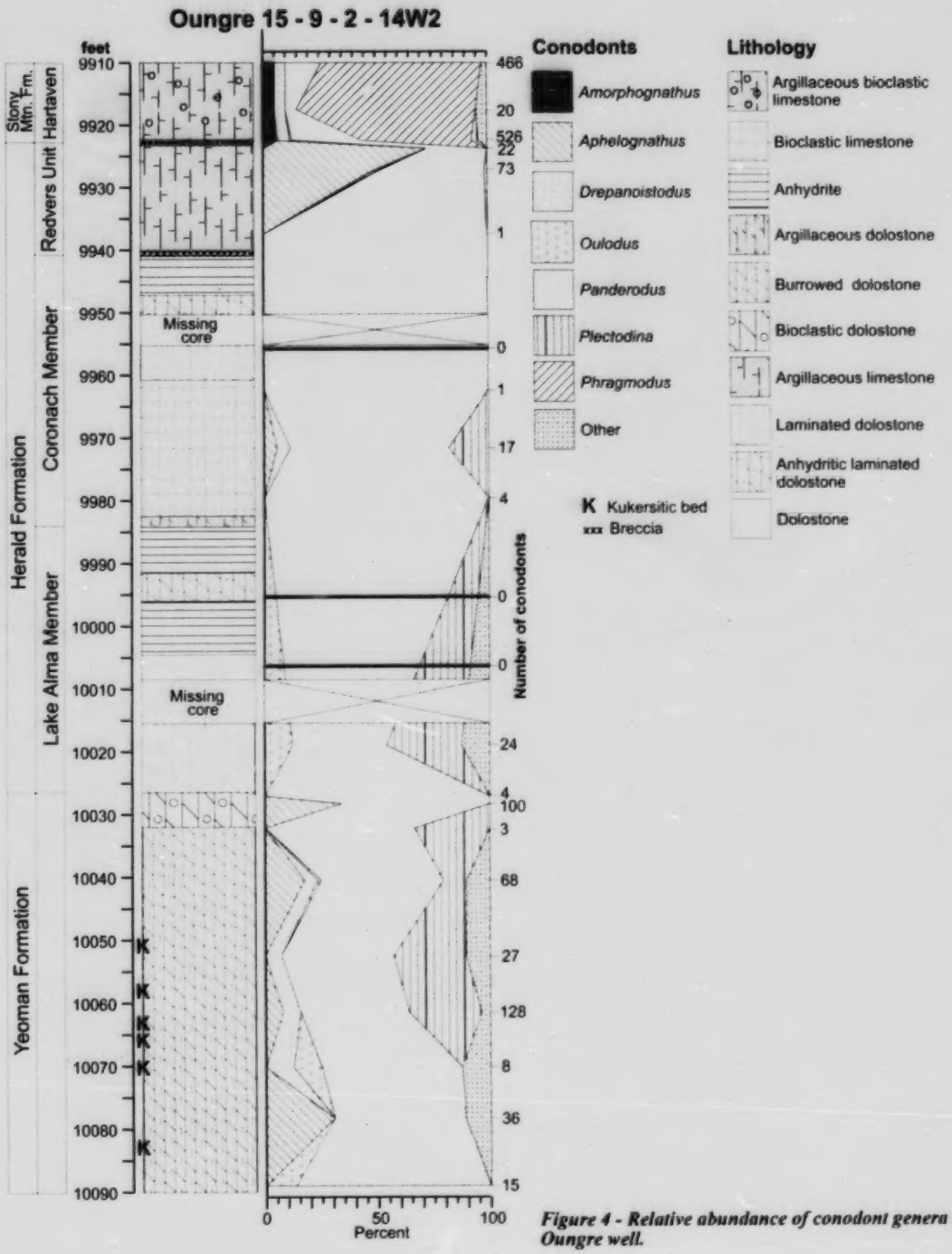

Figure 4 - Relative abundance of conodont genera in the Oungre well.

CDR Shell FPC Oungre 15-9-2-14W2

	Yeoman									Herald										Stony Mountain			
	10069.0 (C-257699)	10078.3 (C-257700)	10070.2 (C-257701)	10061.5 (C-257702)	10052.5 (C-257703)	10040.5 (C-257704)	10032.2 (C-257705)	10028.3 (C-257706)	10027.1 (C-257707)	10019.0 (C-257708)	10006.55 (C-257709)	9985.5.5 (C-257710)	9979.6 (C-257711)	9971.7 (C-257712)	9962.45 (C-257713)	9956.0 (C-257714)	9937.5 (C-257715)	9927.5 (C-257716)	9923.75 (C-257717)	9922.45 (C-257718)	9917.5 (C-257719)	9910.0 (C-257720)	
Amorphognathus ordovicicus	0	0	0	0	0	0	0	0	0	0	0	0	0	0	0	0	0	0	0	34	1	24	
Aphelognathus aff. *A. divergens*	0	0	0	0	0	0	0	34	0	0	0	0	0	0	0	0	0	35	16	0	0	0	
Aphelognathus sp.	0	11	0	10	0	12	0	0	0	0	0	0	0	1	0	0	0	0	0	0	0	0	
Belodina confluens	0	3	0	3	2	0	0	0	0	0	0	0	0	0	0	0	0	0	0	6	0	2	
Culumbodina occidentalis	0	0	0	0	0	1	0	0	0	0	0	0	0	0	0	0	0	0	0	0	0	0	
Drepanoistodus suberectus	0	0	1	10	2	4	0	0	0	0	0	0	0	1	0	0	0	1	0	30	1	23	
Oulodus? sp.	2	0	1	0	0	1	0	0	0	3	0	0	0	0	0	0	0	1	0	4	0	0	
Panderodus bergstroemi	0	0	0	0	0	0	0	0	0	7	0	0	0	0	0	0	0	0	0	0	0	0	
Panderodus gibber	0	0	0	0	0	0	0	0	1	0	0	0	0	0	0	0	0	0	0	3	0	0	
Panderodus gracilis	13	17	5	60	14	35	2	66	3	3	0	0	4	12	1	0	1	35	6	157	1	75	
Panderodus panderi	0	4	0	2	0	2	0	0	0	0	0	0	0	0	0	0	0	0	0	5	0	0	
Parabelodina denticulata	0	0	0	0	0	0	0	0	0	1	0	0	0	0	0	0	0	0	0	0	0	0	
Parabelodina cf. *P. denticulata*	0	0	0	0	0	0	0	0	0	2	0	0	0	0	0	0	0	0	0	0	0	0	
Paroistodus? *nowlani*	0	0	0	0	0	0	0	0	0	0	0	0	0	0	0	0	0	0	0	2	0	0	
Phragmodus undatus	0	0	0	0	0	0	0	0	0	0	0	0	0	0	0	0	0	0	0	260	16	333	
Plectodina aculeatoides	0	0	0	41	9	0	1	0	0	0	0	0	0	0	0	0	0	0	0	0	0	0	
Plectodina florida	0	0	0	0	0	7	0	0	0	0	0	0	0	0	0	0	0	0	0	16	0	0	
Plectodina sp.	0	0	0	0	0	0	0	0	0	8	0	0	0	3	0	0	0	0	0	0	0	0	
Plegagnathus sp.	0	0	0	0	0	0	0	0	0	0	0	0	0	0	0	0	0	0	0	3	0	2	
Pseudobelodina vulgaris vulgaris	0	1	1	1	0	0	0	0	0	0	0	0	0	0	0	0	0	0	0	2	0	1	
Pseudobelodina? *dispansa*	0	0	0	1	0	2	0	0	0	0	0	0	0	0	0	0	0	0	0	2	1	1	
Pseudobelodina sp.	0	0	0	0	0	3	0	0	0	0	0	0	0	0	0	0	0	0	0	0	0	0	
Pseudooneotodus mitratus	0	0	0	0	0	0	0	0	0	0	0	0	0	0	0	0	0	0	0	1	0	0	
Rhipidognathus sp.	0	0	0	0	0	0	0	0	0	0	0	0	0	0	0	0	0	1	0	0	0	0	
Staufferella brevispinata	0	0	0	0	0	0	0	0	0	0	0	0	0	0	0	0	0	0	0	0	0	5	
Walliserodus sp.	0	0	0	0	0	1	0	0	0	0	0	0	0	0	0	0	0	0	0	1	0	0	
Total	**15**	**36**	**8**	**128**	**27**	**68**	**3**	**100**	**4**	**24**	**0**	**0**	**4**	**17**	**1**	**0**	**1**	**73**	**22**	**526**	**20**	**466**	**1543**
Mass (grams):	400	456	400	468	400	522	400	334	400	623	400	242	200	197	300	333	400	498	300	297	250	218	8038

Table 3 - Numerical distribution of conodont species by sample depth in feet and GSC locality number in the Oungre well.

The recurrence of *Plectodina* sp. at 10,019.0 ft (3053.8 m) and at 9971.7 ft (3039.4 m) may be indicative of deeper water. A single specimen of *Rhipidognathus*, representative of extremely shallow water, occurs in the upper part of the Herald Formation at 9927.5 ft (3025.9 m).

The faunal change into the Stony Mountain Formation is made dramatic by the abundance of *Amorphognathus* and *Phragmodus* representative of deeper water biofacies and an implied major transgression.

Imperial Hartaven 2-11-10-9W2

Imperial Hartaven 2-11-10-9W2 contains core from the Herald and Stony Mountain formations from which five samples were taken from the uppermost 47 ft (14.3 m) of the Herald Formation including the Redvers unit and most of the Coronach Member, and thirteen samples from 91 ft (27.7 m) of Stony Mountain Formation, ranging through the Hartaven, Gunn, and Gunton members (Figure 5).

Biostratigraphy

The distribution of conodont species in the Hartaven well is shown in Table 4. Conodonts from the Coronach Member and Redvers unit of the Herald Formation are similar to those recovered from this interval in the Oungre 15-9-2-14W2 and Holdfast 14-12-23-26W2 wells. They are dominated by specimens of the simple cone genera *Panderodus* and *Drepanoistodus*. The most abundant denticulate form is referable to *Aphelognathus*. This species is referred to *A.* aff. *A. divergens*. This interval is undoubtedly Late Ordovician, but its precise location within the Maysvillian-Richmondian interval is uncertain. It is likely Late Maysvillian, but the relationship of the species of *Aphelognathus*, the only abundant denticulate genus, needs to be clarified to support this view (see comments above under the Oungre well).

The basal sample of the Stony Mountain Formation yields an abundant fauna that includes the internationally recognized zonal fossil *Amorphognathus ordovicicus*, which ranges from mid-Maysvillian through Richmondian and into the Gamachian, and an enormously abundant influx of *Phragmodus undatus*.

Specimens of *Oulodus rohneri* Ethington and Furnish, an indicator of Richmondian or younger Late Ordovician age, occur within the upper part of the Hartaven Member of the Stony Mountain Formation (GSC loc. C-257728, 7469.7 ft (2276.8 m). Also present is the first occurrence of the Richmondian *Staufferella brevispinata* Nowlan and Barnes. Specimens of *O. rohneri* also occur in the lower part of the Gunton Member (GSC loc. C-257733; 7429 ft; 2264.4 m).

The high abundance and diversity in the Hartaven and Gunn members drop off drastically in the Gunton Member. Abundance runs from an astonishing 4200 specimens per kilogram in the Hartaven Member, to five specimens per kilogram in the Gunton Member. No biostratigraphically diagnostic forms occur above 7418.5 ft (2261.2 m) in the Gunton Member.

Paleoecology

The yield from samples of the Coronach Member is generally too sparse to provide worthwhile information on biofacies; however, one sample (C-257723 at 7513.7 ft; 2290.2 m) is within the *Apehlognathus* biofacies. The Redvers unit reveals a shallow depositional episode by the dominance of specimens of *Aphelognathus*, and the sample at 7498.5 ft (2285.5 m) (GSC loc. C-257724) includes specimens of *Rhipidognathus*, indicating extremely shallow conditions. The topmost sample in the Redvers yielded only two specimens of *Panderodus*.

Dramatic deepening of the basin during Hartaven time is indicated by the abundance of the deep water forms *Phragmodus* and *Amorphognathus*. The relative abundance of *Phragmodus* is reduced at the base of the Gunn Member (GSC loc. C-257729; 7467.2 ft; 2276.0 m) and specimens of the shallower water genus *Oulodus* increase in abundance, although simple cones, especially *Panderodus*, dominate the faunas above this level. Slight deepening of the basin in the upper Gunn Member is signified by the reappearance of *Phragmodus* and *Plectodina*, but their number is greatly reduced. The base of the Gunton Member of the Stony Mountain Formation is still within the *Oulodus* biofacies, but immediately above, abundance and diversity completely drops off with simple cone genera being the only representatives. In the senior author's opinion, the cone genera represent pelagic conodont forms and that the entire Gunton succession may have been deposited in water too shallow to accommodate any benthic forms.

4. Discussion

The biostratigraphic data confirm an Edenian-Maysvillian age for the Yeoman Formation, especially as based on the presence of species of *Culumbodina*. Specimens of *Parabelodina denticulata* and a related form occur in the upper Yeoman and lower Herald formations and thereby suggest a Maysvillian age for this part of the section. The precise age of the upper part of the Herald remains in doubt because of the difficulty of identifying sparse specimens of *Aphelognathus*. However, recovery of *Parabelodina denticulata* and *Aphelognathus divergens*, an indicator of Richmondian age, from the correlative Fort Garry Member of the Red River Formation in Manitoba (Elias *et al.*, 1988) suggests that the upper Herald is Richmondian, but the presence of *Aphelognathus divergens* cannot be confirmed.

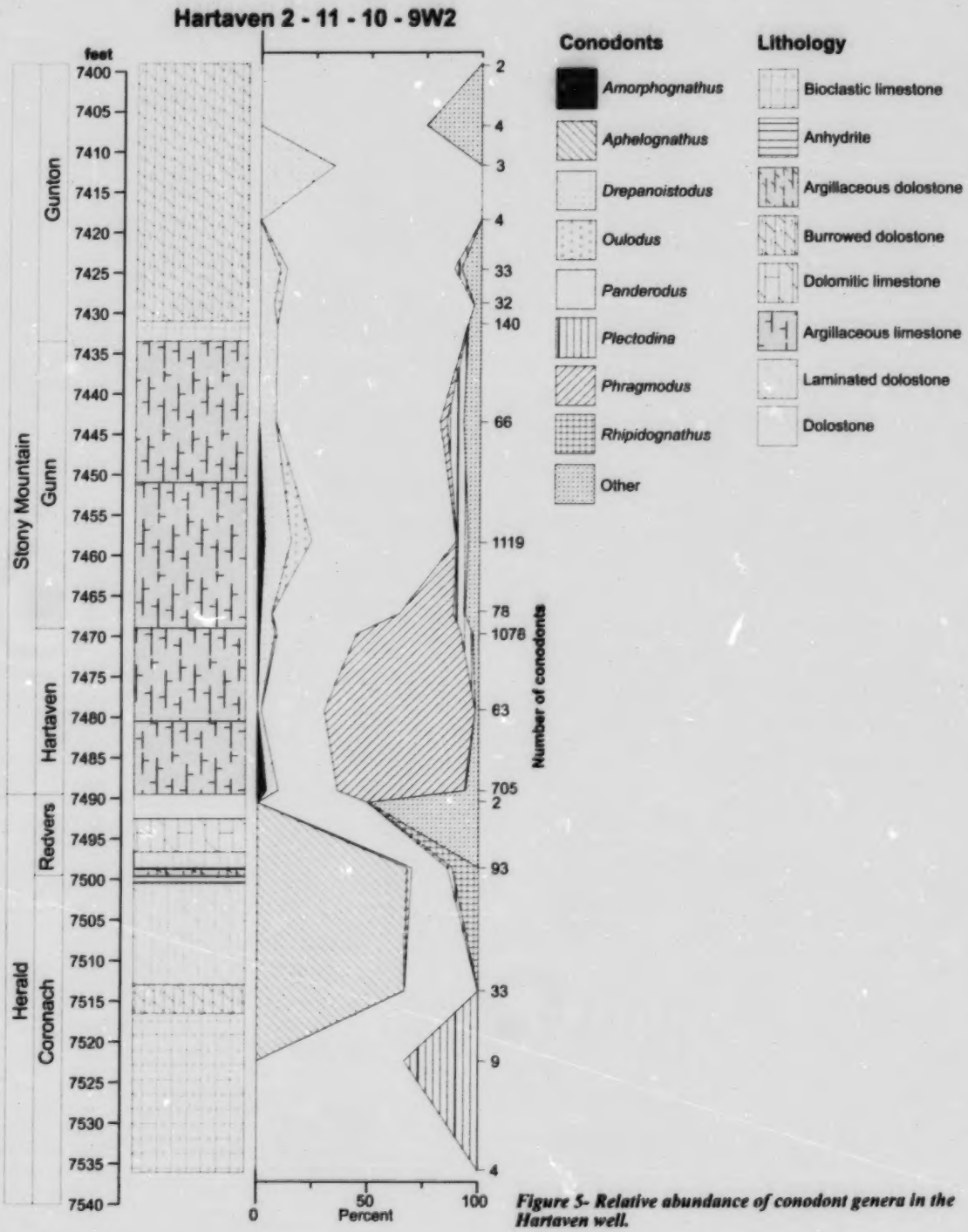

Figure 5- Relative abundance of conodont genera in the Hartaven well.

Imperial Hartaven 2-11-10-9W2

	Herald					Stony Mountain												
	7535.8 (C-257721)	7522.3 (C-257722)	7513.7 (C-257723)	7498.5 (C-257724)	7490.5 (C-257725)	7489.0 (C-257726)	7479.1 (C-257727)	7469.7 (C-257728)	7467.2 (C-257729)	7458.2 (C-257730)	7443.4 (C-257731)	7431.4 (C-257732)	7429.0 (C-257733)	7424.5 (C-257734)	7418.5 (C-257735)	7411.7 (C-257736)	7406.7 (C-257737)	7399.0 (C-257738)	
Amorphognathus ordovicicus	0	0	0	0	0	28	0	0	0	0	0	0	0	0	0	0	0	0	
Amorphognathus sp.	0	0	0	0	0	0	0	8	1	31	0	0	0	0	0	0	0	0	
Apelognathus aff. *A. divargens*	0	0	22	63	0	0	0	0	0	0	0	0	0	0	0	0	0	0	
Belodina confluens	0	0	0	0	0	0	0	0	0	12	0	0	0	2	0	0	0	0	
Belodina sp.	0	0	0	0	0	0	0	0	0	0	0	1	0	0	0	0	0	0	
Coelocerodontus trigonius	0	0	0	0	0	0	1	0	1	0	0	0	0	0	0	0	0	0	
Drepanoistodus suberectus	0	0	0	0	0	38	1	76	4	137	5	11	2	3	0	1	0	0	
Oulodus rohneri	0	0	0	0	0	0	0	11	0	0	0	0	1	0	0	0	0	0	
Oulodus ulrichi	0	0	0	0	0	0	0	0	0	103	0	0	0	0	0	0	0	0	
Oulodus sp.	0	0	0	2	0	0	0	0	0	0	0	0	0	1	0	0	0	0	
Padnerodus bergstroemi	0	0	3	0	0	0	0	0	0	0	0	0	0	0	0	0	0	0	
Panderodus gibber	0	0	0	2	0	4	0	10	1	39	0	5	0	0	0	0	0	0	
Panderodus gracilis	4	6	8	13	1	177	18	362	44	641	49	116	27	25	4	2	3	2	
Panderodus panderi	0	0	0	0	0	8	0	16	0	53	0	0	1	0	0	0	0	0	
Paroistodus? nowlani	0	0	0	0	0	9	0	0	0	3	0	0	0	0	0	0	0	0	
Phragmodus undatus	0	0	0	0	0	406	43	508	19	0	0	0	0	0	0	0	0	0	
Phragmodus? sp.	0	0	0	0	0	0	0	0	0	0	2	0	0	0	0	0	0	0	
Plectodina florida	0	0	0	2	0	0	0	56	4	58	0	0	0	0	0	0	0	0	
Plectodina sp.	0	3	0	0	1	3	0	0	0	0	5	0	0	1	0	0	0	0	
Plegagnathus dartoni	0	0	0	0	0	0	0	0	0	15	0	0	0	0	0	0	0	0	
Plegagnathus nelsoni	0	0	0	0	0	0	0	8	0	0	0	0	0	0	0	0	0	0	
Plegagnathus sp.	0	0	0	0	0	3	0	0	0	0	1	0	1	1	0	0	0	0	
Pristognathus bighornensis	0	0	0	0	0	0	0	0	0	0	2	0	0	0	0	0	0	0	
Pseudobelodina vulgaris vulgaris	0	0	0	0	0	18	0	13	0	18	0	4	0	0	0	0	0	0	
Pseudobelodina? dispansa	0	0	0	0	0	11	0	1	4	7	2	3	0	0	0	0	1	0	
Rhipidognathus symmetricus	0	0	0	11	0	0	0	0	0	0	0	0	0	0	0	0	0	0	
Staufferella brevispinata	0	0	0	0	0	0	0	4	0	0	0	0	0	0	0	0	0	0	
Walliserodus amplissimus	0	0	0	0	0	0	0	5	0	2	0	0	0	0	0	0	0	0	
Total:	**4**	**9**	**33**	**93**	**2**	**705**	**63**	**1078**	**78**	**1119**	**66**	**140**	**32**	**33**	**4**	**3**	**4**	**2**	**3468**
Mass (grams):	300	305	300	357	350	499	400	415	300	265	300	596	350	345	350	409	400	449	6690

Table 4 - Numerical distribution of conodont species by sample depth in feet and GSC locality number in the Hartaven well.

1
2
3
4
5
6
7
8
9
10
11
12
13
14
15
16
17
18
19
20
21
22
23
24
25
26
27
28
29
30
31
32
33
34

Figure 6 - Illustrations of conodonts from the Upper Ordovician of Saskatchewan (specimens arranged alphabetically by genus and species, A to P).
1 to 4) *Amorphognathus ordovicicus* ***Branson and Mehl. 1, Outer lateral view, Pb element, x71, GSC 120873; 2, outer lateral view, M element, x85, GSC 120874; 3, lateral view, Sd element, x97, GSC 120875; 4, oral view, broken Pa element, x91, GSC 120876. All specimens from the lower part of the Stony Mountain Formation in the Oungre well: 1 and 2 from GSC loc. C-257718, 3 and 4 from GSC loc. C-257720.***
5 to 15) *Aphelognathus* ***aff.*** *A. divergens* ***Sweet. 5, Inner lateral view, Sc element, x55, GSC 120877; 6, posterior view, Sb element, x51, GSC 120878; 7, posterior view, Sa element, x54, GSC 120879; 8, posterior view, Sb element, x49, GSC 120880; 9, inner lateral view, Sc element, x76, GSC 120881; 10, inner lateral view, M element, x60, GSC 120882; 11, inner lateral view, M element, x78, GSC 120883; 12, outer lateral view, Pb element, x31, GSC 120884; 13, lateral view, Pa element, x79, GSC 120885; 14, lateral view Pa element, x59, GSC 120886; 15, Pa element, x68, GSC 120887. Specimens 6, 7, 9, 11, 12, and 14 are from GSC loc. C-257706 in the Yeoman Formation in the Oungre well; specimens 5, 8, 10, and 13 are from GSC loc. C-257724 in the upper part of the Herald Formation, Hartaven well; specimen 15 is from GSC loc. C-322654 in the Herald Formation, Holdfast well.***
16 and 17) *Belodina confluens* ***Sweet. 16, Lateral view, compressiform element, x67, GSC 120888; 17, lateral view, grandiform element, x61, GSC 120889. Both specimens from GSC loc. C-322668 in the Yeoman Formation, Holdfast well.***
18) *Coelocerodontus trigonius* ***Ethington. Lateral view, x75, GSC 120890, from the Stony Mountain Formation in GSC loc. C-257729, Hartaven well.***
19) *Culumbodina occidentalis* ***Sweet. Lateral view, x43, GSC 120891, from the Yeoman Formation, GSC loc. C-322668, Holdfast well.***
20) *Culumbodina penna* ***Sweet. Lateral view, x92, GSC 120892, from the Yeoman Formation, GSC loc. C-322668, Holdfast well.***
21 and 22) *Drepanoistodus suberectus* ***(Branson and Mehl). 21, Lateral view, oistodontiform r element, x84, GSC 120893; 22, lateral view, q element, x80, GSC 120894. Both specimens from the basal Stony Mountain Formation in GSC loc. C-257718, Oungre well.***
23, 25, 26, and 31) *Oulodus ulrichi* ***(Stone and Furnish). 23, Lateral view, Sc element, x52, GSC 120895; 25, inner lateral view, Pb element, x60, GSC 120896; 26, inner lateral view, M element, x80, GSC 120897; 31, posterior view, laterally broken Pa element, x70, GSC 120898. All specimens from the Stony Mountain Formation, GSC loc. C-257730, Hartaven well.***
24) *Oulodus rohneri* ***Ethington and Furnish. Posterior view, Pa element, x85, GSC 120899, from the Stony Mountain Formation, GSC loc. C-257733, Hartaven well.***
27) *Panderodus gibber* ***Nowlan and Barnes. Lateral view, x80, GSC 120900, from basal Stony Mountain Formation, GSC loc. C-257726, Hartaven well.***
28) *Panderodus panderi* ***(Stauffer). Lateral view, x65, GSC 120901, from the basal Stony Mountain Formation, GSC loc. C-257726, Hartaven well.***
29) *Panderodus gracilis* ***(Branson and Mehl). Lateral view, x75, GSC 120902, from the basal Stony Mountain Formation, GSC loc. C-257726, Hartaven well.***
30) *Parabelodina denticulata* ***Sweet. Lateral view, x100, GSC 120903, from the Herald Formation, GSC loc. C-322660, Holdfast well.***
32 and 34) *Parabelodina* ***cf.*** *P. denticulata* ***Sweet. 32. Lateral view, x131, GSC 120904; 34, lateral view, x120, GSC 120905. Specimen 32 from the Herald Formation, GSC loc. C-322658, Holdfast well and specimen 34 from the Herald Formation, GSC loc. C-257708, Oungre well.***
33) *Paroistodus? nowlani* ***Zhen, Webby and Barnes. Inner lateral view, oistodontiform element, x137, GSC 120906, from the basal Stony Mountain Formation, GSC loc. C-257726, Hartaven well.***

A striking turnover in the conodont fauna occurs at the base of the Stony Mountain Formation. *Amorphognathus ordovicicus*, the worldwide index for Middle Maysvillian and younger Late Ordovician strata, is found together with extremely abundant *Phragmodus undatus*. Specimens of *Oulodus rohneri* in the lower part of the Stony Mountain Formation confirm a Richmondian age for the unit. Conodont abundance decreases drastically in the upper part of the Stony Mountain Formation and diagnostic forms are absent. Previous work (Norford *et al.*, 1998; Nowlan and Haidl, 1999) has shown that the remainder of the Stony Mountain and the lower part of the Stonewall are Richmondian and that the Ordovician-Silurian boundary occurs within the Stonewall Formation.

Conodont biofacies, expressed in terms of relative abundance curves for genera, show marked changes in depositional environment from the base of the Yeoman, through the Herald, and into the Stony Mountain Formation. Yields from the basal part of the Yeoman are sparse, but the forms present (e.g. *Oulodus*) are suggestive of shallow water deposition. General deepening followed, as indicated by the increase in species of *Plectodina* throughout much of the middle and upper part of the Yeoman Formation (Figures 3 and 4). Within this interval, increases in the relative abundance of *Aphelognathus* suggest distinct shallowing episodes.

One such shallowing episode is reflected by higher energy fabrics in the "transitional" unit at the top of the Yeoman in several wells (including Oungre) (Pratt *et al.*, 1996; Canter, 1998; Kreis and Kent, 2000), and in sub-aerially exposed surfaces in the lower portion of the laminated carbonate unit of the Lake Alma Member (Kent and Kissling, 1998; Kreis and Kent, 2000). The recurrence of *Plectodina* within Lake Alma laminated carbonates in the Oungre well may reflect a deepening event associated with deposition of the upper portion of this laminated unit. In the Holdfast well, the presence of burrowed fossiliferous dolostone between beds of Lake Alma laminated strata also suggests a deepening event. The relative abundance of *Aphelognathus* in this fossiliferous unit and the overlying laminated unit suggests shallower conditions than in the middle part of the Yeoman. However, paleoecological interpretation of the Lake Alma sequence based on conodonts is limited in this well because the lower laminated bed was not sampled. Further detailed sampling in this and other cores is required to determine whether or not a sequence boundary separates lower Lake Alma laminated strata from overlying carbonates and basin-centred, subaqueously deposited Lake Alma evaporites as suggested by Canter (1998).

Specimens of *Rhipidognathus* are present in the upper part of the Herald Formation in both the Holdfast and Hartaven wells (Figures 3 and 5). This suggests an extreme shallowing episode and a possible period of emergence. Lithological evidence for sub-aerial exposure in this part of the stratigraphic section is reported by Kreis and Kent (2000).

1
2
3
4
5
6
7
8
9
10
11
12
13
14
15
16
17
18
19
20
21
22
23
24
25
26
27
28
29
30

The striking concentration of deep and possibly cooler water conodonts *Amorphognathus* and *Phragmodus* at the base of the Stony Mountain Formation indicates a major transgression and a rise in sea level or the introduction of a cooler water mass. Based on evidence from the Hartaven well, this deep water episode persists through the Hartaven Member and into the lower part of the Gunn Member. While specimens of *Phragmodus* continue to be present in upper samples from the Gunn, they are much less abundant and the proportionate decrease in number of *Plectodina* suggest shallowing (Figure 5). The Gunton Member of the Stony Mountain Formation produces few conodonts suitable for biofacies analysis.

Figure 7 - Illustrations of conodonts from the Upper Ordovician of Saskatchewan (specimens arranged alphabetically by genus and species, P to W).
1 to 8) *Phragmodus undatus* ***Branson and Mehl. 1, Lateral view, Sc element, x77, GSC 120907; 2, lateral view, Sc element, x93, GSC 120908; 3, lateral view, Sd element, x75, GSC 120909; 4, inner lateral view, M element, x55, GSC 120910; 5, inner lateral view, M element, x86, GSC 120911; 6, inner lateral view, Pb element, x74, GSC 120912; 7, outer lateral view, Pa element, x75, GSC 120913; 8, outer lateral view, Pa element, x81, GSC 120914. Specimens 1, 3, 4, 6, and 7 from basal Stony Mountain Formation in GSC loc. C-257718, Oungre well; specimens 2, 5, and 8 from basal Stony Mountain Formation in GSC loc. C-257726, Hartaven well.***
9 to 13) *Plectodina aculeatoides* ***Sweet. 9, Inner lateral view, Sc element, x90, GSC 120915; 10, posterior view, Sb element, x107, GSC 120916; 11, inner lateral view, M element, x95, GSC 120917; 12, inner lateral view, Pb element, x62, GSC 120918; 13, lateral view, Pa element, x92, GSC 120919. All specimens from Yeoman Formation, GSC loc. C-257702, Oungre well.***
14 to 18 and 21) *Plectodina florida* ***Sweet. 14, Inner lateral view, Sc element, x98, GSC 120920; 15, posterior view, Sb element, x98, GSC 120921; 16, posterior view, Sc element, x116, GSC 120922; 17, inner lateral view, M element, x74, GSC 120923; 18, inner lateral view, Pb element, x77, GSC 120924; 21, lateral view, Pa element, x111, GSC 120925. All specimens from Stony Mountain Formation in the Hartaven well: 14, 15, 16, 18, and 21 from GSC loc. C-257730 and 17 from C-257729.***
19) *Plegagnathus nelsoni* ***Ethington and Furnish. Lateral view, x98, GSC 120926, from the Herald Formation, GSC loc. C-322654, Holdfast well.***
20 and 23) *Pseudobelodina? dispansa* ***(Glenister). 20, Lateral view, broad element, x80, GSC 120927; 23, lateral view, slender element, x69, GSC 120928. Specimen 20 from basal Stony Mountain Formation, GSC loc. C-257726, Hartaven well and specimen 23 from Yeoman Formation, GSC loc. C-322665, Holdfast well.***
22) *Pristognathus bighornensis* ***Stone and Furnish. Posterior view, Pa element, x70, GSC 120929, from Stony Mountain Formation, GSC loc. C-257731, Hartaven well.***
24 and 28) *Pseudobelodina vulgaris vulgaris* ***Sweet. 24, Inner lateral view, x64, GSC 120930; 28, lateral view, x100, GSC 120931. Specimen 24 from Yeoman Formation, GSC loc. C-322665, Holdfast well and specimen 28 from Yeoman Formation, GSC loc. C-257740, Pangman well.***
25 and 30) *Rhipidognathus symmetricus* ***Branson, Mehl and Branson. 25, Posterior view, symmetrical element, x45, GSC 120932; 30, posterior view, asymmetrical element, x33, GSC 120933. Both specimens from upper part of Herald Formation, GSC loc. C-257724, Hartaven well.***
26, 27, and 29) *Walliserodus amplissimus* ***(Serpagli). 26, Inner lateral view, Sc element, x91, GSC 120934; 27, lateral view, Sa element, x92, GSC 120935; 29, posterior view, Sa element, x100, GSC 120936. All specimens from the lower part of the Stony Mountain Formation, GSC loc. C-257728, Hartaven well.***

5. Future Work

More detailed sampling combined with lithologic studies are required to facilitate sequence stratigraphic interpretation of Upper Ordovician strata. The data presented here are integrated with geochemical data on the neodymium isotopes and samarium-neodymium ratios of conodont and rock samples from many of the same samples (Fanton *et al.*, in review). The combination of biostratigraphic and paleoecological data with these geochemical tools provides insight into the submergence history of the craton in the Williston Basin area. Integration of these types of lithological, geochemical, and paleontological data is planned for correlative sections of Manitoba and Saskatchewan, probably in the Weyburn-Midale area and over the Ordovician-Silurian boundary interval in Saskatchewan and Manitoba.

6. References

Amsden, T.W. and Miller, A.K. (1942): Ordovician conodonts from the Bighorn Mountains of Wyoming; J. Paleont., v16, p301-306.

Barnes, C.R. and Fåhraeus, L.E. (1975): Provinces, communities, and the proposed nektobenthic habit of Ordovician conodontophorids; Lethaia, v8, p133-149.

Brindle, J.E. (1960): The faunas of the Lower Paleozoic carbonate rocks in the subsurface of Saskatchewan; Sask. Dep. Miner. Resour., Rep. 52, 45p.

Canter K.L. (1998): Facies, cyclostratigraphic, and secondary diagenetic controls on reservoir distribution, Ordovician Red River Formation, Midale Field, southern Saskatchewan; Eighth International Williston Basin Symposium, Core Workshop Volume, Regina, October 1998, Saskatchewan, North Dakota and Montana Geol. Soc., p41-65.

Carlson, C.C. (1960): Stratigraphy of the Winnipeg and Deadwood formations in North Dakota; N. Dakota Geol. Surv., Bull. 35, 149p.

Elias, R.J., Nowlan G.S., and Bolton, T.E. (1988): Paleontology of the type section of the Fort Garry Member, Red River Formation (Upper Ordovician), southern Manitoba; New Mexico Bureau Mines Miner. Resour., Mem. 44, p341-359.

Ethington, R.L. and Furnish, W.M. (1960): Upper Ordovician conodonts from southern Manitoba; J. Paleont., v34, p265-274.

Fanton, K.C., Holmden, C., Nowlan, G.S., and Haidl, F.M. (in review): $^{143}Nd/^{144}Nd$ and Sm/Nd stratigraphy of Late Ordovician epeiric sea carbonates; Geochim. Cosmochim. Acta.

Furnish, W.M., Barragy, E.J., and Miller, A.K. (1936): Ordovician fossils from the uppermost part of the type section of the Deadwood Formation, South Dakota; Amer. Assoc. Petrol. Geol. Bull., v20, p1329-1341.

Haidl, F.M., Longman, M.W., Pratt, B.R., and Bernstein, L.M. (1997): Variations in lithofacies in Upper Ordovician Herald and Yeoman formations (Red River), North Dakota and southeastern Saskatchewan; *in* Wood, J. and Martindale, B. (comp.), Can. Soc. Petrol. Geol.–Soc. Econ. Paleont. Mineral., Core Conference, Calgary, p5-39.

Kendall, A.C. (1976): The Ordovician carbonate succession (Bighorn Group) of southeastern Saskatchewan; Dep. Miner. Resour., Rep. 180, 185p.

_____ (1977): Origin of dolomite mottling in Ordovician limestones from Saskatchewan and Manitoba; Bull. Can. Petrol. Geol., v25, p480-504.

Kent, D.M. (1960): The evaporites of the Upper Ordovician strata in the northern part of the Williston Basin; Sask. Dep. Min. Resour., Rep. 46, 46p.

Kent, D.M. and Haidl, F.M. (1999): Geology of Ordovician Winnipeg and Red River rocks, southeast Saskatchewan; Depositional environments and reservoir potential of Lower and Middle Paleozoic rocks in Saskatchewan, Can. Soc. Petrol. Geol., Calgary, CSPG Short Course G-4, unpubl. notes, p1-37.

Kent, D.M. and Kissling, D.L. (1998): Covert facies of the Red River C Laminated Member, northern Williston Basin; *in* Christopher, J.E., Gilboy, C.F., Paterson, D.F., and Bend, S.L. (eds.), Eighth International Williston Basin Symposium, Sask. Geol. Soc., Spec. Publ. No. 13, p24.

Kessler, L.G. (1991): Subsidence controlled stratigraphic sequences and the origin of shelf sand ridges, Winnipeg Group (Middle Ordovician) Manitoba, Saskatchewan and North Dakota; *in* Christopher, J.E. and Haidl, F.M. (eds.), Sixth International Williston Basin Symposium, Sask. Geol. Soc., Spec. Publ. No. 11, p1-13.

Kissling, D.L. (1997): Rethinking the configurations of Red River reservoirs; Fifth International Williston Basin Horizontal Well Workshop; Sask. Energy and Mines and North Dakota Geol. Survey.

_____ (1999): Life and death roles of Red River Thalassinoides; Abstracts, Rocky Mtn. Sect., Amer. Assoc. Petrol. Geol. Bull., v83, p1184.

Kreis, L.K. (2000): Geology of the Middle Ordovician Winnipeg Formation in Saskatchewan, Lower Paleozoic Map Series, Sask. Energy Mines, Open File Rep. 2000-2, Sheet 3 of 8.

Kreis, L.K. and Kent, D.M. (2000): Basement controls on Red River sedimentation and hydrocarbon production in southeastern Saskatchewan; *in* Summary of Investigations 2000, Volume 1, Saskatchewan Geological Survey, Sask. Energy Mines, Misc. Rep. 2000-4.1, p21-42.

Longman, M.W. and Haidl, F.M. (1996): Cyclic deposition and development of porous dolomites in the Upper Ordovician Red River Formation, Williston Basin; *in* Longman, M.W. and Sonnenfeld, M.D. (eds.), Paleozoic Systems of the Rocky Mountain Region, Rocky Mtn. Sec., Soc. Econ. Paleont. Mineral., p29-46.

Norford, B.S., Nowlan, G.S., Haidl, F.M., and Bezys, R.K. (1998): The Ordovician-Silurian boundary interval in Saskatchewan and Manitoba; *in* Christopher, J.E., Gilboy, C.F., Paterson, D.F., and Bend, S.L., (eds.), Eighth International Williston Basin Symposium, Sask. Geol. Soc., Spec. Publ. No. 13, p27-45.

Norford, B.S., Haidl, F.M., Bezys, R.K., Cecile, M.P., McCabe, H.R., and Paterson, D.F. (1994): Middle Ordovician to Lower Devonian strata of the Western Canada Sedimentary Basin; *in* Mossop, G.D. and Shetsen, I. (comp.), Geological Atlas of the Western Canada Sedimentary Basin; Can. Soc. Petrol. Geol./Alta. Resear. Counc., p109-127.

Nowlan, G.S. (in review): Stratigraphy and conodont biostratigraphy of Upper Ordovician strata in the subsurface of Alberta, Canada; Palaeont.

Nowlan, G.S. and Barnes, C.R. (1981): Late Ordovician conodonts from the Vaureal Formation, Anticosti Island, Quebec; Geol. Surv. Can., Bull. 329, p1-49.

Nowlan, G.S. and Haidl, F.M. (1999): New conodont data from the Ordovician-Silurian boundary interval in southeastern Saskatchewan; *in* Summary of Investigations 1999, Volume 1, Saskatchewan Geological Survey, Sask. Energy Mines, Misc. Rep. 99-4.1, p12-16.

Oberg, R. (1966): Winnipeg conodonts from Manitoba; J. Paleont., v40, p130-137.

Pratt, B.R., Bernstein, L.M., Kendall, A.K., and Haidl, F.M. (1996): Occurrence of reefal facies in Red River strata (Upper Ordovician), subsurface Saskatchewan; *in* Summary of Investigations 1996, Saskatchewan Geological Survey, Sask. Energy Mines, Misc. Rep. 96-4, p147-152.

Seddon, G. and Sweet, W. C. (1971): An ecologic model for conodonts; J. Paleont., v45, p869-880.

Stasiuk, L.D (1991): Organic petrology and petroleum formation in Paleozoic rocks of northern Williston Basin, Canada; unpubl. Ph.D. thesis, Univ. Regina, 312p

Stasiuk, L.D., Kybett, B.D., and Bend, S.L. (1993): Reflected light microscopy and micro-FTIR of Upper Ordovician Gloeocapsomorpha prisca alginite in relation to paleoenvironment and petroleum generation, Saskatchewan, Canada; Org. Geochem., v20, p707-719.

Stone, G.L. and Furnish, W.M. (1959): Bighorn conodonts from Wyoming; J. Paleont., v33, p211-228.

Sweet, W.C. (1979): Late Ordovician conodonts and biostratigraphy of the western Midcontinent Province; Brigham Young University, Geology Studies, v26, p45-86.

_____ (1982): Conodonts from the Winnipeg Formation (Middle Ordovician) of the northern Black Hills, South Dakota; J. Paleont., v56, p1029-1049.

_____ (1984): Graphic correlation of upper Middle and Upper Ordovician rocks, North American Midcontinent Province, U.S.A.; *in* Bruton, D.L. (ed.), Aspects of the Ordovician System, Palaeont. Contrib. Univ. Oslo, No. 295, p23-35.

Sweet W.C. and Bergström, S.M. (1984): Conodont provinces and biofacies of the Late Ordovician; *in* Clark, D.L. (ed.) Conodont Biofacies and Provincialism, Geol. Soc. Amer., Spec. Pap. 196, p69-87.

O and C Isotopes of the Middle Devonian Lower Winnipegosis, Brightholme and Ratner Carbonates, Elk Point Basin, Southeastern Saskatchewan

Hairuo Qing [1], Katherine M. Bergman [1], and Orrin Cameron [1]

Qing, H., Bergman, K.M., and Cameron, O. (2001): O and C isotopes of the Middle Devonian Lower Winnipegosis, Brightholme and Ratner carbonates, Elk Point Basin, southeastern Saskatchewan; *in* Summary of Investigations 2001, Volume 1, Saskatchewan Geological Survey, Sask. Energy Mines, Misc. Rep. 2001-4.1.

Abstract

The depositional environment and stratigraphic relationships of the Brightholme and Ratner units of the Middle Devonian Elk Point Group are topics of considerable debate. A total of 20 limestone and dolostone samples from Lower Winnipegosis, Ratner, and Brightholme strata in four wells in south-central Saskatchewan were analyzed for $\delta^{18}O$ and $\delta^{13}C$ in order to test whether or not oxygen and carbon isotopes can be used to characterize the depositional environment and constrain the stratigraphic relationships of these units.

The $\delta^{18}O$ values of both limestone and dolostone samples from the Lower Winnipegosis, Brightholme, and Ratner are lower than the estimated values for Middle Devonian marine calcite and dolomite, which suggests that the original $\delta^{18}O$ signatures of these carbonates have been modified by post-depositional diagenetic processes. Their $\delta^{18}O$ values, therefore, cannot be used to characterize the depositional environments of these stratigraphic units.

The $\delta^{13}C$ values of the Ratner and Lower Winnipegosis limestones and dolostones are similar to or slightly lower than the estimated Middle Devonian seawater values. The main source of carbon for the Ratner and the Lower Winnipegosis carbonates is, therefore, inorganic carbon from Middle Devonian seawater. The $\delta^{13}C$ values of Brightholme limestone and dolostone, however, are lower than those of Ratner and Lower Winnipegosis carbonates. Accordingly, the low $\delta^{13}C$ values of Brightholme carbonate are interpreted to have resulted from mixing of inorganic carbon of Middle Devonian seawater with organic carbon released to the pore water from organic-rich sediments. Carbon isotopes are a potential tool for characterizing and differentiating the Brightholme from the Ratner.

1. Introduction

The depositional environment and stratigraphic relationships of the Brightholme and Ratner units of the Middle Devonian Elk Point Group are not clearly understood.

Stoakes *et al.*, (1987) introduced the informal name "Brightholme member" for the thin organic-rich shale and/or laminated mudstone that overlies the Lower Winnipegosis carbonate. The most recently proposed depositional model (Jin *et al.*, 1997; Jin and Bergman, 1999) for the Brightholme suggests that it is the off-reef basin facies of the Upper Winnipegosis Formation (Figure 1).

Shearman and Fuller (1969) interpreted the laminites of the Ratner as intertidal deposits analogous to modern sabkha algal mats, implying rapid and complete sea-level drawdown after the termination of Winnipegosis reef development. In contrast, Kendall (1975) argued for a deep-water origin because of the gradational contact, lateral continuity, and perfect preservation of individual laminae. Davies and Ludlam (1973) postulated a stratified water column and an anoxic bottom environment. Jin *et al.* (1997) and Jin and Bergman (1998) interpreted the Ratner as the initial deposits of a stratified water column in a restricted basin. Maiklem (1971), Jin *et al.* (1997), and Jin and Bergman (1998, 1999) proposed a partial drawdown of at least 30 m based on the presence of vadose diagenetic features in the Keg River and Upper Winnipegosis carbonate deposits. The stratigraphic relationship of the Ratner is not clear. Jones (1965) first described the laminite as an inter-reef facies of the Upper Winnipegosis. Reinson and Wardlaw (1972) formally proposed the Ratner Member as a distinct stratigraphic unit of the Winnipegosis Formation. Kendall (1975) first argued that the Ratner was entirely post-Winnipegosis and should be part of the Prairie Formation (Figure 1). Petrological and stratigraphic studies of the Winnipegosis–Prairie Evaporite transition (Jin *et al.*, 1997; Jin and Bergman, 1998, 1999) indicate that deposition of the Ratner was genetically related to intense vadose diagenesis of the Winnipegosis reefs under fluctuating rates of marine water seepage into the basin and therefore is post-Winnipegosis (Figure 1).

2. Study Area and Methodology

The study area is contained between Townships 22 and 50, Ranges 20W2 to 10W3 (Figure 2). Samples for oxygen and carbon isotope analysis were taken from

[1] Department of Geology, University of Regina, Regina, SK S4S 0A2.

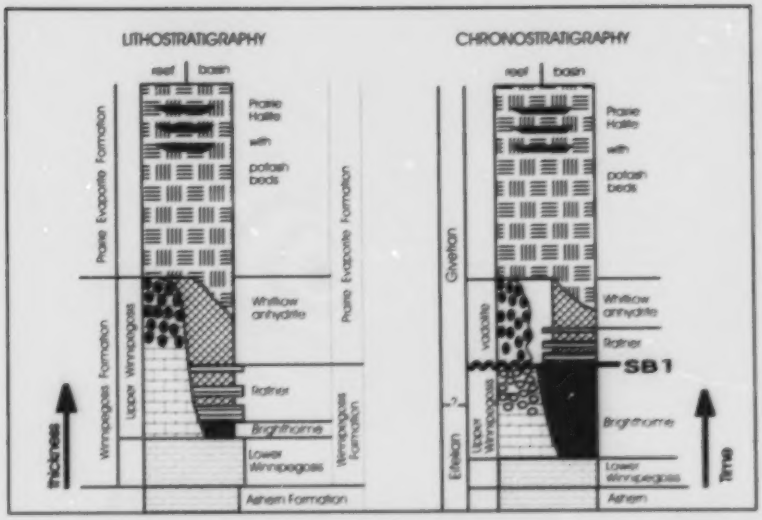

Figure 1 - Comparison of lithostratigraphic and chronostratigraphic relationships between Winnipegosis carbonate and Brightholme shale, Ratner laminite, and Whitkow anhydrite (from Jin and Bergman, 1999).

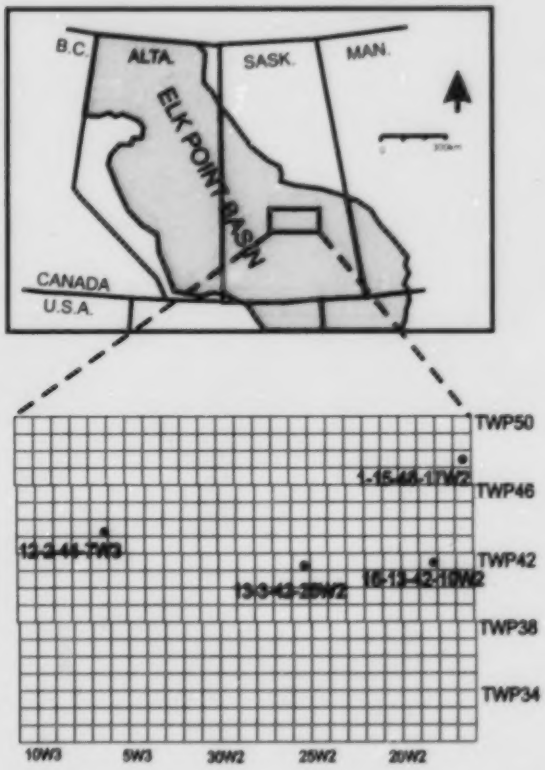

Figure 2 - Schematic map of the Elk Point Basin, showing the study area and locations of wells sampled for isotopic analyses.

four wells in south-central Saskatchewan (Figure 2). Wells were chosen for sampling on the bases of: 1) the completeness and quality of core in the Brightholme unit, and 2) composition of the sediment. Five samples were collected from each well (Table 1): two from the Lower Winnipegosis 10 cm and 1 m below the contact with the Brightholme; two samples in the Brightholme 10 cm and 1 m above the Lower Winnipegosis contact, and one sample from the Ratner. They were obtained using a drill press equipped with a small masonry bit. Oxygen and carbon isotopic analyses were performed at the University of Saskatchewan.

3. Results and Discussions

The measured oxygen and carbon isotopes are reported in Table 1 and plotted in Figure 3. The $\delta^{18}O$ and $\delta^{13}C$ values of marine calcite precipitated from Middle Devonian seawater are estimated to be in the ranges -5 to -3 ‰ PDB and 0.5 to 2.5 ‰ PDB (Figure 3) respectively, based on the analyses of well preserved brachiopod shells and marine cement (Popp *et al.*, 1986). The $\delta^{18}O$ values of brachiopod shells from the Middle Devonian Presqu'ile barrier at Pine Point vary between -3.8 to -4.2 ‰ PDB and $\delta^{13}C$ values are around 1.9 ‰ PDB (Qing, 1998). If a mean value of 2.5 ‰ is taken as the fractionation between dolomite and calcite (Major *et al.*, 1992), then the primary isotopic signatures of dolomite precipitated from normal Middle Devonian seawater should have $\delta^{18}O$ values from -2.5 to -0.5 ‰ PDB and $\delta^{13}C$ from 0.5 to 2.5 ‰ PDB (Figure 3). Dolomite formed by slightly evaporated Middle Devonian seawater prior to gypsum precipitation should have $\delta^{18}O$ values higher than -2.5 to -0.5 ‰ PDB.

Most limestone samples from Lower Winnipegosis, Brightholme, and Ratner strata have a similar range of $\delta^{18}O$ values, from -5.6 to -7.3 ‰ PDB (Figure 3). These values are slightly lower than that of Middle Devonian marine calcite (-5 to -3 ‰ PDB). One Ratner sample, however, has a $\delta^{18}O$ value (-4.9 ‰ PDB) close to the lower end value for Middle Devonian marine calcite. This suggests that the original $\delta^{18}O$ signatures of these Middle Devonian marine limestones have been modified and/or overprinted by post-depositional diagenetic processes. Their present $\delta^{18}O$ values, therefore, cannot be used as a parameter to differentiate the Brightholme from the Ratner. The $\delta^{18}O$ values for the Brightholme dolomite (-7.6 to -8.8 ‰ PDB) and the Ratner dolomite (-7.5 to -11.0 ‰ PDB) overlap (Figure 3) and are much lower than the expected value for Middle Devonian marine dolomite (-2.5 to -0.5 ‰ PDB), indicating later diagenetic

Table 1 - Sample location, formation, location relative to the Lower Winnipegosis (LWIN)–Brightholme (BRHM) contact, depths, composition, and $\delta^{18}O$ and $\delta^{13}C$ values (‰ PDB); RTNR, Ratner.

Well Location	Formation	Location relative to LWIN/BRHM contact	Depth (m)	Composition	$\delta^{18}O$	$\delta^{13}C$
16-13-42-19W2	LWIN	1 m below	844.1	Dolostone	-6.46	1.39
16-13-42-19W2	LWIN	10 cm below	843.2	Dolostone	-7.24	0.57
1-15-48-17W2	LWIN	1 m below	522.2	Dolostone	-6.23	1.33
1-15-48-17W2	LWIN	10 cm below	521.3	Dolostone	-6.76	0.68
				Avg.	-6.67	0.99
12-2-44-7W3	LWIN	1.2 m below	940.7	Limestone	-6.21	0.77
12-2-44-7W3	LWIN	20 cm below	939.7	Limestone	-6.10	-0.59
13-3-42-16W2	LWIN	1 m below	996.1	Limestone	-5.94	0.69
13-3-42-16W2	LWIN	10 cm below	995.2	Limestone	-5.70	-1.59
				Avg.	-5.99	-0.18
16-13-42-19W2	BRHM	25 cm above	842.8	Dolostone	-7.76	-0.05
16-13-42-19W2	BRHM	1 m above	842.1	Dolostone	-8.18	-0.73
1-15-48-17W2	BRHM	10 cm above	521.1	Dolostone	-7.60	-0.39
1-15-48-17W2	BRHM	1 m above	520.2	Dolostone	-8.80	-1.86
				Avg.	-8.09	-0.76
12-2-44-7W3	BRHM	10 cm above	939.4	Limestone	-6.24	-0.95
12-2-44-7W3	BRHM	1 m above	938.5	Limestone	-5.60	-2.45
13-3-42-16W2	BRHM	10 cm above	995	Limestone	-5.59	-1.13
13-3-42-16W2	BRHM	1 m above	994.1	Limestone	-6.45	-3.28
				Avg.	-5.97	-1.95
16-13-42-19W2	RTNR	4.9 m above	838.2	Dolostone	-7.50	0.74
1-15-48-17W2	RTNR	7.9 m above	513.3	Dolostone	-10.99	0.96
				Avg.	-9.25	0.85
12-2-44-7W3	RTNR	2.8 m above	936.7	Limestone	-4.88	0.21
13-3-42-16W2	RTNR	3.5 m above	991.6	Limestone	-7.33	0.62
				Avg.	-6.11	0.42

alteration of their original marine $\delta^{18}O$ values. The $\delta^{18}O$ values from the measured Devonian dolomites, therefore, cannot be used to characterize the depositional environments of the Brightholme or the Ratner.

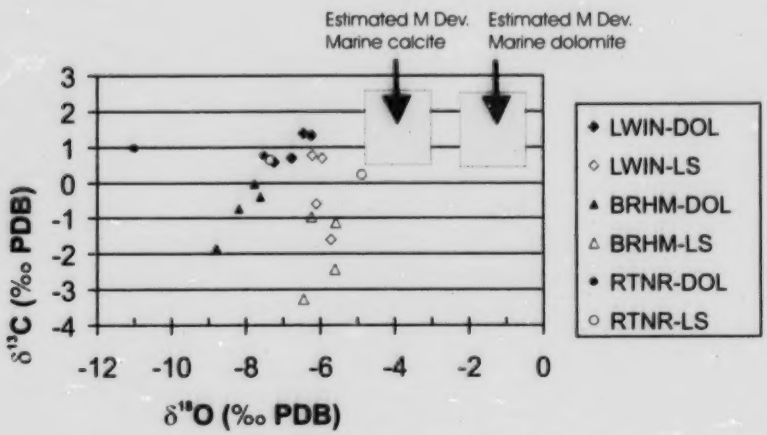

Figure 3 - Cross plot of $\delta^{18}O$ and $\delta^{13}C$ values (‰ PDB). LWIN, the Lower Winnipegosis; BRHM, Brightholme; RTNR, Ratner; LS, limestone; and DOL, dolostone (see text for discussions).

The $\delta^{13}C$ values of the Ratner limestone (range 0.2 to 0.6 ‰ PDB, avg. 0.4 ‰ PDB) are similar to the estimated values of Middle Devonian marine calcite (0.5 to 2.5 ‰ PDB). The Lower Winnipegosis limestone $\delta^{13}C$ values range from -1.6 to 0.8 ‰ PDB, and average -0.2 ‰ PDB, slightly lower than that of Middle Devonian marine calcite (Figure 3). This suggests that the main source of carbon for the Ratner and Lower Winnipegosis limestones was inorganic carbon derived from Middle Devonian seawater. Contrary to oxygen isotopic values, post-depositional diagenetic processes, including dolomitization, have little effect on the original $\delta^{13}C$ signatures of Ratner and Lower Winnipegosis limestone deposits. This interpretation is supported by the $\delta^{13}C$ values of the Ratner dolomite (0.7 to 1.0 ‰ PDB, avg. 0.9 ‰ PDB) and the Lower Winnipegosis dolomite (0.6 to 1.4 ‰ PDB, avg. 1.0 ‰ PDB), which also fall within the range for Middle Devonian marine dolomite (Figure 3).

The $\delta^{13}C$ values of Brightholme limestones (-1.0 to -3.3 ‰ PDB, avg. -2.0 ‰ PDB) are lower than those of Ratner and Lower Winnipegosis limestones, as well as lower than Middle Devonian marine calcite (Table 1; Figure 3). Thus, in addition to inorganic carbon from Middle Devonian seawater, another source of lighter carbon has been incorporated with the Brightholme limestone. Organic matter in marine sediments has $\delta^{13}C$ values from -10 to -20 ‰ PDB (Anderson and Arthur, 1983). The $\delta^{13}C$ value of pore water from organic-rich sediments can decrease rapidly and overprint the $\delta^{13}C$ signature of the original seawater. This process is related to the release of organic carbon into pore water from organic-rich sediments during decomposition of organic matter (Anderson and Arthur, 1983). The low $\delta^{13}C$ values of Brightholme limestones can, therefore, be attributed to the mixing of inorganic carbon from Middle Devonian seawater with carbon derived from organic matter. This is consistent with the dark black colour of the rock and high TOC values (avg. ~4%, maximum ~31%) for the

Brightholme (Osadetz and Snowdon, 1995). Carbon isotopes thus provide a potential means of characterizing the Brightholme and possibly differentiating it from the Ratner.

4. Conclusions

The $\delta^{18}O$ values of both limestones and dolostones from the Lower Winnipegosis, Brightholme, and Ratner are lower than those of Middle Devonian marine calcite and dolomite, suggesting that the original $\delta^{18}O$ signatures of these carbonates have been modified and/or overprinted by post-depositional diagenetic processes. Their $\delta^{18}O$ values, therefore, cannot be used to characterize the depositional environments of the Brightholme or the Ratner members.

The $\delta^{13}C$ values of the Ratner and Lower Winnipegosis carbonates are similar to, or slightly lower than, the estimated values of Middle Devonian marine calcite. The main source of carbon for the Ratner and the Lower Winnipegosis carbonates, therefore, is inorganic carbon derived from Middle Devonian seawater. Post-depositional diagenetic processes, including dolomitization, have had little effect on their original $\delta^{13}C$ signatures.

The $\delta^{13}C$ values of Brightholme limestones and dolostones are lower than those of the Ratner and Lower Winnipegosis carbonates and can be attributed to the mixing of inorganic carbon from Middle Devonian seawater with carbon from organic sources. Carbon isotopes, therefore, provide a potential method to characterize and differentiate the Brightholme from the Ratner.

5. Acknowledgments

We thank Saskatchewan Energy and Mines (SEM) Subsurface Laboratory for access to the facility and core sampling, and Dr. Chris Holmden at the University of Saskatchewan for the isotope analyses. This project was funded by a grant from the Potash Corporation of Saskatchewan (PCS) and with matching support from an NSERC IOR grant.

6. References

Anderson, T.F. and Arthur, M.A. (1983): The carbon cycle and carbon isotopes; *in* Stable Isotopes in Sedimentary Geology, SEPM Short Course No. 10, p1.80-1.151.

Davies, G.R. and Ludlam, S.D. (1973): Origin of laminated and graded sediments, Middle Devonian of western Canada; Geol. Soc. Amer. Bull., v84, p3527-3546.

Jin, J. and Bergman, K.M. (1999): Sequence stratigraphy of the Middle Devonian Winnipegosis carbonate-Prairie Evaporite transition, southern Elk Point Basin; Carbonates and Evaporites, v14, p64-83.

_____ (1998): Occurrences of Middle Devonian Ratner laminite in the distal part of the Elk Point Basin; *in* Kreis, L.K. (ed.), Eighth International Williston Basin Symposium, Core Workshop, Sask. Geol. Soc., N. Dakota Geol. Soc., Montana Geol. Soc., Regina, p89-104.

Jin, J., Bergman, K., Haidl, F., Blair, M., and Ricci, A. (1997): Vadose diagenesis of the Winnipegosis carbonate and the origin of the Ratner laminite and Whitkow anhydrite, Middle Devonian, southern Saskatchewan; *in* Summary of Investigations 1997, Saskatchewan Geological Survey, Sask. Energy Mines, Misc. Rep. 97-4, p197-212.

Jones, L. (1965): The Middle Devonian Winnipegosis Formation of Saskatchewan; Sask. Dep. Miner. Resour., Rep. 98, 101p.

Kendall, A.C. (1975): The Middle Devonian Winnipegosis and lower Prairie Evaporite formations of the commercial potash areas; *in* Summary of Investigations 1975 by the Saskatchewan Geological Survey, p61-65.

Maiklem, W.R. (1971): Evaporative drawdown – a mechanism for water-level lowering and diagenesis in the Elk Point Basin; Bull. Can. Petrol. Geol., v19, p487-503.

Major, R.P., Lloyd, R.M., and Lucia, F.J. (1992): Oxygen isotope composition of Holocene dolomite formed in a humid hypersaline setting; Geol., v20, p586-588.

Osadetz, K.G. and Snowdon, L.R. (1995): Significant Paleozoic Petroleum Source Rocks in the Canadian Williston Basin: Their Distribution, Richness, and Thermal Maturity Southeastern Saskatchewan and Southwestern Manitoba; Geol. Surv. Can., Bull. 487, 60p.

Popp, B.N., Anderson, T.F., and Sandberg, P.A. (1986): Textural, elemental, and isotopic variations among constituents in Middle Devonian limestones, North America; J. Sed. Petrol., v56, p715-727.

Qing, H. (1998): Petrography and geochemistry of early-stage, fine- and medium-crystalline dolomites in the Middle Devonian Presqu'ile at Pine Point, Canada; Sediment., v45, p433-446.

Reinson, G.E. and Wardlaw, N.C. (1972): Nomenclature and stratigraphic relationships, Winnipegosis and Prairie Evaporite formations, central Saskatchewan, Bull. Can. Petrol. Geol., v20, p301-320.

Shearman, D.J. and Fuller, J.G.C.M. (1969): Anhydrite diagenesis, calcitization, and organic laminites, Winnipegosis Formation, Middle Devonian,

Saskatchewan; Bull. Can. Petrol. Geol., v17, p496-525.

Stoakes, F., Cambell, C., Hassler, G., Dixon, R., and Forbes, D. (1987): Sedimentology and Hydrocarbon Source Potential of the Middle Devonian Winnipegosis Formation of South-eastern Saskatchewan; Stoakes Campbell Geoconsulting, unpubl. rep., 98p.

Carbonate/Evaporite Deposits of the Shell Lake Marker Bed, Middle Devonian Elk Point Basin, Rocanville, Saskatchewan

Arden K.A. Marsh [1], Katherine M. Bergman [1], and Jisuo Jin [2]

Marsh, A.K.A., Bergman, K.M., Jin, J. (2001): Carbonate/evaporite deposits of the Shell Lake Marker Bed, Middle Devonian Elk Point Basin, Rocanville, Saskatchewan; *in* Summary of Investigations 2001, Volume 1, Saskatchewan Geological Survey, Sask. Energy Mines, Misc. Rep. 2001-4.1.

1. Introduction

Many interpretations of the depositional environments of both the Winnipegosis and Prairie formations of the Middle Devonian (Givetian), Elk Point Group (Figure 1) have been proposed (Holter, 1969; Wardlaw and Reinson, 1971; Reinson and Wardlaw, 1972; Kendall, 1975, 1989; Martindale *et al.*, 1991; Horita *et al.*, 1996; Jin *et al.*, 1997; Jin and Bergman, 1999). However, only a few of these studies (Jordan, 1967; Holter, 1969; Reinson and Wardlaw, 1972; Kendall, 1989; Horita *et al.*, 1996) have discussed the origin of the sediments forming the Shell Lake Marker Bed of the Prairie Evaporite (Figure 2), which has been interpreted by Reinson and Wardlaw (1972) and Martindale *et al.* (1991) as having been deposited in an overall continuous brining upward succession. The evaporation of water from the restricted Elk Point Basin (Figure 1) allowed for an increase in brine concentration and direct precipitation of chemical sediments (Kendall, 1989), including dolomite, anhydrite, and halite. These interpretations of the depositional conditions were based on limited subsurface data which did not permit detailed study of the vertical relationships of the sediments in the marker bed.

The purpose of this study is a description of the vertical variation of the carbonate/evaporite succession of the Shell Lake Marker Bed exposed over a lateral extent of 61 m (200 ft) on the walls of a lower incline in the Potash Corporation of Saskatchewan (PCS) Rocanville potash mine at Rocanville, Saskatchewan (Figures 1 and 3). This 14.7 m (48.2 ft) thick, flat-lying bed is composed of a cyclic but sometimes variable repetition of anhydrite, dolomite, anhydrite, and halite (Figure 4). The dolomite between anhydrite layers suggests that the brine was replenished by open-marine waters and that the brining upward succession was not continuously progressive. Accordingly, sediments of the Shell Lake Marker Bed appear to have been deposited under salinity conditions that varied from open marine to highly saline. The exposure suggests the possibility of multiple smaller scale brining upward cycles within the large scale brining upward succession (Figure 4).

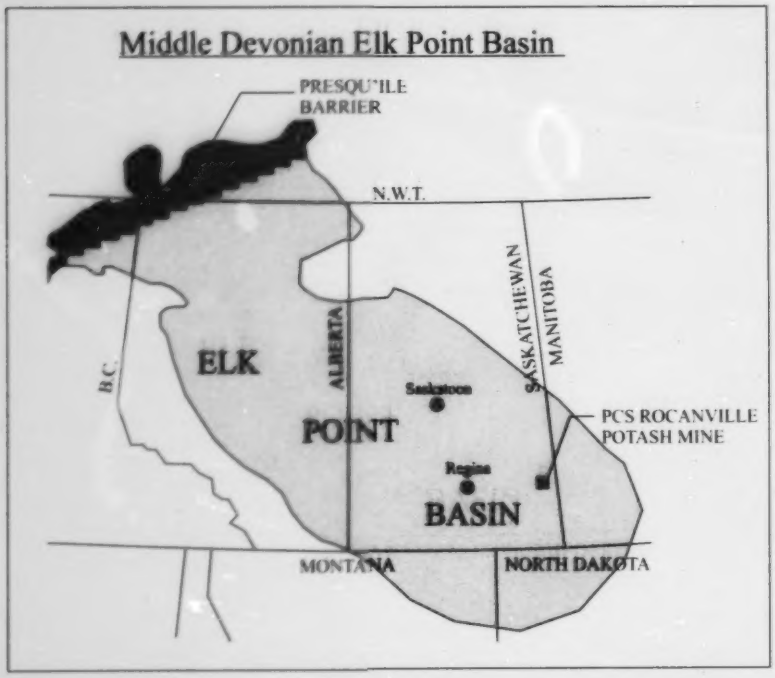

Figure 1 - Map of the Middle Devonian Elk Point Basin, illustrating basin shape, geographical location of the basin, and location of the study area (PCS Rocanville potash mine). Simplified from Kendall (1989).

[1] Department of Geology, University of Regina, Regina, SK S4S 0A2; Katherine.Bergman@uregina.ca.
[2] Department of Earth Sciences, University of Western Ontario, London, ON N6A 5B7; Jjin@julian.uwo.ca.

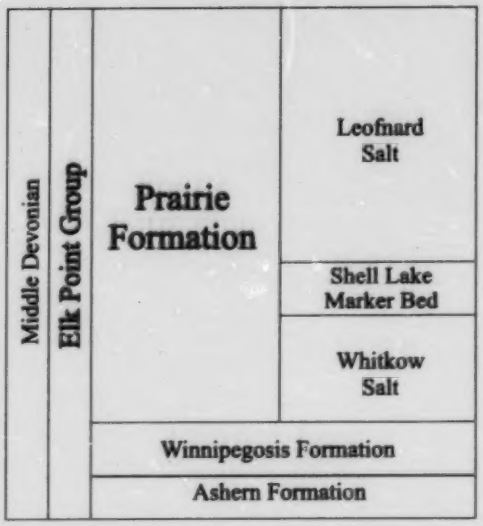

Figure 2 - Stratigraphic column showing the general relationship of the Shell Lake Marker Bed to other stratigraphic units in the study area.

2. Regional Geology and Stratigraphy

During deposition of the Middle Devonian Elk Point Group (Givetian), the Elk Point Basin was situated between latitudes 10° and 20° South (Horita *et al.*, 1996) and was "sack" shaped (Figure 1). It covered an area of approximately 425 000 km^2 (Horita *et al.*, 1996) extending from the present day Northwest Territories in the northwest to the Dakotas and southwestern Manitoba in the southeast. The basin was isolated from the open ocean to the north by the Presqu'ile Barrier Reef, which limited the free exchange of marine water (Figure 1). This restricted the production of carbonate sediments and enhanced the production of evaporite by an increase in salinity in the basin (Kendall, 1989).

The Elk Point Group is composed of chemically and organically precipitated sediments that can be used to infer relative sea-level changes (Jin *et al.*, 1997; Jin and Bergman, 1999) from variations in brine concentrations at the time of deposition (Kendall, 1989; Horita *et al.*, 1996). It is subdivided into three formations (O-Y) (Figure 2): 1) the Ashern Formation comprises an argillaceous microcrystalline dolostone with interbedded dolomitic shale, and basal anhydrite (Jin *et al.*, 1997); 2) the Winnipegosis Formation includes carbonate reefs (Kent, 1968); and 3) the thick Prairie Formation is composed of halite and potash, minor dolomite and anhydrite (Holter, 1969). The Prairie Formation is subdivided into the Whitkow Salt/anhydrite (the mineralogical composition of this unit depends on its relationship to the carbonate reefs of the Winnipegosis Formation) at the base, overlain successively by the medial Shell Lake Marker Bed, and the Leofnard Salt, a unit composed mainly of halite, with potash beds (Figure 2).

3. Shell Lake Marker Bed

a) Regional

The Shell Lake Marker Bed, ranging from 6 to 32 m in thickness, can be traced throughout the southern part of the Elk Point Basin (south of the Meadow Lake Escarpment) (Holter, 1969; Reinson and Wardlaw, 1972). The variation in thickness appears to be related to the pinnacle reefs of the Upper Winnipegosis Formation (Kendall, 1989). In general, the Shell Lake Marker Bed is thinner in close proximity to reefal structures (Jordan, 1967; Holter, 1969; Wardlaw and Reinson, 1971; Kendall, 1989; Meijer Drees, 1996).

The presence in the Prairie Evaporite of a unit termed the "Middle Anhydrite" was first recognized by Jordan (1967) and described by Holter (1969) as the Shell Lake Gypsum. The lowermost 5 to 7 m of the Shell Lake Marker Bed are typically composed of anhydrite making identification of the contact with the underlying Whitkow Member difficult. Wardlaw and

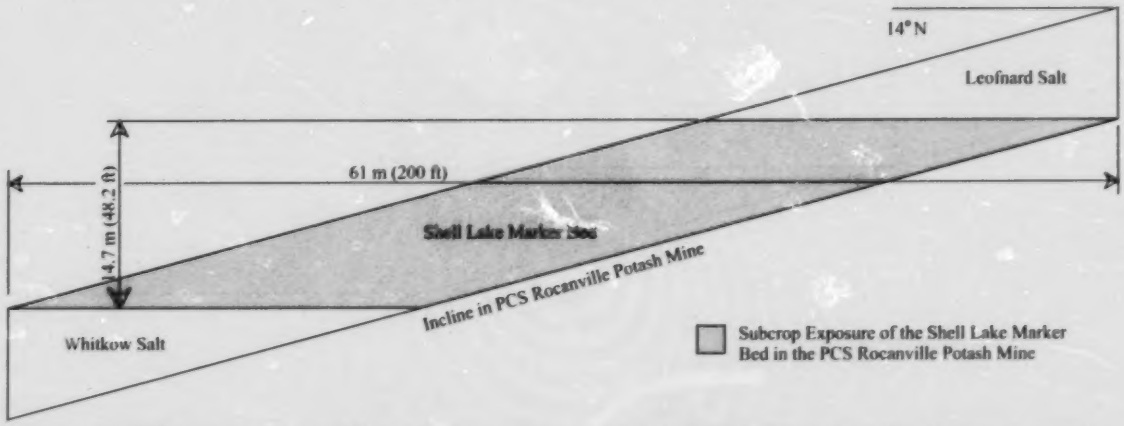

Figure 3 - Graphical representation of the exposed section of the Shell Lake Marker Bed on the walls of a lower incline in the Rocanville potash mine; the incline slopes at 14°, and trends toward the north.

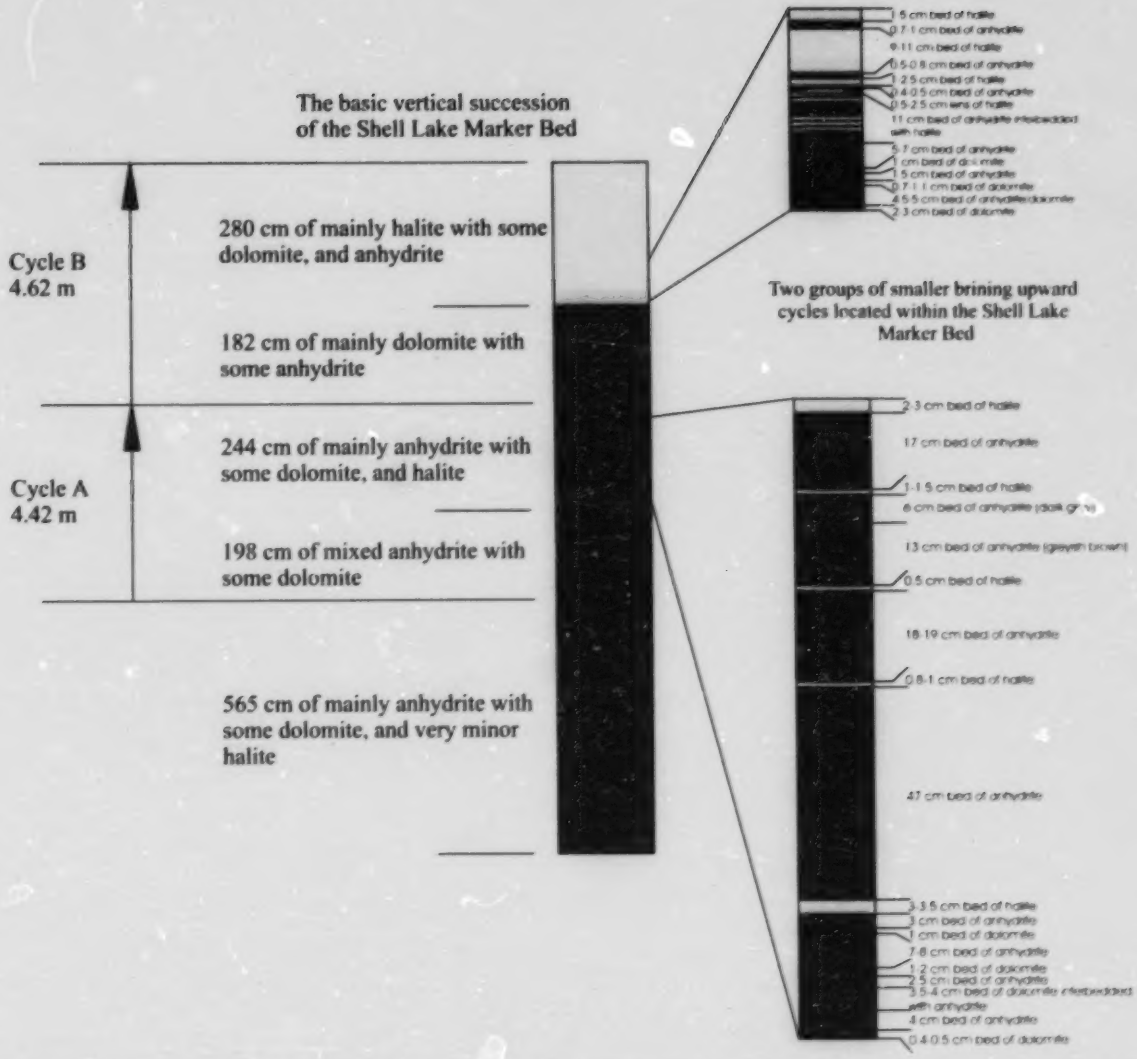

Figure 4 - Five main lithological units of the Shell Lake Marker Bed at Rocanville, Saskatchewan and detailed view of two groups of multiple small-scale brining upward cycles within the two large-scale cycles (A and B).

Reinson (1971) and Reinson and Wardlaw (1972) were unable to distinguish the anhydrite of the Shell Lake Member from that of the Whitkow Member. Kendall (1975) described the Shell Lake as a "sequence of bedded to laminated anhydrite and dolomite" that is difficult to distinguish from the Whitkow Member. More recently Meijer Drees (1996) suggested that the Shell Lake was a difficult unit to define, particularly where the Whitkow Member is composed of anhydrite. Recent papers (Kendall, 1989; Horita *et al.*, 1996) have focused on the driving mechanisms (sea-level fall, basin desiccation, groundwater flow, and brine mixing) that controlled the formation of sediments in the Prairie Evaporite with less emphasis on the nomenclature and definition of individual members.

Descriptions of the vertical variability of the mineralogical composition of this unit reflect the following factors: 1) the general variability in thickness of the Shell Lake Marker Bed in the southern part of the basin, causing the inclusion and omission of certain beds within the unit; 2) the control of various diagenetic processes (including dissolution), which may have varied over geologic time within different parts of the basin; and/or 3) a paucity of subsurface data. The vertical variability of the various sedimentary layers in this unit in other parts of the basin is not known and is beyond the scope of this study.

b) Detailed Lithologic Sequence and Evidence for Cyclicity, Rocanville Potash Mine

The Shell Lake Marker Bed at the Rocanville mine exposure shows a general overall brining upward trend from anhydrite at the basal contact to halite at the top contact (Figure 4). It comprises five main units dominated by the following lithologies (in ascending order) 1) anhydrite, 2) interbedded dolomite/anhydrite, 3) anhydrite, 4) dolomite, and 5) halite (Figure 4). Cracks in the upper 72 to 85 cm of the exposure are infilled by potash. The succession is described in detail in Figure 5 and Table 1. The basal contact of the Shell Lake Marker Bed with the Whitkow Salt is shown in Figure 6. The upper contact with the Leofnard Salt is illustrated in Figure 7.

Detailed vertical measurement (millimetre to centimetre scale) and analysis of the recorded data appear to indicate two different scales of brining upward cycles which suggest a hierarchical system based on cyclostratigraphy (Schwarzacher, 1993). The identification of brining upward cycles is based on the precipitation order of sediments from seawater undergoing increasing concentration (Tucker, 1996). Dolomite ($CaCO_3$) precipitates at a sea-water concentration factor of 1.8, anhydrite ($CaSO_4$) at 3.8, and halite (NaCl) at 10.6. Each brining upward cycle comprises dolomite, anhydrite, and finally halite (Figure 5).

Two large-scale brining upward cycles are present (Figure 5). The lower, 4.42 m thick, is composed of mixed dolomite/anhydrite (1.98 m) overlain by anhydrite (2.44 m). The upper is 4.62 m thick and is composed of dolomite (1.82 m) overlain by halite (2.80 m). These two large-scale cycles are composed of a recorded thirty-three smaller scale (3 cm to 1.53 m in thickness) brining upward cycles which begin 5 m above the basal contact of the Shell Lake Marker Bed, and continue through to the upper contact (Figure 5). Up to 25 of the smaller scale cycles are, however, either incomplete or interrupted (e.g. Cycle 8, Figure 5) possibly due to: 1) non-deposition because of a change in sea-water concentration (probably decreased concentration resulting from influx of open-marine water) that prevented the precipitation of one (or more) of the minerals within any particular cycle; or 2) dissolution at some time after precipitation because of groundwater flow or some other process.

The small-scale cycle (Cycle 17) at the base of the upper large-scale cycle has important implications when considering either sea-level and/or sea-water concentration in the basin at the time of deposition (Figure 8). This zone, 1.5m thick, has 86 layers of dolomite, and 85 layers of anhydrite. The anhydrite interbeds are 1 to 40 mm thick and are thicker toward the middle of this cycle. The dolomite interbeds are 1 to 10 mm thick, with the thickest 46 cm above the base of the cycle. The anhydrite-dolomite interbeds in the lower 32 cm of the unit representing Cycle 17 appear to be partially deformed and contain large (up to 10 cm across) pisolitic (Figure 9) and stromatolitic (Figure 10) structures that indicate a reduction in salinity within the Middle Devonian Elk Point Basin at the time of deposition. The composition and biologic structures of these sediments in this zone were interpreted to indicate a return to an open marine basin (Reinson and Wardlaw, 1972), or alternatively a breech of the Presqu'ile Barrier (Jin *et al.*, 1997).

That halite was the only direct precipitate in these cycles is most likely. The dolomite in the Shell Lake Marker Bed is coarse (up to 1 mm), and angular to subangular in shape, suggesting that the sediment was originally precipitated as limestone and diagenetically altered by dolomitization (Boggs, 1995; Tucker, 1996). The anhydrite is most likely the product of dewatered gypsum (Kent, 1968; Logan, 1987). Dehydration of gypsum ($CaSO_4 \cdot 2H_2O$) to form anhydrite ($CaSO_4$) occurred during burial because of increased temperature and pressure. However, these changes do not affect the validity of the brining upward cycles that are recognized in the Shell Lake Marker Bed. Dolomite (and/or limestone) precipitates at a lower sea-water concentration than anhydrite (and/or gypsum), which precipitates at a lower sea-water concentration than halite.

4. Discussion

At the time of deposition of the Elk Point Group, the Elk Point Basin was located at 10° to 20° South latitude (Horita *et al.*, 1996). To the north, the flow of marine water into the basin was hindered by the Presqu'ile Barrier. Rapid evaporation (Maiklem, 1971) raised the concentration of sea water to critical values that allowed for the precipitation of dolomite and/or limestone, anhydrite and/or gypsum, halite, and potash. If the rate of evaporation of seawater from the basin had been constant, and the brine not periodically replenished, the succession would have been composed of thin units of dolomite and/or limestone, overlain by a thick unit of anhydrite and/or gypsum, followed by a thick (hundreds of metres) halite interval and finally potash with no interruption in the brining upward sequence (Kendall, 1989). This is not the sedimentary succession that is preserved. The repetitive precipitation of carbonate and evaporite indicates that the rate of evaporation was not constant, and that sometimes fresh seawater must have been added to the basin so that complete drawdown did not occur (Maiklem, 1971).

The thickness of the sediments found in the Middle Devonian Elk Point Basin could not be produced simply by static precipitation from sea water as suggested by Kendall (1989) and Maiklem (1971). Sediment types in the basin vary in thickness and composition because of the variation in seawater concentration at the time of deposition, such that sedimentation cycles are observed in the Prairie Formation (Figure 5). The vertical variation observed in the deposits of the Shell Lake Marker Bed is interpreted as a hierarchical cyclostratigraphic succession.

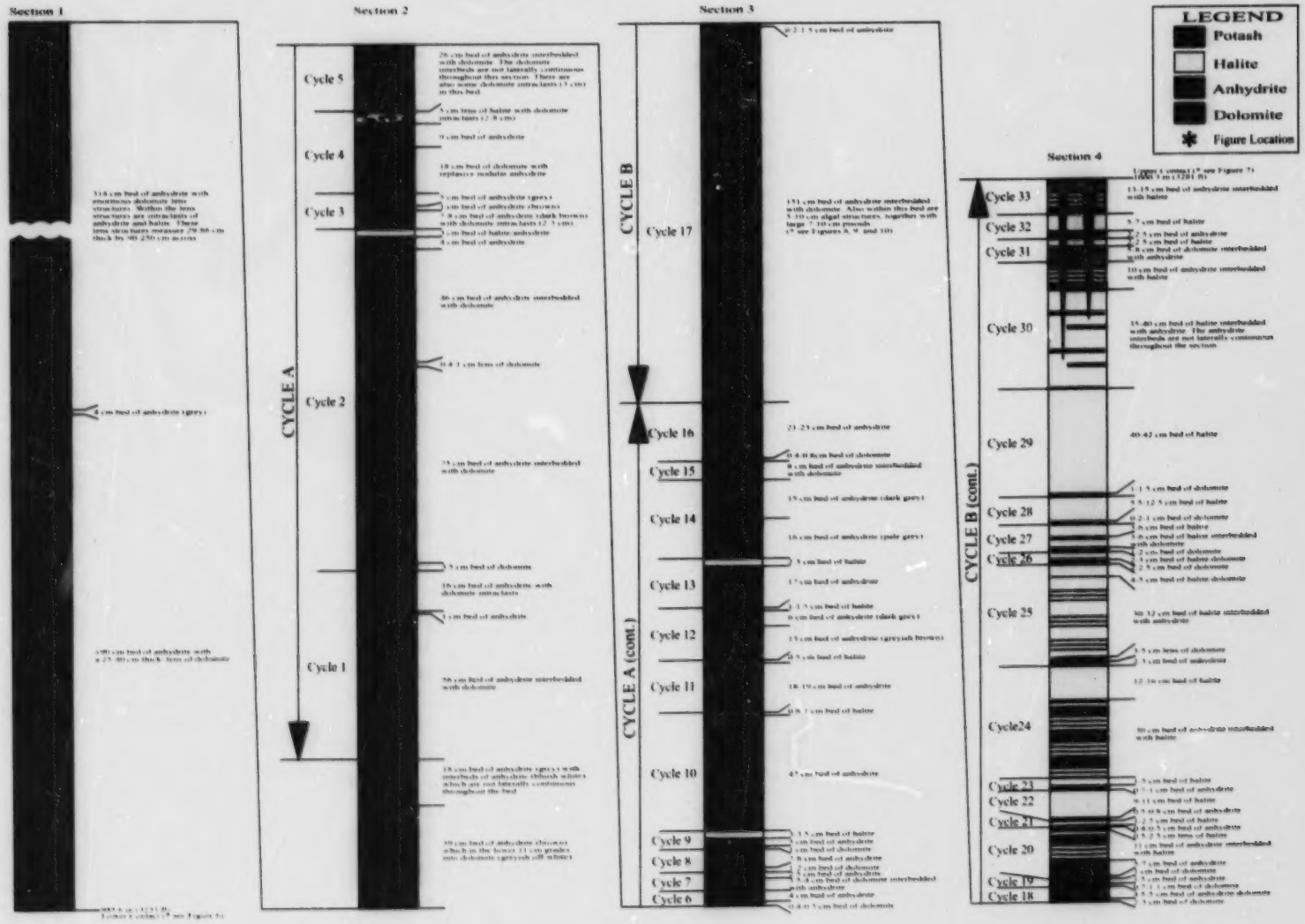

Figure 5 - Detailed vertical section of the Shell Lake Marker Bed at Rocanville, Saskatchewan showing the two large-scale cycles (A and B) and numbered small-scale cycles that make up cycles A and B. Detailed description of the section is given in Table 1. Locations of Figures 6 through 10 are indicated by asterisks.

Table 1 - Detailed description of the vertical variation of sediment in the Shell Lake Marker Bed at Rocanville, Saskatchewan. *potash mine in August 1998. For this particular study, the exposure of the Shell Lake Marker Bed has been described from its*

BED	DATA AND ANALYSIS
1	13 to 15 cm bed of anhydrite interbedded with halite, plus some potash infill in vertical cracks. These halite interbeds are not laterally continuous throughout the bed. The anhydrite in this bed is bluish grey in colour and the halite is white to smoky brown in colour. The thickness of the halite interbeds varies from 2 to 5 mm. A 10 to 12 mm thick band of slightly darker anhydrite appears 22 to 25 mm from the top of this bed, and is laterally continuous throughout the subcrop. This bed is the top contact of the Shell Lake Marker Bed with the Leofnard Salt.
2	5 to 7 cm bed of coarsely crystalline halite, with potash infill in vertical cracks in the bed. The halite in this bed is white to smoky brown in colour. The potash infill (continuing from the bed above) is brownish red in colour, indicating the presence of carnallite within the potash.
3	2 to 2.5 cm bed of bluish grey massive anhydrite. There is potash infill in vertical cracks that are continued from the beds above.
4	2 to 2.5 cm bed of whitish clear to smoky brown coarsely crystalline halite. There is still potash infill in vertical cracks that continue from the beds above.
5	5 to 8 cm bed of dolomite interbedded with massive anhydrite. The dolomite interbeds vary in thickness from 5 to 30 mm, and the anhydrite interbeds vary in thickness from 5 to 15 mm. The dolomite in this bed is a pale yellowish brown and the anhydrite is a greyish brown. Potash infill in is seen in vertical cracks that continue throughout the beds above.
6	10 cm bed of anhydrite interbedded with halite. The anhydrite in this bed is bluish grey in colour, and approx. 5 mm thick (in alternating bands). The halite is white to smoky brown in colour, and approx. 10 mm thick (in alternating bands). Potash infill is still seen in vertical cracks that are continued from the beds above.
7	35 to 40 cm bed of finely crystalline halite, with a several interbeds of anhydrite that are not laterally continuous throughout the subcrop. The halite in this bed is a clearish smoky brown to an opaque pale brown colour, and the anhydrite is a bluish grey. Potash infill that is seen in beds #1 to #6, in vertical cracks terminates in this bed.
8	40 to 42 cm bed of coarsely crystalline white to off-white halite, with no visible inclusions of other minerals.
9	1 to1.5 cm bed of powdery white to very pale grey dolomite.
10	5.5 to 12.5 cm bed of coarsely crystalline white to smoky brown halite.
11	0.2 to 1 cm bed of powdery white dolomite.
12	3 to 6 cm bed of coarsely crystalline clear to smoky brown halite.
13	3 to 6 cm bed of clear to smoky brown halite interbedded with powdery white dolomite. The halite varies from 2 to 5 mm in thickness, and the dolomite interbeds vary from 1 to 2 mm in thickness.
14	1 to 2 cm bed of very pale brown massive dolomite.
15	2 to 3 cm bed of coarsely crystalline clearish smoky brown halite interbedded with powdery white dolomite. The halite in this bed is 2 to 3 mm thick and the dolomite interbeds are up to 1 mm thick.
16	2 to 2.5 cm bed of very pale brown massive dolomite.
17	4 to 5 cm bed of clearish smoky brown coarsely crystalline halite interbedded with powdery white dolomite. The halite in this bed is 3 to 5 mm thick and the dolomite is up to 1 mm thick.
18	30 to 32 cm bed of clearish smoky brown halite interbedded with brown to off-white enterolithic anhydrite. The halite and anhydrite in this bed vary greatly in thickness. The halite is 15 to 60 mm thick and the anhydrite is 5 to 45 mm thick.
19	3 to 5 cm bed of powdery white dolomite, that is not laterally continuous throughout the section of subcrop.
20	2 to 3 cm bed of bluish grey massive anhydrite.
21	12 to 16 cm bed of coarsely crystalline smoky brown halite.
22	30 cm bed of greyish blue massive anhydrite interbedded with coarsely crystalline smoky brown halite. The anhydrite in this bed is 5 to 15 mm thick and the halite is 5 to 10 mm thick.
23	1 to 5 cm bed of white to off-white coarsely crystalline halite.
24	0.7 to 1 cm bed of finely laminated brownish grey anhydrite. The laminations in this bed are less than 1 mm thick.
25	9 to 11 cm bed of white to off-white coarsely crystalline halite.
26	0.5 to 0.8 cm bed of finely laminated brownish grey anhydrite. The laminations in this bed are approximately 0.5 mm thick.
27	1 to 2.5 cm bed of white to off-white coarsely crystalline halite.
28	0.4 to 0.5 cm bed of finely laminated brownish grey anhydrite. The laminations in this bed are approximately 1 to 1.5 mm thick.
29	0.5 to 2.5 cm bed of white to off-white coarsely crystalline halite that is not laterally continuous throughout the exposed subcrop. Note: beds #24, #26, and#28 appear to look like storm/flood type deposits.
30	11 cm bed of interbedded contorted brownish grey anhydrite (contortions are 5 to 10 mm in thickness) with white to off-white coarsely crystalline halite.
31	5 to 7 cm bed of coarsely laminated pale brown, dark brown, and bluish grey anhydrite. The laminations in this bed are 2 to 10 mm thick.
32	1 cm bed of powdery off-white dolomite.
33	1.5 cm bed of laminated pale brown to dark brown anhydrite. The laminations in this bed are too fine to measure, but the colour of the laminations changes from pale brown to dark brown after 3 mm (from the top of the bed) for 3 mm, and then changes back to pale brown.
34	0.7 to 1.1 cm bed of powdery off-white dolomite.
35	4.5 to 5 cm bed of enterolithic anhydrite with three to four fine (up to 1 mm) interbeds of powdery off-white dolomite. The dolomite interbeds are not laterally continuous throughout the section.
36	2 to 3 cm bed of finely laminated off-white to pale brown dolomite. The laminations in this bed are less than 1 mm thick.
37	0.2 to 1.5 cm bed of massive greyish anhydrite.
38	151 cm unit of massive and laminated anhydrite interbedded with powdery off-white dolomite. The anhydrite interbeds are 1 to 40 mm thick and are thicker toward the middle of the unit. The dolomite-anhydrite interbeds in the lower 32 cm of the unit appear to be partially deformed. Within this partially deformed section are large (up to 10 cm across) pisolitic, and stromatolitic structures that may indicate a reduction in salinity within the Middle Devonian Elk Point Basin at the time of deposition. The dolomite interbeds are 1 to 10 mm thick, with the thickest dolomite interbed 46 cm above the base of the unit. A total of 86 layers of dolomite and 85 layers of anhydrite are present.
39	21 to 23 cm bed of laminated bluish grey to medium brown anhydrite. The laminations in this bed are 2 to 10 mm thick and appear to fine upward.

***Note:** The following description of the Shell Lake Marker Bed is taken from field notes that were produced at the PCS Rocanville Upper Contact (Bed #1) to the Lower Contact (Bed #82). Figure 5 graphically represents the information in this table.*

BED	DATA AND ANALYSIS
40	0.4 to 0.8 cm bed of powdery pale-brown dolomite.
41	8 cm bed on enterolithic and laminated anhydrite in various shades of grey, interbedded with pale to medium brown dolomite. The dolomite interbeds in this bed are up to 1 mm thick.
42	15 cm bed of dark grey laminated anhydrite. The laminations in this bed are 1 to 8 mm thick.
43	16 cm bed of pale grey with bluish grey and pale brown laminated, and contorted (in the upper 11 cm of this bed) anhydrite. The laminations in this bed are 1 to 6 mm thick.
44	2 to 3 cm bed of clear to smoky brown coarsely crystalline halite.
45	17 cm bed of dark greyish brown contorted anhydrite. The contorted laminations in this bed are up to 1 mm thick.
46	1 to 1.5 cm bed of clear to smoky brown coarsely crystalline halite.
47	6 cm bed of moderately contorted and laminated dark greyish brown anhydrite.
48	13 cm bed of laminated greyish brown anhydrite. The laminations in this bed are 1 to 5 mm thick.
49	0.5 cm bed of coarsely crystalline smoky brown halite.
50	18 to 19 cm bed of grey, and greyish brown finely laminated anhydrite. The laminations in this bed are too thin to measure with any accuracy, but can be seen clearly with a hand lens.
51	0.8 to 1 cm bed of clear to smoky brown coarsely crystalline halite.
52	47 cm bed of thickly laminated, and moderately contorted (in the lower 20 cm of this bed) bluish grey to brown anhydrite. The laminations in this bed are 1 to 5 mm thick.
53	3 to 3.5 cm bed of coarsely crystalline white to clear halite.
54	3 cm bed of brown laminated anhydrite, with the inclusion of bluish white bands of anhydrite within the bed. The laminations in this bed are 1 to 3 mm thick.
55	1 cm bed of brown dolomite interbedded with dark greyish brown laminated anhydrite. The laminations in this bed are less than 1 mm thick.
56	7 to 8 cm bed of grey to brown very finely laminated (too thin to measure with any accuracy) anhydrite.
57	1 to 2 cm bed of white to pale grey dolomite.
58	2.5 cm bed of finely laminated brown anhydrite. The laminations in this bed are less than 1 mm thick.
59	3.5 to 4 cm bed of greyish white dolomite interbedded with brown massive anhydrite.
60	4 cm bed of finely laminated brown anhydrite. The laminations in this bed are less than 1 mm thick.
61	0.4 to 0.5 cm bed of greyish white powdery dolomite.
62	26 cm bed of laminated brown to grey anhydrite with fine pale brown dolomite interbeds (no more than 3 mm thick and is not laterally continuous throughout this bed). There are also some small (3 cm diameter) intraclasts of powdery white dolomite.
63	5 cm bed of clear to white coarsely crystalline halite that pinches out within this section of subcrop. This bed also contains intraclasts of powdery white dolomite of various sizes (two are 2 cm by 3 cm across, and two are 2 cm by 8 cm across, also many other smaller intraclasts that are less than 2 cm across).
64	9 cm bed of thickly laminated (these laminations are also contorted) grey and brown anhydrite . The grey laminations in this bed are 5 to 10 mm thick. The degree of contortion of the laminations is highly variable throughout this bed.
65	18 cm bed of turbated powdery white dolomite with replacement anhydrite.
66	5 cm bed of brown massive anhydrite with grey enterolithic anhydrite. The enterolithic bands are 5 mm thick throughout this bed.
67	1 cm bed of very finely laminated medium brown anhydrite. The laminations in this bed are too small to measure with any accuracy, but they can be seen with a hand lens.
68	7 to 8 cm bed of medium to dark brown contorted anhydrite. There are powdery white dolomite intraclasts within this bed (2 to 3 cm in thickness, and 7 to 23 cm in width).
69	3 cm bed of white halite interbedded with medium brown massive anhydrite.
70	4 cm bed of very finely laminated (less than 1 mm thick) medium brown anhydrite.
71	46 cm bed of contorted brown anhydrite interbedded with off-white dolomite. The dolomite interbeds are mostly 1 mm thick. However, there are a few of the dolomite interbeds that are 10 to 15 mm thick. The contorted anhydrite interbeds within this bed vary in thickness from 10 to 30 mm.
72	0.4 to 1 cm lens of powdery white to off-white dolomite. This lens of dolomite is not laterally continuous throughout the section of subcrop.
73	75 cm bed of brownish grey laminated anhydrite interbedded with white dolomite. The laminations of anhydrite in this bed are 1 to 5 mm thick and the dolomite interbeds in this bed are 5 to 8 mm thick.
74	3.5 cm bed of beige to brownish grey mottled dolomite.
75	16 cm bed of medium brown massive anhydrite, with nodules of off-white powdery dolomite.
76	1 cm bed of grey finely laminated anhydrite. The laminations in this bed are less than 1 mm thick.
77	56 cm bed of brown to grey massive anhydrite interbedded with off-white dolomite. The dolomite interbeds in this bed are 5 to 15 mm thick.
78	18 cm bed of grey massive anhydrite with interbeds of bluish white anhydrite, that are not laterally continuous throughout the bed.
79	39 cm bed of greyish brown massive anhydrite with the lower 11cm of this bed gradually altered to a greyish off-white dolomite.
80	314 cm bed of massive brown anhydrite with three enormous lens type structures. The upper lens measures 24 cm in thickness by 115 cm across, and is composed of clear to smoky brown halite with an off-white dolomite matrix, making the structure almost conglomeratic in appearance. The top surface of this lens (which is the top contact of this bed) is flat, but the lower surface is dish shaped. There are halite intraclasts in this bed that measure 2 to 45 mm across. The next lens is 86 cm into this (from the top contact of this bed) and measures 86 cm in thickness and 250 cm across. This lens type structure is made up of clear halite, and grey anhydrite in a lacy dolomite matrix, and also has a conglomeratic appearance. Another mass of the same conglomeratic appearance appears 119 cm into this bed. This lower mass is 29 cm in thickness and 90 cm across.
81	4 cm bed of massive grey anhydrite.
82	190 cm bed of massive medium brownish grey anhydrite, with a 25 to 40 cm thick by 460 cm across powdery white dolomite lens, that is not laterally continuous throughout the section of subcrop. This lens type structure may have been produced by the post-depositional dissolution of the anhydrite within this bed. This bed marks the lowermost contact with the Whitkow Halite, and thus the base of the Shell Lake Marker Bed.

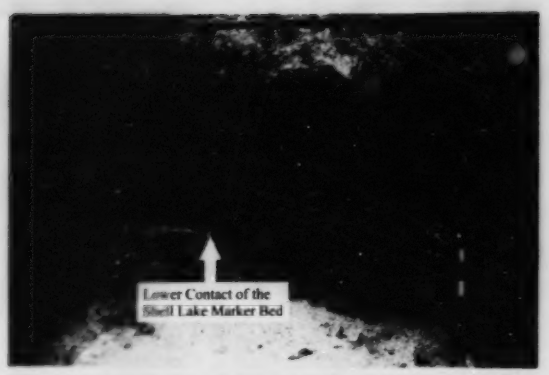

Figure 6 - Lower contact (arrow) of the massive anhydrite (Bed #82, Table 1) of the Shell Lake Marker Bed with the halite of the Whitkow Salt. Scale bar is 50 cm.

Figure 7 - Upper contact (arrow) of the interbedded anhydrite and halite (Bed #1, Table 1) of the Shell Lake Marker Bed with the halite of the Leofnard Salt. Scale bar is 50 cm.

Figure 8 - Anhydrite and dolomite interbeds (Bed #38, Table 1), interpreted to indicate a major brine refreshening cycle (Cycle 17, Figure 5). The pisoids (Figure 9) and stromatolites (Figure 10) are found in this interval. Scale bar is 50 cm.

Figure 9 - Pisoid (arrow) contained in the interval of massive anhydrite interbedded with dolomite (Bed #38, Table 1; Cycle 17, Figure 5).

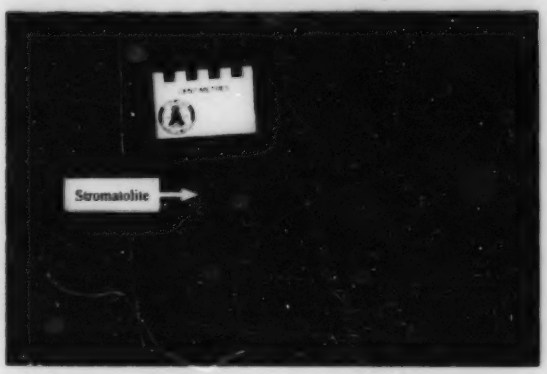

Figure 10 - Stromatolitic structure (arrow) contained in the interval of massive anhydrite interbedded with dolomite (Bed #38, Table 1; Cycle 17, Figure 5).

5. Summary and Conclusions

Observations and detailed measurements were made on an exposure of the Shell Lake Marker Bed at the Rocanville Potash Mine and brining upward cycles were documented in detail. The concentration of the brine must have been periodically replenished by open marine water as evidenced by the repetitive precipitation of carbonate and evaporite recorded in the 33 small-scale brining upward cycles that constitute the overall brining upward Shell Lake succession (Figure 5).

6. Acknowledgments

We thank the Potash Corporation of Saskatchewan (PCS), Rocanville Division mine, for allowing access to the subcrop. In particular we thank Terry Danyluk (PCS, Saskatoon), Vance Thom (PCS, Rocanville), and George Williams (PCS, Rocanville). Dr. Hairuo Qing of the Department of Geology at the University of

Regina and Fran Haidl, Petroleum Geology Branch, Saskatchewan Energy and Mines, read early versions of the manuscript and provided useful comments. We also thank Andrew Nimegeers for his field support. This project was funded by a grant from PCS with matching support from an NSERC IOR grant.

7. References

Boggs, S. (1995): Principles of Sedimentology and Stratigraphy; Second Edition, Prentice-Hall, Upper Saddlehaven, 727p.

Holter, M.E. (1969): The Middle Devonian Prairie Evaporite of Saskatchewan; Sask. Dep. Miner. Resour., Rep. 123, 63p.

Horita, J., Weinberg, A., Das, N., and Holland, H.D. (1996): Brine inclusions in halite and the origin of the Middle Devonian prairie evaporites of western Canada; J. Sed. Resear., v66, no5, p956-964.

Jin, J. and Bergman, K.M. (1999): Sequence stratigraphy of the Middle Devonian Winnipegosis carbonate–Prairie Evaporite transition, southern Elk Point Basin; Carbonates and Evaporites, v14, p64-83.

Jin, J., Bergman, K.M., Haidl, F.M., Blair, M.J., and Ricci, A. (1997): Vadose diagenesis of the Upper Winnipegosis carbonate and the origin of the Ratner laminite and Whitkow anhydrite, Middle Devonian, southern Saskatchewan; *in* Summary of Investigations 1997, Saskatchewan Geological Survey, Sask. Energy Mines, Misc. Rep. 97-4, p197-212.

Jordan, S.P. (1967): Saskatchewan reef trend looks big; Oilweek, v17, p10-12.

Kendall, A.C. (1975): The Middle Devonian Winnipegosis and lower Prairie Evaporite formations of the commercial potash areas; Summary Report of Investigations of the Saskatchewan Geological Survey, Sask. Dep. Miner. Resour., p61-65.

_____ (1989): Brine mixing in the Middle Devonian of western Canada and its possible significance to regional dolomitization; Sed. Geol., v64, p271-285.

Kent, D.M. (1968): The Geology of the Upper Devonian Saskatchewan Group and Equivalent Rocks in Western Saskatchewan and Adjacent Areas; Sask. Dep. Miner. Resour., Rep. 99, 224p.

Logan, B.W. (1987): The MacLeod Evaporite Basin Western Australia: Holocene Environments, Sediments and Geological Evolution; Amer. Assoc. Petrol. Geol., 133p.

Maiklem, W.R. (1971): Evaporative drawdown - a mechanism for water-level lowering and diagenesis in the Elk Point Basin; Bull. Can. Petrol. Geol., v19, p487-503.

Martindale, W., Erkmen, U., Metcalfe, D., and Potts, E. (1991): Winnipegosis buildups of the Hitchcock area, southeastern Saskatchewan – a case study; *in* Christopher, J.E. and Haidl, F.M. (eds.), Sixth International Williston Basin Symposium, Sask. Geol. Soc., Spec. Publ. No. 11, p47-63.

Meijer Drees, N.C. (1996): Devonian Elk Point Group of the Western Canada Sedimentary Basin; *in* Mossop, G. and Shetsen, I. (comp.), Geological Atlas of the Western Canada Sedimentary Basin, Can. Assoc. Petrol Geol./Alta. Resear. Counc., p129-147.

Reinson, G.E. and Wardlaw, N.C. (1972): Nomenclature and stratigraphic relationships, Winnipegosis and Prairie Evaporite formations, central Saskatchewan; Bull. Can. Petrol. Geol., v20, no2, p301-320.

Schwarzacher, W. (1993): Cyclostratigraphy and the Milankovitch Theory; Elsevier, New York, 225p.

Tucker, M.E. (1996): Sedimentary Petrology: An Introduction to the Origin of Sedimentary Rocks; Blackwell Science, Cambridge, 260p.

Wardlaw, N.C. and Reinson, G.E. (1971): Carbonate and evaporite deposition and diagenesis, Middle Devonian Winnipegosis and Prairie Evaporite Formations of south-central Saskatchewan; Amer. Assoc. Petrol. Geol. Bull., v55, no10, p1759-1786.

Mississippian Madison Formation Low-gravity Oilfields in Southwestern Saskatchewan: Examples of Unconformity Diagenesis Controlling Reservoir Quality

D.M. Kent [1] and L.K. Kreis

Kent, D.M. and Kreis, L.K. (2001): Mississippian Madison Formation low-gravity oilfields in southwestern Saskatchewan: Examples of unconformity diagenesis controlling reservoir quality; *in* Summary of Investigations 2001, Volume 1, Saskatchewan Geological Survey, Sask. Energy Mines, Misc. Rep. 2001-4.1.

1. Introduction

The Mississippian rocks of southwestern Saskatchewan, unlike their counterparts on the eastern flank of the Williston Basin, have yielded exclusively low-gravity oil shows in cores, drill cuttings, and drillstem tests since the early days of exploration in both southeastern Alberta and southwestern Saskatchewan. However, the potential of the rocks for commercial oil production has commonly been overlooked because of the extremely low API (11° to 13°) in Mississippian core and drillstem tests. Twenty-four of these oil shows were identified from the area bounded by Range 20 west of the Third Meridian, the Alberta/Saskatchewan boundary, and Townships 1 and 15, inclusive (Kent and MacEachern, 1990). The most impressive was from a drillstem test of the Coop et al Battle Creek 1-27-3-26W3 well that recovered 1262 m (4140 ft) of 11° API oil from Mississippian rocks immediately beneath the sub-Mesozoic unconformity. Subsequent tests of the same well yielded mainly water, leading to eventual abandonment of the well. However, this discovery identified the Battle Creek area as having potential for low-gravity oil production, and, in 1966, Western Decalta offset the 1-27 well with two boreholes at 1A-27-3-26W3 and 6-27-3-26W3. The former was abandoned shortly after completion, but the latter produced oil from the Madison Formation at the same stratigraphic level as the discovery well for about one-and-a-half years (1966 to 1968) until a fire at the treater caused abandonment. A third well, Canadian Reserve Decalta 15-22-3-26 W3, produced 11 695 m^3 (73,562 barrels) of oil from 1972 to 1985 when it was plugged back to become a Jurassic producer. In 1989, Cirque Energy revived Madison production in the 6-27 well and drilled additional vertical and horizontal wells at Battle Creek. Kent (1995) reported that the horizontal wells significantly improved the productivity of the reservoir. More recently, additional discoveries have been made at Rangeview, Rangeview East, Divide, and an area northwest of Battle Creek herein referred to as Battle Creek West (Figure 1).

Approximately 100 new wells have penetrated Mississippian strata in the study area since Kent and Kreis (1995) outlined an exploration model for Mississippian reservoirs in southwestern Saskatchewan. They provide additional information which gives new insights into the geology of the area.

The localities of interest in this paper all lie within Townships 1 to 6 and Ranges 22 to 30 west of the Third Meridian. The five producing localities, Battle Creek, Battle Creek West, Divide, Rangeview, and Rangeview East have a total of 27 vertical and directionally drilled wells and six horizontals that have produced or are producing low-gravity oil from the Madison. Twenty-three of the wells are classified as suspended or plugged back. The majority of these are in the area encompassing Rangeview, Rangeview East, and Divide.

The rocks of interest lie on the western flank of the Sweetgrass Arch and have a general regional southeasterly dip of about 2.5 m/km toward the centre of the Williston Basin. The Paleozoic strata underlying the area are approximately 870 m thick, consisting of 200 to 350 m of Cambrian siliciclastics belonging to the Deadwood and Earlie formations, and 520 to 670 m of Ordovician, Devonian, and Mississippian rocks that are mainly carbonates. The youngest rocks of the carbonate succession belong to the Mississippian Madison Formation. They directly overlie the predominantly siliciclastic Devonian/Mississippian Three Forks Group which comprises (in ascending order) the Torquay, Big Valley, and Bakken formations.

In much of the study area, the rocks immediately superjacent to the Madison belong to the Middle Jurassic Gravelbourg Formation, a mixed unit of carbonates and fine siliciclastics. However, in places, the basal part of the Gravelbourg includes brecciated zones in which the clasts are in either chalky limestone or mudrock matrix. These breccias and superjacent finely crystalline carbonates locally form a continuous reservoir with the underlying Madison rocks. The remainder of the succession above the Gravelbourg is dominated by siliciclastics of Jurassic, Cretaceous and Tertiary ages and is >1200 m thick.

Locally, the disconformable Mississippian/Jurassic contact is marked by a pronounced paleotopography developed on incised or karsted Mississippian strata (Kent and Kreis, 1995). Regionally, an angular

[1] D.M. Kent Consulting Geologist Ltd., 86 Metcalfe Road, Regina, SK S4V 0H8.

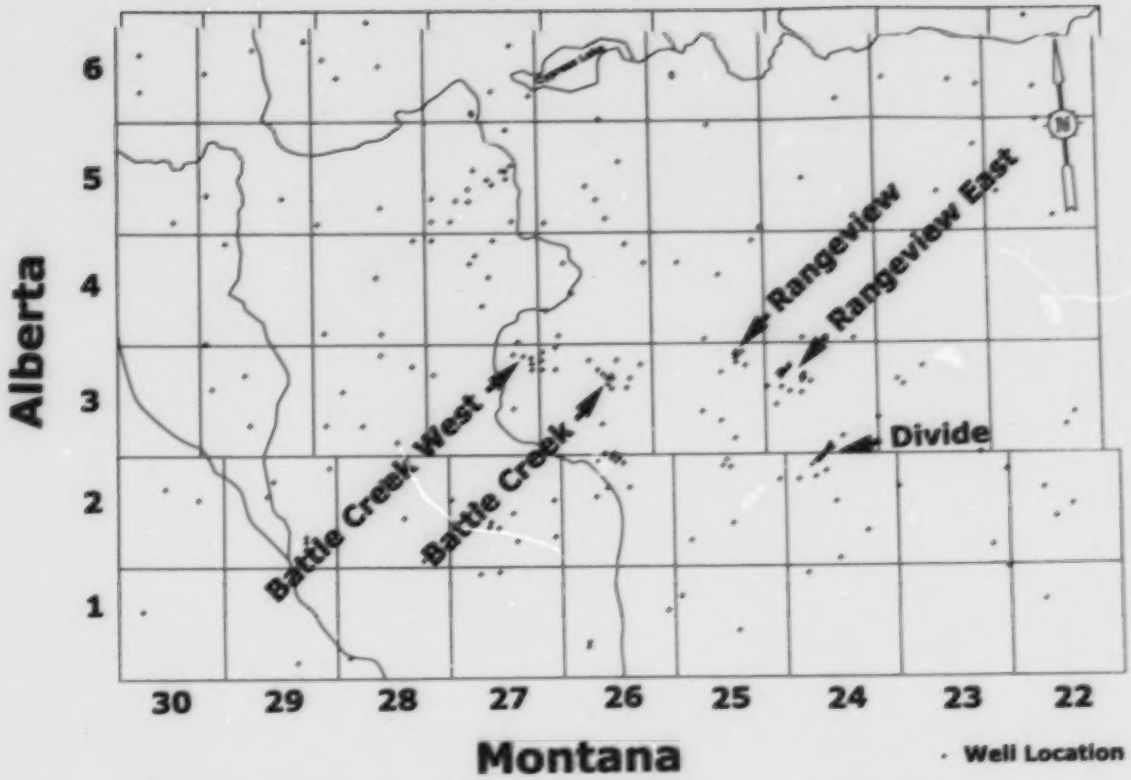

Figure 1 - Map of the study area showing the distribution of the low-gravity oil-producing areas.

relationship between Mississippian and Jurassic rocks also exists. Kent and Kreis (1995) show a well-developed dissected upland on the unconformity surface in the southwestern corner of Saskatchewan, extending from at least Range 20 west of the Third Meridian to the Alberta boundary. The upland is onlapped by progressively younger Jurassic strata. Both Battle Creek and the two Rangeview fields lie on promontories on the northeast-facing slope of the upland (Figure 2). In addition to paleotopographic relief on the sub-Mesozoic unconformity, a monadnock-like feature on the Precambrian erosion surface appears to have been rejuvenated during the Laramide Orogeny. It underlies the Battle Creek region, its influence apparently extending into the Rangeview area. The feature appears as a broad eastward-plunging anticline (Figure 3), part of which is identified as the Battle Creek Structure (Sawatzky *et al.*, 1960; Kent and MacEachern, 1990; Kreis *et al.*, 2000). The combination of sub-Mesozoic paleotopography and structure appears to have played an important role in creating traps for the hydrocarbons at the Battle Creek, Battle Creek West, Rangeview, Rangeview East, and Divide fields.

2. Descriptive Geology of the Oil-bearing Strata

a) Madison Formation

Kent (1974) correlated the Mississippian rocks of southwestern Saskatchewan with the Madison Group of Montana (Figure 4), but as the contacts between the formations comprising that group could not be easily identified, he suggested that the entire Mississippian succession in southwestern Saskatchewan be recognized as one formation, the Madison, but subdivided it into two marker-defined units: the younger Killdeer Beds and the older Strathallen Beds. The former is correlated with the Ratcliffe Beds and the latter with the Souris Valley, Tilston, Frobisher-Alida, and Midale beds of southeastern Saskatchewan (Figure 4). The Killdeer Beds are present only in an area east of Range 13 west of the Third Meridian and therefore are not present in the study area.

The Strathallen Beds extend from the base of the Madison Formation to the sub-Mesozoic unconformity and attain a maximum thickness of 225 m. This marker-defined unit includes three lithotypes: 1) unit A: a basal slightly argillaceous, burrow-mottled, glauconitic, fossil-bearing lime mudstone; 2) unit B: a laminated lime mudstone with partings of finely

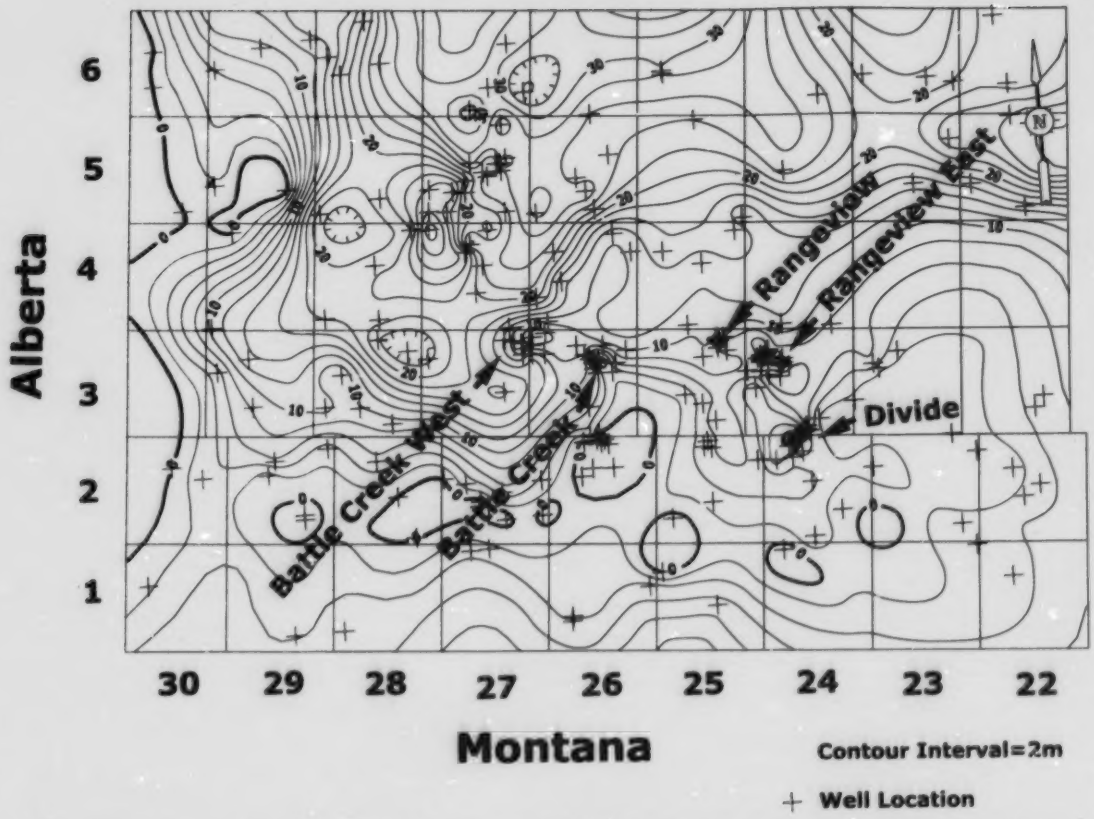

Figure 2 - Isopach map of Upper Watrous (?) and lower Gravelbourg strata overlying the Madison Formation. The map largely reflects the paleotopography of the sub-Mesozoic surface of unconformity prior to deposition of these strata.

disseminated organic carbon emphasizing the interlaminar surfaces; and 3) unit C: a succession of crinoidal packstones and grainstones interbedded with wackestones and lime mudstones. This latter unit subcrops at the sub-Mesozoic unconformity and is host to the low-gravity oil reservoirs at Battle Creek, Battle Creek West, Rangeview, Rangeview East, and Divide.

The thickness of unit C is largely a function of the depth to which erosion has extended below the sub-Mesozoic unconformity and varies from 30 to 160 m, but averages about 130 m. The unit comprises lime mudstones, skeletal wackestones, and crinoidal packstones and grainstones. In places, the former two lithologies alternate with thin beds of the latter two. In other places, the packstones and grainstones of unit C are as much as 30 m thick. Although dominated by crinoidal debris, typically disarticulated columnals and plates, they also contain brachiopod valve fragments, particles of bryozoan zooaria, and solitary corals. By contrast, the wackestones and lime mudstones incorporate a wide variety of organisms including crinoids, bryozoans, brachiopods, pelecypods, ostracods, and corals. Some of the crinoidal grainstones are crossbedded (Kent and MacEachern, 1990) and apparently correlate with the Madison outcrops in the Sweetgrass Hills, some 150 km to the southwest of the study area, where crossbedded crinoidal grainstones vary from 1.25 m thick foreset tabular bodies exposed across several metres of outcrop face, to beds 0.15 to 0.3 m thick which are interbedded with repeated successions of lime mudstone and stromatolites.

The scarcity of cores in the study area makes difficult the determination of the facies relationships within the Madison. Evidence from the few cores in the Battle Creek area suggests that oil shows are in highly micritic rocks, ranging from lime mudstones to wackestones and wacke-packstones, immediately subjacent to the unconformity.

The micrite-rich rocks are, for the most part, unstratified to poorly stratified, but locally include skeletal packstone to grainstone lenses and layers that range from 3 to 30 cm thick. They are intercalated with concentrations of thin partings of greyish green and, rarely, reddish brown, fissile claystone. Skeletal remains are dominantly crinoidal and brachiopodal, but, in places, solitary rugosan and fine-branching tabulate corals such as *Syringopora* are also present. In thin section, the micrite encloses a trace to 2% detrital

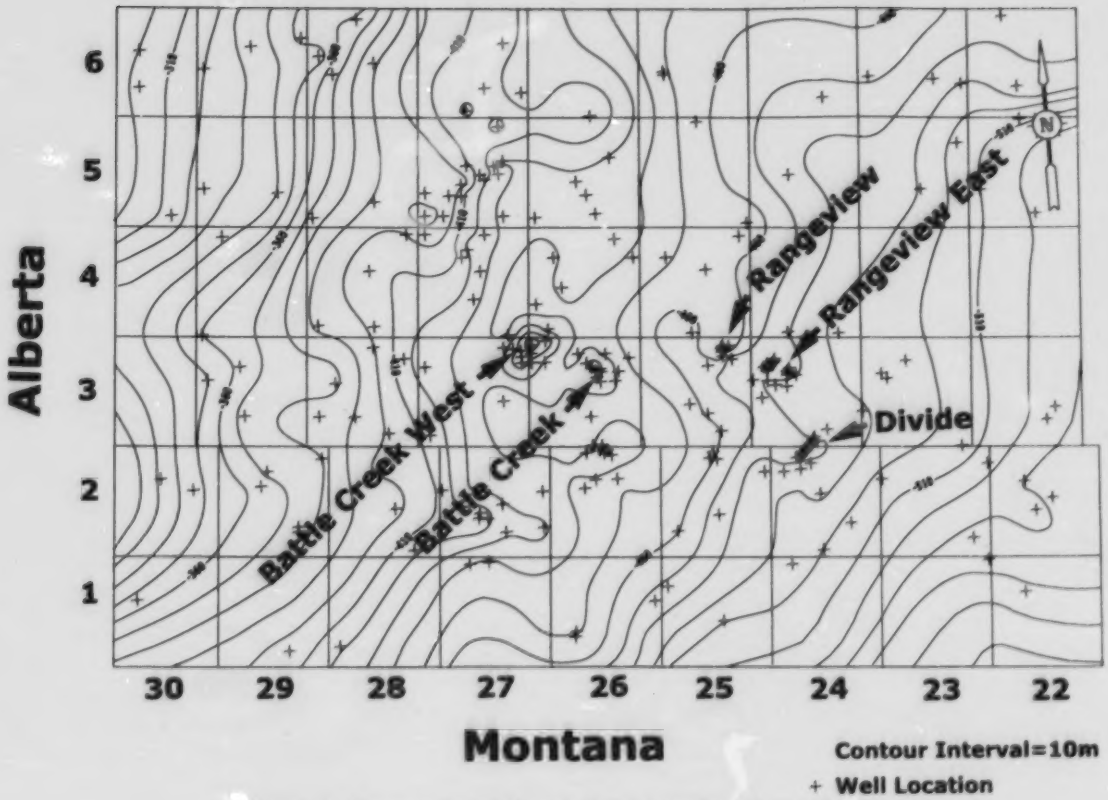

Figure 3 - Structure map on the sub-Mesozoic surface of unconformity.

quartz, and locally shows neomorphic alteration to microspar. Chert is a common accessory in all lithotypes. It is present as nodules and stringers that are clearly visible in hand specimen, and, in thin section, as a fibrous, partial to complete replacement of fossil fragments. Anhydrite may fill solution cavities or replace matrix and fossil debris.

Abundant crinoidal remains and lesser amounts of brachiopod valve and bryozoan zoaria fragments typically range from 0.5 to 7.5 mm across. They generally dominate the packstone and grainstone lithotypes. The amount of micrite in the packstones varies markedly, and in places, the rocks could be more appropriately called wacke-packstones. Thin sections from cores of two separate wells indicate that the fossil fragments in some of the grainstones and packstones may have been partially or totally micritized. Elsewhere, the fragments are fairly well preserved, although some interpenetration and fracturing of in-contact skeletal particles have been observed. Equant calcite spar and syntaxial mono-crystalline overgrowths are the main cementing components of these rocks. Alizarin red S/potassium ferricyanide staining demonstrates that both ferroan and non-ferroan calcite cements are present with the latter being more abundant. The staining shows a zonation of the equant spar thereby indicating phases of ferroan and non-ferroan calcite growth. This zonation is also supported by cathodoluminescence microscopy.

A large area of the subcrop of unit C is dolomitized, particularly the micrite in the lime mudstones, wackestones, and packstones (Kent, 1974). Dolomitization extends to a depth of about 10 m beneath the sub-Mesozoic unconformity. In addition, skeletal particles and equant calcite cement subjacent to the unconformity are extensively dissolved. In places, the rocks are also intensely fractured, reaching the stage of crackle brecciation. Where developed to an extreme, this crackle breccia is difficult to distinguish from the basal breccia of the Gravelbourg.

Cores from wells at 9-19-3-24W3, 16-6-3-25W3, and 14-26-3-25W3 show, proximal to the sub-Mesozoic unconformity, between 0.5 and 1.4 m of white, massive-appearing anhydrite with coarse tabular to acicular crystals beneath the basal breccia of the Gravelbourg or within the upper part of the Madison. The anhydrite is 1.5 m and 0.6 m below the top of the Madison in, respectively, the 9-19 and 16-6 wells, and rests on Madison rocks in the 14-26 well. The anhydrite in the core from the 16-6 well contains silicified carbonate clasts with crinoid columnals, bryozoan zoaria, and brachiopod valves, all of which

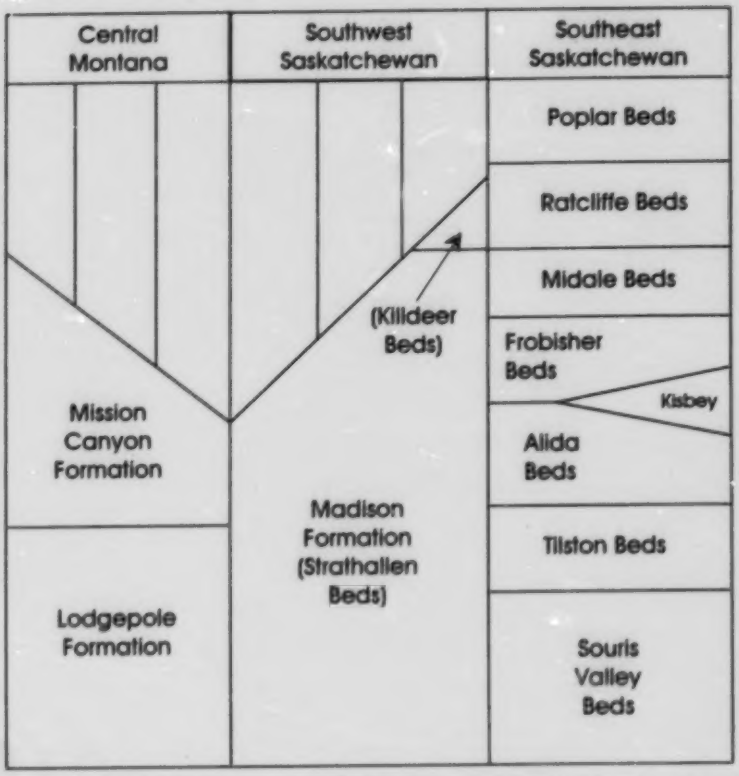

Figure 4 - Mississippian nomenclature chart for southern Saskatchewan and central Montana.

are obvious Madison fossils. However no fossils were observed in the black chert clasts of the 14-26 well.

b) Gravelbourg Formation

The Middle Jurassic Gravelbourg Formation overlies the Mississippian throughout the study area. Its thickness ranges from a minimum of 0 m in the west and in an east-west zone along Township 2 to more than 32 m in the 7-12-6-27W3 well. Some of the thickest deposits shown on the isopach map (Figure 2) may include Upper Watrous dolostone and anhydrite between the base of the lower Gravelbourg and the underlying Madison. Elsewhere, picking the Gravelbourg-Madison contact on well logs without the benefit of core has led to the erroneous inclusion of part of the lower unit of the Gravelbourg within the Mississippian. The error is particularly prevalent where a breccia containing clasts of Madison carbonate is present in the basal part of the Gravelbourg. This mis-identification is due to the high carbonate content of the lower Gravelbourg, giving rise to similar resistivity and SP log signatures for the two units. However, the lower Gravelbourg has a distinct argillaceous signature on the gamma ray curve, which contrasts with the pronounced non-argillaceous character of the Madison. In addition, the differences are easily determined in core through the fossil content and basic lithologic characteristics.

The Gravelbourg is informally divided into two members. The lower member is characterized by yellowish grey to pale yellowish brown, laminated, extremely finely crystalline to sublithographic, partially pyritic dolomicrite layers interbedded with dark grey to dark greenish grey calcareous mudrock. The upper member is dominantly a medium grey to dark greenish grey mudrock with lesser amounts of interbedded siltstone and silty very fine-grained sandstone. The lower member commonly contains chalcedony and megaquartz-filled vugs at or near the contact with the overlying unit, thereby suggesting a period of exposure and disconformity between the two members. The chalcedony is medium bluish grey and the megaquartz is typically present as clear, colourless prisms with bipyramidal terminations. These silica-filled vugs are consistently found at approximately the same stratigraphic level throughout southern Saskatchewan (Kreis, 1991).

Brecciation at the Base of the Gravelbourg

Cores from widely distributed wells have brecciated interbeds in the basal portion of the lower Gravelbourg. At the 1A-27-3-26W3 and 6-27-3-26W3 wells, breccia beds which directly overlie the sub-Mesozoic unconformity surface range in thickness from 0.3 to 2 m and are composed of chert fragments in a matrix ranging from fine quartz sand to marl (Figure 5). At the 6-35-3-25W3 well, two breccia layers with a combined thickness greater than 4 m are present (Figures 5 and 6). Both breccias are matrix-supported and contain 1 to 60 mm diameter, subangular to subrounded clasts of Madison chert and carbonate as recognized through their constituent fossils, especially the abundant crinoid columnals. The matrix of the upper breccia is very pale orange, extremely finely crystalline, earthy dolomicrite; the lower breccia has a dark greenish grey, fairly well indurated, dolomitic mudrock matrix. The upper breccia is also present in the 14-26-3-25W3 core but a one metre thick, massive-appearing anhydrite with very dark grey, angular chert clasts near the base is found in place of the lower breccia.

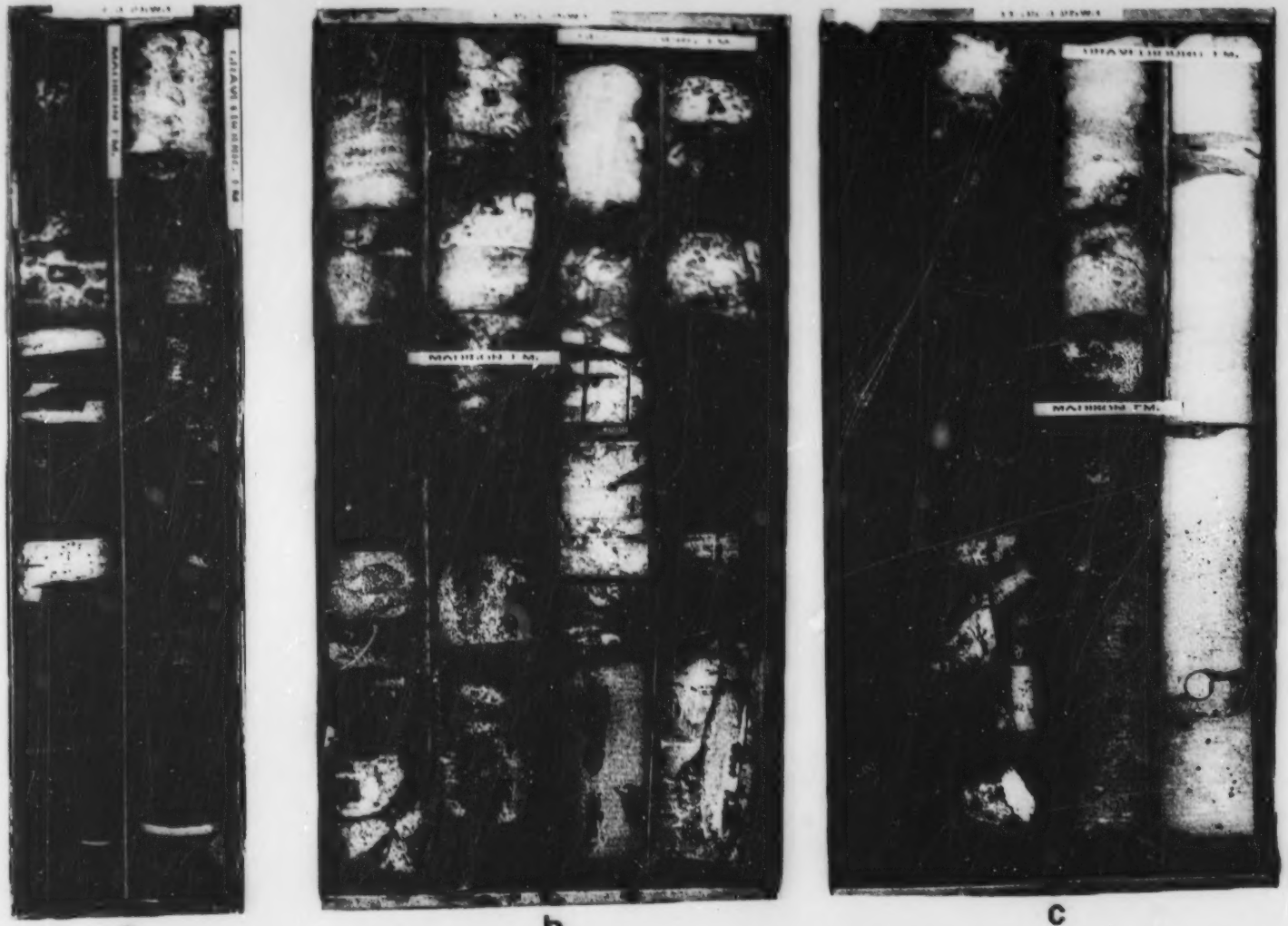

a b c

Figure 5 - Core photographs illustrating the Mississippian-Gravelbourg contact in the: (a) 6-27-3-26W3, (b) 6-35-3-25W3, and (c) 11-35-3-25W3 wells. Crackle brecciation (CB) is recognizable in the 6-27-3-26W3 core. The two types of breccia (A and B) found in the lower Gravelbourg, as illustrated in Figure 6, are visible in the 6-35-3-25W3 well.

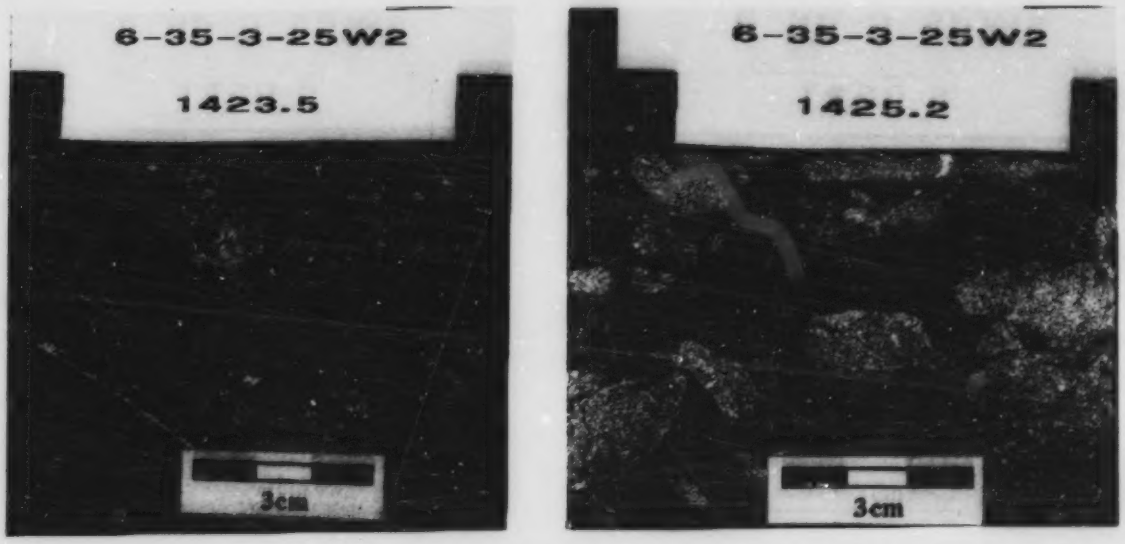

Figure 6 - Two types of breccia found in the lower Gravelbourg. The breccia in the hand specimen on the left is made up of black and dark grey chert clasts. It is typical of the lower Gravelbourg and is widely distributed throughout southern Saskatchewan. It is identified as A in Figure 5. The breccia in the specimen on the right contains clasts of Mississippian carbonate in a mudrock matrix. It is identified as B in Figure 5.

3. Interpretive Geology

a) Depositional History of the Oil-bearing Strata

The three Mississippian lithologic units are interpreted as representing a basin to shelf succession (Kent, 1974). Unit A was deposited below fairweather wave base and is transitional between the underlying deposits of the Bakken Formation and the deeper-water rocks of unit B. Unit B includes both deeper water and slope carbonates, specifically debris flows and tempestites. The rocks of unit C formed in a broad, shallow-sloping, outer ramp setting. Sporadically occurring, thick accumulations of crinoidal grainstone and packstone in unit C represent banks or mounds formed on this outer ramp.

Control wells are, for the most part, so widely distributed that determining the geometry of the thicker grainstone and packstone accumulations is difficult. However, at two localities where wells are sufficiently closely spaced, the thick accumulation of crinoidal grainstone may represent outer ramp banks or mounds. Their high-angle crossbedding suggests current conditions similar to those for crossbedded grainstones observed in Mississippian outcrops on Sage Creek in the Sweetgrass Hills. The geometry and fabric of the outcrop bodies indicate an origin as sand waves. Elsewhere in this Mississippian exposure, however, other crossbedded grainstones appear to be part of high-energy shallowing upward cycles. Since these crossbedded grainstones alternate with laminated carbonates, they may represent ephemeral shoals that vertically accreted to sea level and were then covered by tidal flat deposits. The crossbedded grainstones of the subsurface may be referred to one or the other of these outcrop settings.

The overlying rocks of the lower Gravelbourg are transgressive deposits. In the study area, this transgression flooded a surface on which karsting had played an important role in creating the paleotopography. The surface had probably been irregular and rolling, and had been breached in places by solution holes and collapsed caverns.

b) Influence of Diagenesis on Reservoir Quality

Diagenetic processes that acted upon the heavy oil-bearing rocks of southwestern Saskatchewan (Kent and MacEachern, 1990) include mechanical and early chemical compaction, micritization of skeletal debris, and stages of cementation, chertification, anhydritization, dolomitization, and solution (Figure 7). Micritization, cementation, chertification, dolomitization and solution are of specific significance to characterization of the reservoir rocks in the heavy-oil producing areas.

Strata in the Madison below the reservoir rocks show that the growth of calcite cement in the interparticle porosity of grainstones and packstones has resulted in extensive occlusion of porosity. Alizarin red S/potassium ferricyanide staining and cathodoluminescence analyses indicate that both non-ferroan and ferroan calcite are present. The distribution of ferroan and non-ferroan calcite suggests that cementation commenced with non-ferroan calcite during shallow burial and terminated with ferroan calcite in the deep burial stage (Dorobecki, 1987;

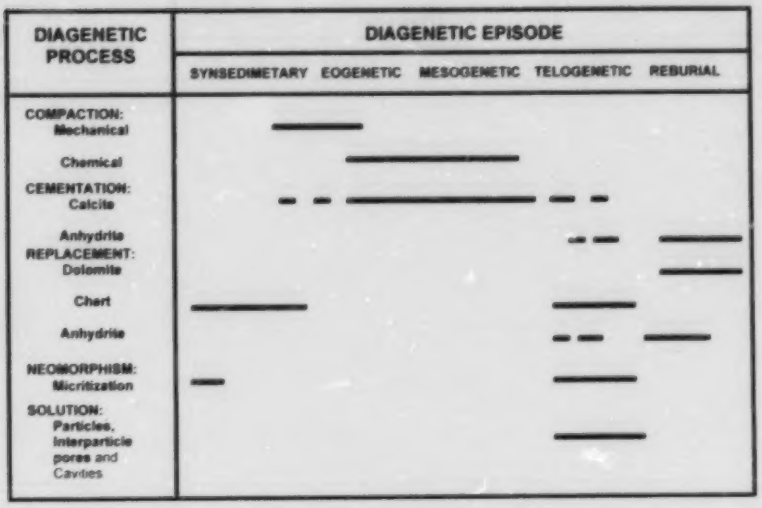

Figure 7 - Chronology of diagenetic events.

Read, 1980). However, in the reservoir zone, solution by meteoric water evidently played a major role in the exhumation of interparticle porosity through total or partial removal of the occluding cements. The less stable ferroan calcite probably acted as the site for initial solution. Meteoric solutions also created biomoldic pores, as well as enhancing pore and pore throat sizes by partial removal of skeletal components rimming the walls of the pore systems. They also produced metre-sized cavities that were later filled by anhydrite.

Partial to total micritization of skeletal remains made the Madison rocks more susceptible to solution and dolomitization, resulting in improved intercrystal porosity. Partial micritization is commonly manifested in micritic rims, but it may also be recognized as large patches of micrite in skeletal particles. In addition to replacing micritized skeletal remains, dolomite has replaced micrite-rich rocks, enhancing their fluid storage and conducting capabilities. In contrast, chertification and anhydrite cementation are two diagenetic processes that have significantly destroyed porosity and have created potential barriers to fluid migration.

According to Kent (1974), dolomitization appears to have been confined to the paleotopographically high regions of the sub-Mesozoic erosion surface. The paragenetic sequence summarized in Figure 7 identifies dolomitization of the rocks subjacent to the sub-Mesozoic unconformity as a re-burial phenomenon, which, according to Kent and Kreis (1995), occurred while the erosion surface was being flooded by lower Gravelbourg marine waters. A mechanism similar to this was proposed for the origin of present-day dolomite in carbonates of the Bahama Banks (Whitaker *et al.*, 1994). In this Jurassic setting, marine waters with salinities slightly above normal are presumed to have refluxed through the Mississippian carbonates immediately beneath the erosion surface, dolomitizing a shallow zone beneath the unconformity. The dolomitized zone was extended laterally as seawater progressively inundated the exposure surface. This process operated only where lower Gravelbourg seawater was in direct contact with the underlying Mississippian rocks. Where Mississippian carbonates are overlain by interbedded dolostone, anhydrite and dolomitic mudstone of the Watrous Formation, they are not dolomitized.

Some of the chert found in the Mississippian is most likely early diagenetic, especially that found in the thinly layered rocks of unit B. Most of the chert in this unit appears to be a replacement of carbonate. In some cores, the chert appears as though it may have been disturbed during seafloor slumping. The porosity-occluding chert is a combination of chalcedonic and megaquartz (Kent, 1974). The fasciculate crystals grew isopachously on the margins of the pores and the megaquartz filled the remaining void. In addition, some chalcedonic quartz replaced skeletal remains. This chert is commonly found in strata near the sub-Mesozoic unconformity, suggesting that the silica may have been produced during exposure or possibly leached from overlying siliciclastic sediments.

The anhydrite is rarely replacive and more commonly void filling. The voids range from interparticle and vuggy pores to fractures and metre-sized cavities (Kent, 1974; Kent and MacEachern, 1990). The thick anhydrite intervals and associated breccias in the 9-19-3-24W3, 16-6-3-25W3, and 4-26-3-25W3 wells in the Rangeview area suggest anhydrite infill of karst solution holes or caverns.

4. Development and Production History

As previously noted, Mississippian low-gravity oil reservoirs in southwestern Saskatchewan have gone through several phases of exploration and exploitation. Following a long period of relative dormancy from 1968 to 1989, Cirque Energy gave new life to the Battle Creek area with the reactivation of the 6-27-3-26W3 well and the drilling of two horizontal wells. A flurry of drilling activity in 1994 to 1995, firstly by Inverness and later by Renaissance and Merit, resulted in the discovery of more low-gravity reserves in Mississippian strata at Rangeview, Rangeview East, and Divide. More recent drilling (1999) has led to the discovery of additional Mississippian low-gravity reserves in the Battle Creek West area. Since 1966, Mississippian wells in the study area have produced

374 863 m^3 of oil (2.36 x 10^6 BO). Battle Creek is the most prolific and oldest producing area. Its Mississippian reservoir rocks have yielded 280 202 m^3 of oil (1.76 x 10^6 BO) (Table 1).

Table 1 demonstrates that large volumes of water accompanying oil production detrimentally influence the life-expectancy of Mississippian producing wells. Production histories for most wells show that the water/oil ratios become greater than unity after only a few months of production.

5. Controls on Reservoir Distribution and Future Exploration

Kent and Kreis (1995) proposed that further exploration for low-gravity oil reservoirs might be most fruitful along the north-facing flank of the previously described paleo-upland region. Production data suggest that the most favourable reservoir and trapping conditions occur where a deep-seated structure apparently causes draping of subcropping strata such as at Battle Creek West and Battle Creek. Figures 2 and 3 demonstrate that Rangeview, Rangeview East, and Divide are controlled primarily by paleotopographic positive elements on the Madison subcrop. Each of these paleotopographic features is identifiable by thinning of the overlying lower Gravelbourg Member. In addition diagenesis, particularly the processes of solution and dolomitization, also played an important role in forming the reservoir pore systems in all of the localities. Solution resulted in the exhumation of early cemented interparticle porosity as well as the creation of biomoldic vugs and karst-related cavities. Although many of the latter are filled by anhydrite, prefill roof- and wall-collapse produced a fracture system that enhanced reservoir potential. Dolomitization improved the reservoir quality of the micritic rock. Porosity-enhancing diagenetic processes, including solution and dolomitization, created reservoir rocks with pore volumes averaging 27% and gas permeabilities ranging from 87 to 542 md (Kent and MacEachern, 1990).

Using these criteria, low-gravity oil reservoirs may be present in the paleotopographically highest Mississippian rocks at several localities where the lower Gravelbourg is thin or absent in Township 2 between Ranges 22 and 29 west of the Third Meridian (Figure 2). Areas of possible hydrocarbon entrapment are further defined where evidence of structural closure is present (Figure 3). One of the more highly potential of these is in the Supreme area of Township 2, Range 27 west of the Third Meridian, where oil has been observed in a Mississippian core, and a drillstem test from a second well recovered sulphurous oil and water (Kent and MacEachern, 1990). Another region of high potential is in Township 2, Range 26 west of the Third Meridian where two positive paleotopographic features occur on the Mississippian subcrop. Their oil-bearing potential is enhanced by their position near the northern edge of the Mississippian paleo-upland. A third locality may be an area around the 7B-16-2-22W3 well. A heavily oil-stained core was taken from the Upper Member of the Shaunavon Formation and geophysical well logs show porosity near the Mississippian subcrop. Unfortunately, the Mississippian was neither cored nor drillstem tested, and cuttings are inconclusive.

Kent and MacEachern (1990) also recommended the Oxarat structure for potential oil discovery. The Imperial et al Oxarat 14-7-5-27W3 well was drillstem tested in the Mississippian. The test straddled the unconformity between the lower Gravelbourg and Madison and yielded 1286 m of sulphurous gas-cut and oil-cut water. Although outside the zone where the Madison subcrop is dolomitized, the presence of oil suggests the structure may have some Mississippian potential. Its prospectivity is underscored by a cumulative production of over 21 000 m^3 oil and only 11 m^3 water from perforations in the uppermost part of the Lower Gravelbourg in the Canyon Creek Battle Creek 6-23-5-27W3 well.

6. Summary and Conclusions

The Battle Creek Madison low-gravity oil pool has a long but interrupted production history. The initial vertical wells had high yields, in spite off the low gravity of the oil and the carbonate composition of the reservoir rocks. The subsequent drilling of several horizontal wells has significantly improved that production. Additional exploration in the area since 1994 has brought on stream several other Mississippian Madison low-gravity oil-producing areas, namely Battle Creek West, Rangeview, Rangeview East, and Divide. These Mississippian reservoirs have yielded a total of 374 863 m^3 of oil (2.36 x 10^6 BO) (Table 1).

Four factors contributing to oil entrapment and the high productivity within Mississippian strata in the Battle Creek area are: 1) diagenetic alteration of the reservoir rocks; 2) structural attitude and paleotopographic setting on the sub-Mesozoic unconformity surface; 3) an active water drive; and 4) bottom hole temperatures in the order of 57°C. In terms of diagenetic alteration, micritization of skeletal debris, solution and

Table 1 - Cumulative oil and water production for low-gravity oil producing areas of southwestern Saskatchewan.

Field	No. of Wells	Cumulative Oil (m^3)	Cumulative Water (m^3)	Gross WOR	Production Period
Battle Creek	8	280 201.8	5 300 134.4	18.9	08/66-03/00
Battle Creek West	5	10 734.2	12 090.3	1.13	03/98-03/00
Rangeview	5	44 102.6	480 889.4	10.9	06/94-03/00
Rangeview East	10	34 654.0	203 739.2	5.8	01/95-08/97
Divide	5	5 170.8	77 511.1	15.0	12/95-01/98
Total		**374 863.4** [1]	**6 074 364.4** [2]	**16.2**	

Note: [1] 2,358,504.1 BO (barrels of oil); [2] 3,822,4980.4 bw (barrels of water);
WOR, water to oil ratio.

dolomitization of micritic textures have been important porosity- and permeability-enhancing processes. However, all three processes would not have been as effective had not the paleotopographic position of the reservoir rock been positive so the Madison was exposed at the pre-Mesozoic erosion surface. Oil entrapment at Battle Creek and Battle Creek West is aided by Laramide orogenic rejuvenation of a Precambrian structurally controlled monadnock that underlies the Battle Creek area. It may have also played a role in creating trapping conditions at Rangeview, Rangeview East, and Divide.

Drillstem tests from wells penetrating the Mississippian Madison in the Battle Creek area indicate that an active water drive is probably maintained by recharge in the Montana highlands to the south. This water drive has established a northerly fluid migration and a northward hydrodynamic displacement of the trapped oil at Battle Creek, Battle Creek West, Rangeview, Rangeview East, and Divide. The high bottom hole temperatures in the area have undoubtedly improved the fluidity of the oil in spite of its low API gravity.

The main exploration targets in this part of southwestern Saskatchewan have, in recent years, been shallower reservoirs such as the oil-bearing Middle Jurassic Shaunavon and the gas-prone Upper Cretaceous Second White Specks Formation. Both commonly occur on regional structures and positive paleotopographic features that may also have low-gravity oil in Mississippian rocks. Termination of wells in shallower reservoirs may mean that operators have missed potential production from the Mississippian.

7. Acknowledgments

The authors acknowledge the assistance of Doug Harvey, graduate student, University of Regina, who gathered much of the production data for the study area.

8. References

Dorobecki, S.L. (1987): Petrography, geochemistry, and origin of burial diagenetic facies, Siluro-Devonian Helderberg Group (carbonate rocks), central Appalachians; Bull. Amer. Assoc. Petrol. Geol., v71, p492-514.

Kent, D.M. (1974): A Stratigraphic and Sedimentologic Analysis of the Mississippian Madison Formation in Southwestern Saskatchewan; Sask. Dep. Miner. Resour., Rep. 141, 85p.

_____ (1995): Horizontal well production from Mississippian strata, Battle Creek Field, southwestern Saskatchewan: New life for a dormant reservoir; Third Internat. Williston Basin Horizontal Well Workshop, North Dakota Geol. Surv./Sask. Energy Mines, pB9-1 to B9-20.

Kent, D.M. and Kreis, L.K. (1995): Trapping mechanisms for Mississippian heavy oil reservoirs in southwestern Saskatchewan; *in* Summary of Investigations 1995, Saskatchewan Geological Survey, Sask. Energy Mines, Misc. Rep. 95-4, p129-134.

Kent, D.M. and MacEachern, J.A. (1990): Heavy Oil Potential of the Mississippian Madison Formation in Southwestern Saskatchewan; University of Regina, Energy Research Unit Contribution No. 199, Sask. Energy Mines, Open File Rep., 70p.

Kreis, L.K. (1991): Stratigraphy of the Jurassic System in the Wapella-Moosomin Area, Southeastern Saskatchewan; Sask. Energy Mines, Rep. 217, 90p.

Kreis, L.K., Ashton, K.E., and Maxeiner, R.O. (2000): Geology of the Precambrian basement and Phanerozoic strata in Saskatchewan; Lower Paleozoic Map Series, Sask. Energy Mines, Open File Rep. 2000-2, Sheet 1 of 8.

Read, J.F. (1980): Carbonate ramp to basin transitions and foreland basin evolution, Middle Ordovician, Virginia Appalachians; Bull. Amer. Assoc. Petrol. Geol., v64, p1575-1612.

Sawatzky, H.B., Agarwal, R.G., and Wilson, W. (1960): Helium Prospects in Southwest Saskatchewan; Sask. Dep. Miner. Resour., Rep. 49, 26p.

Whitaker, F.F, Smart, P.L., Vahrenkamp, V.C., Nicholson, H., and Wogelius, R.A. (1994): Dolomitization by near normal seawater (?), field evidence from the Bahamas; *in* Purser, B., Tucker, M., and Zenger, D. (eds.), Dolomites, IAS Special Publ. No. 21, p111-132.

Onlap within the Mississippian Midale Beds of Southeastern Saskatchewan

J.H. Lake [1]

Lake, J.H. (2001): Onlap within the Mississippian Midale Beds of southeastern Saskatchewan; *in* Summary of Investigations 2001, Volume 1, Saskatchewan Geological Survey, Sask. Energy Mines, Misc. Rep. 2001-4.1.

The Midale Beds in southeastern Saskatchewan have been economically important for many years. In the last decade, drilling activity has resurged due largely to development of horizontal drilling technology. The location of the subcrop edge of the Midale Beds and of oil pools within this unit are outlined in Figure 1.

The Midale Beds were deposited in the Williston Basin Mississippian epeiric sea. Their lithological variation has made interpretation of their environments of deposition difficult. In contrast to a ramp facies type, shallow-water facies have been found to extend down dip for tens of kilometres. Midale strata onlap the Frobisher Evaporite surface, which appears to have had considerable relief because unconformities related to underlying depositional cycles had not been fully accommodated by Midale time (major erosional events had, for example, taken place at the end of Alida and after the first cycle of Frobisher deposition). In addition, uplift and tilting occurred at the end of Frobisher Evaporite time. This is evident because the Midale Beds pinch out toward the east (Figure 2). The lower portion of the Midale Beds, informally known as the "Vuggy", onlaps the Frobisher Evaporite in the Weyburn, Midale, and Steelman pools but did not transgress the evaporite in fields farther east because of increased relief. The Vuggy sediments were exposed and eroded, developing an extensive vuggy secondary

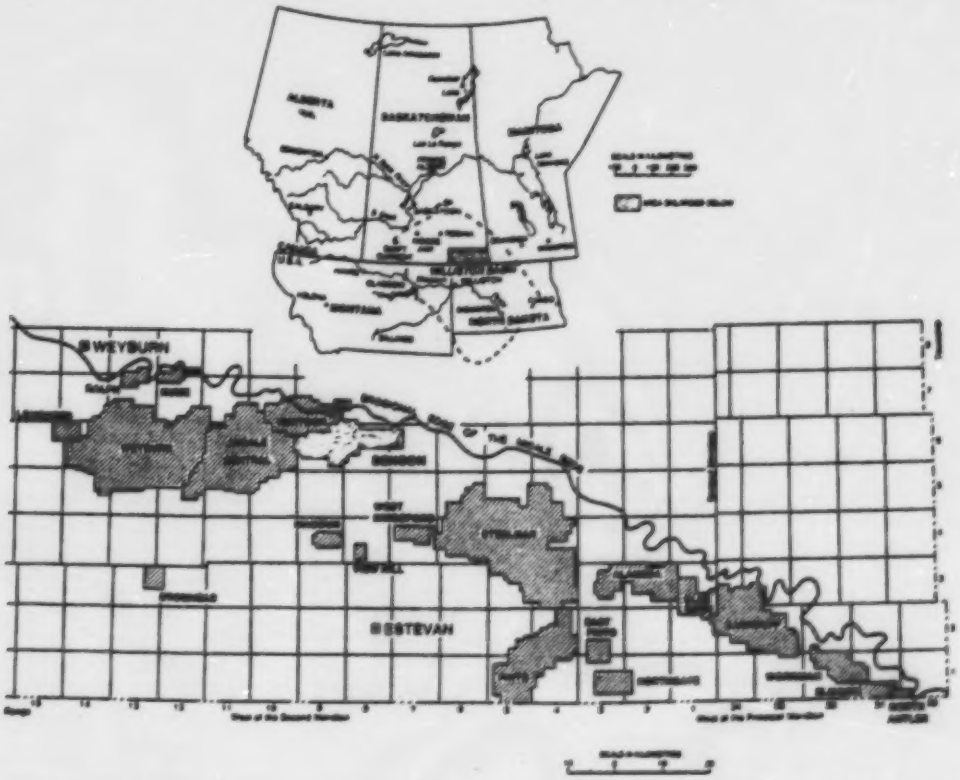

Figure 1 - Distribution of oil pools along the Midale Beds subcrop edge in southeastern Saskatchewan (after Smith, 1980).

[1] Lake Geological Services Inc., 1911 MacDonald Drive, Swift Current, SK S9H 1M1.

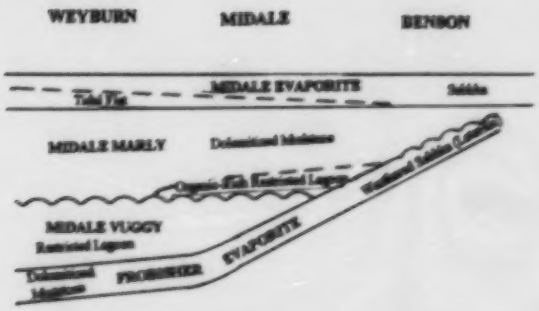

Figure 2 - Idealized west-east cross section through the Midale Beds in southeastern Saskatchewan. The Midale Vuggy and Marly onlap the Frobisher Evaporite. At Benson Pool, the Midale Evaporite onlaps the Frobisher Evaporite, which here and to the east shows laterite development due to exposure and weathering soon after deposition.

porosity. Evidence of exposure includes soil development on top of the Vuggy at Steelman Pool. The southwesterly erosional trend influenced subsequent Marly sedimentation.

The Midale Marly overlies the Midale Vuggy and onlaps the Frobisher Evaporite surface with considerable relief at Benson Pool. The Marly is so thin that the Midale Evaporite beds almost onlap the Frobisher Evaporite (Figure 2). It varies in reservoir quality. At Weyburn Pool, all shallow-water facies show extensive reflux dolomitization. In pools to the east, the reservoir is restricted to a single shallowing event within the Midale. Here, dolomitization took place when conditions were restricted and local ponding occurred, enabling fresh-water mixing to take place (Figure 3). Dolomitization was greatest in the most restricted lagoons. The rock is limestone and is not of reservoir quality in areas that were not exposed to fresh-water mixing. East of Weyburn, the Midale Marly contains abundant organic-rich layers that were originally deposited in restricted-circulation bays. In these layers are transported crinoids, *Syringopora*, bivalves, and oolites introduced by storm activity from outside the organic-rich bays. Very shallow-water conditions are interpreted from the abundance of calcispheres, ostracods, and *Ortonella* algae. Figure 3 shows the geometry and shallow nature of these accumulations (modified after Lake, 1998).

The underlying and overlying evaporites likewise show a shallowing trend in facies variations from west to east. Across most of the Weyburn Pool, the Frobisher Evaporite is an argillaceous dolomitized mudstone deposited seaward of the sabkha (Figures 4 and 5). In contrast, it includes near-sabkha tidal-flat mudstone and exposed sabkha facies (including extensive laterization of the carbonate fraction) at Benson and pools farther east (Figure 6). The Midale Evaporite contains stacked argillaceous tidal-flat mudstone (referred to as the "Three Fingers" in local drilling terminology) at Weyburn. In contrast, equivalent rocks are near-sabkha tidal-flat mudstone at Benson and pools to the east.

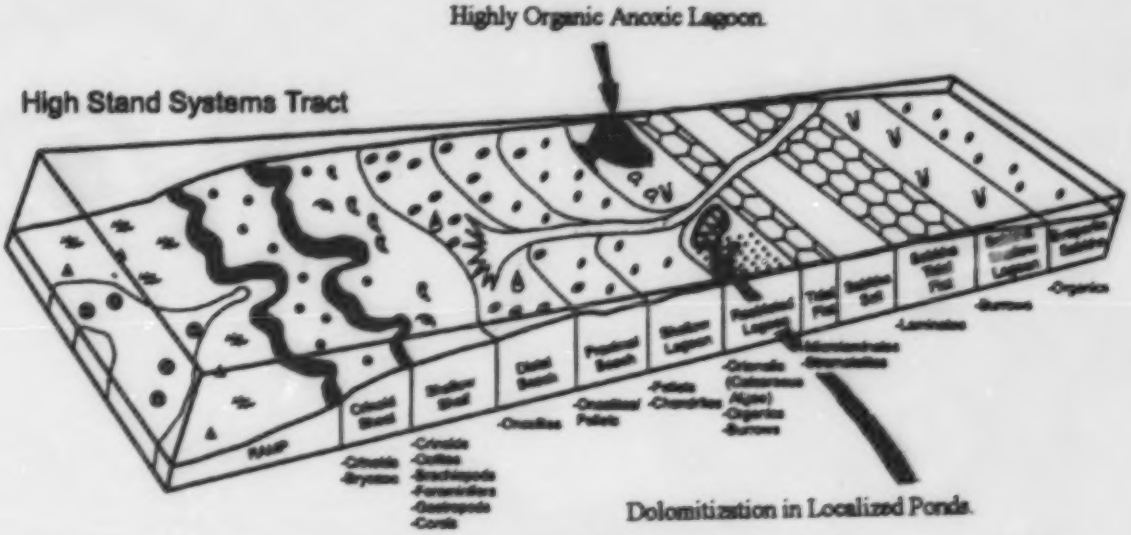

Figure 3 - Facies model for the Midale Beds (modified after Lake, 1998). Midale Marly dolomitization occurred in very restricted lagoonal ponds adjacent to the sabkha margin. Highly organic-rich lagoons also developed in response to restricted circulation (contain calcispheres, crinoids, and coral allochems transported by storms).

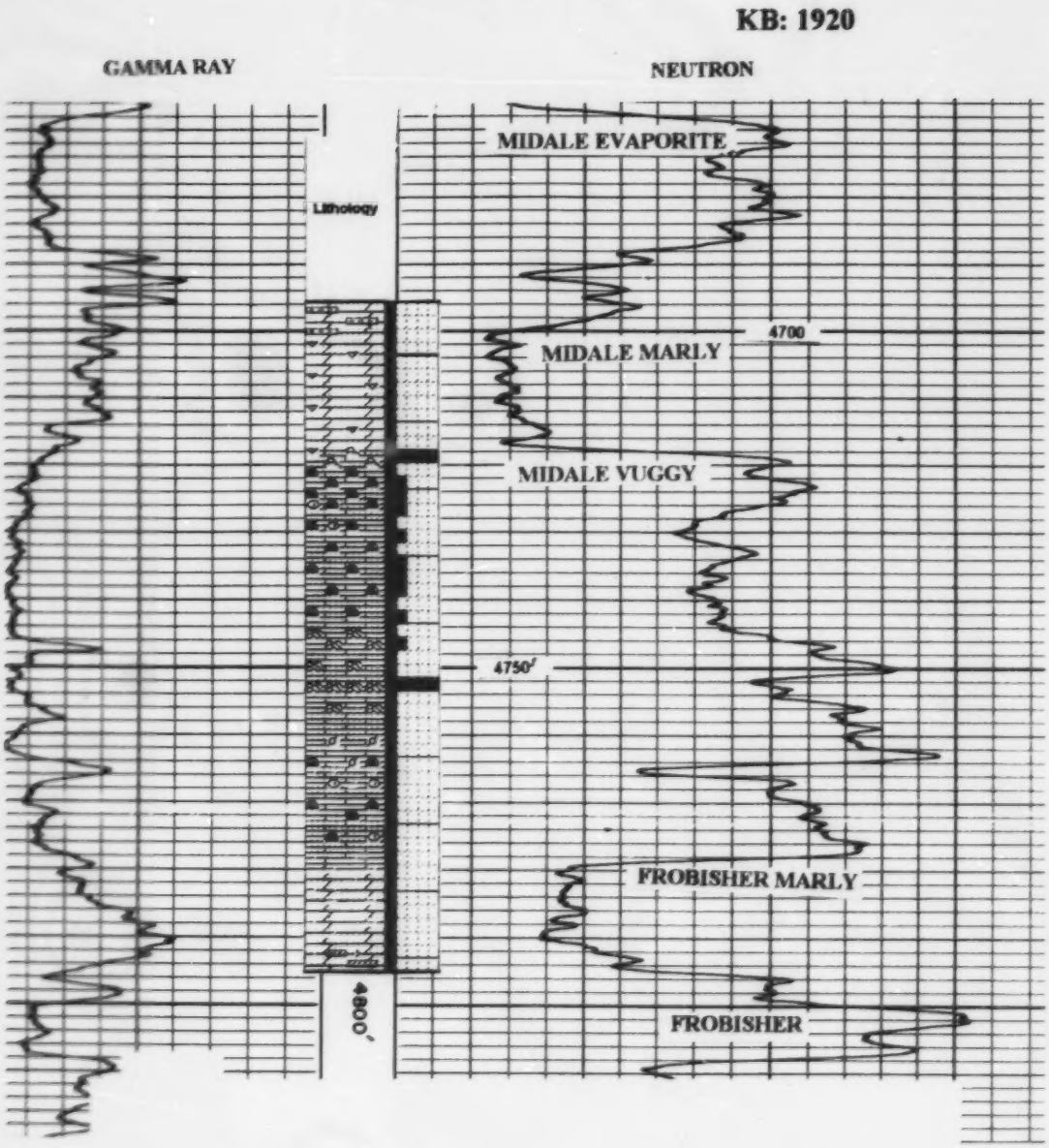

Figure 4 - Typical Midale Beds interval at Weyburn. The Frobisher Marly is a dolomitized mudstone facies distal to the Frobisher Evaporite. The Midale Vuggy is relatively thick and contains stacked Ortonella mudstones and wackestones. The Midale Marly is dolomitized mudstone with Planolites burrows. The Midale Evaporite contains stacked tidal-flat mudstones at the base (locally named the "Three Fingers"). Refer to legend on Figure 6.

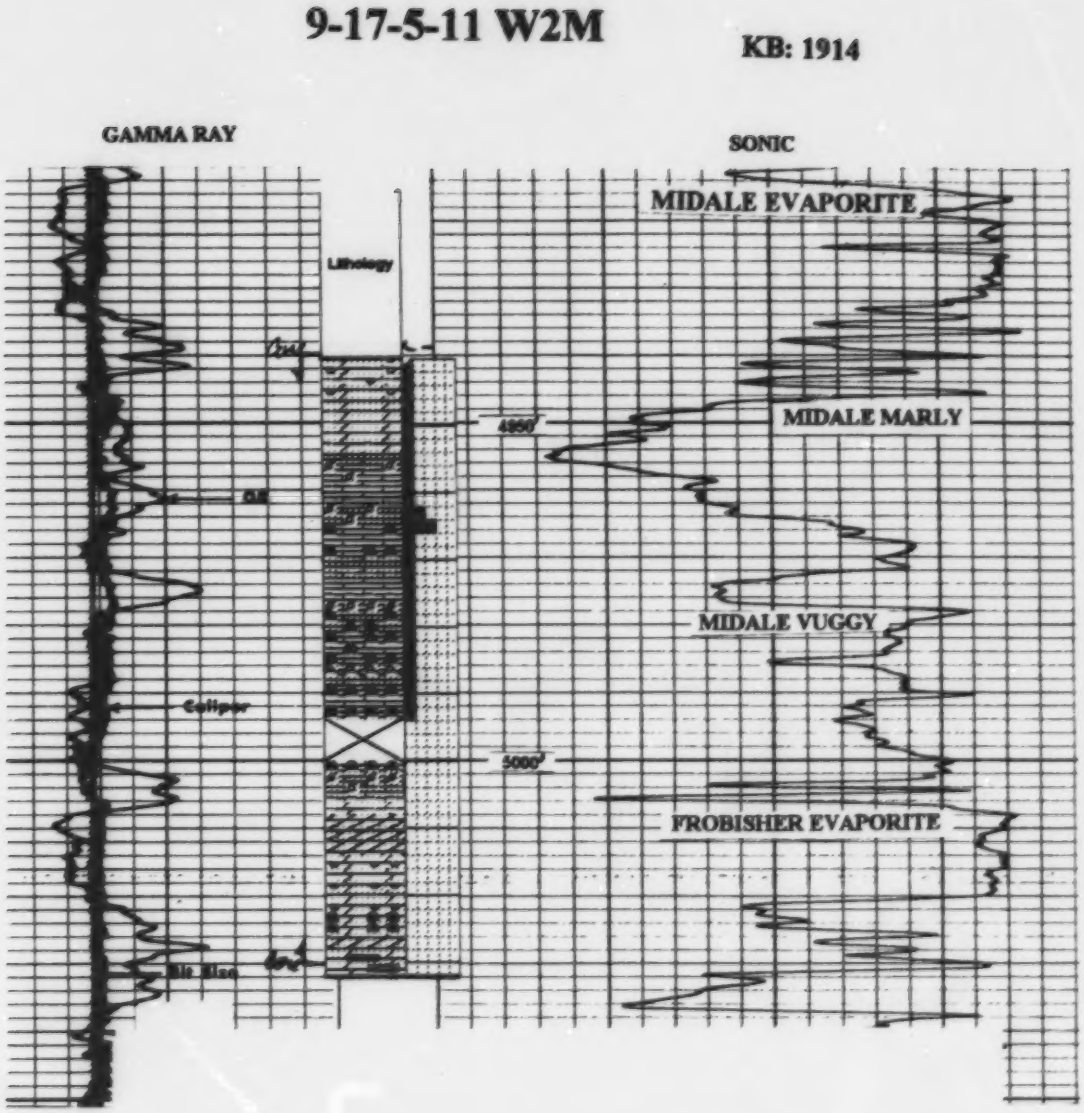

Figure 5 - Typical Midale Beds interval at Midale Pool. The Midale Vuggy contains stacked Ortonella mudstones with some vuggy porosity development. The lower part of the Midale Marly is organic-rich lime wackestone with crinoids and calcispheres. It is included with the Marly because of its close association with the overlying very restricted lagoonal dolomitized mudstone. The limestone facies of the Marly was deposited in a shallow lagoon with restricted circulation immediately adjacent to the sabkha/shoreline. The upper part of the Midale Marly is dolomitized mudstone. The Midale Evaporite contains stacked tidal-flat mudstone at the base (locally named the "Three Fingers"). Refer to legend on Figure 6.

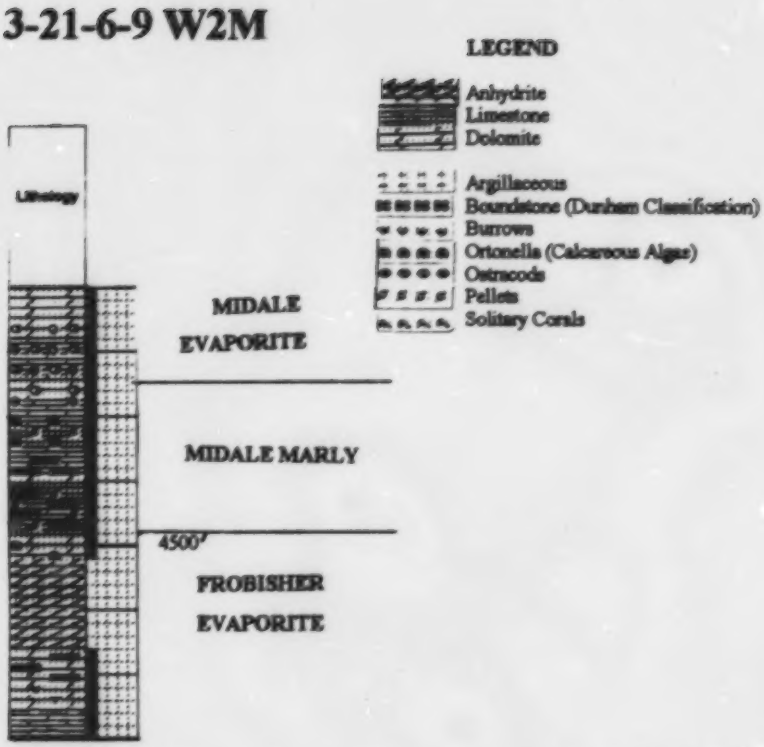

Figure 6 - Typical Midale Beds interval at Benson Pool (core description; no geophysical logs available to the author). The basal pelletal mudstone of the Midale Marly was exposed and underwent anhydrite infill of dissolution vugs. Above, it contains ostracod, Ortonella, and pelletal mudstone, with reservoir development restricted to the uppermost very restricted lagoonal mudstone. The Midale Evaporite contains stacked near-sabkha tidal-flat mudstone and organic-rich restricted lagoonal mudstone.

References

Lake, J.H. (1998): A Mississippian epeiric shelf facies model for the Williston Basin; *in* Christopher, J.E., Gilboy, C.F., Paterson, D.F., and Bend, S.L. (eds.), Eighth International Williston Basin Symposium, Sask. Geol. Soc., Spec. Publ. No. 13, p69-71.

Smith, S.R. (1980): Petroleum Geology of the Mississippian Midale Beds, Benson Oil Field, southeastern Saskatchewan, Sask. Miner. Resour., Rep. 215, 98p and accomp. maps.

Investigating CO_2 Storage Potential of Carbonate Rocks during Tertiary Recovery from a Billion Barrel Oil Field, Weyburn, Saskatchewan: Part 1 – the Geoscience Framework (IEA Weyburn CO_2 Monitoring and Storage Project)

C.F. Gilboy, F.M. Haidl, L.K. Kreis, and O.G. Burrowes [1]

Gilboy, C.F., Haidl, F.M., Kreis, L.K., and Burrowes, O.G. (2001): Investigating CO_2 storage potential of carbonate rocks during tertiary recovery from a billion barrel oil field, Weyburn, Saskatchewan: Part 1 – the Geoscience Framework (IEA Weyburn CO_2 Monitoring and Storage Project); *in* Summary of Investigations 2001, Volume 1, Saskatchewan Geological Survey, Sask. Energy Mines, Misc. Rep. 2001-4.1.

1. Introduction

In Western Canada, the application of CO_2 injection for enhanced 'tertiary' oil recovery is a relatively recent addition to the arsenal available to reservoir engineers. The first successful application of CO_2 as a miscible fluid in Western Canada began in 1984 at Joffre Field, a Cretaceous marine siliciclastic reservoir in southern Alberta. A significant portion of the remaining proven conventional oil reserves in Western Canada resides in large, mature Paleozoic carbonate fields such as the Mississippian Weyburn Field in southeastern Saskatchewan. In combination with economically dictated tertiary recovery schemes, these large fields have potential as suitable sites for future geological storage of anthropogenically produced greenhouse gases. An immediate challenge to geoscientists is to assess the ability of these carbonate containers to store CO_2 for geologically significant lengths of time. Storage of this kind is currently in progress in siliciclastic rocks beneath the North Sea, where, at the Sleipner Field, the Norwegian oil company, Statoil, has been injecting about one million tons/year CO_2 into a saline aquifer, the 1000 m deep Middle to Late Miocene Utsira Formation, since 1996.

The CO_2 miscible flood recently initiated by PanCanadian at the Weyburn Field provides an ideal natural laboratory to begin an investigation into a carbonate-reservoir assessment process. To this end, the International Energy Agency (IEA) and a consortium of industry and government partners have designed a comprehensive suite of research and monitoring activities with, as their prime objective, assessing the capacity of a carbonate oil reservoir to store CO_2 over time. For monitoring purposes, the Weyburn Field has several advantages over Sleipner, in particular its easy access, the availability of very extensive pre-CO_2 injection geological and reservoir data dating from the field's discovery in 1954, and the dense drilling pattern that will help enable CO_2 movement to be readily tracked. A multinational, multidisciplinary approach is being used, with six main task areas initially involved: 1) collecting field data and samples; 2) investigating the wider geoscience framework; 3) geochemical sampling, monitoring, and prediction; 4) monitoring CO_2 movement; 5) evaluating CO_2 storage performance; and 6) calculating the economics of CO_2 storage. Project and task interim results are expected to be reported at regular intervals in a variety of ways including future *Summaries of Investigations*, with final products becoming publicly available in 2004 or 2005. The overall budget is estimated at over $14 million (Canadian). Whilst a substantial proportion of the required funding is now in place, efforts to obtain the balance continue.

2. Objectives

To help the project meet its objective, the main problems to be investigated in the geoscience framework task area include: i) the distribution of porosity and permeability within the Weyburn reservoir, in laterally equivalent strata and in underlying and overlying rocks; ii) the distribution and role of fractures within the Weyburn reservoir, in laterally equivalent strata and in underlying and overlying rocks; iii) the distribution of fluids within the Weyburn reservoir, in laterally equivalent strata and in underlying and overlying rocks; iv) factors controlling the distribution of porosity, permeability, fractures, and, ultimately, fluid flow; v) migration pathways of the injected CO_2; and vi) CO_2 trapping mechanisms in the reservoir. Resolving such problems requires understanding of the relationships between sedimentation, diagenesis, salt dissolution, tectonics, and fluid flow pathways and barriers of the entire sedimentary section from the contact of Precambrian crystalline basement with Cambrian sediments to the present-day surface over a distance of up to 100 km from the Weyburn Field (Figure 1).

3. Project Structure

The geoscience framework project has been subdivided into five main components: 1) pre-Mississippian geology; 2) Mississippian and post-Mississippian

[1] PanCanadian Resources, 150 - 9th Avenue SW, P.O. Box 2850, Calgary, AB T2P 2S5.

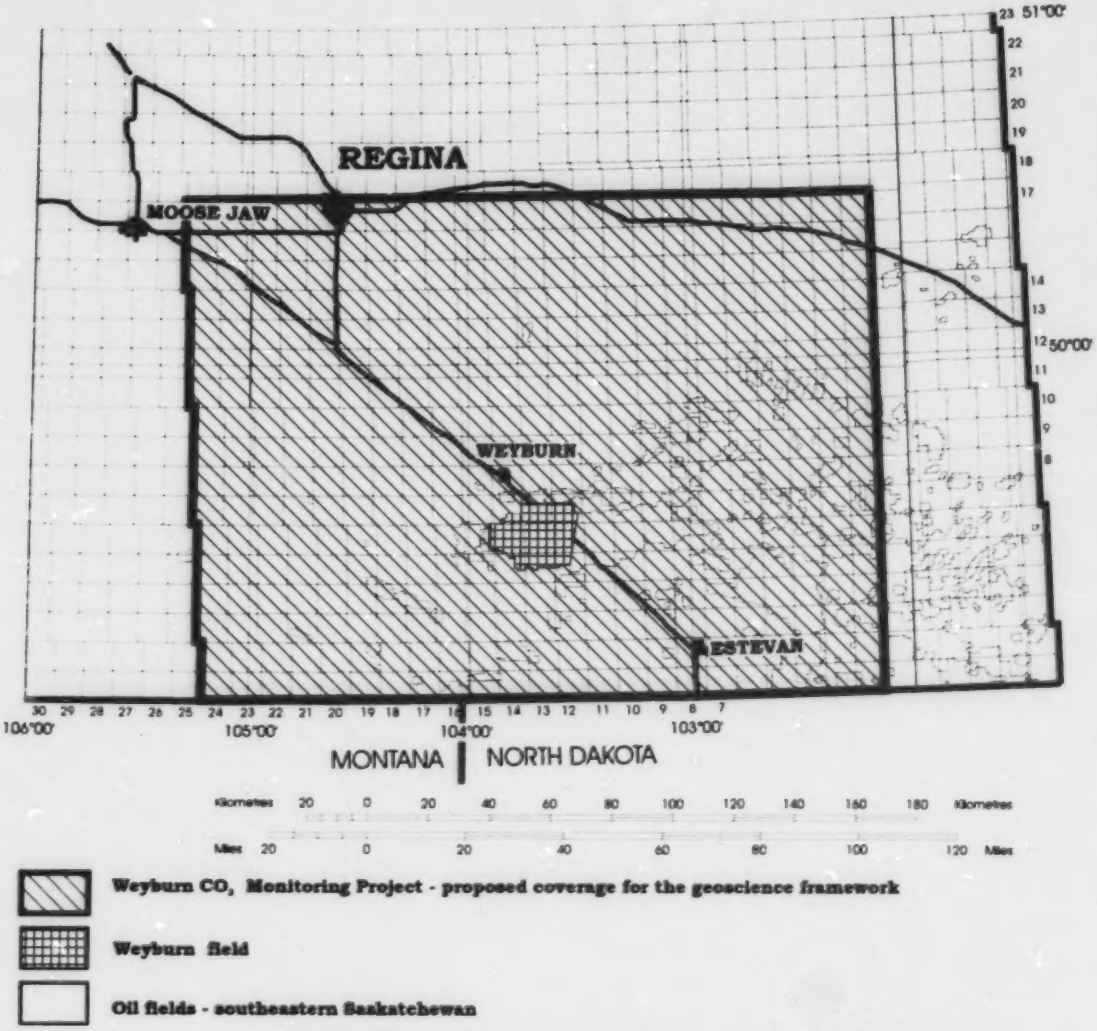

Figure 1 - Location of the IEA CO_2 Monitoring and Storage Project's Geoscience Framework study area.

geology; 3) hydrogeology; 4) reflection seismic studies; and 5) geoscience synthesis (Figure 2). In addition, detailed Weyburn Field geological information from PanCanadian and other sources will be incorporated into all components as necessary.

In order to produce valid and valuable results, the need to assemble a team with expertise in different geoscience disciplines was recognized from the project's early beginnings in 1999. Saskatchewan Energy and Mines took a lead role in inviting experts from the earth sciences departments of several western Canadian universities to participate (Figure 2). Also recognized was the need for a contract research scientist who, based with Saskatchewan Energy and Mines, will co-ordinate the various tasks and have overall responsibility for synthesizing and interpreting the various datasets to build a comprehensive geoscience framework of the study area.

4. Project Participants

Saskatchewan Energy and Mines, under the leadership of Chris Gilboy, is responsible for pre-Mississippian geology and for co-ordination of the project. The study of the geology of Devonian strata, with emphasis on evaporite distribution in the study area, will be led by Kim Kreis. Fran Haidl will co-ordinate studies of the influence of the geological evolution of pre-Mississippian strata on the sedimentology, diagenesis, and distribution of porosity and permeability in Mississippian reservoirs.

The University of Alberta, under the leadership of Dr. Ben Rostron, is responsible for quantifying the 3-D fluid-flow rates and directions with a primary objective of identifying potential CO_2 leakage pathways.

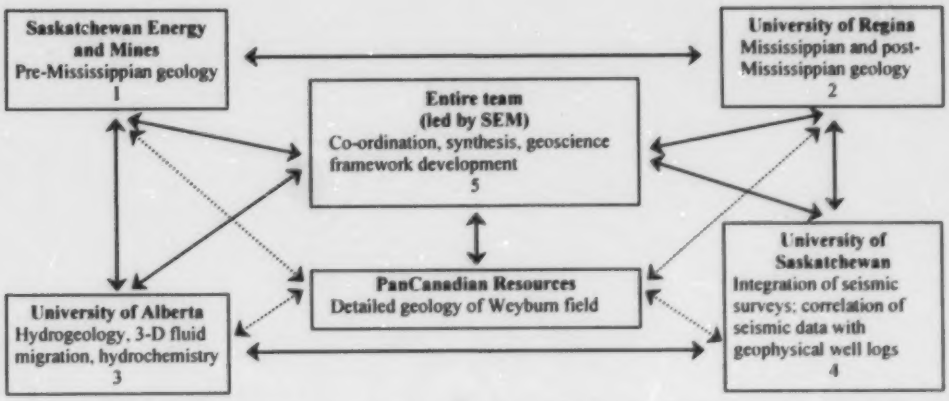

Figure 2 - Information-flow diagram for participants in the Geoscience Framework synthesis (not shown are the direct links between 1 and 4, and 2 and 3).

The University of Saskatchewan, under the leadership of Dr. Zoli Hajnal, is initially to reprocess existing seismic reflection and wireline information, then, in collaboration with the co-ordinating geoscientist, to integrate the resulting data with geological information supplied by other team members to build a three-dimensional stratigraphic model of the study area.

The University of Regina, under the leadership of Dr. Hairuo Qing, is to study the geology of Mississippian and post-Mississippian strata with emphasis on stratigraphic, sedimentological, diagenetic, and fracture-trend analyses. Dr. Katherine Bergman is a co-researcher with responsibility primarily for clastic strata above Mississippian rocks.

PanCanadian Resources, through its Voyageur Business Unit, will provide geological expertise and information that is helpful towards clarifying understanding of geological relationships in and immediately around the Weyburn Field.

5. Current Status

In mid-February 2001, budgets were allocated to team partners in the following amounts:

University of Alberta	$50,000
University of Saskatchewan	$148,000
University of Regina	$50,000
Saskatchewan Energy and Mines	$110,000
Total	**$358,000**

At the time of writing (early March 2001), various agreements have yet to be signed and other minor logistical obstacles overcome before research into the geoscience framework of the wider Weyburn area begins in earnest.

Investigating CO_2 Storage Potential of Carbonate Rocks during Tertiary Recovery from a Billion Barrel Oil Field, Weyburn, Saskatchewan: Part 2 – Reservoir Geology (IEA Weyburn CO_2 Monitoring and Storage Project)

G. Burrowes [1]

Burrowes, G. (2001): Investigating CO_2 storage potential of carbonate rocks during tertiary recovery from a billion barrel oil field, Weyburn, Saskatchewan: Part 2 – reservoir geology (IEA Weyburn CO_2 Monitoring and Storage Project); *in* Summary of Investigations 2001, Volume 1, Saskatchewan Geological Survey, Sask. Energy Mines, Misc. Rep. 2001-4.1.

1. Introduction

The Weyburn Field (Figures 1 and 2) covers an area of about 180 km^2 (70 square miles) and produces 29° API gravity crude oil from Mississippian shallow-water carbonates at a mean depth of 1450 m. Pay thickness ranges from 5 m to over 30 m with an average of about 10 m. Following its discovery in 1954, the Weyburn Field was produced by primary depletion for about 10 years (Figure 3). In an effort to arrest declining production, an inverted nine-spot waterflood scheme was introduced in 1964 targeting the higher permeability lower limestone member of the Midale carbonate. After achieving maximum rates of more than 7000 m^3/day by 1966, pool production declined to less than 2000 m^3/day by 1985. An aggressive vertical infill drilling program (to 40° to 60° acre spacing) was initiated in 1986. It arrested production decline, returning production to almost 4000 m^3/day. Horizontal drilling, introduced at Weyburn in 1991, became the preferred production strategy over the ensuing 10 years. Unlike the earlier vertical phase, horizontal drilling targets the largely unswept reserves in the low-permeability, high-porosity dolostone within

Figure 1 - Location of the Weyburn Field, Williston Basin.

[1] PanCanadian Resources, 150 - 9th Avenue SW, P.O. Box 2850, Calgary, AB T2P 2S5; E-mail: Geoffrey.Burrowes@pancanadian.ca.

Discovered:	1954
Area:	70 sq. miles
Current oil rate:	18,000 BOPD
Number of wells:	1016 total
	660 vert. oil
	158 hz. oil
	197 inj.
Sour crude:	25-34 API
Depth:	1450m (4760 ft)
OOIP:	1,400 MMbbls
Cum. Prod. (12/98):	351 MMbbls
Total recovery to date:	5%

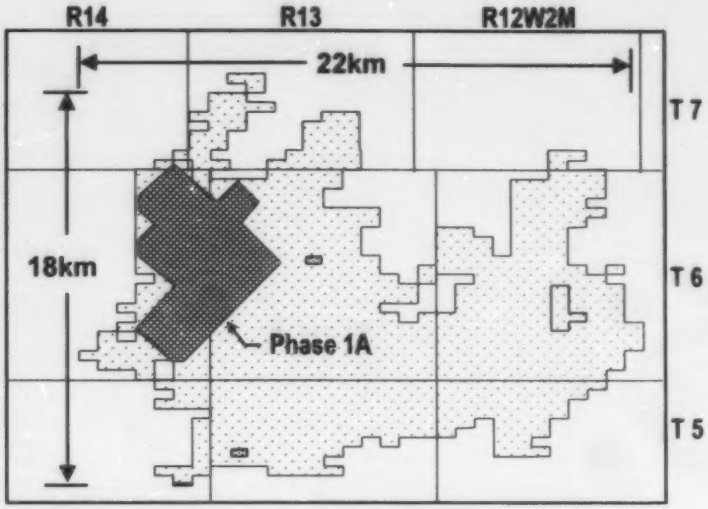

Figure 2 - Summary of Weyburn reservoir data showing outline of field and initial Phase 1A area of the CO_2 flood.

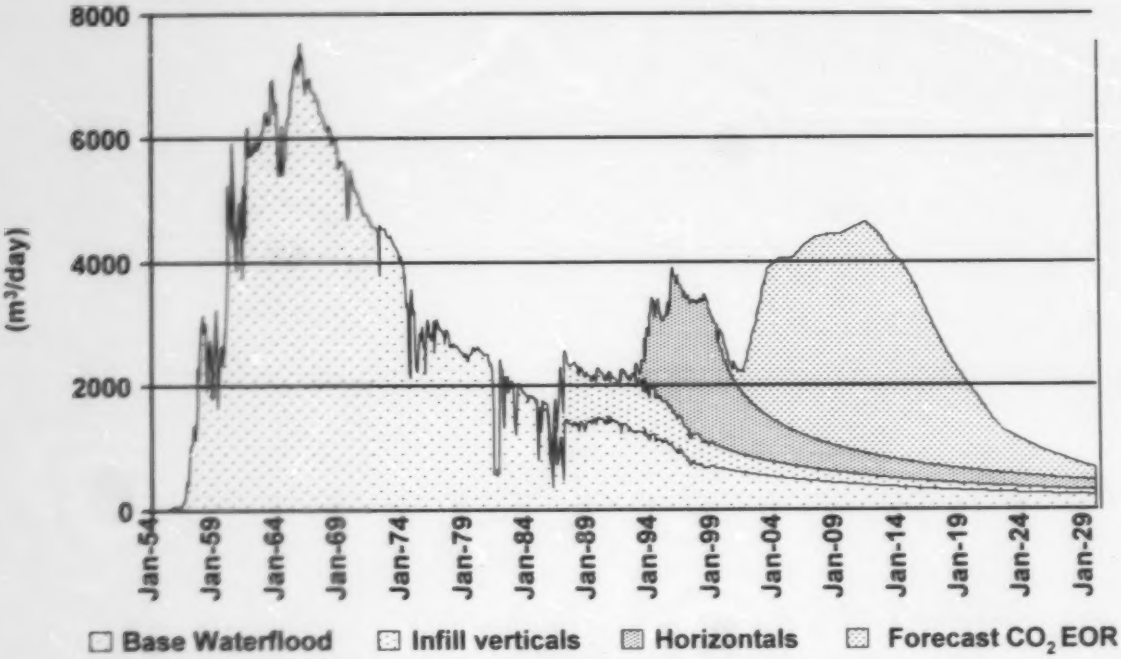

Figure 3 - Production history and forecast, Weyburn Field, Saskatchewan.

the upper Midale. By the mid-1990s, planning for a CO_2 miscible flood was well underway and CO_2 injection began in the Fall of 2000 in the 19 pattern, Phase 1A area (Figure 2). A variety of engineering, geochemical, and seismic efforts are currently underway to monitor progress of the miscible front and optimize sweep efficiency.

2. Regional Setting – The Trap

The 1.4 billion barrel (0.2 billion m^3) Weyburn Field in southeastern Saskatchewan is one of several large oil fields discovered along the Mississippian subcrop belt of the northern Williston Basin (Figure 4). Reservoired hydrocarbons have accumulated in a series of combined stratigraphic, diagenetic and hydrodynamic traps. Progressive northeasterly incision of the Mississippian succession below the sub-Jurassic

unconformity has created ideal trapping conditions where porous shallow-marine carbonate is regionally juxtaposed against relatively impermeable, fine-grained 'red bed' siliciclastics of the Triassic to Jurassic Watrous Formation (Figure 5). The efficiency of hydrocarbon trapping at the Mississippian subcrop is further enhanced by widespread, primary, cycle-capping anhydrite within the Mississippian section, as well as by widespread, sub-unconformity, diagenetic "caprock" of anhydritized dolostone (Kendall, 1975; Kent, 1987, 1999). More locally, such as at Weyburn, a 'hydrodynamic' trapping component is also created by high irreducible water saturations in updip, very low-permeability cryptocrystalline dolostone underlying the unconformity. The development of such subtle hydrodynamic traps is documented by Coalson *et al.* (1994).

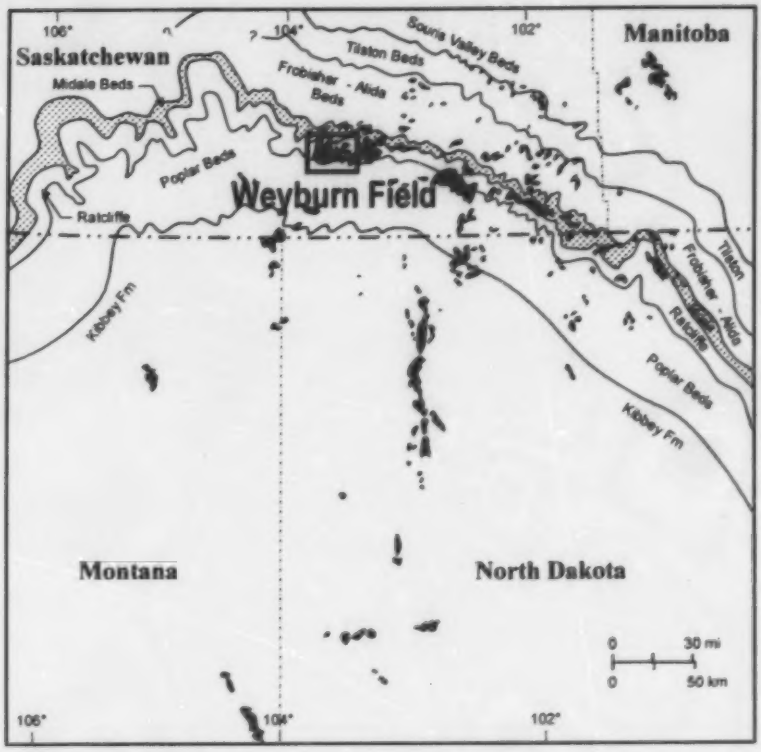

Figure 4 - Mississippian subcrop trends and oilfields, Williston Basin (from Kent, 1983).

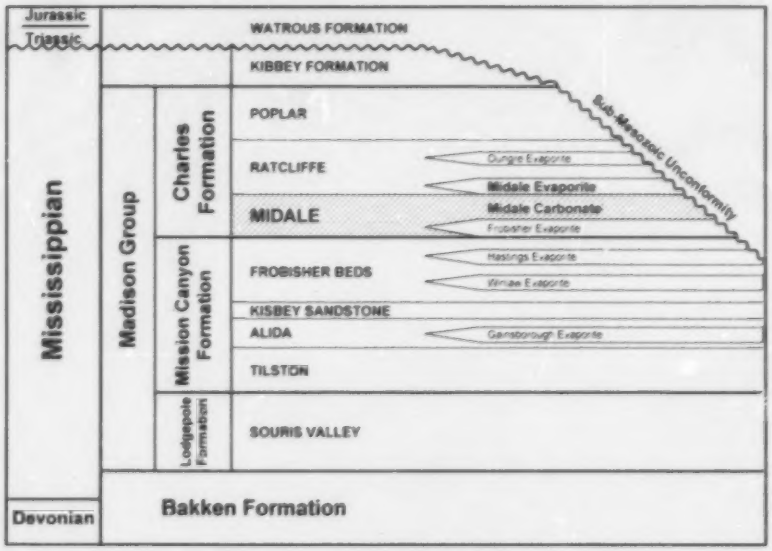

Figure 5 - Mississippian stratigraphy, southeast Saskatchewan.

The presence of bottom seal across the Weyburn Field is problematic. With the exception of northerly margins of the field where the Frobisher Anhydrite is present, Midale reservoir carbonate directly overlies dolostone of the Frobisher Marly. Furthermore, historical drillstem test results and log evaluations suggest that the original free-water level within the field extended well into the Frobisher beds (Weyburn Sub-Committee, 1962). In reality, however, significant communication with Frobisher reservoirs is tempered by widespread metasomatic anhydrite replacement at the base of the Midale and by scarcity of reservoir-quality units within the upper Frobisher beds (Frobisher Marly beds under Weyburn are generally dominated by non-reservoir argillaceous, silty, and anhydritic dolostone and marl). On the reservoir production time scale, therefore, communication with Frobisher reservoirs is probably local and limited.

3. Midale Stratigraphy

At Weyburn Field, oil is trapped within Osagean-age Midale strata of the Madison Group (Figure 5). As is common throughout the Upper Mississippian succession of the Williston Basin, alternating porous carbonate and impermeable anhydrite record fluctuating sea levels and episodic isolation and evaporation within a shallow water intracratonic basin.

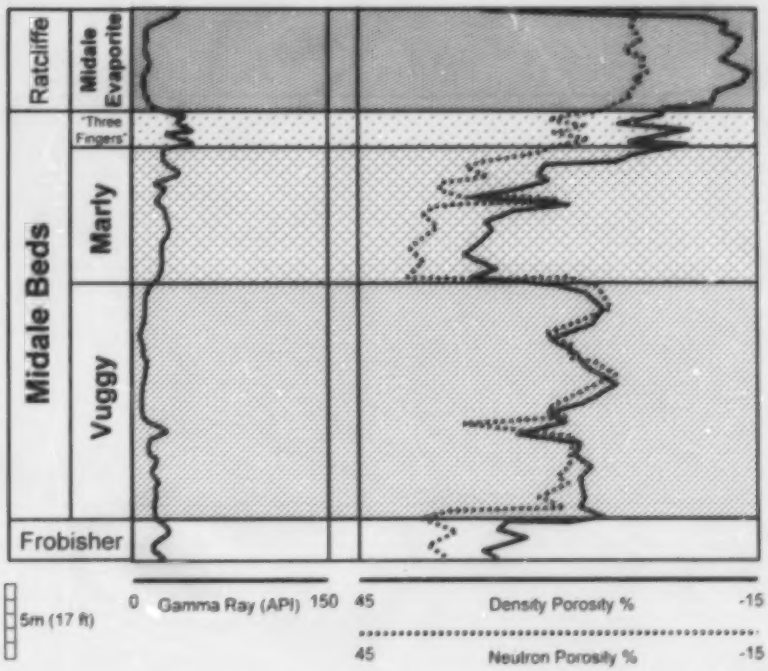

Figure 6 - Typical log response and major reservoir zones within the Midale reservoir.

The reservoir lies between low permeability dolostone and anhydrite of the Frobisher and anhydrite of the Midale Evaporite. Though locally reduced in thickness to only a few metres by erosion on the sub-Jurassic unconformity, the Midale Evaporite forms a regional top seal across the field. Figure 5 illustrates Midale stratigraphy relative to a typical reservoir log response.

The Midale carbonate reservoir is informally subdivided into a lower limestone-dominated unit called the "Vuggy", and an upper, mainly dolostone unit referred to as the "Marly" (Figure 6). Thickness ranges from 10 to 22 m in the Vuggy and 1 to 11 m in the Marly. Core-based sequence stratigraphic interpretation by PanCanadian (Figure 7) indicates that the Vuggy can be subdivided into two sequences separated by a mappable surface of subaerial exposure and erosion. Heterogeneous calcareous, algal/coated-grain/pisolitic wackestone, packstone and grainstone, with visible "vuggy" and fenestral porosity, are characteristic of the lower Vuggy. Patchy cementation by calcite, anhydrite, and dolomite adds to the overall heterogeneity. Internal higher order cyclicity within the lower Vuggy permits further breakdown of this unit for purposes of reservoir modelling (V2 to V6; Figure 7). Mapping of the lower Vuggy reveals a generally northeasterly trend of 'shoal' thicks and 'intershoal' thins (Figure 8).

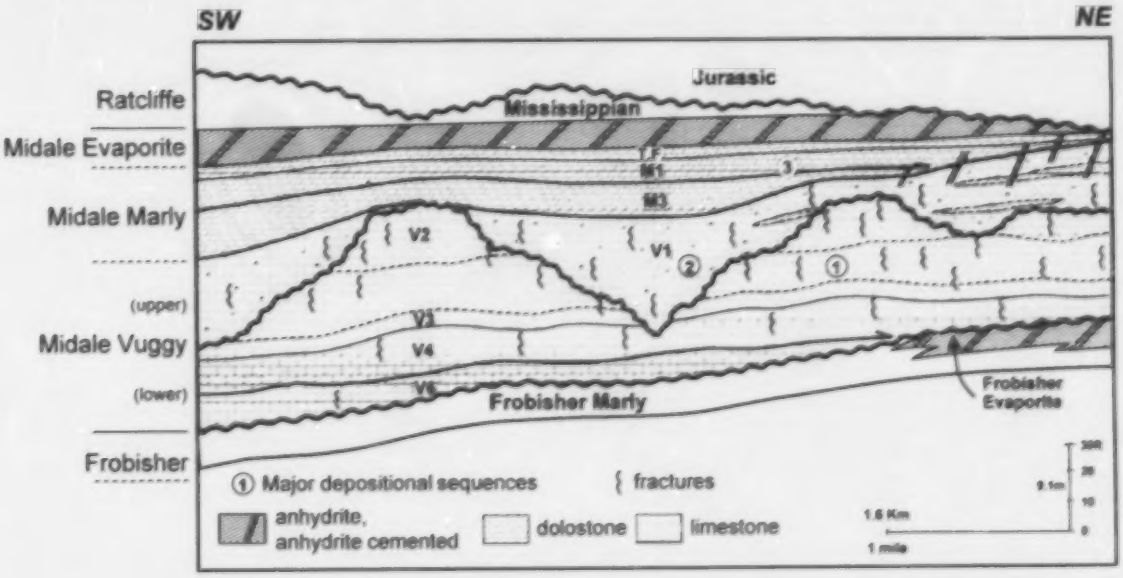

Figure 7 - Midale geological model illustrating depositional sequences and reservoir flow units. T.F., Three Fingers; M1 and M3, Marly units as discussed in text.

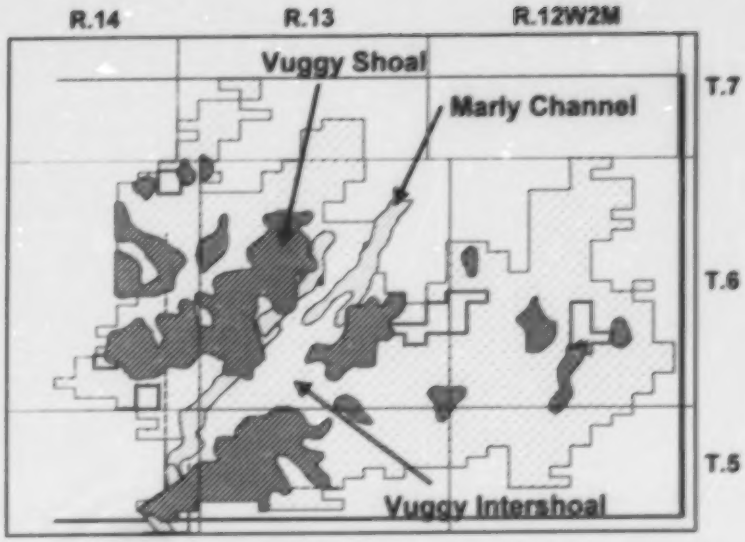

Figure 8 - Generalized distribution of Midale Vuggy shoal and intershoal areas, Weyburn Field (from Churcher and Edmunds, 1994).

The overlying upper Vuggy sequence (V1) is distinguished in core by the general absence of coarse vuggy pores and by depositional fabrics dominated by abraded skeletal packstone and wackestone. Upper Vuggy thickness generally varies inversely with that of the lower Vuggy, with thick upper Vuggy associated with thin, 'off-shoal' lower Vuggy.

High porosity, microsucrosic Marly dolostone with mud-dominated fabrics abruptly overlies the upper Vuggy. Isopachs of the Marly illustrate a generally southwestward thickening wedge that, in cross section, appears to onlap the upper Vuggy surface to the northeast. Two Marly layers (M1 and M3; Figure 7) are distinguished based on a widespread, low porosity, calcareous marker bed (M2) within the Marly. Below the capping Midale Evaporite, a thin (1 to 3 m thick) transitional unit of laminated, silty, and anhydritic dolostone is commonly referred to as the "Three Fingers" (due to its characteristic gamma response; see Figure 6). This unit is considered to be non-reservoir facies in most areas.

4. Depositional Environments

Kent (1984, 1999) and Lake (1998) have discussed regional aspects of Mississippian Madison deposition within the Williston Basin and generally agree that the characteristic style of sedimentation indicates a periodically restricted, shallow epeiric sea. Typical features include extremely low-angle depositional slopes coupled with predominance of shallow-water facies exhibiting abrupt vertical facies transitions on a regional scale. The carbonate reservoir at Weyburn represents an erosional remnant of a considerably more extensive marginal ramp on the northern flank of the Williston Basin. Phase 1A area sedimentological core studies by PanCanadian suggest the presence of four distinct depositional settings that reflect responses of an intracratonic epeiric ramp to significant eustatic fluctuations. The inferred spatial relationships of these environments are summarized in Figure 9.

Initial lower Vuggy deposition occurred in response to the early phases of a major transgression over the Frobisher surface. Stacked, strongly progradational cycles with evidence of repeated subaerial exposure record deposition within a marginal marine, peritidal island/lagoon complex. This style of sedimentation ceased abruptly in response to major sea-level fall and subaerial exposure. Up to 8 m of relief on the lower Vuggy surface was developed by a combination of depositional topography and erosional incision. Considerable porosity enhancement probably also occurred at this stage.

Significant sea-level rise resulted in major inundation of the shelf over the eroded lower Vuggy and in a change in depositional setting to dominantly subtidal, open-marine mid-ramp influenced by storm- and wave-reworking. Blanket-like deposition of the distinctive non-vuggy, skeletal-rich beds of the upper Vuggy largely infilled the lower Vuggy topography.

A widespread *Thalassinoides*-burrowed layer marks a third major shift in depositional style within the Midale beds. Upper Vuggy grain-dominated textures abruptly give way to extensively bioturbated, mud-dominated textures in the Marly. The predominance of skeletal and non-skeletal algal remains, ostracods, and the introduction of terrestrial silt and clay suggest a shift to a more proximal, quiet-water subtidal setting. The apparent regional extent of these environments seaward of an evaporitic coastal plain, represented by the overlying upper Marly and Midale Evaporite, argues for deposition within an extensive epeiric lagoon that may have developed in response to regional isolation of the Williston Basin. Depositional environments may have included both distal, relatively deep, outer ramp equivalents and proximal, very shallow restricted euryhaline bays. Within the Marly, an overall brining-upward and shallowing-upward succession is suggested by the upward change from a diverse *Cruziana* ichnofacies to a *Planolites/ Chondrites*-dominated ichnofacies with algal lamination (see Keswani and Pemberton,1993). Marly deposition culminated in silty, anhydritic tidal flat and sabkha dolo-laminites of the upper Marly "Three Fingers" zone. Subsequent deposition of the Midale Evaporite records the final shift to fully coastal marine to continental evaporitic salinas and playas.

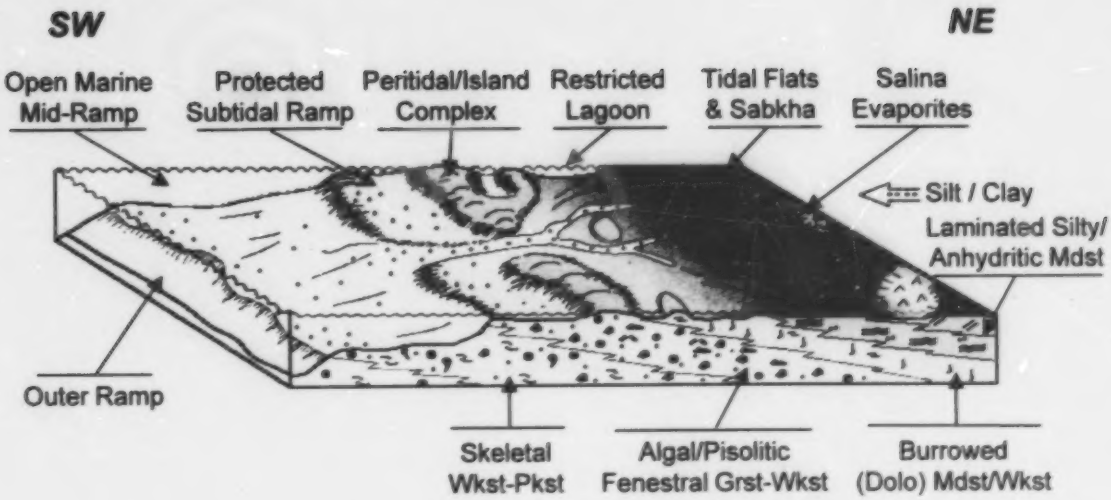

Figure 9 - Diagrammatic representation of Midale depositional environments. Mdst, mudstone; Wkst, wackestone, Grst, grainstone; Pkst, packstone; and Dolo, dolomitized.

5. Reservoir Characteristics

Table 1 summarizes the key reservoir parameters of the Midale beds in the Weyburn Field. Markedly different flow characteristics between the lower Vuggy, upper Vuggy, and Marly reflect the combination of: a) different primary depositional settings and textures, b) markedly different secondary diagenetic overprints, and c) varying rheological responses to imposed stress. Lower Vuggy reservoir characteristics (extreme heterogeneity, low to moderate porosity, low to high permeabilities) are predictable products of texturally diverse peritidal deposits overprinted by complex near-surface and burial dissolution and cementation. On the other hand, the relatively homogeneous reservoir characteristics of the upper Vuggy (low to moderate porosity, low permeability) directly reflect more uniform, finer grained depositional textures and absence of strong diagenetic overprints.

Reservoir characteristics of the Marly (homogeneity, high porosity, low permeability) are, foremost, a function of early dolomitization of 'bio-homogenized', mud-dominated fabrics. Variations in reservoir quality within the Marly occur mainly in response to variations in degree of dolomitization, and a general upward trend to finer crystalline, lower permeability fabrics. Severely reduced reservoir quality is commonly associated with partial dolomitization within either thin skeletal-rich packstones or organic-rich, microstylolitic beds; both of these are widespread at the top of the M3 zone and combine to form a correlatable low-permeability zone separating M1 and M3.

Table 1 - Summary of Midale reservoir characteristics, Weyburn Field.

Reservoir Zone	Lithology & Textures	Porosity (avg.%, Type)	Matrix Permeability (avg.,md)	Heterogeneity	Fracture Density
Marly (M1, M3)	Dolostone mudstone wackestone	20-37 (26) intercrystalline moldic	<0.1 - 100 (10)	Low bioturbation dolomitization	Low - Moderate (2-4 m spacing) >25% O-unfract
Upper Vuggy (V1)	Limestone packstone wackestone	2-15 (10) interparticle intraparticle	<0.01 - 20 (1)	Medium thick bedded bioturbation	High (<1 m spacing)
Lower Vuggy (V2-V8)	Limestone mudstone to grainstone	5-20 (15) fenestral vuggy	<1 - 500 (20)	High well bedded, high order cyclicity complex diagenesis	Moderate - High (<1-2 m spacing) microfractured

6. Fractures

One of the more prominent features of the Weyburn Midale reservoir is sub-vertical natural fractures, both open and cemented. Not only are these obvious in numerous well cores, but are also clearly imaged on borehole image logs. Analysis of these image logs indicates that the dominant fracture orientation is parallel to the current southwest-northeast orientation of maximum horizontal stress (Bell and Babcock, 1986; Adams and Bell, 1991). Secondary southeast-northwest fracture trends have also been defined (Bunge, 2000). Churcher and Edmunds (1994) have estimated fracture spacing at between 0.3 and 10 m, with

highest densities in the upper Vuggy and lowest in the Marly. Although the low fracture density in the Marly appears to be inconsistent with the normally more brittle response of crystalline dolostones, the very high porosity and sucrosic textures appear to have induced a more ductile response to stress.

The degree to which fractures affect directional reservoir permeability, flow characteristics, and producibility is difficult to determine. Perhaps the strongest evidence for their influence is the pronounced preferred "on-trend" water breakthrough response during waterflood. However, much of this effect is possibly a by-product of northeasterly propagation of fractures under high injection pressures, combined with the preferred northeasterly orientation of the high-permeability lower Vuggy shoals. Furthermore, history matching of the breakthrough response does not require permeabilities significantly higher than average, core-based matrix permeabilities. Also, PanCanadian's analysis of scattered transient pressure data does not lend strong support for dual porosity reservoir behaviour. The classic dual porosity response may, however, be partly masked by either the interaction of the markedly different Marly and Vuggy flow systems, or the homogenizing effect of microfracturing, which is widely observed in thin sections of the lower Vuggy.

These ambiguities have made it difficult to develop a satisfactory, comprehensive fracture model for the Weyburn reservoir. The extent to which fractures will influence CO_2 flood performance remains a key issue to be addressed by the IEA Weyburn CO_2 Monitoring and Storage Project. One of the avenues PanCanadian and the IEA are pursuing is the acquisition of multicomponent 3-D seismic data to assist in spatial characterization of the fracture system.

7. Flood Monitoring

A critical element of successful, efficient tertiary recovery schemes involves diligent monitoring of flood conformance as well as the overall progress of the flood front. PanCanadian is addressing this process through monitoring of production fluid composition and volumes, chemical tracer studies and muticomponent 4-D seismic.

Production testing on individual wells will be done regularly in five newly constructed satellite stations. Each satellite is equipped with a three-phase test separator for measuring oil, water, and gas flow rates. Produced gas is monitored for CO_2 using infra-red analyzers and dragar tube sampling. Samples of produced oil, water, and gas will be periodically collected for more detailed compositional analysis. A tracer study will be implemented in March 2001 using perflourocarbons to trace CO_2 injection gas at seven injection wells. The study will determine CO_2 conformance in three flood patterns and assist in designing flood operations. A screening study has also been initiated at University of Regina to evaluate commercially available CO_2 surfactants and diverting agents for CO_2 mobility control.

Together with the Colorado School of Mines, PanCanadian will be acquiring four multicomponent 3-D seismic surveys within the initial Phase 1A area over a period of about three years; the key baseline survey was acquired in 1999. The seismic surveys will use the latest techniques to acquire P and S wave data in an attempt to monitor the progress of the flood front and to improve spatial resolution of reservoir properties (porosity-thickness and fracture-permeability). Interpretation of the seismic data is to be enhanced by the co-ordinated acquisition of two multicomponent 3-D vertical seismic profiles (VSPs) as well as single-well and cross-well (horizontal to horizontal) seismic tomography.

8. References

Adams, J. and Bell, J.S. (1991): Crustal stresses in Canada; *in* Slemmons, D.B., Engdahl, E.R., Zoback, M.D., and Blackwell, D.D. (eds.), Neotectonics of North America, Decade Map Volume 1, Geol. Soc. Amer., Boulder, p376-386.

Bell, J.S. and Babcock, E.A. (1986): The stress regime of the Western Canadian Basin and implications for hydrocarbon production; Bull. Can. Petrol. Geol., v34, p364-378.

Bunge, R.J. (2000): Midale reservoir fracture characterization using integrated well and seismic data, Weyburn Field, Saskatchewan; unpubl. M.Sc. thesis, Colorado School of Mines, 218p.

Churcher, P.L. and Edmunds, A.C. (1994): Reservoir characterization and geologic study of the Weyburn Unit, southeastern Saskatchewan; PanCanadian Petroleum Ltd., internal rep., 80p.

Coalson, E.B., Goolsby, S.M., and Franklin, M.H. (1994): Subtle seals and fluid-flow barriers in carbonate rocks; *in* Dolson, J.C., Hendricks, M.L., and Wescott, W.A. (eds.), Unconformity-related Hydrocarbons in Sedimentary Sequences, Guidebook for Petroleum Exploration and Exploitation in Clastic and Carbonate Sediments, Rocky Mtn. Assoc. Geol., Denver, p45-58.

Kendall, A.C. (1975): Anhydrite replacements of gypsum (satin-spar) veins in the Mississippian caprocks of southeastern Saskatchewan; Can. J. Earth Sci., v12, p1190-1195.

Kent, D.M. (1983): Mississippian reservoirs in Williston Basin; Comptes Rendues, Ninth International Congress on Carboniferous Stratigraphy, v4, p99-110.

_____ (1984): Carbonates and associated rocks of the Williston Basin – their origin, diagenesis and economic potential; Rocky Mtn. Sec., Soc.

Econ. Paleont. Mineral., Short Course Notes, 137p.

_____ (1987): Mississippian facies, depositional history, and oil occurrences in Williston Basin, Saskatchewan and Manitoba; *in* Peterson, J.A., Kent, D.M., Anderson, S.B., Pilatzke, R.H., and Longman, M.W. (eds.), Williston Basin: Anatomy of a Cratonic Oil Province, Rocky Mtn. Assoc. Geol., Denver, p157-170.

_____ (1999): A re-examination of the process of formation and diagenesis of coated-grain accumulations and contiguous facies in the Mississippian of southeastern Saskatchewan; *in* Summary of Investigations 1999, Volume 1, Saskatchewan Geological Survey, Sask. Energy Mines, Misc. Rep. 99-4.1, p17-26.

Keswani, A.D. and Pemberton, S.G. (1993): Sedimentology, ichnology, and paleoecology of the Mississippian Midale carbonates in the Williston Basin, Radville area, Saskatchewan: Preliminary interpretation; *in* Haan, J.D., Jang, K., and Webb, T. (eds.), Carboniferous to Jurassic – Pangea, Core Workshop Guidebook. Can. Soc. Petrol. Geol., Calgary, p206-228.

Lake, J.H. (1998): A Mississippian epeiric shelf model for the Williston Basin; *in* Christopher, J.E., Gilboy, C.F., Paterson, D.F., and Bend, S.L. (eds.) Eighth International Williston Basin Symposium, Sask. Geol. Soc., Spec. Publ. No. 13, p69-71.

Weyburn Sub-Committee (1962): Effective oil pore volume, Midale Beds reservoir, Weyburn Field, Saskatchewan; Weyburn Working Engineering-Geological Sub-Committee, Pore Volume Group, 1962 Report, 110p.

Paleomagnetic Indications for a Late Paleozoic Age for Part of the Watrous Formation, Williston Basin, Southern Saskatchewan

Randolph J. Enkin [1], Judith Baker [1], and K.G. Osadetz [2]

Enkin, R.J., Baker, J., and Osadetz, K.G. (2001): Paleomagnetic indications for a Late Paleozoic age for part of the Watrous Formation, Williston Basin, southern Saskatchewan; *in* Summary of Investigations 2001, Volume 1, Saskatchewan Geological Survey, Sask. Energy Mines, Misc. Rep. 2001-4.1.

1. Introduction

The Williston Basin is a Phanerozoic epicratonic basin about 800 km in diameter underlying southern Saskatchewan, Manitoba, and the adjacent United States of America (Figure 1). The basin contains several significant petroleum provinces and mineral deposits (e.g. Burrus *et al.*, 1996), and has thus been the focus of detailed exploration. However, there remain profound uncertainties concerning the origin, tectonics, and even stratigraphy of the basin. These uncertainties hamper the understanding of its petroleum systems.

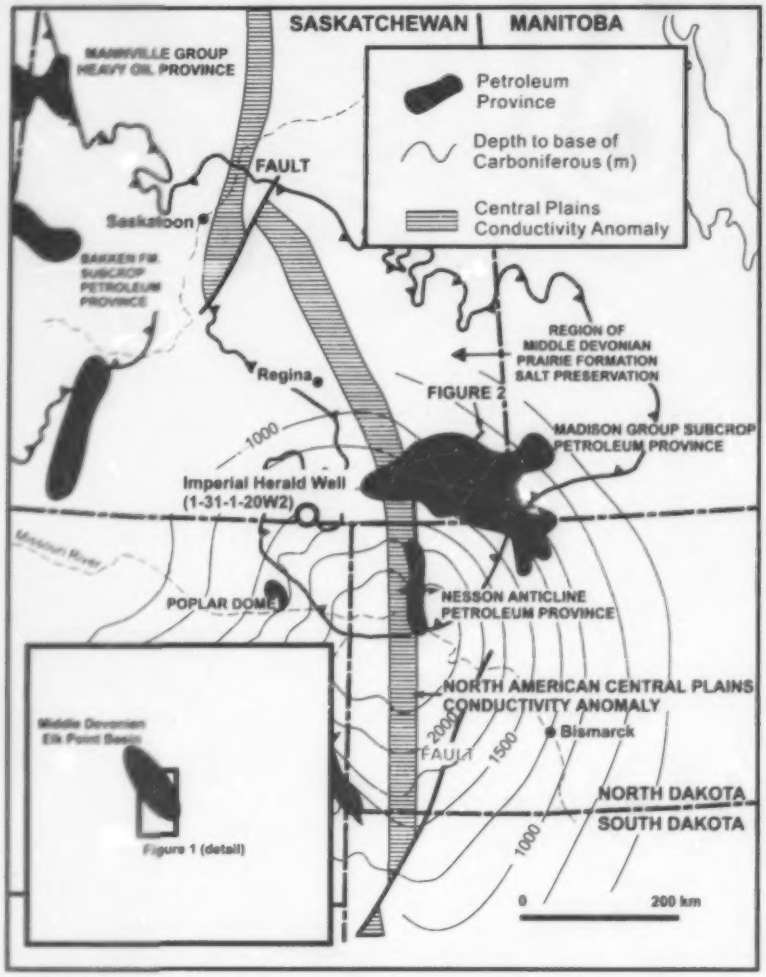

Figure 1 - Regional setting, major tectonic elements, and petroleum provinces of the Williston Basin. Basin form-lines are indicated by the depth to the base of the Carboniferous Madison Group.

The Watrous Formation (Milner and Thomas, 1954) is composed of red bed siliciclastics and anhydrites (Christopher, 1984; Edwards *et al.*, 1994). The formation onlaps a major regional unconformity underlain by the deeply eroded Paleozoic carbonate succession (Figure 2). These usually "tight" rocks are commonly cap rocks to the Mississippian subcrop oil fields. The formation has been a minor oil producer, from more sandy porous lithologies, as typified by the Waskada Field in southwestern Manitoba that was discovered in 1980.

The Watrous Formation is informally split into "upper" and "lower" members. The upper member is dominated by anhydrites and is considered to be of Jurassic age (Christopher, 1984). The lower member has been correlated to the Lower Jurassic upper Spearfish Formation which crops out in North Dakota. Others suggest this member may be as young as Middle Jurassic (see Edwards *et al.*, 1994).

[1] Geological Survey of Canada - Pacific, 9860 West Saanich Road, POB 6000, Sidney, BC V8L 4B2.
[2] Geological Survey of Canada, 3303 - 33rd Street NW, Calgary, AB T2L 2A7.

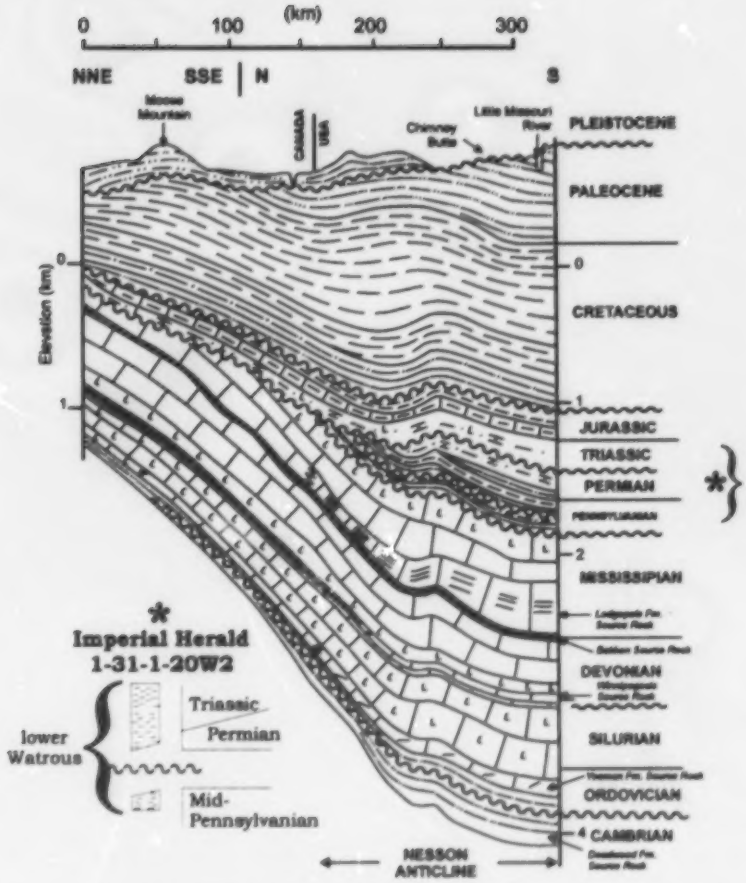

Figure 2 - Section of Williston Basin illustrating the Phanerozoic stratigraphic succession after Burrus et al. (1996). Location of this section is indicated in Figure 1. The interpreted stratigraphic position of the lower member of the Watrous in the analyzed core is shown in the inset in the lower left-hand corner of the diagram.

In an attempt at better determining the age of this non-fossiliferous formation, we sampled core from an oil exploration well for paleomagnetic study. The observed magnetic inclination gives the paleolatitude at which the rocks were situated at the time of magnetization. By comparing the paleolatitude history of the site, derived from North America's apparent polar wander path (APWP), with the observed paleolatitude, we can determine the age of the magnetization. If the magnetization is primary, we can date the age of sediment deposition.

We sampled the Imperial Herald core (1-31-1-20W2; 49.1°N, 104.5°W, approximately 160 km south of Regina), because it lies near the centre of the Williston Basin and has excellent recovery of the lower member of the Watrous Formation. The Watrous Formation was picked between depths of 5206 and 5593 ft (1586.8 and 1704.7 m), and the bottom 110 feet (33.5 m) were almost continuously recovered. The Watrous Formation is underlain by the Charles Formation of the Carboniferous Madison Group.

2. Methods

We drilled 2.5 cm diameter minicores perpendicular to the core axis. Since the original core was almost vertical, our minicores were taken parallel to the near- horizontal strata. Where the rock was massive and red-pigmented, we sampled every 2 to 3 ft (60 to 90 cm).

Magnetic remanence was measured on an Agico JR5-A spinner magnetometer. Magnetic susceptibilities were measured using a Sapphire SI2-B meter. We measured both full core and minicore susceptibility. Thermal demagnetizations were performed with an ASC TD-48 furnace, over 12 to 15 steps up to 700°C. Magnetic remanence directions were determined by Principal Component Analysis, using programs developed by the first author (available on request).

3. Results

The core of the lower Watrous consists mostly of red to orange mudstone to siltstone with rare beds of sandstone. Common ripple marks and cross bedding indicate shallow-water deposition. Reduction spots are common, and usually have sharp edges. They are early diagenetic features, and apparently have not been altered by subsequent fluid motions.

Characteristic demagnetization curves are plotted in Figure 3. The natural remanent magnetizations (NRM) are typical of red sediments (geometric mean 5.34 mA/m ±48%). The samples are relatively efficiently magnetized (Koenigsberger ratio K_N = NRM/induced magnetization = 1.34 ±45%) compared to similar rocks which usually have $K_N < 1$. However, about half of the magnetization is a drilling induced overprint. This component, roughly parallel to the direction of minicoring, is removed by heating to 150° or 200°C. The remaining magnetization remains very stable to about 500°C. The dominant magnetic carrier is clearly hematite (with a Curie Temperature T_C = 680°C), as most of the stable magnetization unblocks between 600° and 700°C heating, well above the T_C of magnetite, 580°C. The remanence direction held by the hematite is easily determined by line-fitting this high

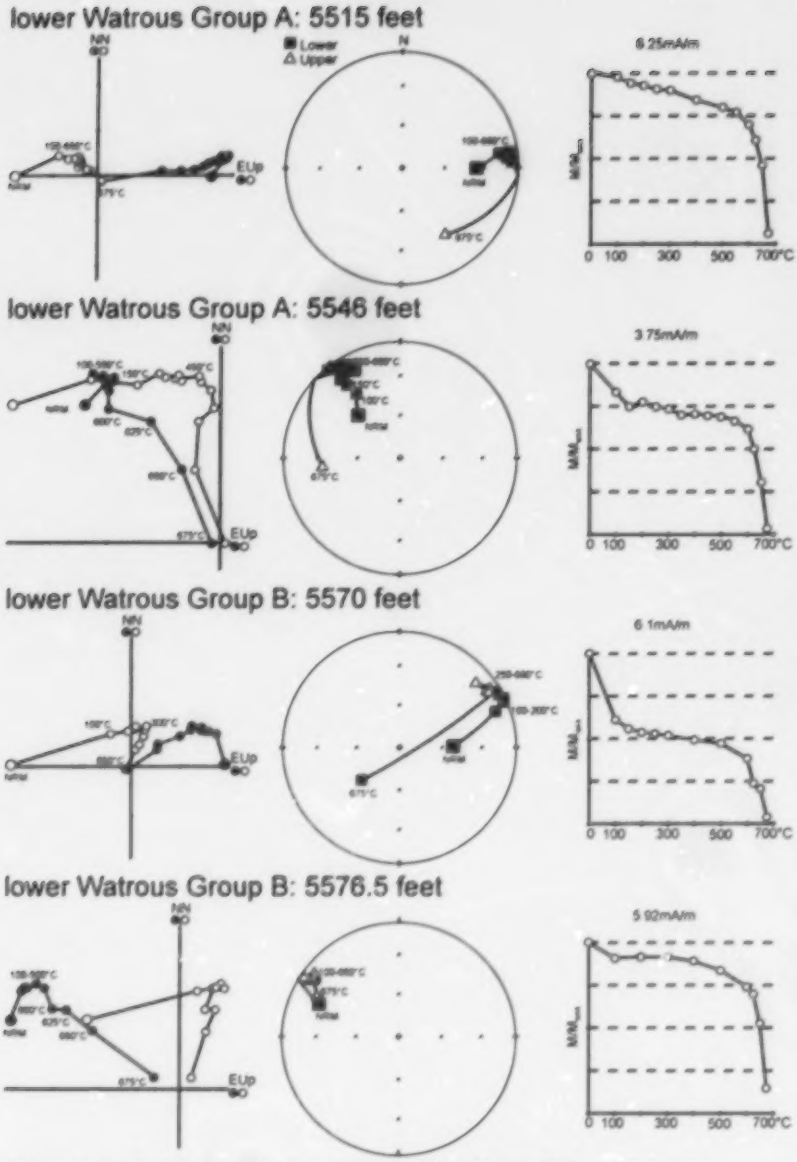

Figure 3 - Typical demagnetization characteristics of lower Watrous Formation specimens, illustrated as orthogonal projections, stereographs, and magnetic intensity as a function of thermal demagnetization step.

temperature segment. About 20% of the samples were unsuitable, since the remanence was demagnetized at much lower temperatures and gave either incoherent directions, or only drilling overprint directions.

The observed remanence directions clearly separate into two groups (Figure 4). The A group, from depths of 5484 to 5560 ft (1671.5 to 1694.7 m), has positive (down) inclinations, while the B group, from 5563 to 5583 ft (1695.6 to 1701.7 m), has negative (up) inclinations. The declinations are random. However, from core segments which we could piece together, we attempted to orient the core using the faint present-field overprint which survived the drilling overprint. The resolution is low, but we find north-west declinations in the A group, and southerly declinations in the B group. This indicates that the A group is truly normal polarity, while the B group has reverse polarity and is not a normal polarity magnetization from when North America was situated in the southern hemisphere.

The mean inclination of group A is 25.1° ±4.1°, N = 49, Fisher precision k = 14.9 (method of Enkin and Watson, 1996). This observed inclination is consistent with the expected inclination derived from the North American APWP for ages between 209 to 311 Ma (Pennsylvanian through Triassic) (Figure 5). Note, in particular, that North America drifted rapidly northward during latest Triassic and Early Jurassic time, and that the expected inclination for all more recent times is far steeper than what we observe. Thus we can be sure that these rocks did not suffer a post-Triassic remagnetization.

The observed polarity is normal, and during most of Pennsylvanian and Permian times, the geomagnetic field has persistent reverse polarity, a period known as the Kiaman Reverse Chron. Thus we conclude that the age of this interval of the Watrous Formation is between latest Permian to Triassic time (260 to 209 Ma), likely during one normal polarity chron.

The B group has significantly shallower inclination (-13.5° ±3.8°, N = 25, k = 34.7). This result is consistent with the North American APWP between the ages of 351 and 303 Ma (Mississippian through Pennsylvanian) (Figure 5). There are reversals before the Kiaman Reverse Chron, so it is not possible to constrain the age using magnetic polarity as confidently as with the A group. But since we observed no reversals in this interval of the core, we consider it likely to have post-dated the start of the Kiaman at about 315 Ma.

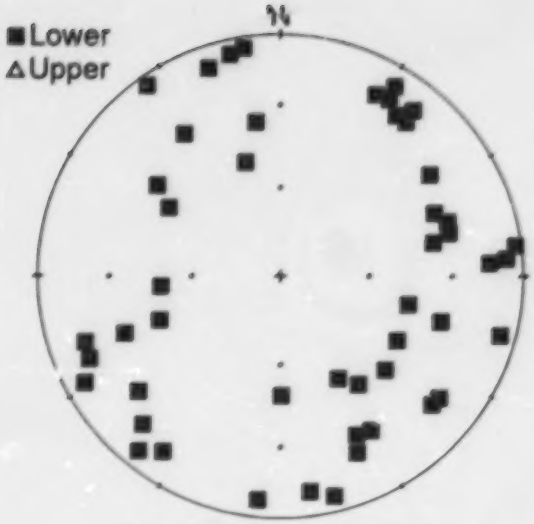

lower Watrous Group A
5484-5560 feet

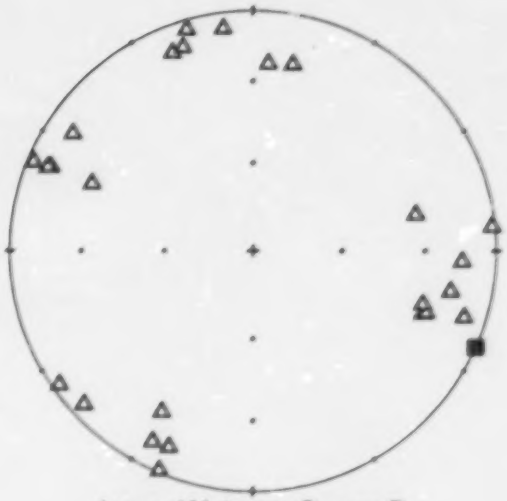

lower Watrous Group B
5563-5583 feet

Figure 4 - Stereographs of the lower Watrous Groups A and B. The declinations are random, but the polarities and inclinations are well defined.

4. Discussion and Conclusion

The basic stratigraphy of a region must be established before questions concerning the regional setting of deposition, subsequent deformation and hydrocarbon generation can be answered. Watrous stratigraphy is both complicated and uncertain. Edwards *et al.* (1994, p273) quote Cumming (1956): "It is almost traditional that papers on the Watrous should express doubt concerning the age and correlation of that formation, and in this respect the present report is no exception". They go on to say, "We maintain the tradition". While recognizing the preliminary nature of our study, we feel confident in saying that the lower Watrous recovered in the Imperial Herald core was not deposited after Triassic time, and is most likely latest Permian to Triassic in age. Furthermore, a period of tens of millions of years is missing near the bottom of the Watrous in this core. The lowest 20 ft (6.1 m) is of Paleozoic, probably mid-Pennsylvanian, age.

Our study on sub-Watrous portions of the core indicates that only the red sediments retain stable magnetizations. The possibility exists that the Charles Formation has suffered pervasive remagnetization during Permian time. This observation was also suggested from the paleomagnetic study of Devonian Prairie Formation evaporites in Saskatchewan (Koehler *et al.*, 1997). Clearly further study on core material from around the Williston Basin is essential to delineate the stratigraphic and hydrothermal history of the region.

5. Acknowledgments

We thank the staff at the Subsurface Geological Laboratory of Saskatchewan Energy and Mines for help accessing the core, and Glenda Rathwell and Jennifer Porter for excellent laboratory assistance.

6. References

Besse, J. and Courtillot, V. (1991): Revised and synthetic apparent polar wander paths of the African, Eurasian, North American and Indian plates, and true polar wander since 100 Ma; J. Geophys. Resear., v96, p4029-4050.

Burrus, J., Osadetz, K.G., Wolf, S., Doligez, B., Visser, K., and Dearborn D. (1996): A two-dimensional regional model of Williston Basin hydrocarbon systems; Amer. Assoc. Petrol. Geol. Bull., v80, p265-291.

Christopher, J.E. (1984): Depositional pattern and oil field trends in the Lower Mesozoic of the northern Williston Basin, Canada; *in* Lorsong, J.A. and Wilson, M.A. (eds.), Oil and Gas in Saskatchewan, Sask. Geol. Soc., Spec. Publ. No. 7, p83-102.

Cumming, A.D. (1956): The Watrous strata in Saskatchewan; *in* First International Williston Basin Symposium, N. Dak. Geol. Soc./Sask. Geol. Soc., Sask. Geol. Soc., p165-169.

Edwards, D.E., Barclay, J.E., Gibson, D.W., Kvill, G.E., and Halton, E. (1994): Chapter 17, Triassic strata of the Western Canada Sedimentary Basin; *in* Mossop, G. and Shetsen, I. (comp.), Geological Atlas of the Western Canada Sedimentary Basin, Can. Soc. Petrol. Geol./Alta. Resear. Counc., p259-275.

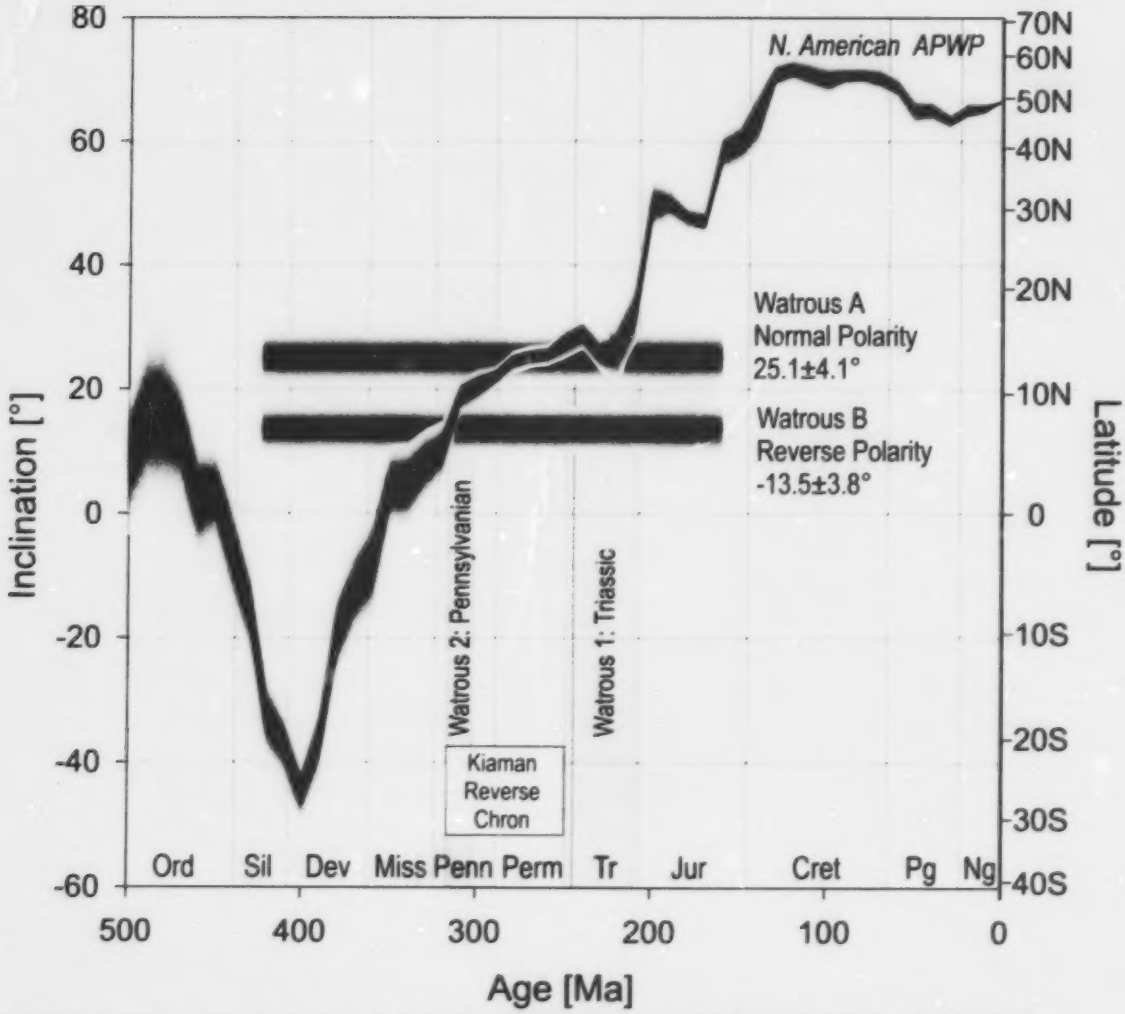

Figure 5 - The paleomagnetic inclination history of the Williston Basin (calculated at 49°N, 105°W, using the North American apparent polar wander path compiled by Van der Voo (1990), Wynne et al. (1992), and Besse and Courtillot (1991)), compared to the observed inclinations of the two levels of lower Watrous Formation sampled at the Imperial Herald well: A 5484 to 5560 ft (1671.5 to 1694.7 m), and B 5563 to 5583 ft (1695.6 to 1701.7 m). The uncertainty bands show 95% confidence intervals.

Enkin, R.J. and Watson G.S. (1996): Statistical analysis of paleomagnetic inclination data; J. Geophys. Internat., v126, p495-504.

Koehler, G., Kyser, T.K., Enkin, R.J., and Irving, E. (1997): Paleomagnetic and isotopic evidence for the diagenesis and alteration of evaporites in the Paleozoic Elk Point Basin, Saskatchewan, Canada; Can. J. Earth Sci., v34, p1619-1629.

Milner, R.L. and Thomas, G.E. (1954): Jurassic System in Saskatchewan; *in* Western Canada Sedimentary Basin – a Symposium, Amer. Assoc. Petrol. Geol., Ralph Leslie Rutherford Memorial Volume, p250-267.

Van der Voo, R. (1990): Paleozoic paleomagnetic poles from Europe and North America and comparisons with continental reconstructions; Rev. Geophys., v28, p167-206.

Wynne, P.J., Irving, E., Schulze, D.E., Halls, D.C., and Helmstaedt, H.H. (1992): Paleomagnetism of three Canadian Rocky Mountain diatremes; Can. J. Earth Sci., v29, p35-47.

Isotopic Data (Sr, S, and O) from Anhydrites in the Northern Williston Basin, and Pennsylvanian Ages for the Watrous and Amaranth Formations of Saskatchewan and Manitoba [1]

R.E. Denison [2], H.R. Krouse [3], and T.P. Poulton [4]

Denison, R.E., Krouse, H.R., and Poulton, T.P. (2001): Isotopic data (Sr, S, and O) from anhydrites in the northern Williston Basin, and Pennsylvanian ages for the Watrous and Amaranth formations of Saskatchewan and Manitoba; *in* Summary of Investigations 2001, Volume 1, Saskatchewan Geological Survey, Sask. Energy Mines, Misc. Rep. 2001-4.1.

1. Introduction

Strontium, sulphur, and oxygen isotopic ratios provide important information regarding the marine character, freshwater influence, circulation characteristics, and age of deposition of anhydrites and gypsums. This report presents the first data indicating an age (Late Pennsylvanian) for the previously undated upper members of the Watrous and Amaranth evaporitic formations in southern Saskatchewan and Manitoba. It also presents preliminary results from a more limited examination of Devonian through Jurassic(?) samples from other evaporite units in the northern Williston Basin. We have determined 109 strontium isotope ratios of core samples of anhydrite from 19 widely separated boreholes in Saskatchewan, Manitoba, and North Dakota (Figure 1) and two outcrop localities of gypsum from South Dakota. Sulphur and oxygen isotope ratios were determined on 36 of these anhydrite/gypsum samples. Most of the samples come from the Upper Watrous Member, but other units were sampled as well.

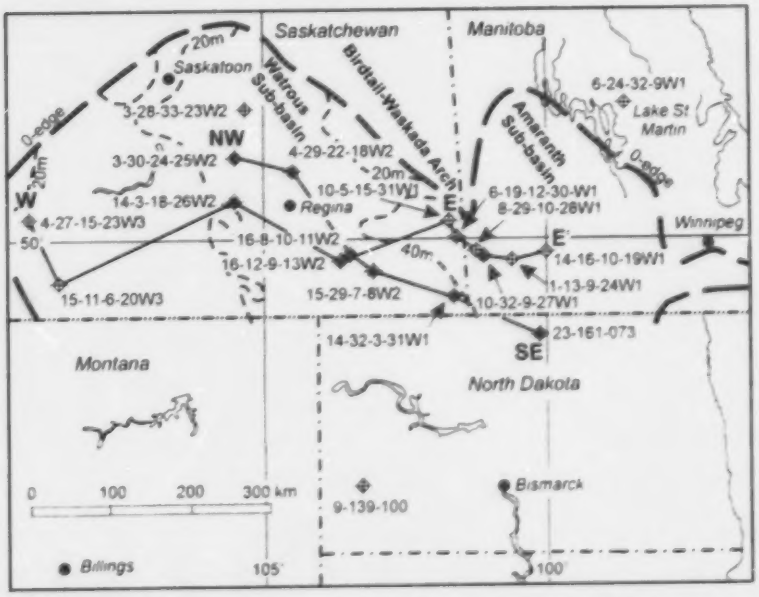

Figure 1 - Location of wells from which samples were analyzed. Three outcrop samples from two locations in South Dakota are not shown. Locations of cross sections W-E, NW-SE, and E-E' are shown. The wells yielding typical Upper Watrous strontium values indicating Pennsylvanian ages are shown in black. The 0-edge showing the limits of the Upper Watrous (heavy dashed line) and the 20 m and 40 m isopachs (light dashed lines) are approximated from electronic data bases of formation picks.

2. Watrous and Amaranth Formations

The Watrous Formation and its correlative in Manitoba, the Amaranth Formation, are subdivided into lower and upper members. Neither has been the subject of detailed sedimentologic analysis. The lower members of each formation consist of red and red-brown, partly dolomitic mudstones and siltstones, with minor sandstones with pitted grains. They contain minor anhydrite laminae, blebs and fracture fills (see descriptions by Milner and Thomas, 1954; Stott, 1955; Barchyn, 1982; Christopher, 1990, p677; McCabe, 1990, p11-12; Kreis, 1991). On well logs, the red beds are characterized by a high gamma ray signature. This red-bed unit infills irregularities of the underlying weathered erosional surface on Devonian to Mississippian rocks in Saskatchewan and progressively older rocks down to Precambrian basement eastward in Manitoba. The Lower Watrous reaches at least 30 m in thickness.

[1] Geological Survey of Canada Contribution No. 2000280
[2] Geosciences, The University of Texas at Dallas, Box 830688, Richardson, TX 75080
[3] Department of Physics, University of Calgary, 2500 University Drive NW, Calgary, AB T2N 1N4
[4] Geological Survey of Canada, 3303 - 33rd Street NW, Calgary, AB T2L 2A7

The Lower Watrous red beds are continuous southward into northern Montana and northwestern North Dakota (Francis, 1956; LeFever *et al.*, 1991), where they are considered to be a northern extension of the upper part of the Spearfish Formation and are generally assigned a Triassic age (see Dow, 1967; Carlson, 1968, 1993; McLachlan, 1972) (Table 1).

The Upper Watrous (Evaporite) Member of southern Saskatchewan contains varying proportions of anhydrite, more than 50% in some wells, interbedded with buff or grey argillaceous limestone, dololutite and calcareous or dolomitic mudstone. Some of the buff dololutites are cryptalgal-laminated. The Upper Watrous overlaps the margins of the lower red-bed unit around the northern edges of the Williston Basin (Christopher, 1990, p677), and its basal contact with the Lower Watrous is sharp to apparently gradational. The anhydrite occurs as small nodules or in massive pure beds up to 1.5 m thick, in which it has a "chicken-wire" texture (Kreis, 1991, p10) consisting of coalesced nodules. No extended sequences of laminated beds, nor enterolithic, teepee or sabkha-like breccias have been observed.

The upper boundary is apparently gradational with the lowest Gravelbourg mudstones and dolomitic limestones. However, beyond the northeastern limit of the basal beds of the Lower Gravelbourg, the Upper Watrous is brecciated and contains secondary anhydrite fracture fills below the unconformity at its top (Kreis, 1991). The Upper Watrous exceeds 40 m in thickness.

Table 1 - Table of formations, showing conventional age assignments (left), revised age assignments (right), and proposed correlations (bold). Columns are adapted from Bluemle** et al. **(1986), Kreis (1991), LeFever** et al. **(1991), Poulton** et al. **(1994), and Richards** et al. **(1994).

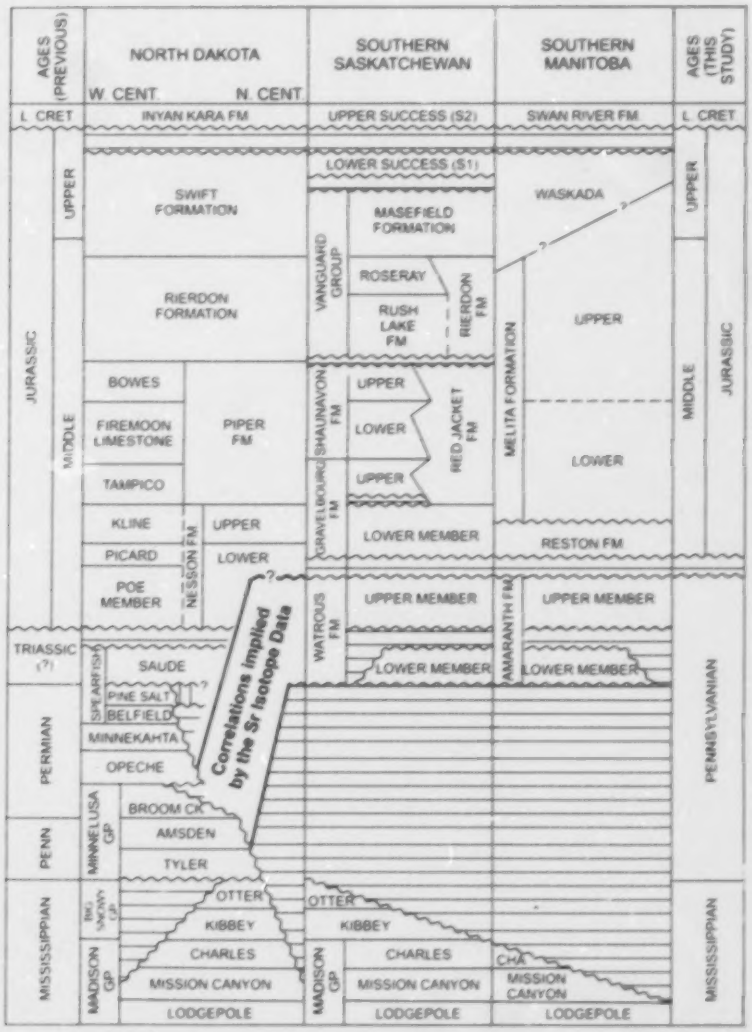

The correlative Upper Amaranth anhydrite unit in Manitoba contains interbeds of shale and dolostone, and chert concretions are present at the top (McCabe, 1990, p11). Descriptions of the Upper Watrous and Amaranth formations are available in Milner and Thomas (1954), Stott (1955), Barchyn (1982), Christopher, (1990), McCabe (1990), and Kreis (1991).

The Upper Watrous–Amaranth evaporite unit correlates southward with the Poe Member of the lower Piper and the lower Nesson Formation in northern North Dakota (LeFever *et al.*, 1991). Regional distributions of these strata are described in Peterson (1972), Imlay (1980), and Anna (1986).

3. Age Constraints on the Watrous and Amaranth Formations

Determining the age of deposition for evaporite units is one of the great geologic challenges. Because evaporites generally lack definitive flora or fauna, their age is usually determined by lateral correlation with open marine rocks or, as is the case with the Watrous evaporites, by stratigraphic bracketing (Holser, 1992). Pocock (1972) reported palynomorphs from both the Lower and Upper Watrous, including a minor marine component of microplankton

from the upper member, but they do not permit precise age assignments.

The youngest rocks underlying the Watrous and Amaranth formations of western Canada are Mississippian (but mid-Pennsylvanian strata underlie equivalents in adjacent North Dakota) and the oldest overlying rocks are Middle Jurassic. The latitude of these constraints has allowed the Watrous to be assigned a variety of ages, most recently Middle Jurassic(?) for the upper part and Triassic(?) for the lower (Poulton *et al.*, 1994; Edwards *et al.*, 1994).

The youngest dated rocks below the Watrous Formation are Serpukhovian (Mississippian) – the Otter Formation of the Big Snowy Group (Richards *et al.*, 1994). In adjacent northern North Dakota and northeastern Montana, the youngest rocks underlying the Spearfish-Nesson-Piper succession are DesMoinesian, and possibly Early Missourian (Pennsylvanian) – the uppermost Minnelusa Formation (Mallory, 1972).

The oldest dated strata above the Upper Watrous in Saskatchewan (Upper Gravelbourg and Shaunavon formations) are Middle Jurassic, possibly Late Bajocian based on contained faunas and on indirect dates from the Piper in adjacent Montana (Wall, 1960; Paterson, 1968; Poulton, 1984). These formations are a shallow marine, limestone-rich, heterogeneous unit containing sandstones and shales. Below these, and above the Watrous, is a dolomitic, argillaceous limestone or calcareous mudstone unit that has yielded small bivalves and fish fossils, foraminifera, ostracods, and palynomorphs, none of which provides a firm age and some of which suggest stressed marine environments (Lower Gravelbourg, see Kreis, 1991). Samples from the Lower Gravelbourg collected during this study have produced mainly nonmarine palynomorphs indicating Jurassic (probably Middle Jurassic) or younger ages (J. Utting and J. White, pers. comm., 2001). This leads to interpreting a major regional unconformity between the Lower Gravelbourg and the Upper Watrous, contradicting the apparently gradational contact indicated by Kreis (1991). At least one worker (e.g. Stott, 1955) considered the Upper Amaranth anhydrite in Manitoba to grade up into the undated Reston limestone above it, and considered it to be Middle Jurassic, while the chert concretions at the top of the anhydrite suggested an unconformable relationship to McCabe (1990, p11).

The oldest dated marine Jurassic strata in Montana above Watrous equivalents is the middle limestone member of the Piper Formation, dated as Late Bajocian because of the similarity of molluscs within it to those of the Rich Member of the Twin Creek Limestone of Utah. This unit, in turn, is dated by its gradational relationship with the underlying Sliderock Member, which contains a varied early Late Bajocian assemblage (Imlay, 1980, p80). The lower member of the Piper is suggested to be late Early Bajocian (Middle Bajocian, Imlay, 1980), based on a possible equivalence with the lithologically different Sawtooth Formation at Swift Reservoir, northwestern Montana.

Assuming these ages to be correct, the Kline (limestone and dolostone), Picard (red shale), and Poe Evaporite (gypsum) members of the Nesson Formation are undated.

4. Strontium Isotopes in Seawater and Evaporites

Strontium isotope ratios in seawater varied with time. This variation is recorded in calcium-bearing fossils and minerals precipitated from seawater (e.g., Burke *et al.*, 1982; McArthur, 1994; Veizer *et al.*, 1999). Because the mixing time of the oceans is thousands of years and the residence time of strontium is millions of years, the open oceans contain perfectly mixed strontium isotopes. The $^{87}Sr/^{86}Sr$ ratio curve is constructed by determining the isotope ratio in samples of known age that have retained the original seawater ratio (reviewed by Veizer *et al.*, 1997). The quality of the age assignment and selection of samples that have retained the original ratio are crucial in the construction of the curve. By convention, the seawater curve is said to be rising or increasing (ratio increasing with decreasing age) or falling or declining (ratio decreasing with decreasing age).

Evaporites represent a special challenge because they can be precipitated from brines derived from seawater, continental water, or mixtures of the two (hybrid waterbodies). In order to determine the age of sedimentation for anhydrite/gypsum beds using strontium isotope stratigraphy, the evaporites must first be shown to carry a marine isotopic signal. Establishing a marine origin is based on the consistency of isotopic results from different stratigraphic intervals within the unit at different geographic locations (Denison *et al.*, 1998). The mixing of marine and meteoric water (Bryant *et al.*, 1995) invariably leads to an inconsistent isotope signal at different localities (e.g. the present-day Baltic Sea, Andersson *et al.*, 1992, 1994). The ratio in mixed waters also varies with time (e.g. San Francisco Bay over the last 4,300 years, Ingram and DePaolo, 1993; varves in the Permian Whitehorse gypsum, Denison *et al.*, 1998). If a marine isotope signal can be identified from evaporite results, the age can be determined or constrained by comparison with the established global seawater strontium curve.

The strontium isotope ratio of a hybrid water body can be either higher or lower than seawater, depending on the geology of the area supplying meteoric runoff to the salina (Denison *et al.*, 1998). Therefore, the isotope ratios of evaporites derived from a hybrid brine scatter along a line anchored by the isotopic composition of contemporaneous seawater and the mean of the meteoric contribution. The Watrous isotopic evidence indicates that the meteoric influence in the salina carried strontium more radiogenic than contemporary seawater. The lowest isotopic values determined in a particular well are therefore closest to marine water.

5. Sulphur and Oxygen Isotopes in Seawater Sulphate and Evaporites

Sulphur isotopic ratios also vary in seawater with time (see the review of Strauss, 1997). Because sulphur and strontium ratios vary independently, the results can be used together to reduce the stratigraphic ambiguity caused by oscillations in both curves. A limited comparison of isotope results from the same samples shows that strontium is much more sensitive to meteoric influence than is sulphur (Denison *et al.*, 1998). The sulphur isotopic variation is less well defined than that of strontium because evaporites, traditionally used in defining the curve, are difficult to date precisely and are not uniformly represented in the geologic record (Strauss, 1999). Unfortunately, the depositional age indicated by the Watrous strontium results is one of the time intervals in which the seawater sulphur isotope curve is not well defined. Nevertheless, some of the 36 sulphur isotope ratios determined in this study proved useful and definitive in differentiating evaporites other than those deposited from Watrous seas.

Changes in the S- and O-isotope compositions of SO_4^{2-} by three processes are reasonably well understood (Krouse, 1987). These are summarized in Figure 2 with respect to present oceanic SO_4^{2-}. Of primary importance is the fact that O-isotope exchange between SO_4^{2-} and H_2O is extremely slow and therefore is not shown. During bacterial SO_4^{2-} reduction (BSR), unreacted SO_4^{2-} becomes enriched in heavier isotopes of both sulphur and oxygen. In many laboratory experiments and field studies, plots of $\delta^{18}O$ vs. $\delta^{34}S$ yield a slope of 0.25 (e.g. Mizutani and Rafter, 1969; Krouse, 1987) which perhaps relates to the atomic ratio of sulphur to oxygen in the sulphate structure. However, further laboratory investigations show that the oxygen isotope composition of unreacted SO_4^{2-} is dependent upon that of the solvent water (e.g. Mizutani and Rafter, 1973). This is attributed to exchange of O-isotopes between intermediates in the conversion coupled with back reaction to SO_4^{2-}. In Figure 2, the range of slope for SO_4^{2-} reduction is somewhat arbitrary. For SO_4^{2-} reduction in bottom waters ($\delta^{18}O$=0 ‰) of stratified lakes in the Canadian Arctic, the slope is 0.5 (Jeffries *et al.*, 1984). Presumably the slope can be larger for SO_4^{2-} reduction occurring in evaporated water with higher $\delta^{18}O$ values.

During crystallization of hydrated $CaSO_4$, ^{34}S, and ^{18}O are favoured over ^{32}S and ^{16}O by factors of 1.016 and 1.036 respectively (Holser *et al.*, 1979). Hence the $\delta^{18}O$ and $\delta^{34}S$ values of SO_4^{2-} decrease with a slope of about 2.

Admixture of continental SO_4^{2-} usually reduces both the $\delta^{34}S$ and $\delta^{18}O$ values of oceanic SO_4^{2-}. For the most part this arises from oxidation of mineral sulphides and organic matter in H_2O with varying negative $\delta^{18}O$ values. During oxidation of lower valence sulphur compounds, O in SO_4^{2-} arises from both H_2O and O_2 in an approximate ratio of 2:1 (see review of Van Stempvoort and Krouse, 1994).

SO_4^{2-} reduction followed by quantitative HS^- re-oxidation leads to increase or decrease along the y-axis of Figure 2 dependent upon the $\delta^{18}O$ value of the associated water.

Whereas the individual trends in Figure 2 fall into two quadrants, combinations of these trends can generate data in all quadrants.

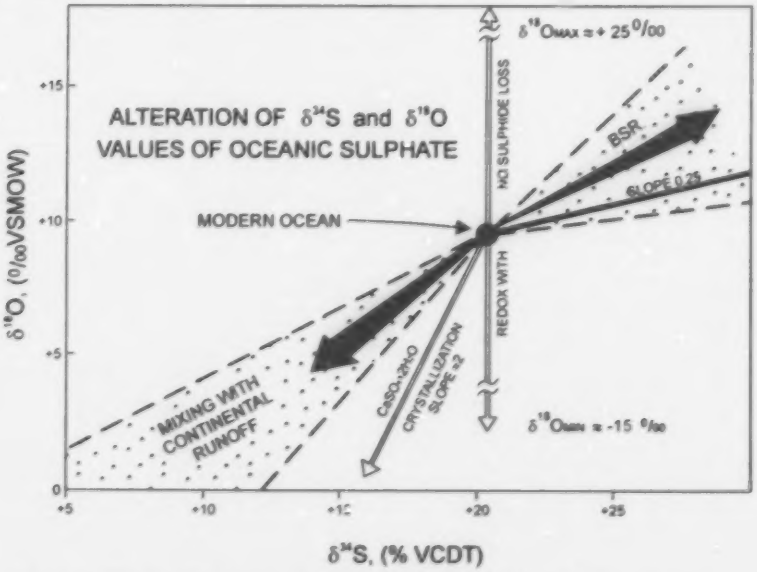

Figure 2 - Effects of major processes that alter the sulphur and oxygen isotope compositions of oceanic SO_4^{2-}. The modern ocean has been chosen as the reference point. This point has moved over geological time in response to the various processes shown. See text for explanation.

Evaporite formation of $CaSO_4 \cdot 2H_2O$ is accompanied by $\delta^{34}S$ and $\delta^{18}O$ shifts of about +1.6 and +3.6 with respect to the sulphate in solution, which in turn responds over time to the processes shown in Figure 2. Detailed sampling of long cores for isotopic determination of sulphate has seldom been attempted. In some studies, remarkable consistency of $\delta^{34}S$ and $\delta^{18}O$ values has been found over depth intervals of hundreds of metres (e.g. Shakur, 1982). Long term trends have also been found. For example, in the Lower Permian Mount Bayley Formation of the Sverdrup Basin, the $\delta^{34}S$ and $\delta^{18}O$ values both decreased with decreasing depth from about +15 ‰ to +12 ‰ over an interval of 335 m (Shakur, 1982). This author also found a similar average trend for the Middle Pennsylvanian Otto Fiord Formation in the same basin.

Cycles of smaller $\delta^{34}S$ and $\delta^{18}O$ changes were found in both cores over depth intervals of the order of 10 m.

Cycles of $\delta^{34}S$ and $\delta^{18}O$ changes have also been identified over distances of less than 1 m in modern evaporites, e.g. Trucial Coast (Butler *et al.*, 1973). In that study, over 90% of the original SO_4^{2-} had mineralized. Changes in long term trends by erosion by continental brines were recognized by changes in $\delta^{34}S$ values.

6. Sample Preparation and Analysis

For $^{87}Sr/^{86}Sr$ analysis, the anhydrite and gypsum samples were dissolved in pure water. The strontium was separated and analyzed using techniques described by Kirkland *et al.* (2000). Results from these samples are reported as $^{87}Sr/^{86}Sr$ and the difference between this and modern seawater (Δ_{SW}).

Δ_{SW} = (unknown - $^{87}Sr/^{86}Sr$ modern seawater) x 10^5

More than 100 measurements of modern seawater (0.709173) yield a weighted mean difference of Δ_{SW} +106.7 ±0.3 for the NBS $SrC0_3$ standard. All published results are normalized to these values.

For sulphur and oxygen analysis, raw samples were dissolved in dilute HCl followed by $BaSO_4$ precipitation with a 10% $BaCl_2$ solution. The low pH minimizes $BaCO_3$ precipitation but it also reduces the half time for O-isotope exchange between SO_4^{2-} and H_2O. Therefore, solutions should not be left standing for long periods. After decantation, the $BaSO_4$ was washed twice with deionized H_2O. After the third addition of H_2O, the supernatant was tested for the presence of Cl^- by adding $AgNO_3$. Washing was continued until Cl^- could not be detected. The $BaSO_4$ was then oven dried at 110°C.

For sulphur isotope analysis, SO_2 was prepared by heating a $BaSO_4$-V_2O_5-SiO_2 mixture as described by Yanagisawa and Sakai (1983).

For oxygen isotope analysis, CO_2 was produced by heating an intimate mixture of $BaSO_4$ and pure graphite at approximately 1000°C. The mixture was placed in a "canoe" made from platinum sheet stock pinched on both ends by machined electrical leads (Sakai and Krouse, 1971). Any CO_2 generated in the reaction was converted to CO_2 by electrical discharge in a cell partially immersed in liquid N_2.

Isotopic analysis of CO_2 and SO_2 were carried out in highly modified Micromass 903 and 602 dual inlet, simultaneous collection mass spectrometers.

Reproducibility of isotopic data was better than ±0.2 ‰ and ±0.4 ‰ for $\delta^{34}S$ and $\delta^{18}O$ respectively.

7. Isotope Results and Discussion

Multiple samples were chosen from individual beds and from vertically adjacent beds from wells over a wide region. The isotope results show that not all the Watrous evaporites were deposited in the same salina and that they most likely represent several ages of deposition. With one exception (at Lake St. Martin, Manitoba), the evaporites, particularly the thickest gypsums, were deposited from marine water.

The locations of samples from the Watrous Formation are shown in correlated cross sections by arrows (Figures 3, 4, and 5).

The isotope ratios determined are shown on Tables 2 and 3 and compiled on Figures 6 and 7. A strong peak centres near $^{87}Sr/^{86}Sr$ 0.70828 (Δ_{SW} -90) with a lesser number of both higher and lower values. The samples represented by the peak are mostly from the more massive anhydrites in the Watrous Formation. An example of the consistency of results can be seen in the five determinations from the interval between 4248 to 4263 ft (1294.8 to 1299.4 m) in the KCL Home Viewfield 15-29-7-8W2 well. The mean of these values is 0.708269 ±7 (Δ_{SW} -90.4) with every determination agreeing within error. Results from other wells are equally consistent (Tables 2 and 3). Anhydrites that yield higher ratios are present in some of these Watrous wells. Their values are near Δ_{SW} -110 (0.70807). All are from the highest stratigraphic samples, suggesting a younger age. The range of single-well results is interpreted as the change in seawater during Watrous deposition, from Δ_{SW} -90 to Δ_{SW} -110 (0.70827 to 0.70807).

If the strontium values more radiogenic than the peak are due to meteoric influence, then an explanation for the 15 less radiogenic values is needed. The stratigraphic position of some of these anhydrites gives an important clue. In the wells from which an extended section was sampled, the lowest isotope ratios were generally determined from the highest stratigraphic horizons. The explanation for this may be that these younger anhydrites record the systematic change in the seawater strontium isotope ratio with time. A single gypsum/anhydrite bed several metres thick represents the evaporation of an enormous volume of seawater but little geologic time, thousands rather than millions of years (see discussion of Denison *et al.*, 1998). A systematic change in the seawater ratio due to age differences would not be expected even in the thickest gypsum/anhydrite beds (e.g. the KCL Home Viewfield 15-29-7-8W2 well) because of the rapid deposition rates. When evaporite beds are separated, the intervening beds almost certainly represent substantially more time or even interrupted sedimentation. Where the samples can be placed in stratigraphic context, the anhydrite yielding a lower ratio, indicating a younger age, is from a bed physically separated from beds yielding $^{87}Sr/^{86}Sr$ of 0.70827 (Δ_{SW} -90). Because demonstrably younger samples generally yield lower ratios, all samples with lower ratios, even isolated samples for which there is no stratigraphic context, are regarded as younger. The

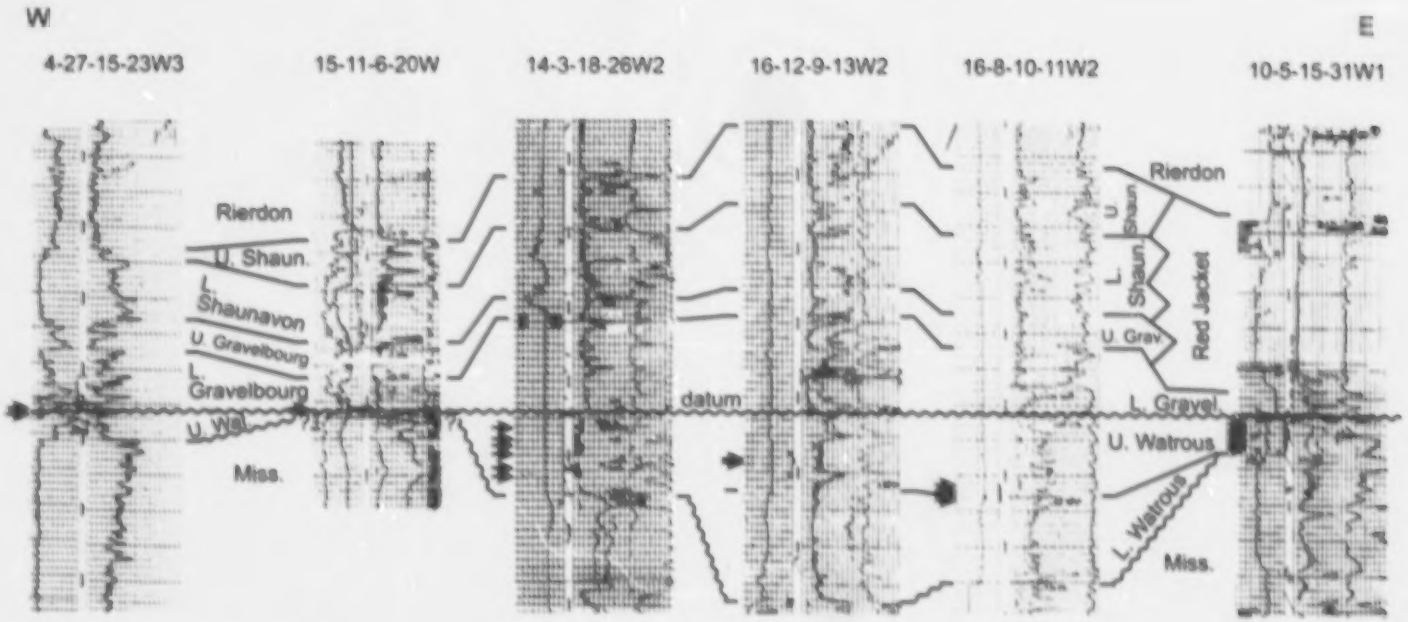

Figure 3 - Cross section W-E. Formation tops in the Saskatchewan wells are from K. Kreis. In all cross sections, cores through the anhydrite-bearing interval are not abundant, and the quality of geophysical logs is highly variable, particularly in the older wells. The sample intervals in all cross sections, shown by arrows, are approximate because of the minor discrepancies between depths interpreted from cores and logs. Datum - top of Upper Member, Watrous Formation.

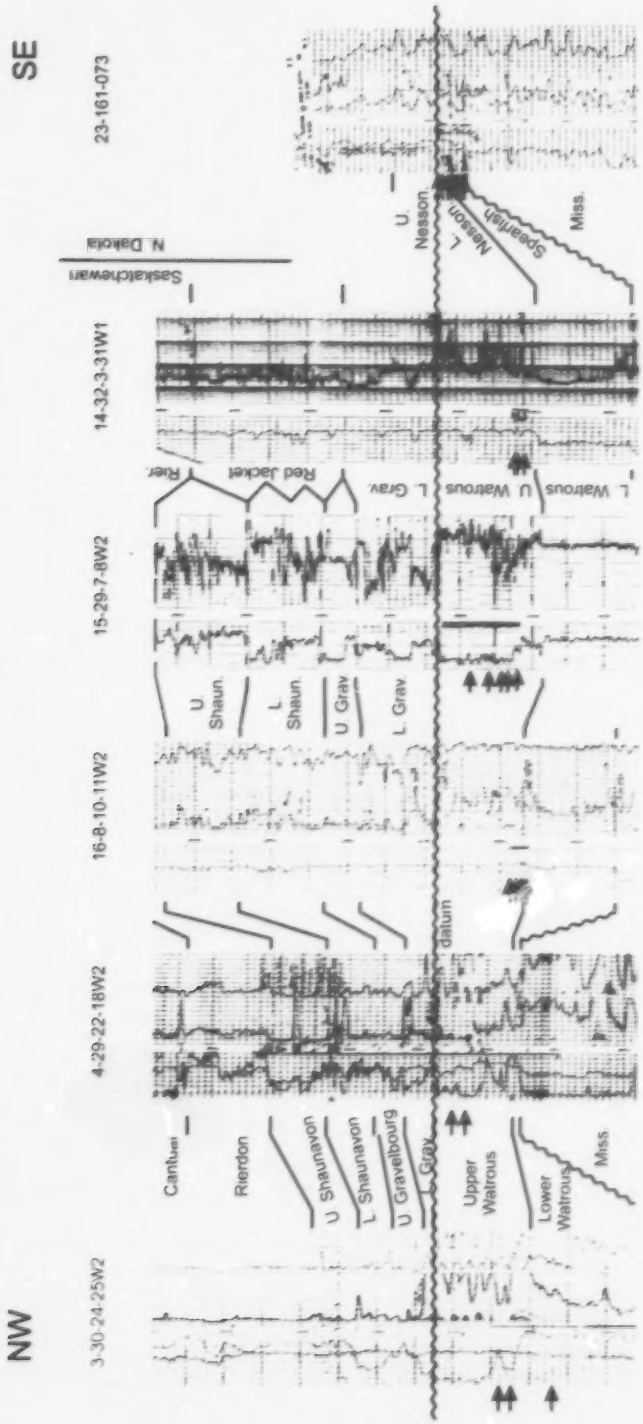

Figure 4 - Cross section NW-SE. Formation tops in the North Dakota well 23-161-073 are after LeFever et al. (1991).

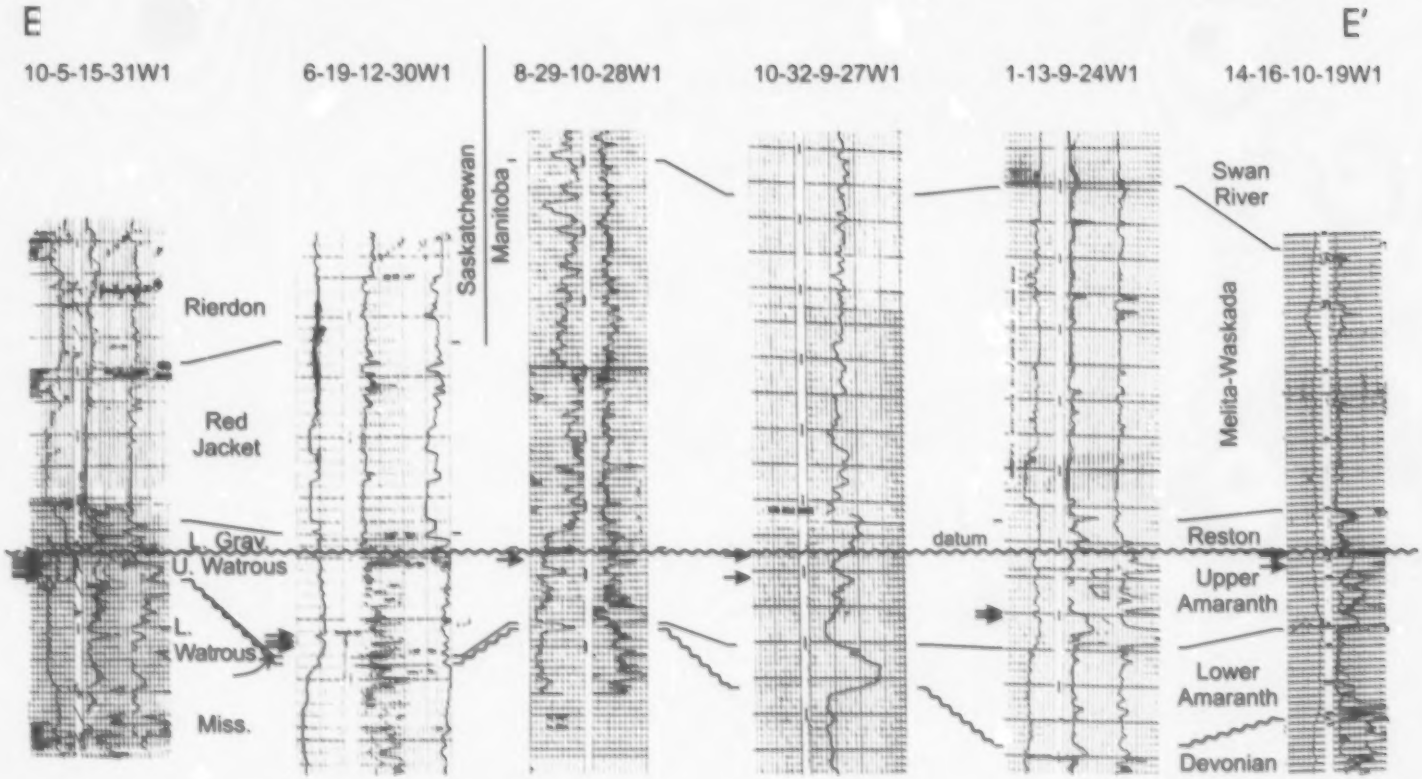

Figure 5 - Cross section E-E'. The formation tops in the Manitoba wells are taken from picks cards prepared by H. McCabe and supplied by R. Bezys, both of Manitoba Energy and Mines..

Table 2 - Strontium isotopic ratios and the core depths from which samples were taken.

Well ID	Depth (feet except 6-19-12-30-W1)	$^{87}Sr/^{86}Sr$	ΔSW
4-27-15-23W3	3457.0	0.707805±17	-136.9
	3460.0	0.707887±17	-128.6
	3461.0	0.707916±16	-125.7
15-11-8-20W2	4910.0	0.707553±13	-162.0
	4910.5	0.707549±14	-162.4
	4911.0	0.707596±14	-157.7
	4911.5	0.707581±16	-159.2
16-12-9-13W2	3986-88	0.708271±5	-90.2
	3986-88	0.708269±11	-90.4
	3986-88	0.708294±9	-87.9
16-8-10-11W2	3818.0	0.708287±13	-88.6
	3821.0	0.708283±17	-91.0
	3827.0	0.708286±16	-88.7
	3836.0	0.708335±12	-83.8
	3836.0	0.708270±10	-90.3
	3836.0	0.708267±8	-90.6
14-32-3-31W1	3478.0	0.708269±17	-90.4
	3479.5	0.708284±17	-88.9
	3483.0	0.708289±13	-90.5
	3484.5	0.708294±18	-88.9
	3485.0	0.708285±15	-89.8
	3489.5	0.708286±16	-88.7
	3490.0	0.708264±16	-90.9
	3491.0	0.708281±18	-89.2
	3492.0	0.708269±19	-90.4
10-5-15-31W1	2188.0	0.708047±16	-112.6
	2190.0	0.708052±11	-112.1
	2191.0	0.708047±14	-112.6
	2192.5	0.708055±17	-111.8
	2193.0	0.708117±13	-105.6
	2200.0	0.708165±15	-100.8
	2201.0	0.708079±17	-109.4
	2203.0	0.708123±17	-105.0
	2203.0	0.708083±8	-109.0
	2204.0	0.708052±15	-112.1
	2204.5	0.708072±10	-110.1
	2208.0	0.708075±16	-109.8
	2210.5	0.708169±16	-100.4
	2213.0	0.708071±13	-110.2
	2214.5	0.708072±17	-110.1
	2217.0	0.708049±15	-112.4
	2221.0	0.707988±16	-118.5
	2221.5	0.707910±9	-126.3
	2222.0	0.707945±14	-122.8
6-19-12-30W1	782m	0.708271±17	-90.2
	783m	0.708212±12	-96.1
	789m	0.708241±15	-93.2
	790.7m	0.708174±10	-99.9
	791m	0.708236±11	-93.7
	791.3m	0.708278±6	-89.5
	791.5m	0.708268±11	-90.5
23-161-073, ND	2616-18	0.708230±16	-94.3
	2616-18	0.708295±16	-87.7
	2616-18	0.708282±16	-89.1
	2618-20	0.708267±14	-90.6
	2618-20	0.708294±8	-87.9
	2618-20	0.708280±16	-89.3
	2618-20	0.708278±18	-89.5
	2618-20	0.708266±12	-90.7
	2618-20	0.708265±15	-90.8
	2622.0	0.708271±10	-90.2
	2638.0	0.708286±14	-88.7
	2648-52	0.708273±6	-90.0
	2648-52	0.708349±15	-82.4
	2652-56	0.708352±15	-82.1
	2652-56	0.708448±16	-72.5
	2652-56	0.708476±14	-69.8
	2657-58	0.708351±11	-82.2
	2657-58	0.708447±6	-72.6
09-139-100, ND	7674-77	0.708081±16	-109.2
	7677-78	0.707952±16	-122.1
	7677-78	0.707920±12	-125.3
	7677-78	0.708149±11	-102.4

Table 3 - Strontium, sulphur, and oxygen isotopic ratios and the core depths from which samples were taken.

Well ID	Depth (in feet)	$^{87}Sr/^{86}Sr$	ΔSW	$\delta^{34}S$	$\delta^{18}O$
3-30-24-25W2	2455.0	0.708270±15	-90.3	20.1	17.5
	2477.5	0.708466±12	-70.7	20.0	16.8
	2531.0	0.708615±14	-55.8	19.8	15.6
14-3-18-26W2	3361.0	0.708178±10	-99.5	20.9	18.5
	3375.0	0.708182±15	-99.1	19.8	18.2
	3385.5	0.708276±17	-89.7	20.0	18.6
	3398.0	0.708339±9	-83.4	20.0	18.1
	3417.0	0.708408±13	-76.5	19.2	17.8
	3421.5	0.708413±12	-76.0	19.4	16.7
4-29-22-18W2	2346.0	0.708092±9	-108.1	20.2	17.1
	2374.0	0.708200±12	-97.3	20.5	16.6
15-29-7-8W2	4219.5	0.708184±12	-98.9	19.7	17.3
	4248.0	0.708268±18	-90.5	19.9	17.4
	4252.5	0.708276±7	-89.7	19.2	15.1
	4257.0	0.708271±13	-90.3	18.9	16.7
	4261.0	0.708258±9	-91.5	20.1	17.4
	4263.0	0.708274±12	-89.9	19.3	17.1
	4275.0	0.708333±9	-84.0	19.7	17.7
08-29-10-28W1	2275.0	0.707976±10	-119.7	21.7	15.1
10-32-9-27W1	2286.0	0.708314±12	-85.9	20.9	17.1
	2311.0	0.708278±11	-89.5	20.8	17.2
01-13-09-24W1	1900.0	0.708286±15	-90.7	20.9	15.2
	1905.0	0.708300±16	-87.3	21.5	16.1
14-16-10-19W1	1364.0	0.707833±14	-134.0	22.3	9.2
	1365.0	0.707900±17	-127.3	22.8	8.9
	1383.0	0.708018±15	-115.5	20.2	14.7
(Devonian)	2125.0	0.708133±18	-104.0	20.6	13.8
06-24-32-9W1	97.0	0.708620±13	-55.3	21.0	15.8
(L St Martin)	107.0	0.708780±5	-39.3	24.5	17.8
	113.0	0.708773±13	-40.0	24.6	8.7
3-28-33-23W2	1737	0.708261±12	-91.2	20.3	1.1
	1753-57	0.708281±13	-89.2	20.1	2.1
(Dev-Duperow)	1893.5	0.708318±19	-85.5	26.5	5.7
Robinson Flat outcrop, SD		0.708184±13	-98.9	10.2	5.9
Robinson Flat outcrop, SD		0.707684±11	-148.9	10.8	9.1
Beaver Road outcrop, SD		0.707314±16	-185.7	10.3	5.5

Watrous sequence must have been deposited during a period of declining seawater strontium ratios consistent with the global curve, and because of the systematic spread of isotope ratios, evaporites assigned to the Upper Watrous must represent a substantial amount of time (millions of years).

The sulphur isotope compositions of samples definitely identified with the Watrous are remarkably consistent ($\Delta^{34}S$ = +19.9 ±0.6 ‰) with no discernable difference from the upper and lower parts of the sequences sampled. The sulphur isotopic composition varies within a smaller range in seawater than strontium and is less sensitive to influence from meteoric water. The 10 samples yielding sulphur isotope values outside the error of the mean of Watrous results, and not precipitated from the Watrous waterbody, also yield anomalous strontium ratios; some are known to be of different age (Figures 6 and 7).

Values of $\delta^{34}S$ and $\delta^{18}O$ are plotted in Figures 8 to 10 as a function of depth in three wells from which four or more samples were analyzed. At Dillman Lindley 14-3-18-26W2 (Figure 8), $\delta^{34}S$ and $\delta^{18}O$ values generally increase with decreasing depth. In the KCL Home Viewfield well (15-29-7-8W2), pronounced minima in the ratios occur at 4250 ft (1295.4 m) (Figure 9). The δ-values above and below this interval are in very close agreement. Two possible explanations for such minima are apparent: extensive $CaSO_4 \cdot 2H_2O$ crystallization lowered both the $\delta^{18}O$ and $\delta^{34}S$ values or an influx of a continental brine may have taken place. In any case,

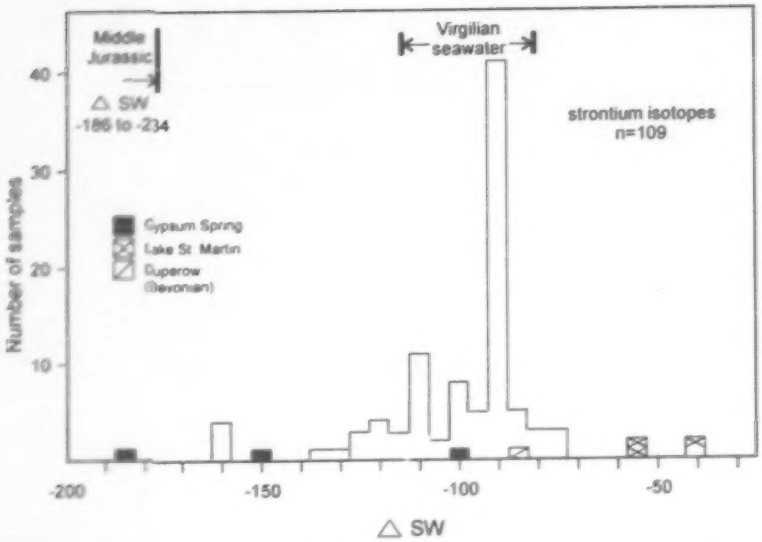

Figure 6 - Histogram plot of all strontium isotope results showing a strong peak at Δ_{SW} -90 (0.70827). Samples with higher ratios are interpreted as derived from hybrid brines (mixtures of marine and meteoric water). Lower ratio samples are interpreted as younger or older than those in the Watrous deposition peak. Range of Δ_{SW} of Virgilian seawater from Denison et al. (1994); Middle Jurassic range taken from Jones et al. (1994b).

the isotopic composition of SO_4^{2-} must have been "reset" after these minima by an incursion of more open ocean water.

A plot of $\delta^{34}S$ vs. $\delta^{18}O$ values for the wells in Figures 8 and 9 is more informative (Figure 10). For both wells, all but one point fall along a trend which is in the regime of dominant bacterial sulphate reduction (BSR; Figure 2). In each case, one point falls significantly below the trends. This implies that in both wells, evidence is present of an episode which lowered $\delta^{34}S$ and $\delta^{18}O$ values.

Data for the three samples from the Lake St. Martin borehole (at 6-24-32-9W1; Figures 10 and 11) differ from the previous figures in that with a relatively constant $\delta^{34}S$ value, a swing of 9 ‰ in $\delta^{18}O$ is apparent. This is suggestive of an incursion of continental water which oxidized sulphide produced from BSR with very little sulphide loss (trend along the negative y-axis in Figure 2).

On the $\delta^{18}O$ vs. $\delta^{34}S$ plot of Figure 10, data from two nearby wells, West and East Daly (8-29-10-28W1, 10-32-9-27W1), fall along a negative slope.

In summary, $\delta^{34}S$ and $\delta^{18}O$ values in cores from two wells have positive slopes consistent with BSR. Both have minima followed with "resetting" of the δ-values by incursion of more open ocean water. At least one well has a large negative slope on the $\delta^{34}S$ and $\delta^{18}O$ plots which suggests a long term trend of continental influence. Anhydrites yielding higher (more radiogenic) strontium ratios are found in a few wells, commonly in the lower part of the section. These are considered to be the results of seawater mixing with meteoric water.

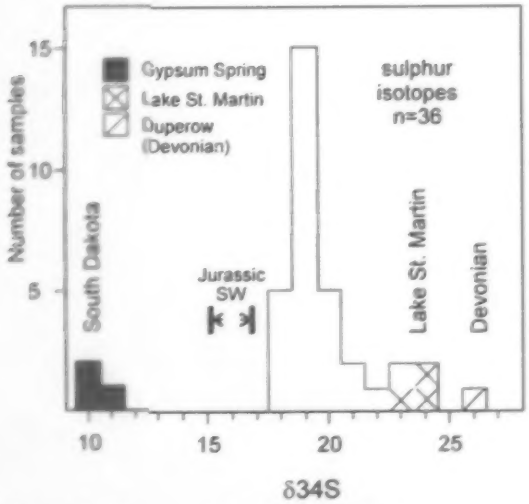

Figure 7 - Histogram of 36 $\delta^{34}S$ values from anhydrite/gypsum samples. The mean of Upper Watrous results is 19.9 ±0.6. Evaporites outside this value are interpreted to be younger or older than those in the peak of Upper Watrous evaporite deposition. Range of $\delta^{34}S$ in Middle Jurassic seawater taken from Strauss (1999).

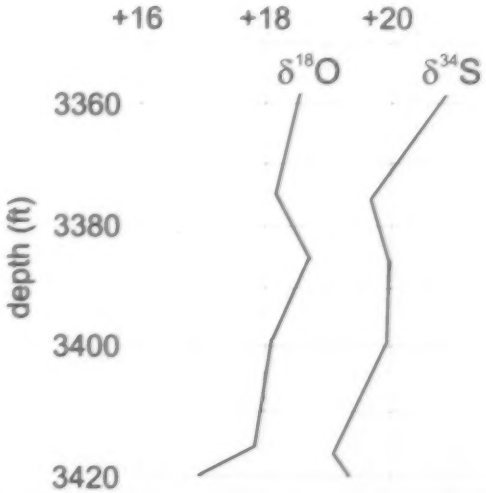

Figure 8 - Variation of $\delta^{18}O$ and $\delta^{34}S$ values with depth in the Dillman Lindley 14-3-18-26W2 well.

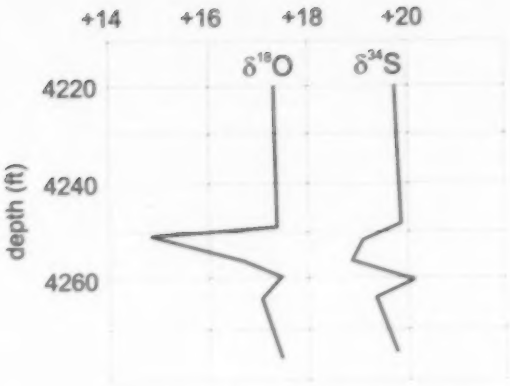

Figure 9 - Variation of $\delta^{18}O$ and $\delta^{34}S$ values with depth in the KCL Home Viewfield 15-29-7-8W2 well.

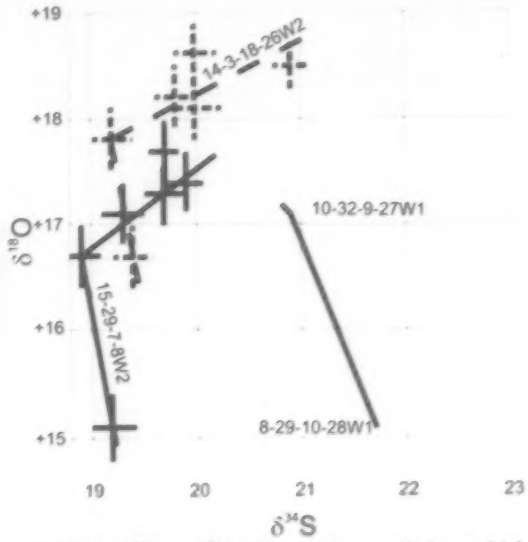

Figure 10 - $\delta^{18}O$ vs. $\delta^{34}S$ values in three wells from which four or more samples were analyzed, and from the West and East Daly wells (10-32-9-27W1 and 8-29-10-28W1). The slopes relate to processes depicted in Figure 2.

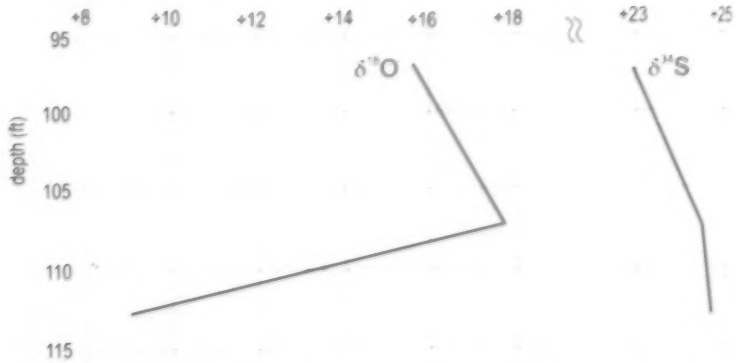

Figure 11 - Variation of $\delta^{18}O$ and $\delta^{34}S$ values with depth in the Lake St. Martin M-05-99 borehole (at 6-24-32-9W1).

8. Isotopic Evidence for the Age of the Watrous

The path of seawater strontium and sulphur isotope ratios with time is determined by analyzing samples of known age that have retained the original seawater ratio. Since the original seawater strontium curve of Burke *et al.* (1982), numerous workers have contributed to a much improved seawater path definition, using improved methods and stratigraphic assignments. The seawater sulphur isotope curve of Claypool *et al.* (1980) and subsequent work has recently been reviewed by Strauss (1999).

The peak of the histograms of strontium isotope values of the Watrous Formation has a mean of 0.708276 ±10 (Δ_{sw} -89.7), representing 41 samples from 12 wells. This value is interpreted as a retained marine ratio because of the isotopic consistency from adjacent intervals in a single well and agreement with results from other wells over a wide area. This seawater value intersects the composite curve of strontium isotopic ratios of Phanerozoic seawater seven times during the Phanerozoic (Figure 12). However, given the stratigraphic constraints for Watrous/Amaranth deposition, one intersection cross-cuts when the curve is declining, i.e. in the latest Pennsylvanian (Figures 12 and 13). The path of seawater strontium isotopes in the Late Pennsylvanian and Early Permian is based on results from stratigraphic sections in northern Oklahoma and adjacent Kansas and the Eastern Shelf of the Permian Basin in Texas (Denison *et al.*, 1994). The seawater ratio falls to near 0.70817 (Δ_{sw} -100) in the mid-Virgilian and remains near this value until the end of the Pennsylvanian, then falls abruptly to near 0.70803 (Δ_{sw} -114) in the earliest Permian (Denison *et al.*, 1994). The values for the lower part of the Upper Watrous Formation centre around 0.70827 (Δ_{sw} -90) and this is equivalent to early Virgilian seawater. The curve of Bruckschen *et al.* (1999) based on analyses of brachiopods would allow Missourian as well as Virgilian ages for the Watrous peak results. Two of the highest Watrous samples yielded values (~Δ_{sw} -110) equivalent to seawater near the Permian/Pennsylvanian boundary.

The $\delta^{34}S$ results from the samples that yielded strontium values in the Δ_{sw} -90 to Δ_{sw} -110 (0.70827 to 0.70807) are very consistent, with a mean of +19.8 ±0.9. Unfortunately, the sulphur seawater curve is not well defined during the Late Pennsylvanian–Early Permian. Strauss (1999) gives no preferred value (his Table 1) for this time interval. The values determined from the Watrous are higher than would be expected from extrapolation through the 40 Ma gap for which there is no preferred seawater value. Detailed data ($\delta^{34}S$ and $\delta^{18}O$) do exist for the Middle Pennsylvanian Otto Fiord and the

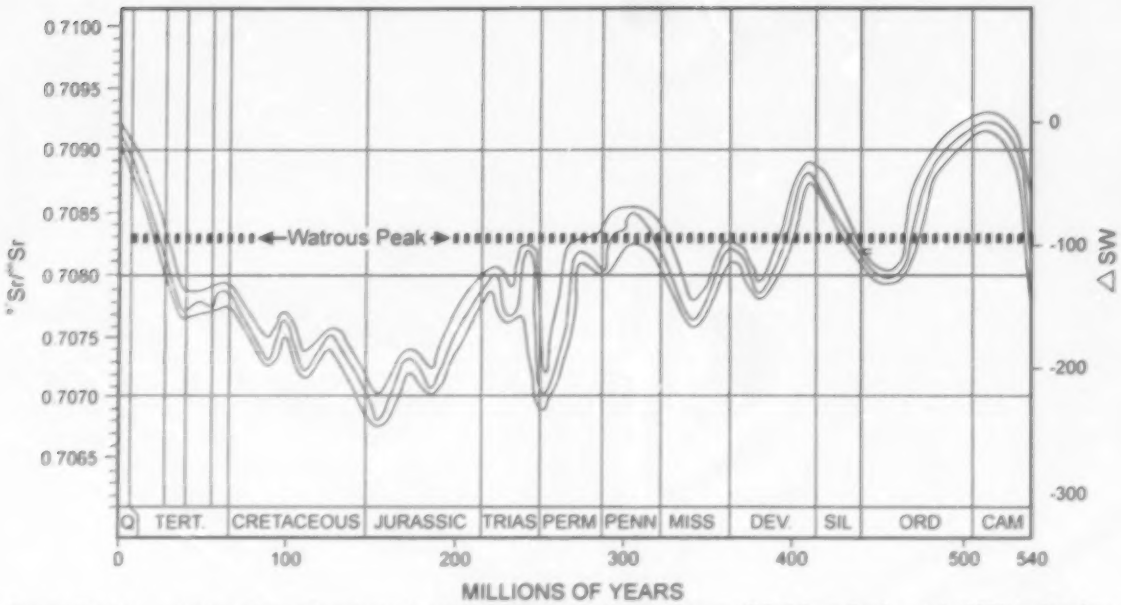

Figure 12 - The variation of strontium isotopic ratios in Phanerozoic seawater, modified from Burke et al. (1982) using data interpreted from the compilations of Howarth and McArthur (1997) and Veizer et al. (1999). The peak value for Watrous values of 0.70827 (Δ_{SW} -90) intersect the curve at seven time intervals but only once with a negative slope during the stratigraphically constrained time for Watrous deposition.

Lower Permian Mt. Bayley evaporite formations in the Sverdrup Basin of the Canadian Arctic (Shakur, 1982), but this basin had periods of very limited connection to the paleo-Pacific Ocean. The average low $\delta^{34}S$ and $\delta^{18}O$ values near +15 ‰ and +13 ‰, respectively, suggest that the isotopic ratios from this basin are not representati e of the open ocean.

The mean of the $\delta^{34}S$ results fits known seawater sulphur during a brief period of declining values recognized in the early Middle Triassic (Jin-Shi and Xue-Lei, 1988). This assumes that the evaporites from China that were used to construct this portion of the curve are correctly correlated to the European stages. Strontium isotopic values are also declining during that interval. Korte (1999) reports marine strontium isotopes values during this time interval in the range of Δ_{SW} -125 to Δ_{SW} -135 (0.70792 to 0.70782), well out of the range of our Watrous results.

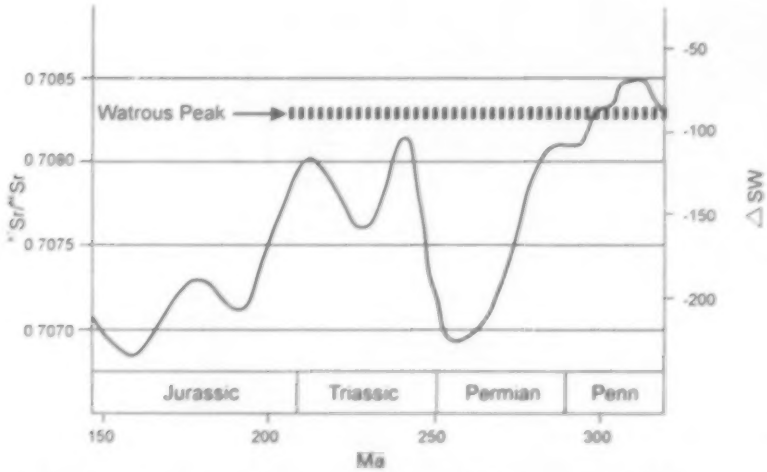

Figure 13 - The variation of strontium isotopic ratios in seawater during the stratigraphically constrained time for Watrous deposition showing peak of Watrous values. Taken from Jones et al. (1994a, 1994b) for the Jurassic, Korte (1999) for the Triassic, Denison et al. (1994) for the Permian, and Denison et al. (1994) and Bruckschen et al. (1999) for the Pennsylvanian. The path of Jurassic seawater is based on UK sample localities; the Triassic from Tethyan realm, West Carpathian and Sicilian localities; and the Permian and Pennsylvanian largely from the southern interior of the United States.

The great consistency of strontium and sulphur isotope results from the Watrous is a clear indication of a marine origin for these evaporites. A 400 km long, northwest-southeast fairway of nine wells through Saskatchewan into North Dakota shows an unequivocal Watrous isotope signal. During the period of stratigraphically constrained deposition, only one time interval is preserved in which Watrous strontium values are known in

seawater. The most likely age of deposition of the lower anhydrites in the Upper Watrous Formation is, therefore, Late Pennsylvanian, with deposition continuing to near the Pennsylvanian-Permian boundary. The consistent Watrous sulphur values neither support nor preclude the Pennsylvanian strontium age assignment.

9. Preliminary Results from Other Samples

Analysis and evaluation of other samples continue, but preliminary results for some of them are available. These include anomalous results from certain wells, some geographically separated from the others, where the correlation to the Upper Watrous was assumed during sampling, but is now debatable. An example is the anhydrite core sample from the Chevron West Daly well (8-29-10-28W1) in Manitoba. None of the sulphur, oxygen or strontium isotope results from this anhydrite are within the Watrous range. Both strontium and oxygen isotope ratios from the higher (presumed Amaranth) samples in the G.D.W. Brandon 14-16-10-19W1 well (1364 and 1365 ft) (415.7 and 416.1 m) fall outside the range of the Watrous. These Manitoba wells occur adjacent to an ancient highland (Birdtail-Waskada Axis), onto which the Upper Watrous, and eventually the overlying Reston limestone, lapped beyond the limits of underlying rocks. This highland partially separated the Amaranth Sub-Basin of southern Manitoba from the larger Watrous sub-basin in southern Saskatchewan (e.g. Kreis, 1991, Figure 3). The presence of the highland and the relative isolation of the Amaranth sub-basin presumably influenced both circulation and meteoric influence of the sea water in this region. Additionally, in some places the Watrous/Amaranth (and eventually northward the overlying Reston) lie directly on Paleozoic rocks, in which evaporites also occur, so possibly some confusion exists regarding the identity of certain evaporites in this situation.

a) Lake St. Martin Impact Structure, Manitoba

Three gypsum cores from the Lake St. Martin impact structure (M-05-99 borehole at 6-24-32-9W1) yielded strontium values dissimilar to those of the Watrous, and sulphur and oxygen values (Figure 11) lie outside the errors for the Watrous. The inconsistent values suggest that these evaporites were not deposited in a body of water well mixed with open oceans. These data do not support a stratigraphic correlation with the Watrous and Amaranth formations from which they are physically separated, as was supposed when the samples were collected, and therefore they do not contribute materially to the age of those units. The evaporites sampled are interlaminated gypsum and buff dolostone, with abundant secondary gypsum veins, unlike Watrous and Amaranth cores and unlike the more massive gypsums that were quarried from within the impact crater. This structure is complicated and remains poorly understood in spite of several radiometric dates having been published (Kohn *et al.*, 1995).

b) North Dakota

The Leonardian (Permian) ages provided by the strontium isotope data from four samples of anhydrite within red siltstones of the Opeche Formation in the Herman May 9-139-100 well conform with the Permian age generally assigned to that formation.

The strontium isotope data from 18 Spearfish and Lower Nesson anhydrite samples in the Sebelius 23-161-073 well conform with those from the Upper Watrous Formation, with which the Lower Nesson of northernmost North Dakota is confidently correlated (LeFever *et al.*, 1991) and thus provide further data supporting the Late Pennsylvanian age of that unit. The upper samples from the 23-161-073 well, from about 2616 to 2622 ft (797.4 to 799.2 m), are from anhydrites within a mainly fine buff dolostone unit (lower Nesson Formation, following LeFever *et al.*, 1991, Col: Lion Oil 23-163-075). Those from 2648 to 2658 ft (807.1 to 810.2 m) are from anhydrites associated with red mudstones ("Spearfish" Formation). These last contain a significant meteoric input signal in the strontium isotopes.

The Pennsylvanian age assigned to the Lower Nesson at the Sebelius well should not be taken as a firm contradiction of the standard interpretation of Middle Jurassic ages for all the Lower Piper or Lower Nesson anhydrites throughout North Dakota and Montana. Rather it suggests the need to re-examine stratigraphic correlations within North Dakota and Montana, for example around northern parts of the Nesson Anticline where the Spearfish Formation (Saude Member) is interpreted to truncate Mississippian through Permian strata (see Anderson, 1974; e.g. 48°30'N Lat., 103°W Long; Dow, 1967; Plate 10, columns 2501, 2182). Re-interpretation from the literature is problematic, but the suggestion offered in Table 1 (Bold face) reflects the strontium isotope results.

c) South Dakota

Three outcrop gypsum samples from the Gypsum Spring Formation at the Robinson Flat and Beaver Road localities along the south and west sides of the Black Hills were analyzed. The strontium values are inconsistent and suggest a large component of meteoric water in an hybrid salina. The sulphur and oxygen ratios are well removed from those of other samples analyzed in this report. The sulphur results are consistent with a mean $\delta^{34}S$ of +10.4 ±0.3 equivalent to Late Permian seawater (Strauss, 1999).

10. Geological Conclusions

Confidently identified Upper Watrous anhydrites, recognized in a number of widely separated wells in Saskatchewan, were precipitated from a hypersaline water body of marine origin (see Figure 1). Some minor influence from meteoric water took place in this

marine-based salina. It shifted with time and location. Relatively short-term isotopic fluctuations, such as those attributed to the influence of meteoric water, can potentially serve to correlate stratigraphic horizons within an evaporitic unit, and give evidence regarding paleogeographic and paleo-oceanographic conditions.

Although the strontium isotope ratio determined on Upper Watrous anhydrites is equivalent to that of seawater seven times during the entire Phanerozoic, it is equivalent to seawater only once during the stratigraphically constrained time of deposition between the Mississippian and the Middle Jurassic. The typical strontium isotope value recorded by the Watrous is equivalent to Virgilian (Pennsylvanian) seawater. The $\delta^{34}S$ results from Watrous evaporites are well defined but less definitive. A recent synthesis of $\delta^{34}S$ in Phanerozoic seawater gives no preferred values for a crucial 40 Ma period during the latest Pennsylvanian-earlier Permian. The only defined time, honoring stratigraphic constraints, that agrees with the Watrous sulphur results is during a spike in $\delta^{34}S$ during the Early and Middle Triassic. Strontium in seawater during this period has a reported value significantly lower than the peak of Watrous results. A Virgilian age of deposition is therefore neither supported nor precluded by the $\delta^{34}S$ results because of a lack of definition of $\delta^{34}S$ in Virgilian seawater.

The strontium isotope evidence indicates that the most likely age of deposition of the lower anhydrites in the upper members of the Watrous (and Amaranth) Formation is Late Pennsylvanian, with deposition continuing to near the Pennsylvanian-Permian boundary. A Jurassic age of deposition for the upper Watrous is precluded by all isotope results. The overlying Lower Gravelbourg and Reston formations remain poorly dated, although palynomorphs conform with a Middle Jurassic age for the former. Considering the revised ages presented here for the Watrous, the age of the overlying units cannot be assumed.

These results open the question of the age of deposition and correlation of all evaporites in the northernmost interior of the United States (Poe, Lower Piper, lower Nesson, Lower Gypsum Spring from place to place) that occupy the same stratigraphic position as the Watrous. The relationships and correlations of these units in northernmost Montana and North Dakota with their supposed equivalents to the south and southwest in those states must be re-examined. Access of the Watrous seas to open ocean water must have been through the Minnelusa (Pennsylvanian) marine facies of North Dakota and Montana.

Intermittently from Ordovician through Late Jurassic time, the Williston Basin was a shallow epicontinental depositional basin. A significant hiatus in sedimentation in the northern part of the basin is interpreted through the absence of any firmly dated strata of Permian through Early Jurassic age. The isotope evidence now associates the red bed and anhydritic Watrous and Amaranth formations with their lithologically more compatible counterparts in the Late Paleozoic, below a major unconformity that is perhaps sub-Middle Jurassic. The overall character of the stratigraphic packages below and above this hiatal interval is different, with evaporites and redbeds comprising a significant portion of the Late Paleozoic strata throughout the western interior U.S., within and beyond Williston Basin. A high-magnitude, short-duration, regional Permian thermal event in the northern part of the basin which reset apatite fission track clocks in the Precambrian crystalline basement was presumably causally associated with the regional uplift that produced the sub-Middle Jurassic unconformity (Osadetz *et al.* 1998).

11. Acknowledgments

F. Haidl and Jim Bamburak initially provided samples from the core archives stored in Saskatchewan and Manitoba. J.E. Christopher, Kim Kreis, Ruth Bezys and Julie LeFever assisted with later collecting. Kreis, Bezys, and LeFever provided correlation data. Nenita Lozano and Jesusa Pontoy-Overend (Isotope Science Laboratory, University of Calgary) provided the sulphur and oxygen isotope measurements. Denise Then prepared the diagrams. Kirk Osadetz, Kreis, Christopher, Bezys, and LeFever provided valuable stratigraphic discussion and insights, while not necessarily agreeing with the conclusions presented here. B.C. Richards provided a thorough and useful review. This study benefited from a NSERC Individual Grant to H.R.K.

12. References

Anderson, S.B. (1974): Pre-Mesozoic paleogeologic map of North Dakota; N. Dakota Geol. Surv., Misc. Map 17.

Andersson, P.S., Wasserburg, G.J., and Ingri, J. (1992): The sources and transport of Sr and Nd isotopes in the Baltic Sea; Earth Planet. Sci. Lett., v113, p459-472.

Andersson, P.S., Wasserburg, G.J., Ingri, J., and Stordal, M.C. (1994): Strontium, dissolved and particulate loads in fresh water and brackish waters: The Baltic Sea and Mississippi Delta; Earth Planet. Sci. Lett., v124, p195-210.

Anna, L. (1986): Geologic Framework of the Ground Water System in Jurassic and Cretaceous rocks in the Northern Great Plains, in Parts of Montana, North Dakota, South Dakota, and Wyoming; U.S. Geol. Surv., Prof. Pap. 1402-B, 18 plates.

Barchyn, D. (1982): Geology and hydrocarbon potential of the Lower Amaranth Formation, Waskada-Pierson area, southwestern Manitoba; Manit. Dep. Energy Mines, Geol. Rep. GR 82-6, 30p.

Bluemle, J.P., Anderson, S.B., Andrew, J.A., Fischer, D.W., and LeFever, J.A. (1986): North Dakota

stratigraphic column; N. Dakota Geol. Surv., Misc. Series 66, Sheet 1.

Bruckschen, P., Oesmann, S., and Veizer, J. (1999): Isotope stratigraphy of the European Carboniferous: Proxy signals for ocean chemistry, climate and tectonics; Chem. Geol., v161, p127-163.

Bryant, J.D., Jones, D.S., and Mueller, P.A. (1995): Influence of fresh water flux on $^{87}Sr/^{86}Sr$ chronostratigraphy in marginal marine environments and dating of vertebrate and invertebrate faunas; J. Paleont., v69, p1-6.

Burke, W.H., Denison, R.E., Hetherington, E.A., Koepnick, R.B., Nelson, H.F., and Otto, J.B. (1982): Variation of seawater $^{87}Sr/^{86}Sr$ throughout Phanerozoic time; Geol., v10, p516-519.

Butler, G.P., Krouse, H.R., and Mitchell, R. (1973): Sulphur-isotope geochemistry of an arid, supratidal evaporite environment, Trucial Coast; *in* Purser, B.H. (ed.), The Persian Gulf, Springer-Verlag, New York, p453-462.

Carlson, C.G. (1968). Triassic-Jurassic of Alberta, Saskatchewan, Manitoba, Montana, and North Dakota; Amer. Assoc. Petrol. Geol. Bull., v52, no10, p1969-1983.

_____ (1993): Permian to Jurassic redbeds of the Williston Basin; N. Dakota Geol. Surv., Misc. Series 78, 21p.

Christopher, J.E. (1990): Watrous; *in* Glass, D.J. (ed.), Lexicon of Canadian Stratigraphy, Volume 4, Western Canada, including eastern British Columbia, Alberta, Saskatchewan and southern Manitoba, Can. Soc. Petrol. Geol., p677.

Claypool, G.E., Holser, W.T., Kaplan, I.R., Sakai, H., and Zak, I. (1980): The age curves of sulphur and oxygen isotopes in marine sulphate and their mutual interpretation; Chem. Geol., v28, p199-260.

Denison, R.E., Kirkland, D.W., and Evans, R. (1998): Using strontium isotopes to determine the age and origin of gypsum and anhydrite beds; J. Geol., v106, p1-17.

Denison, R.E., Koepnick, R.B., Burke, W.H., Hetherington, E.A., and Fletcher, A. (1994): Construction of the Mississippian, Pennsylvanian, and Permian seawater $^{87}Sr/^{86}Sr$ curve; Chem. Geol., v112, p145-167.

Dow, W.G. (1967): The Spearfish Formation in the Williston Basin of Western North Dakota; N. Dakota Geol. Surv., Bull. 52, 28p.

Edwards, D.E., Barclay, J.E., Gibson, D.W., Kvill, G.E., and Halton, E. (1994): Triassic strata of the Western Canada Sedimentary Basin; *in* Mossop, G.D. and Shetson, I. (comp.), Geological Atlas of the Western Canada Sedimentary Basin, Can. Soc. Petrol. Geol./Alta. Geol. Surv., p259-275.

Francis, D.R. (1956): Jurassic Stratigraphy of the Williston Basin Area; Sask. Dep. Miner. Resour., Rep. 18, 69p.

Holser, W.T. (1992): Stable isotope geochemistry of sulphate and chloride rocks; *in* Clauer, N. and Chaudhuri, S. (eds.), Isotopic Signatures and Sedimentary Records, Lecture Notes in Earth Sciences, Vol. 43, Springer-Verlag, Berlin, p154-176.

Holser, W.T., Kaplan, I.R., Sakai, H., and Zak, I. (1979): Isotope geochemistry of oxygen in the sedimentary sulphate cycle; Chem. Geol., v25, p1-17.

Howarth, R.J. and McArthur, J.M. (1997): Statistics for strontium isotope stratigraphy: A robust LOWNESS fit to the marine Sr-isotope curve for 0 to 206 Ma, with look-up table for derivation of numeric age; J. Geol., v105, p441-456.

Imlay, R.W. (1980): Jurassic paleobiogeography of the conterminous United States in its continental setting; U.S. Geol. Surv., Prof. Pap. 1062, 134p.

Ingram, B.L. and DePaolo, D.J. (1993): A 4300 year strontium isotope record of estuarine paleosalinity in the San Francisco Bay, California; Earth Planet. Sci. Lett., v119, p103-119.

Jeffries, M.O., Krouse, H.R., Shakur, M.A., and Harris, S.A. (1984): Isotope geochemistry of stratified lake "A", Ellesmere Island, NWT, Canada; Can. J. Earth Sci., v21, p1008-1017.

Jin-Shi, C and Xue-Lei, C. (1988): Sulphur isotope composition of Triassic marine sulphates of south China; Chem. Geol., v72, p155-161.

Jones, C.E., Jenkyns, H.C., Coe, A.L., and Hesselbo, S.P. (1994a): Strontium isotopic variations in Jurassic and Cretaceous seawater; Geochim. Cosmochim. Acta, v58, p3061-3074.

Jones, C.E., Jenkyns, H.C., and Hesselbo, S.P. (1994b): Strontium isotopes in Early Jurassic seawater; Geochim. Cosmochim. Acta, v58, p1285-1301.

Kirkland, D.W., Denison, R.E., and Dean, W.E. (2000): Parent brine of the Castile evaporites (Upper Permian), Texas and New Mexico; J. Sed. Resear., v70, p749-761.

Kohn, B.P., Osadetz, K.G., and Bezys, R.K. (1995): Apatite fission-rack dating of two crater structures in the Canadian Williston Basin; Bull. Can. Petrol. Geol., v43, no1, p54-64.

Korte, C. (1999): $^{87}Sr/^{86}Sr$-, $\delta^{18}O$-, und $\delta^{13}C$-evolution des Triassischen Meerswassers: Geochemische

und stratigraphische untersuchungen an conodonten und brachiopoden: Bochumer Geologische and Geotechnische Arbiten; Ruhr-Universität Bochum, Heft 52, 171p.

Kreis, L.K. (1991): Stratigraphy of the Jurassic System in the Wapella-Moosomin Area, Southeastern Saskatchewan; Sask. Energy Mines, Rep. 217, 90p.

Krouse, H.R. (1987): Relationships between the sulphur and oxygen isotope composition of dissolved sulphate; Studies on sulphur isotope variations in nature, Proceedings Series, Internat. Atomic Energy Agency, Vienna, p19-29.

LeFever, J.A., Martiniuk, C.D., and Anderson, S.B. (1991): Correlation cross-sections along the United States-Canada international border (North Dakota-Manitoba); N. Dakota Geol. Surv. Rep. Investigation 92/Manit. Energy Mines Petrol. Open File Rep. POF 12-91, Triassic/Jurassic, Sheet 2.

Mallory, W.W. (1972): Regional synthesis of the Pennsylvanian System; *in* Mallory, W.W. (ed.), Geological Atlas of the Rocky Mountain region, Rocky Mtn. Assoc. Geol., Denver, p111-138.

McArthur, J.M. (1994): Recent trends in Sr isotope stratigraphy; Terra Nova, v6, p331-358.

McCabe, H.R. (1990): Amaranth; *in* Glass, D.J. (ed.), Lexicon of Canadian Stratigraphy, Volume 4, Western Canada, including eastern British Columbia, Alberta, Saskatchewan and southern Manitoba, Can. Soc. Petrol. Geol., p11-12.

McLachlan, M.E. (1972): Triassic System; *in* Mallory, W.W. (ed.), Geological Atlas of the Rocky Mountain region, Rocky Mtn. Assoc. Geol., Denver, p166-176.

Milner, R.L. and Thomas, G.E. (1954): Jurassic system in Saskatchewan; Western Canada Sedimentary Basin, Amer. Assoc. Petrol. Geol., Rutherford Memorial Volume, p250-267.

Mizutani, Y. and Rafter, T.A. (1969): Oxygen isotopic composition of sulphates – Part 4; New Zealand J. Sci., v12, p60-68.

_____ (1973): Isotopic behavior of sulphate oxygen in the bacterial reduction of sulphate; Geochem. J., v6, p183-191.

Osadetz, K.G., Hannigan, P.K., Stasiuk, L.D., Kohn, B.P., O'Sullivan, P., Feinstein, S., Everitt, R.A., Gilboy, C.F., and Bezys, R.K. (1998): Williston Basin thermotectonics: Variations in heat flow and hydrocarbon generation; *in* Christopher, J.E., Gilboy, C.F., Paterson, D.F., and Bend, S.L. (eds.) Eighth International Williston Basin Symposium, Sask. Geol. Soc., Spec. Publ. No. 13, p147-165.

Paterson, D.F. (1968): Jurassic Megafossils of Saskatchewan with a Note on Charophytes; Sask. Dep. Miner. Resour., Rep. 120, 135p.

Peterson, J.A. (1972): Jurassic System; *in* Mallory, W.W. (ed.), Geological Atlas of the Rocky Mountain region, Rocky Mtn. Assoc. Geol., Denver, p177-198.

Pocock, S.A.J. (1972): Palynology of the Jurassic sediments of western Canada, Part 2, Marine Species; Palaeontographica, Abt. B, Bd. 137, p85-153.

Poulton, T.P. (1984): The Jurassic of the Canadian western interior from 49°N Latitude to Beaufort Sea; *in* Stott, D.F. and Glass, D.J. (eds.), The Mesozoic of Middle North America, Can. Soc. Petrol. Geol., Mem. 9, p15-41.

Poulton, T.P., Christopher, J.E., Hayes, B.J.R., Losert, J., Tittemore, J., Gilchrist, R.D., Bezys, R., and McCabe, H.R. (1994): Jurassic and lowermost Cretaceous strata of the Western Canada Sedimentary Basin, Chapter 18; *in* Mossop, G.D. and Shetson, I. (comp.), Geological Atlas of the Western Canada Sedimentary Basin, Can. Soc. Petrol. Geol./Alta. Geol. Surv., p297-316.

Richards, B.C., Barclay, J.E., Bryan, D., Hartling, A., Henderson, C.M., and Hinds, R.C. (1994): Carboniferous strata of the Western Canada Sedimentary Basin; *in* Mossop, G.D. and Shetson, I. (comp.), Geological Atlas of the Western Canada Sedimentary Basin, Can. Soc. Petrol. Geol./Alta. Geol. Surv., p221-250.

Sakai, H. and Krouse, H.R. (1971): Elimination of memory effects in $^{18}O/^{16}O$ determinations in sulphates; Earth Planet. Sci. Lett., v11, p369-363.

Shakur, A.S. (1982): $\delta^{34}S$ and $\delta^{18}O$ variations in terrestrial evaporites; unpubl. Ph.D. thesis, Univ. Calgary, 229p.

Stott, D.F. (1955): Jurassic stratigraphy of Manitoba; Manit. Dep. Mines Miner. Resour., Publ. 54-2, 78p.

Strauss, H. (1997): The isotopic composition of sedimentary sulphur through time; Palaeogeog., Palaeoclim., Palaeoecol., v132, p97-118.

_____ (1999): Geological evolution from isotope proxy signals - sulphur; Chem. Geol., v161, p89-101.

Van Stempvoort, D.R. and Krouse, H.R. (1994): Controls of $\delta^{18}O$ in sulphate: Review of experimental data and application to specific environments; *in* Environmental Geochemistry of Sulphide Oxidation, Amer. Chem. Soc. Symposium Series 550, p446-480.

Veizer, J., Buhl, D., Diener, A., Ebneth, S., Podlaha, O. G., Bruckschen, P., Jasper, T., Korte, C., Schaaf, M., Ala, D., and Azmy, K. (1997): Strontium isotope stratigraphy: Potential resolution and event correlation; Palaeogeog., Palaeoclim., Palaeoecol., v132, p65-77.

Veizer, J., Ala, D., Azmy, K., Bruckschen, P., Buhl, D., Bruhn, F., Carden, G. A. F., Diener, A., Ebneth, S., Godderis, Y., Jasper, T., Korte, C., Pawellek, F., Podlaha, O.G., and Strauss, H. (1999): $^{87}Sr/^{86}Sr$, $\delta^{13}C$, $\delta^{18}O$ evolution of Phanerozoic seawater; Chem. Geol., v161, p59-88.

Wall, J.H. (1960): Jurassic microfaunas from Saskatchewan; Sask. Dep. Miner. Resour., Rep. 53, 228p.

Yanagisawa, F. and Sakai, H. (1983): Preparation of SO_2 for sulphur isotope ratio measurements by thermal decomposition $BaSO_4$-V_2O_5-SiO_2 mixtures; Anal. Chem., v55, p985-987.

The Lower Cretaceous Mannville Meadow Lake Basin and its Temporal Counterparts, West-central Saskatchewan

J.E. Christopher [1]

Christopher, J.E. (2001): The Lower Cretaceous Mannville Meadow Lake Basin and its temporal counterparts, west-central Saskatchewan; *in* Summary of Investigations 2001, Volume 1, Saskatchewan Geological Survey, Sask. Energy Mines, Misc. Rep. 2001-4.1.

1. Surficial Topographic Elements

The study area covers the southwestern quarter of the Meadow Lake Basin on the Paleozoic system. It is bounded by Townships 55 and 70 and Ranges 7 west of the Third Meridian and the interprovincial boundary with Alberta at longitude 110° (Figure 1). Verdant forests, rivers, and lakes (Figure 2) laid out on a 100 to 200 m thick blanket of surficial glacial deposits shape a landscape dominated by the Mostoos Hills in the northwest and the Meadow Lake upland in the south, as delineated by the 610 m contour (Figure 3). A central zone of east-northeast-sloping, rolling countryside is incised by the Beaver, Waterhen and Makwa rivers west of longitude 108°, and the north-flowing Green and Beaver rivers in the east. All rivers access major lakes: Primrose and Cold lakes in the northwest and the Doré-Sled-Beaupre lakes complex in the northeast. The smaller lake complexes, such as Ministikwan-Makwa in the southwest, Pierce Lake, Lac des Îsles, Waterhen, and Flotten of the Waterhen river system in the northwest and central district, and Meadow Lake, Chitek, Green, Cowan and Delaronde lakes in the southeast, are either collecting sites in local depressions and/or are widened expressions of the linear stream courses. All drainage runs into the Waterhen and Beaver rivers, which flow toward the east on near parallel courses to longitude 108°. The Beaver bends north at the confluences of the north-flowing Green and Cowan rivers, whereas the Waterhen, to the east of Waterhen Lake, flows northeastward before joining the Beaver. From the east, the Doré River meanders northward as it angles into the Beaver River. In the southwest, the Ministikwan River, entrenched in a reticulate northeast-trending valley, flows into Makwa Lake. From there, the Makwa River flows east and north. On its course to the Beaver River, the Makwa is joined by north-aligned tributaries from the Meadow Lake upland on which the Chitek River, Tea Creek, and Cowan and Delaronde lakes are aligned and elongated north-northwest (N52°W). The larger lakes of the northeastern and central areas are amoeboid in shape and, with the smaller lakes, constitute shrunken remnants of an extensive post-Pleistocene lacustrine regime that drowned the lowlands now controlled by the Beaver-Waterhen river system.

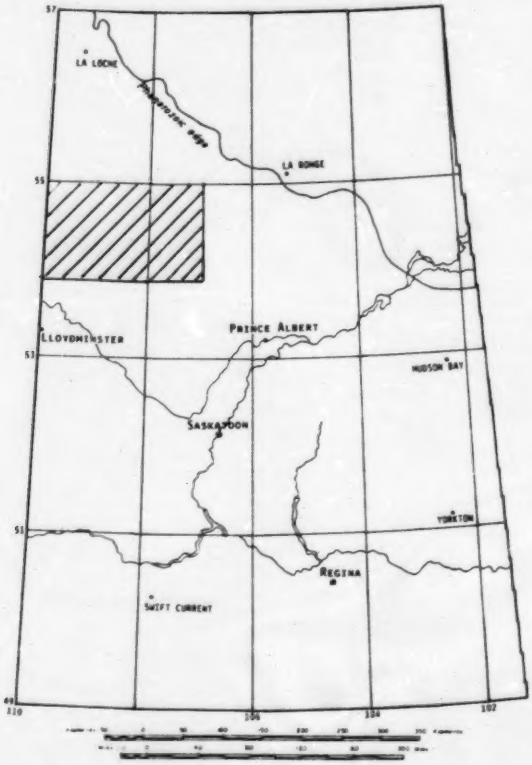

Figure 1 - Location map of the Meadow Lake region, west-central Saskatchewan.

2. The Erosion Surface on the Upper Devonian Souris River Formation

a) Relationship to the Holocene Land Surface

The sub-Cretaceous unconformity surface cuts across the south-dipping Upper Devonian Souris River Formation. It displays a gross morphological congruence with the Holocene land surface (Figure 3). Accordingly, the Mostoos Hills in the northwest of the study area, as delineated by the northern 610 m topographic contour, correspond to an underlying large structural dome on the Souris River Formation. The monocline on the Paleozoic surface created by drape of

[1] J.E. Christopher, Ph.D., P.Geol., Geological Consultant, Regina, SK.

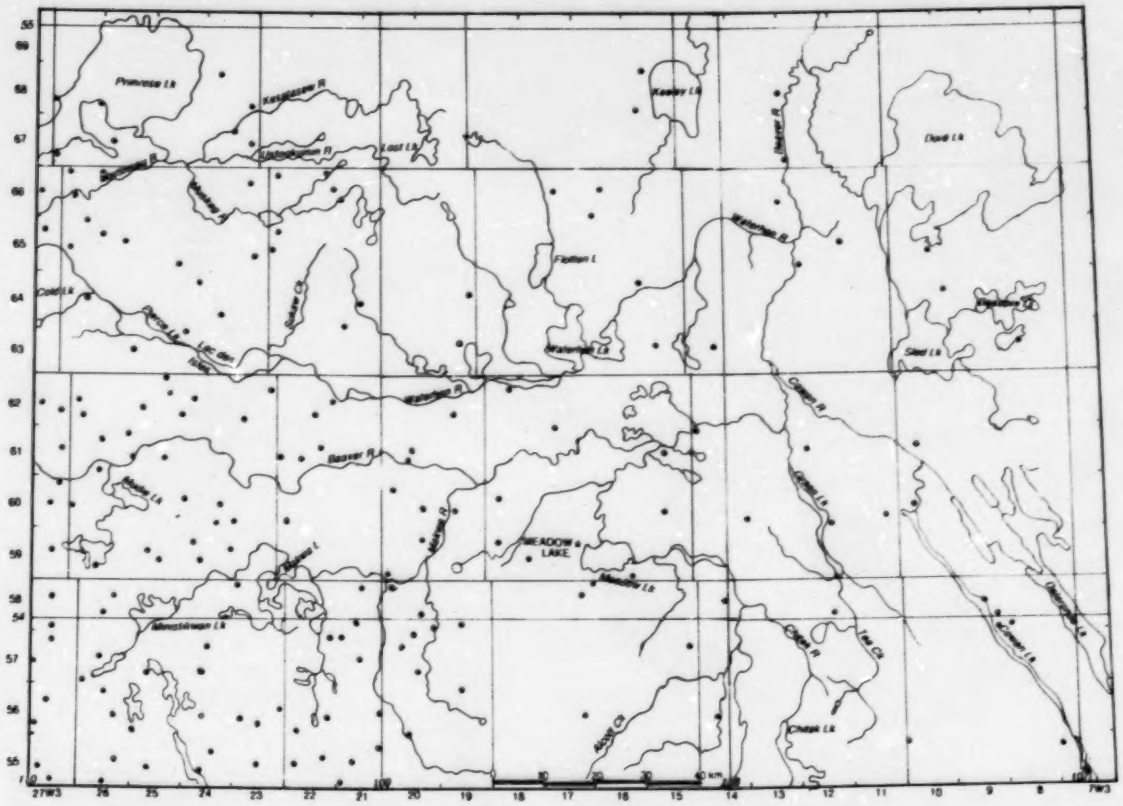

Figure 2 - Map showing rivers, lakes, and well locations (•) in the Meadow Lake region, west-central Saskatchewan.

Dawson Bay, Winnipegosis, and Souris River strata across the Lower Paleozoic Meadow Lake Escarpment (Haidl, 1989) is defined by the closely spaced contours between Township 55 in the extreme southwest through Meadow Lake to Township 63 at the northeastern boundary of the study area. The drainage pattern provides a Holocene surface expression of the Meadow Lake Escarpment by (west to east): 1) the eastward closing U-shaped jog in the course of the easternmost north-flowing tributary to the Makwa River; (2) the eastward elongation and alignment of Meadow Lake and its incoming streams such as the Chitek River; (3) the eastward closing U-shaped bends in the courses of the Green and Cowan rivers, and (4) the westward closing loop in the course of the river entering Sled Lake. The surficial topographic 610 m (msl) contour is deviated to the south from alignment with the escarpment by glacial stripping. On the Devonian erosion surface, the escarpment rises 160 m onto a mesa which is buttressed by the Beaverhill Member of the Souris River Formation and above which a northwesterly topographic grain is projected along the Chitek River, and the Cowan and Delaronde lakes. Below the Souris River Formation, the Meadow Lake Escarpment physically terminates the Lower Paleozoic Big Horn and Deadwood formations from the south (Kreis and Haidl, 1995, 2000; Kreis, 2000). It thereby forms the southern wall of the Lower Devonian Elk Point Basin (Fuzesy, 1980; Meijer-Drees, 1986), the deposits of which comprise the evaporites, carbonates, and red beds of the Lower Devonian Lower Elk Point Group.

b) Relationship to Predecessor Basins

The Lower Elk Point Basin (Grayston *et al.*, 1964) is centred in Alberta and in Saskatchewan is terminated to the north along the Cenozoic erosional edge of the Paleozoic formations, which trends southeasterly from Township 95 at the Alberta boundary to Lac La Ronge at Range 27W2. There, it meets the Meadow Lake Escarpment from the southwest. Accordingly, the Mannville Meadow Lake Basin is a pre-Success and pre-Cantuar successor to the Lower Elk Point Basin. It is tilted southwesterly and shaped by southwesterly plunging re-entrant troughs and irregular domes that reflect the irregular dissolution of the underlying Devonian Elk Point salt beds by formation and meteoric water. The more durable carbonates and red beds, though locally brecciated, constitute the dominant components, but evaporitic beds are present as far east as the La Ronge district. There, a 180 m downdrop of the Middle Devonian Ashern Formation across the Meadow Lake Escarpment indicates a comparable loss of salt section. Apparently the dissolution front retreated from east to west, so that the

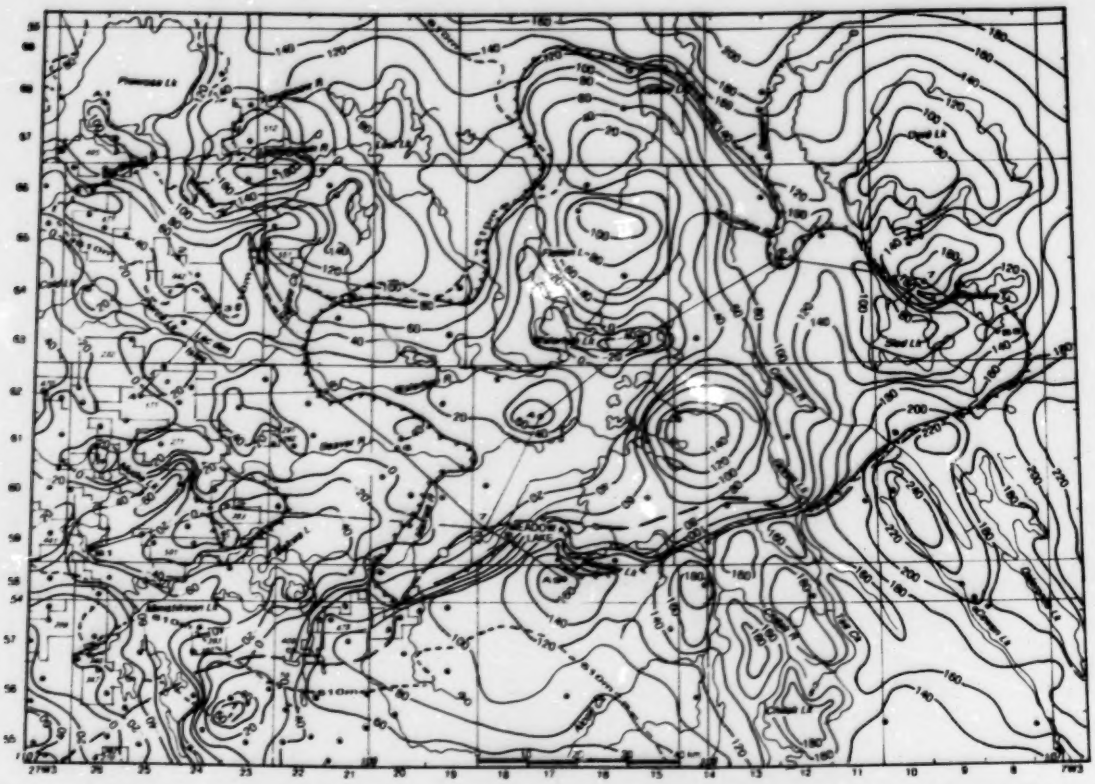

Figure 3 - Structure contour map on the Upper Devonian Souris River Formation in the southwestern portion of the Mannville-Success Meadow Lake Basin, west-central Saskatchewan. Contour interval: 20 m; Holocene topographic contour: 610 m; hachured line: edge of the Success Formation; broken line: Meadow Lake Escarpment; lines B1 to B8 and A1 to A9: trace of stratigraphic cross sections; Mannville natural gas fields outlines and numbers are taken from Saskatchewan Energy and Mines Reservoir Annual (1993).

Lotsberg and Cold Lake salt masses are present west of longitude 109°. Thus, the generally depressed central region on the Paleozoic surface from Doré Lake to Ministikwan Lake is attributable to episodic dissolution of the salt beds, which was especially pronounced in the Jura-Cretaceous (Success) and, less so, in the Cretaceous (Cantuar and Colorado). In that the Holocene amoeboid large and small lake complexes occupy sites corresponding to depressions on the Paleozoic erosion surface, extensive Holocene salt dissolution and collapse of the overlying strata are indicated. This genetic connection between surficial drainage patterns and the Paleozoic erosion surface is used to accentuate structural forms shown in Figure 3, especially in the eastern half of the region where well control points are widely spaced (Figure 2).

c) Relationship to the Precambrian Basement

The structural framework of the Mannville Meadow Lake Basin apparently reflects the geological configuration and topography of the Precambrian basement. One element of this control is shown by the north-south and east-west linear sets. The aeromagnetic pattern of the area (Miles *et al.*, 1997; Kreis, *et al.*, 2000) (Figure 4) shows the central district between longitudes 109° and 108° marked by linear highs and lows which trend north-south and flank a central core of curvilinear, 10 to12 km wide, closed highs and lows. The eastern boundary coincides with the eastern flank of the structural trough on the Paleozoic surface and the northerly aligned Holocene Green River–Beaver River course (this alignment continues north beyond the study area to Lac Ile-à-la-Crosse and into the course of the Mudjatik River on the Precambrian Shield). The western boundary underlies the western limb of the structural depression on the Paleozoic and continues south-southwest under the Makwa River and its north-flowing tributary across the Paleozoic Meadow Lake Escarpment. The broad axial keel of the trough from under Keeley Lake to Waterhen Lake corresponds to a compound aeromagnetic low of similar dimension but partitioned by a pair of curvilinear aeromagnetic highs, which amalgamate south of the Waterhen structural depression on the Paleozoic and enclose most of the triangular area closing to an apex at Meadow Lake. On the Meadow Lake Escarpment, the general aeromagnetic pattern

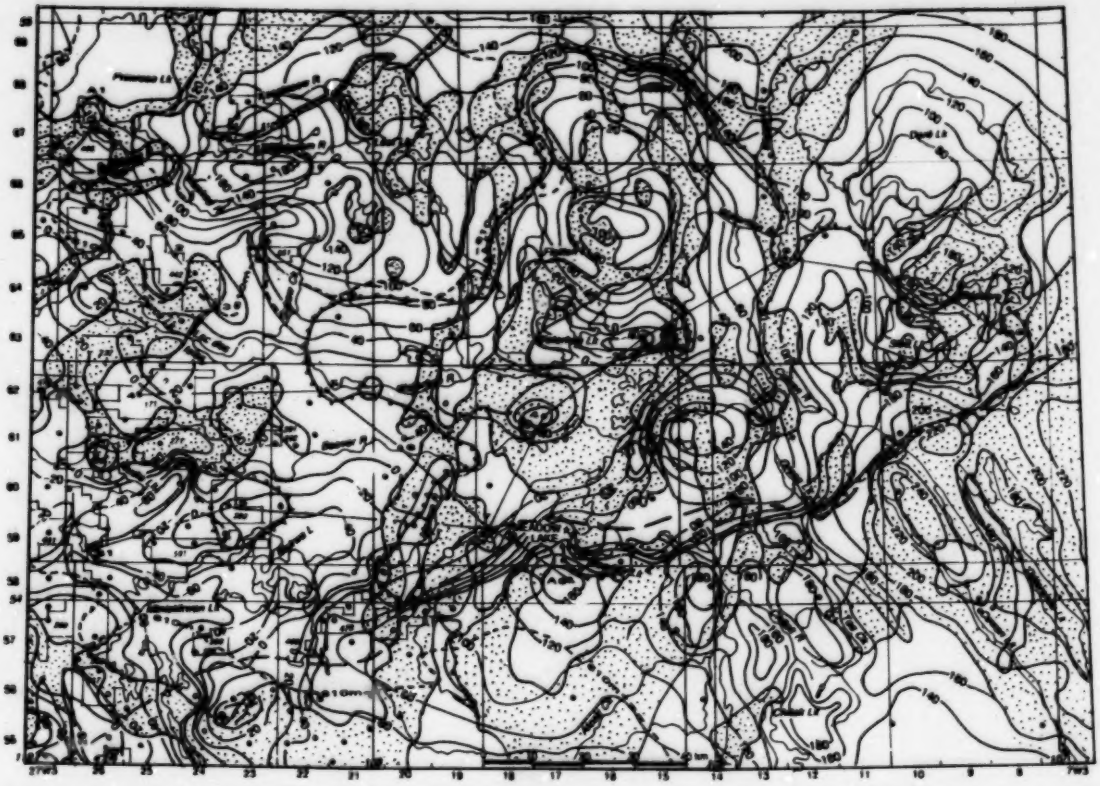

Figure 4 - Overlay of Precambrian basement aeromagnetic patterns on structure contour map of the Upper Devonian Souris River Formation in the southwestern portion of the Mannville-Success Meadow Lake Basin, west-central Saskatchewan; magnetically high areas are stippled.

continues, but the order reverses abruptly, with highs yielding to lows and vice versa.

The linked alternation of magnetic highs and lows, broad across the central district and narrow along the flanks, probably reflects the domal layout of complexly folded metasedimentary rocks. Low magnetic flux emanates from rocks that are low in iron-rich minerals and that are presumed to be dominantly erosion-resistant quartzofeldspathic gneisses, therefore forming paleotopographic highs. The high magnetic areas probably represent iron-rich rocks such as amphibolites and mafic volcanics which were likely more prone to Precambrian weathering and erosion and thus generally occupy paleotopographic lows. The Precambrian topography appears to have been genetically controlled by an antiform that was breached axially along the erosion-prone rocks from Waterhen Lake north to Keeley Lake, but was less breached south to the Meadow Lake Escarpment, where the resistant rocks appear to have provided better cover on the plunge to the south. The narrow flanking magnetic belts represent ridges and valleys of folded rocks outlying the axial region. The north-alignment of the Beaver River and its tributary Green River coincides with a strip of magnetically high Precambrian rocks, more prone to erosion and therefore forming depressions that exercise linear control on present-day surficial streams. The aeromagnetic district to the east angles off toward the northeast in keeping with the regional trend of the Precambrian Wollaston fold belt, and displays relatively wide (20 to 60 km) bands of lows and highs. The magnetic pattern is much flatter than in the central district. Thus, the entire area of Doré and Sled lakes and south to Chitek Lake is incorporated by a belt of magnetic lows, and is adjacent to a comparable band of magnetic highs from Beaupre Lake to Cowan and Delaronde lakes. Assuming that the basement rocks are tightly folded and that the magnetic properties emanate from steeply dipping, thick Wollaston Group metasedimentary rocks, the lower lying belts of iron-rich gneisses and schists (stippled areas in Figure 4) subcrop to the east of a more resistant belt of quartzofeldspathic meta-arkose. The Doré Lake structural low, like the central trough, may be situated over Precambrian domes and/or antiforms, and have acquired their trough-like character by dissolution of the Lower Elk Point salt beds over Precambrian highs.

The eastward shift of aeromagnetic patterns on the north side of the Paleozoic Meadow Lake Escarpment with respect to patterns on the south side indicates that the escarpment originated by faulting. The northeastward increase in the lateral displacements of

the aeromagnetic patterns suggests a right lateral wrench fault with increasing northeasterly tilt of the northern block. Most streams on the northern block west of Meadow Lake flow eastward along the general front of the escarpment and, east of Meadow Lake, north-flowing streams such as the Green, Cowan, and Delaronde-Sled are offset eastward in the vicinity of the escarpment.

West of the central district and south of the west-flowing Ustookumin River, the area from longitude 109° to the Alberta border is characterized by low magnetic flux, which is in keeping with the interpretation of a granitoid terrain. However, between Townships 64 and 61 inclusive, the magnetic low field encloses a compound east-opening U-shaped magnetic high, 800 km^2 in area, partially enclosing a central low. Analogues of this magnetic feature on the Paleozoic erosion surface, though partially masked by the Lower Elk Point salt beds, are: (1) the northwesterly striking salt-dissolution-controlled trough fronting the magnetic body to the east; (2) a similar trough but plunging southwesterly, along the southeastern flank of the magnetic body; and (3) structural highs and lows on the Paleozoic surface corresponding to the arms and central low of the magnetic high. This magnetic feature appears to translate into Precambrian igneous-metamorphic topographic forms analogous to those of the overlying Paleozoic, and may represent a complex mafic, igneous or gneissose rock dome. To the south, under the Ministikwan Lake basin, along latitude 54°, occurs an elliptical, east-aligned locale of extremely low magnetic values. The Makwa Lake trough on the Paleozoic surface rises northeasterly from this site onto the central structural depression beneath Waterhen Lake.

d) Laramide Overprint

Tectonic overprint is also apparent. A Laramide stress field is indicated by the northwesterly (308°) alignment of lakes and rivers on the Holocene Meadow Lake upland in the southeast, by the northwesterly alignment of the Lost Lake drainage in the Mostoos Hills of the northwest, by the southeasterly drainage into Flotten Lake and the Waterhen River of the central region, and by the northwesterly alignment of the major upper Mannville gas fields. On the Paleozoic surface, the complementary northeasterly vector is exemplified by the southwesterly plunge of the Makwa Lake trough. Pervasive northeasterly and northwesterly stress directions, as determined from breakouts in well bores distributed across the Western Canada Sedimentary Basin (Gough and Bell, 1981; Bell and Babcock, 1986; Bell *et al.*, 1994), have been attributed to an origin in the lithosphere. These authors found that the horizontal stress is greatest toward the northeast and least toward the northwest, and that this phenomenon reflects strain in the lithosphere created by drag effects from continental plate motion toward the south-southwest relative to the mantle. They also observed that this asymmetry corresponds to northeasterly trends of enhanced permeability in reservoirs of some of the larger oilfields, such as Pembina and Cold Lake in Alberta. Immediately to the south of the study area, control on the geometry of the Lloydminster heavy oilfields by northwesterly and northeasterly lineaments has been examined by Klovan *et al.* (1986), Mollard, (1987, 1988), and Gregor (1997). These authors concluded that Lloydminster oil pools trend northwesterly and are cut off by northeasterly lineaments. They attributed the local structural relief to small-scale movements along the lineaments by episodic basement activity. Slip along northeasterly lineaments opened northwesterly fractures, which were accessed by formation water that dissolved Elk Point salt beds and created northwesterly oriented subsidence structures in the Mannville strata.

3. The Jura-Cretaceous Success Formation

The Success Formation, as outlined in Figure 3, occupies the structural depression on the Souris River erosion surface between the northerly course of the Beaver River in the east, the Mostoos Hills in the west, and the Meadow Lake Escarpment. The locale is the most northwesterly of the four major homologous bodies of this formation in the province, and all are pre-Cantuar eroded remnants of a once Western Canada-wide Jura-Cretaceous depositional basin (Poulton *et al.*, 1994). Because it is unconformity bounded, its thickness is highly variable. A section, comparable to that at the reference Sohio Western Prairie Insinger 9-16-29-7W2 well (Christopher, 1987) for the Insinger Basin of east-central Saskatchewan, is present at the Cdn Seaboard Meadow Lake 3-21-63-15W3 well (Figure 5, well B5). It is 137.3 m thick, lies between the Souris River and Cantuar formations at a depth of 384.0 to 521.3 m, and consists of three units described below from well cuttings.

a) Unit C (384.0 to 423.6 m)

Sandstone: quartzose, medium grained, buff, partially kaolinite-indurated; lower part of unit includes thin pebbly layers of quartzose gritstone. In the upper part, beds coarsen upward from shale to cemented, fine- and medium-grained quartzose sandstone. Thin coaly layers occur at 396 to 402 m. The unit underlies the coarse-grained, quartzose, weakly cemented sandstone of the Dina Member of the Cantuar Formation.

b) Unit B (423.6 to 467 m)

Sandstone: quartzose, fine to medium grained, interbedded with coaly shale and buff, kaolinitic mudstone; abundant chert over the lower half.

c) Unit A (467 to 521.3 m)

Sandstone: quartzose, coarse and medium grained; subordinate gritstone, light grey; kaolinite and pyrite cemented.

A comparison of the Success section at the B5 (3-21-63-15W3) well with the adjacent B4 (1-33-61-17W3) well reveals that Success strata infill a valley eroded to a depth of 106 m into the Souris River Formation. Because the provenance of the Success mineral suite of

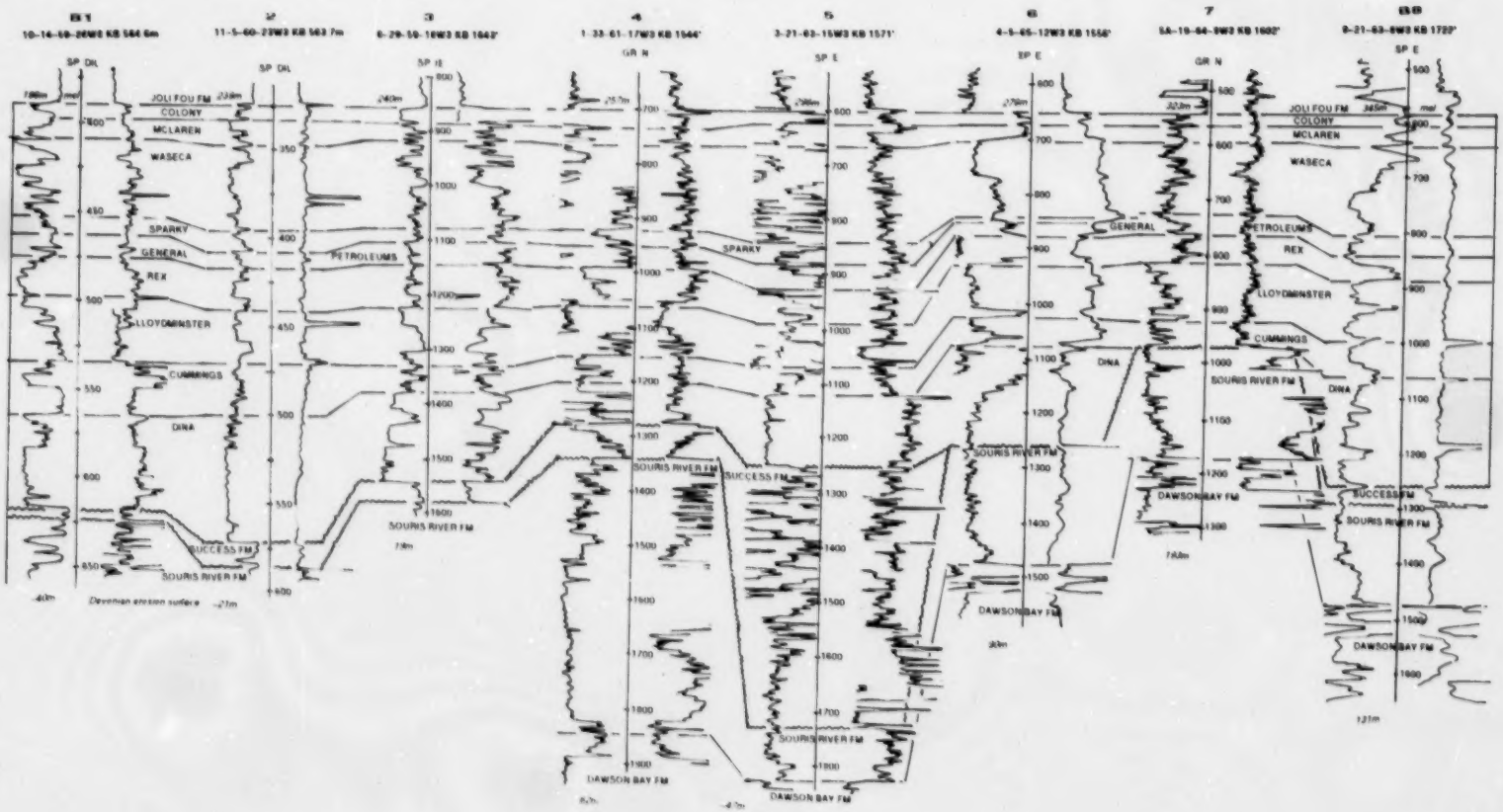

Figure 5 - Southwest-northeast stratigraphic cross section, B1 to B8, of Success and Mannville strata, Meadow Lake Basin, west-central Saskatchewan.

quartz and kaolinite is the Precambrian Shield, the section is evidently part of an open fluviatile system rather than a closed collapse sink. This conclusion is supported by the widespread, relatively uniform thickness (in the range of 40 to 70 m) of the overlying Dina sandstones, and the significantly low structural relief on the Dawson Bay and Joli Fou datums between B5 and B4. The kaolinitic, quartzose sandstones of the Success Formation are distributed throughout the central trough but are thickest in an annulus on the central core between Keeley and Waterhen lakes, reaching a maximum of 137.3 m at the 3-21-63-15W3 reference well (see above). Although pre-Success in age, as they are all capped with Success sedimentary rocks, domes in the structural trough share little else in common, and are: (1) buttes fronting the Paleozoic Meadow Lake Escarpment, i.e. erosional outliers of the Beaverhill Member that forms the upper one-third of the Souris River Formation, see B4 (1-33-61-17W3) and 12-31-61-14W3; (2) drapes of 90 m high Winnipegosis mounds, see 4-5-66-16W3 and 8-30-64-14W3 on the flank of the central dome in the depression, and, on the north-south Precambrian aeromagnetic high that bisects it; and (3) post-Souris River, pre-Cantuar uplift, see B7 (5A-19-64-9W3), as shown by the comparable positions of the Paleozoic erosion surface on the Souris River Formation with respect to the Dawson Bay structural datum at B6 (4-5-65-12W3) and B8 (9-21-63-8W3). Outliers of the Success Formation to the west confirm a wider distribution to beyond the Alberta boundary. Early Cretaceous erosion appears to have stripped the Jura-Cretaceous Success strata from the Paleozoic surface immediately south of the Meadow Lake Escarpment. Success sedimentary rocks in the trough escaped because regional sapping of the Elk Point salt beds in the structural trough had lowered these rocks below the pre-Cantuar erosional base.

4. The Cantuar Formation

Relative relief on the post-Success terrain is subdued and reflects both the widespread planation that followed the Success infill of the earlier topographic surface, and the absence of differential uplift proximal to the study region. Only a gentle westerly tilt toward the Cold Lake Basin of Alberta is indicated by the northeasterly rise on upward decreasing gradients of the intra-Cantuar correlation surfaces (Figure 5). Dina beds are predominantly made up of medium- and coarse-grained, friable, quartzose sandstone with about 1 to 2% kaolinite that, over the upper half, grades to fine-grained sandstone with interbedded mudstone unless interrupted by channel deposits of coarser grade sandstone. They are interpreted to represent fluvial bars in channels of a lateral accretionary flood plain of oxbow, overbank, and, in the upper part, lagoonal deposits. Capping shales and upward-coarsening shale-sandstone sequences indicate the encroachment of estuarine conditions. The general thickness of the sandstone ranges up to 40 m, but increases to more than 70 m (B2, Figure 5; A4, Figure 6) in the distributary thalwegs of the Assiniboia Paleovalley (Christopher, 1984, 1997), which enters the region from the south in the lows under the Bronson-Ministikwan lakes and exits northwest under Cold Lake. Most of the Dina sandstones in the region may have been derived from the Success Formation.

An overall impression of the lithological facies in the Mannville is obtainable from the well cuttings taken in the region, but the nearest full-length core is from the Frenchman Butte A7-3-54-25W3 well, located only 10 km to the south. Above the Dina, most of the Cantuar units tend to downlap toward the east against the rising depositional slope of the Meadow Lake Basin, and are dominated by cycles coarsening upward from argillaceous beds into fine- and medium-grained arenite (Christopher, 1997). Cummings sandstones are generally quartzose and well sorted, and are associated with bioturbated, dark grey sandstone and shale. At the Shell Frenchman Butte well, the basal unit consists of 11 m of friable, well sorted and current-bedded quartzose sandstone above similar sandstone interbedded with dark grey shale, 8 m thick; this indicates progradation over a subsiding depositional base. Sediments were apparently reworked and sourced from within the eastern part of the basin.

Lloydminster and Rex sandstones, by virtue of their mineral suite, represent multiple progradational influxes from the Rocky Mountain system. Medium- and fine-grained quartz, in combination with up to 15% black and dark grey chert, white kaolinite and feldspar, green glauconite and brown siderite, and widespread calcite and pyrite cements characterize their mineral suite. In the nearby Cold Lake Basin of Alberta, where this mineral suite is more proximal, the equivalent Clearwater sandstones are litharenites dominated by rock fragments (28 to 49%) comprising volcanics (3 to 15%), chert (7 to 15%), sedimentary (4 to 13%), dolomite (9%), igneous-metamorphic (3 to 11%), quartz (13 to 25%), plagioclase (5 to 10%), and K-feldspar (4 to 11%); accessories include amphibole, biotite, muscovite, tourmaline, zircon and opaques (McKay and Longstaffe, 1977). A similar suite is found in the Dimmock Creek and Atlas members on the Swift Current Platform in southwestern Saskatchewan (Christopher, 1974), and the Grand Rapids Formation of the Athabasca River Basin and the Wabasca Basin (Keeler, 1980). Here, on the Meadow Lake Basin, the volcanic mineral species are less in evidence, whereas hard, black cherts are in great abundance. As shown in cross section A1 to A8 (Figure 6), the facies are readily identified in the well cuttings across the region, and, at the Frenchman Butte well, are conspicuous in the low-stand deposits characterizing the lower unit of the Lloydminster Member. Bedding cycles 1 and 2 (3.0 and 2.5 m thick respectively) are unconformity-bounded sequences that coarsen upward from dark shale, wavy and ripple-laminated with fine-grained quartzose sandstone, into oxidized and calcite-cemented, fine-grained, quartzose sandstone. Bedding cycle 3 is an 11 m thick quartzose sandstone that coarsens upward from fine to medium grained, and displays a subordinate mineral suite of 10 to 15% black and dark grey chert, white kaolinite altered from feldspar, glauconite, chloritic mudstone,

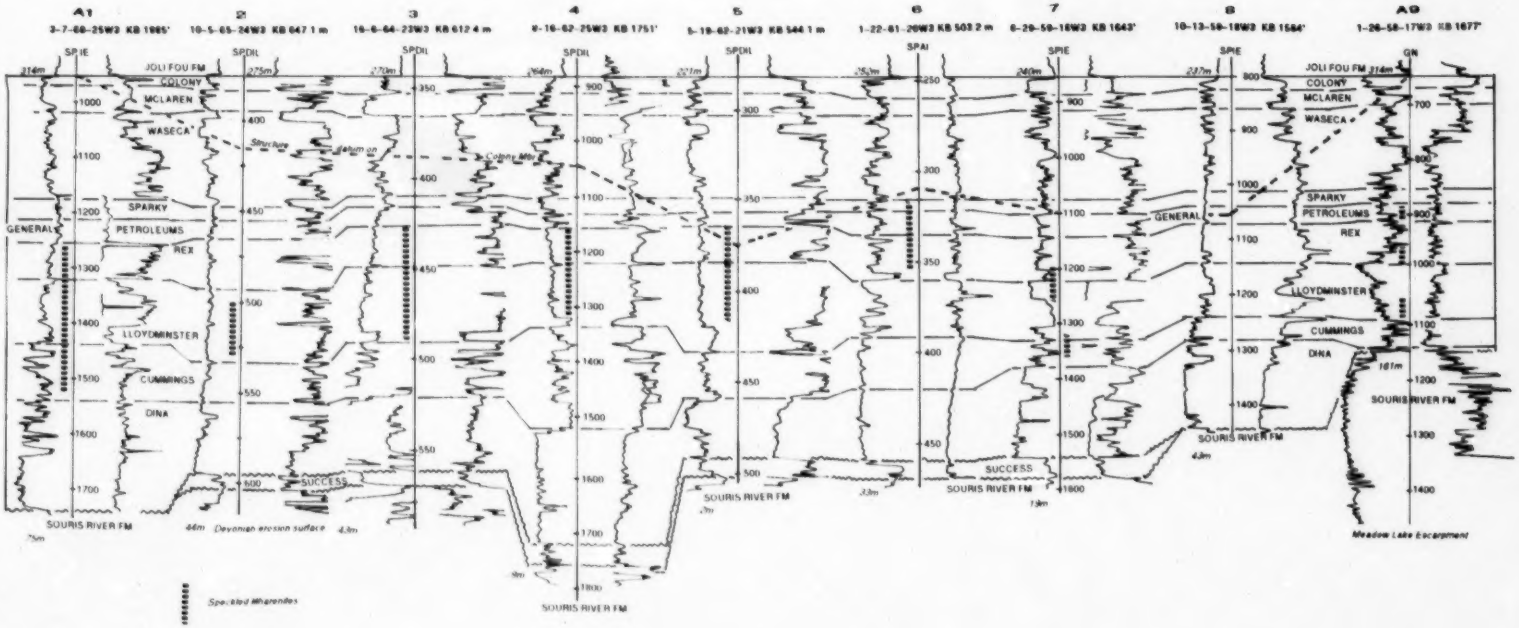

Figure 6 - Northwest-southwest stratigraphic cross section, A1 to A9, of Success and Mannville strata, Meadow Lake Basin, west-central Saskatchewan.

pyritic nodules, and calcitic cements. It is generally bioturbated and indurated throughout. The basal contact is sharp and irregular. Bedding cycle 4, at 5.3 m thick, is half as thick as cycle 3, but shares all of the characteristics and is also unconformity bounded. It is deeply oxidized yellow and brown at the top, and the basal contact is sharp and irregular. In that Mannville beds are broadly lenticular, this four-fold episode of emergence, weathering, deposition, and emergence reflects sea-level changes equivalent to the thickest of the cycles. The high-stand upper Lloydminster strata are dominated by a medial 8.7 m thick cycle 6 consisting of very fine- and fine-grained, quartzose sandstone that is current and low-angle wavy bedded with shale-draped sandy laminae and bioturbation toward the top. The basal bed is a dark grey, fissile shale, 1.5 m thick. The subjacent cycle 5, at 3.4 m thick, is less than half as thick, but likewise displays an upward transition of shale to sandstone. Cycle 7, at 0.4 m thickness, is oxidized and cemented, an eroded remnant of a speckled sandstone body with about 5% of coaly grains.

The speckled sandstones reappear in bedding cycle 1 of the Rex Member as an unconformity-bounded, 8.9 m thick sequence that coarsens upward from dark grey shale, through laminated and intensively burrowed (*Teichichnus)* sandstone and shale into quartzose, bimodally fine- and medium-grained sandstone that contains about 12% black and dark grey chert, sphaerosiderite, and feldspar, and is moderately indurated by calcite and kaolinite. Bedding cycle 2, similar in thickness at 9.15 m, is apparently compounded in that the basal metre-thick bed, though a dark grey, bioturbated shale on an erosion-pitted basal contact, grades upward to include subordinate starved-rippled sandstone lenticles with minerals as in bedding cycle 1. The major body of cycle 2 by virtue of its sharp contact apparently truncates the basal bed and grades upward through swaley, cross-bedded, very fine-grained, quartzose sandstone, into low-angle, planar cross-bedded and flat-bedded, fine-grained, quartzose sandstone. Mudstone and coaly seat-earth caps the cycle. Cycle 2 may represent a build-up of a shoaling sandbar into a barrier beach and lagoon. Bedding cycle 3, though thin at 3.2 m, displays a return of the upward transition to the speckled sandstones of cycle 1, whereas cycle 4, about equally thin at 3.38 m, is similar to the facies of bedding cycle 2. The speckled sandstones by virtue of their mineral suite represent direct input or nearby sourcing by fluviatile channel systems, which with the passage of time shift their location by virtue of shoreline retreat or advance. The intervening current-bedded, well-sorted, quartzose sandstones represent *in situ* shoreline reworking of sands into barrier beaches and shoals on former offshore depositional floors.

Loss of basin accommodation is indicated by the two 6 m thick bedding cycles of the General Petroleums Member. The first coarsens upward from dark grey shale through bioturbated mudstone and sandstone, into very fine- and fine-grained, current- and cross-bedded quartzose sandstone. The second grades upward from very fine-grained, bioturbated, cross-bedded, argillaceous sandstone into flat-laminated and swaley cross-bedded, fine-grained, quartzose sandstone with centimetre-thick truncating cross-sets, and is capped by a 0.5 m thick, black chert and white kaolinite-speckled, quartzose sandstone.

In the Sparky Member, bedding cycle 1 is 4.4 m thick, and is bipartite, with its lower half a black shale with subordinate layers of ripple beds, graded beds and trough cut-and-fill, quartzose sandstone, and its upper half a speckled, black chert and white kaolinite-rich, fine-grained, quartzose sandstone. The 6 m thick, second bedding cycle sandstone is quartzose, fine-grained, massive, weakly indurated, and conglomeratic at the base and siderite-cemented at the top. It is interpreted to be an estuarine channel deposit common to the Sparky Member in the Lloydminster heavy oilfield district. The Sparky is terminated by a regional coal, here less than 0.4 m thick, on a 3.4 m thick, upward coarsening third cycle of shale and very fine-grained, quartzose sandstone.

The Waseca Member at Shell Frenchman Butte is composed of eight bedding cycles, which range in thickness from 2.0 to 5.7 m. This relatively narrow range is atypical of the Waseca in that 10 m thick channel and shoal sandstones are present in many of the wells in the region, as indicated by the logs on the cross sections A1 to A8 and B1 to B8. Waseca units are highly variable lithologically, and, to the northeast on the Meadow Lake paleolowland basin, acquire strong fluviatile inputs from the Precambrian Shield. However, the study area is largely offshore from the eastern Nipekamew delta front (Christopher, 1997), the edge of which is picked up at B6, B7, and B8 (Figure 5). At Shell Frenchman Butte, all cycles shoal upward except for the 2.8 m thick, dual sandstone-mudstone couplets of cycle 2. All sandstones at the top of the upward coarsening cycles are current and cross-bedded, swaley, and trough cross-bedded and ripple bedded. Those of the 3 m thick cycle 4 display opposing cross-sets suggestive of a tidal setting. Mudstones and shales are bioturbated, and the sandstones of cycles 1 to 3 are fine-grained, and of 4 to 7, very fine grained, thereby reflecting a waning depositional energy gradient. The speckled black chert and kaolinite-rich quartzose sandstones appear only in cycles 3 and 7 as distal components of a western influx. The 3.5 m thick, bioturbated, argillaceous, quartzose sandstone of bedding cycle 8 ends in a 0.6 m thick coal bed.

5. Pense Formation

The McLaren and Colony, as used in this paper, are members of the Pense Formation (Christopher, 1984, 1997). Generally the McLaren beds are highly lenticular, and variable in thickness, ranging from decimetre values to a metre or two. In the Shell Frenchman Butte well they are grouped into three bedding cycles. However, quartzose sandstones predominate as stacked, friable, well-sorted, current-bedded, very fine-grained bodies, separated by thinner, bioturbated shale. As shown on the cross sections, 3 to

5 m thick sand bodies are locally present, representing channel inlet and beach depositional environments. The sandstone of bedding cycle 3 at the Frenchman Butte well is a 6.3 m thick, stacked channel succession. A basal shale lies at its contact with the Waseca and a coal bed on a loamy paleosol caps the McLaren Member. The Colony Member is a shallower water repetition of the McLaren, and includes bedding cycles 4, 5, and 6 of the Pense Formation. A black shale, 1.6 m thick, initiates bedding cycle 4, and the three bedding cycles are terminated by loamy mudstones suggestive of paloesols and or marsh deposits, and in cycle 4, by a decimetre-thick coal. Sandstones are very fine grained, quartzose, and variably argillaceous.

6. The Natural Gas Fields

Most of the natural gas fields lie at elevations above the Lloydminster heavy oil-producing region to the south, but not up-dip from the latter. Rather they appear to be components of the Cold Lake heavy oilfield district adjacent to the west in central eastern Alberta. From a geographical overlap with the Lloydminster oilfields, they extend north from Township 52 to Township 68 in a narrow belt between the Alberta boundary and Range 21W3 (Figure 3), and are mostly in upper Mannville (Waseca, McLaren, and Colony) progradational shoreline sandstones built out from the west into offshore more argillaceous, sandy mudstone. They are enclosed on small structural terraces and anticlines and across narrow re-entrant troughs by the easterly shale out, but in the overall structural setting of the large amphitheatre in the western part of the trough extending southwesterly from under Doré Lake, i.e. above the eastern partially dissolutioned mass of the Early Devonian Lower Elk Point salt beds. With more than 25 pools present, this is the second largest gas-producing district of the province. The centrally located Beacon Hill Field encloses the highest reserves (6164.8 x 10^6 m^3) and has produced about 24% of the total cumulative production.

The natural gas reserves crowd the western perimeters of the potentiometric draw-downs of Mannville formation water by the Beaver, Waterhen, and Makwa rivers between Townships 60 and 67 in the north, and the draw-down associated with the North Saskatchewan River between Townships 56 and 52 in the south (Christopher, 1984). At the potentiometric divide in Townships 57 and 58, the natural gas district extends farthest east to include Loon Lake in ranges 21W3 and 20W3. Gas fields in the study area are at extremely shallow depths (274 to 310 m), but the Mannville Formation underlies the shale of the Joli Fou Formation. Geographically, the gas fields can be categorized into three groups:

1) Those located on the southern, western, and northern flanks of structural depression under the Ministikwan and Makwa lakes where the natural gas reserves are apparently held in inward tilted reservoirs by down-flow of meteoric water into the depression. This is also the site of the previously mentioned Precambrian aeromagnetic minimum (Figure 4), and as well, the structural minimum on the Paleozoic erosion surface.
2) The central area between Mudie Lake and the Waterhen River, where the major Beacon Hill and Pierceland gas pools occupy subsidiary knobs and terraces of a broad dome coincident in its location with the aeromagnetic high on the Precambrian.
3) North of the Waterhen River, the fields occupy domal terraces and the crest of the dome on the Paleozoic erosion surface underlying the Mostoos Hills east of Cold Lake and southeast of Primrose Lake.

7. Summary

Precambrian basement to Holocene land surface structural forms, including faults, are widespread throughout the area of study. The effect of the basement forms is transmitted by the effects of salt dissolution on the evaporites of the Devonian Elk Point formations, by repetitive drape effects accentuated and locally inverted by agents of erosion acting in the several major Late Paleozoic, Mesozoic, and Cenozoic hiatuses. Holocene agents acting on the contemporary landforms are continuing the precedents. The Precambrian igneous-metamorphic domain in the western part of the district exhibits less structural differentiation, but probably more effective and larger structural-topographic closures in the context of natural gas entrapment and storage. Leakage of natural gas to the surface is also inhibited by a full coverage of Colorado shale. The central district appears to have been most active tectonically of the three areas, with reactivation of faults, aligned with the Meadow Lake Escarpment and the Beaver River system being the most conspicuous. Drape structures on erosional and collapse forms are widespread and the paths for migratory fluids many. The area appears to be a tectonic boundary zone between the lithologically more massive domain to the west and the Wollaston fold belt to the east. Thus its western flank, as well as the Meadow Lake Escarpment may provide promising mineral exploration prospects. Ten-metre thick Mannville sandstone bodies are abundant, as are the structures available for hydrocarbon infill. Known oil shows are limited to the western part of the Meadow Lake Escarpment. Natural gas prospects decrease northeastward across the eastern area with thinning of the Colorado shale coverage by Cenozoic and Holocene erosion.

8. Acknowledgments

The author thanks Saskatchewan Energy and Mines for permission to publish this paper, which is an offshoot of a Saskatchewan-wide study of the Mannville Group submitted to the department. He gratefully acknowledges the support and critical reviews of C. Gilboy, F. Haidl, and K. Kreis, and the editorial and technical input of E. Nickel and C. Brown.

9. References

Bell, J.S. and Babcock, E.A. (1986): The stress regime of the Western Canadian Basin and implications for hydrocarbon production; Bull. Can. Petrol. Geol., v34, p364-378.

Bell, J.S., Price, P.R., and McLellan, P.J. (1994): In-situ stress in the Western Canada Sedimentary Basin; *in* Mossop, G. and Shetsen, I. (comp.), Geological Atlas of the Western Canada Sedimentary Basin, Can. Soc. Petrol. Geol./Alta. Resear. Counc., p439-446

Christopher, J.E. (1974): The Upper Jurassic Vanguard and Lower Cretaceous Mannville Group of southwestern Saskatchewan; Sask. Dep. Miner. Resour., Rep. 151, 349p.

_____ (1984): The Lower Cretaceous Mannville Group, northern Williston Basin region, Canada; *in* Stott, D.F. and Glass, D.G. (eds.), The Mesozoic of Middle North America; Can. Soc. Petrol. Geol. Mem. 9, p109-126.

_____ (1987): Note on the Jura-Cretaceous section in central southeastern Saskatchewan; *in* Summary of Investigations 1987, Saskatchewan Geological Survey, Sask. Energy Mines, Misc. Rep. 87-4, p194-198.

_____ (1997): Evolution of the Lower Cretaceous Mannville Sedimentary Basin in Saskatchewan; *in* Pemberton, S.G. and James, D.P. (eds.), Petroleum Geology of the Cretaceous Mannville Group, Western Canada, Can. Soc. Petrol. Geol., Mem. 18, p191-210.

Fuzesy, L.M. (1980): Geology of the Deadwood (Cambrian), Meadow Lake and Winnipegosis (Devonian) Formations in West-central Saskatchewan; Sask. Dep. Miner. Resour., Rep. 210, 64p

Gough, D.I. and Bell, J.S. (1981): Stress orientations from oil well fractures in Alberta and Texas; Can. J. Earth Sci., v18, p638-645.

Grayston, L.D., Sherwin, D.F., and Allan, J.F. (1964): Chapter 5 – Middle Devonian; *in* McCrossan, R.G. and Glaister, R.P. (eds.), Geological History of Western Canada, Alta. Soc. Petro. Geol., p49-59.

Gregor, V.A. (1997): Mannville linears in the Lloydminster heavy oil area and their relationship to fractures and fluid flow in the Western Canada Sedimentary Basin; *in* Pemberton, S.G. and James, D.P. (eds.), Petroleum Geology of the Cretaceous Mannville Group; Can. Soc. Petrol. Geol., Mem. 18, p428-474.

Haidl, F.M. (1989): Distribution of Lower Paleozoic strata in the vicinity of the Meadow Lake Escarpment, west-central Saskatchewan; *in* Summary of Investigations 1989, Saskatchewan Geological Survey, Sask. Energy Mines, Misc. Rep. 89-4, p125-132.

Keeler, R.G. (1980): Lower Cretaceous (Mannville Group) Grand Rapids Formation, Wabasca A Oil Sand Deposit area, northeast Alberta; *in* Beck, L.S., Christopher, J.E., and Kent, D.M. (eds.), Lloydminster and Beyond: Geology of Mannville Hydrocarbon Reservoirs, Sask. Geol. Soc., Spec. Publ. No. 5, p96-131.

Klovan, J.E., Gregor. V.A., and Robson, D. (1986): Structural features of the Lloydminster heavy oil area: Underrated trapping mechanisms?; *in* Canada Hydrocarbon Reserves for the 21st Century, Can. Soc. Petrol. Geol., Calgary, prog. abstr., p59.

Kreis, L.K. (2000): Geology of the Middle Cambrian–Lower Ordovician Deadwood Formation in Saskatchewan; Lower Paleozoic Map Series, Sask. Energy Mines, Open File Rep. 2000-2, Sheet 2 of 8.

Kreis, L.K. and Haidl, F.M. (1995): Geology of the Interlake Formation (Silurian); *in* Summary of Investigations 1995, Saskatchewan Geological Survey, Sask. Energy Mines, Misc. Rep. 95-4, 1:2 000 000 scale maps.

_____ (2000): Geology of the Upper Ordovician Red River strata (Herald and Yeoman strata) in Saskatchewan; Lower Paleozoic Map Series, Sask. Energy Mines, Open File Rep. 2000-2, Sheet 4 of 8.

Kreis, L.K., Ashton, K.E., and Maxeiner, R.O. (2000): Geology of the Precambrian Basement and Phanerozoic Strata in Saskatchewan; Lower Paleozoic Map Series, Sask. Energy Mines, Open File Rep. 2000-2, Sheet 1 of 8.

McKay, J.L. and Longstaffe, F.J. (1997): Diagenesis of the Lower Cretaceous Clearwater Formation, Primrose area, northeastern Alberta; *in* Pemberton, S.G. and James, D.P. (eds.), Petroleum Geology of the Cretaceous Mannville Group, Western Canada, Can. Soc. Petrol. Geol., Mem. 181, p392-412.

Meijer Drees, N.C. (1986): Evaporitic Deposits of Western Canada; Geol. Surv. Can., Pap. 85-20, 118p.

Miles, W., Stone, P.E., and Thomas, M.D. (1997): Magnetic and gravity maps with interpreted Precambrian Basement; Geol. Surv. Can. Open File 3488.

Mollard, J.D. (1987): Remote Sensing for Petroleum Exploration and Exploitation in Saskatchewan; Sask. Energy Mines, Tech. Branch, Open File Rep., 205p.

_____ (1988): Fracture lineament research and applications on the Western Canadian plains; First

R.M. Hardy Memorial Lecture, Can. Geotech. J., v25, p749-767.

Poulton, T.P., Christopher, J.E., Hayes, B.J.R., Losert, T., Tittemore, J., and Gilchrist, R.D. (1994): Jurassic and Lowermost Cretaceous strata; *in* Mossop, G. and Shetsen, I. (comp.), Atlas of the Western Canada Sedimentary Basin, Alta. Resear. Counc./Can. Soc. Petrol. Geol., p297-315.

Saskatchewan Energy and Mines Reservoir Annual (1993): Misc. Rep. 89-3, 135p.

Lithofacies Architecture of the Upper Cretaceous Belle Fourche Formation, Saskatchewan, Alberta, and Montana – Its Relationship to Sites of Shallow Biogenic Gas Production

J.L. Ridgley [1] and C.F. Gilboy

Ridgley, J.L. and Gilboy, C.F. (2001): Lithofacies architecture of the Upper Cretaceous Belle Fourche Formation, Saskatchewan, Alberta, and Montana – its relationship to sites of shallow biogenic gas production; *in* Summary of Investigations 2001, Volume 1, Saskatchewan Geological Survey, Sask. Energy Mines, Misc. Rep. 2001-4.1.

1. Introduction

Shallow gas of biogenic origin (Rice and Claypool, 1981; Ridgley, 1998) is produced from various intervals in the Upper Cretaceous Belle Fourche Formation (Figure 1) in Saskatchewan and Alberta, Canada, and Montana, USA. This report is a summary of work in progress to further understand the controls on sites of biogenic gas accumulation in the Belle Fourche. The general region of interest covers a large portion of southern Alberta and southwestern Saskatchewan, south of Township 33, and northern Montana, north of Township 28N. Principal geological structures include the Sweetgrass Arch (incorporating the North Battleford Arch in Saskatchewan, and, in Montana, the South Arch and the Kevin-Sunburst Dome, which are separated by the southwest-northeast-trending Pendroy fault zone), Moose Jaw Syncline, Bowdoin Dome, Bears Paw Mountains, and Cobourg Syncline (Figure 2). In Canada, the western boundary of the study area is defined by the west limb of the Sweetgrass Arch where it forms the eastern margin of the deep Alberta Basin. In Montana, the southern boundary is defined by current production at the south end of Bowdoin Dome and the Bears Paw Mountains, and the western limit is the eastern boundary of the thrust belt. The thermal maturity of organic matter in the Belle Fourche is below the oil-generation window

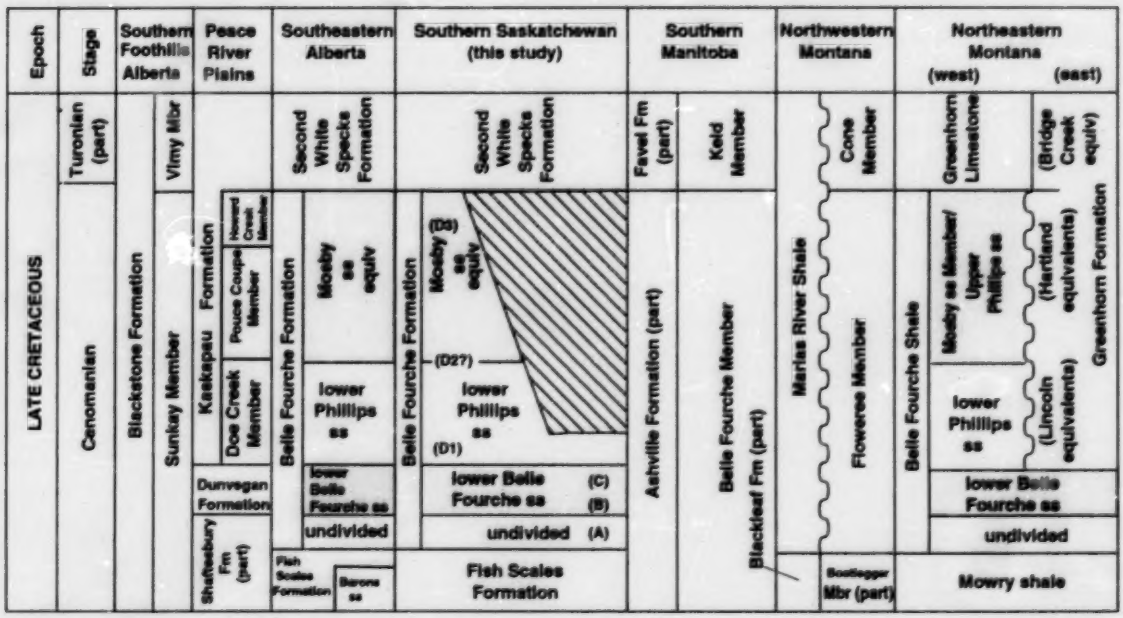

Figure 1 - Chart showing stratigraphic correlations for Belle Fourche, Second White Specks, and Greenhorn formations, and units A, B, C, D1, D2, and D3 of this report in Alberta and Saskatchewan, Canada, and Montana, USA. Position of D2 in the Belle Fourche is approximately shown due to lack of ammonite control. Revised from Bloch et al. (1993) and Ridgley et al. (2000).

[1] U.S. Geological Survey, Central Region, Energy Resources Team, MS939, P.O. Box 25046, DFC, Denver, CO 80225-0046.

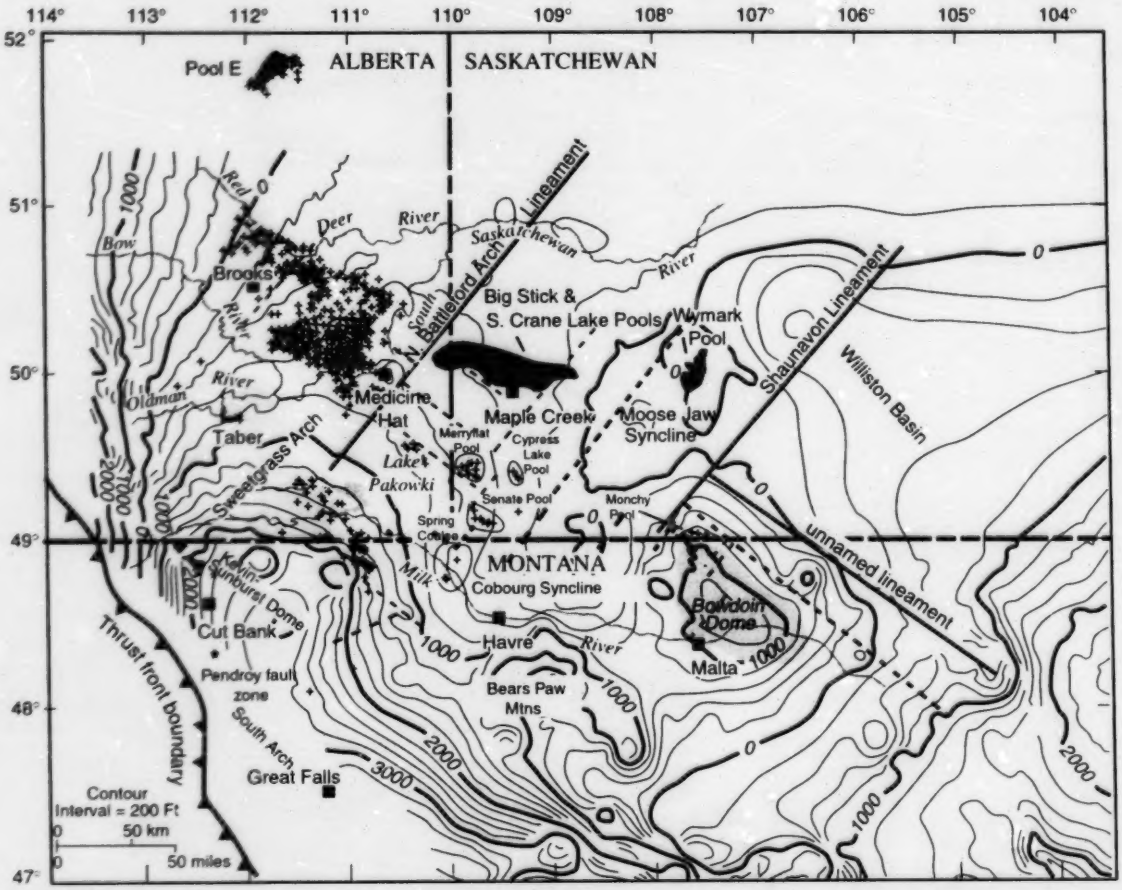

Figure 2 - Location of shallow biogenic gas production from the Belle Fourche and Second White Specks formations, Alberta, Saskatchewan, and Montana. Production in Alberta and Montana is from upper Belle Fourche sandstones (crosses), in Alberta, Saskatchewan, and Montana from lower Belle Fourche sandstones (medium grey shading or stars), and on the Bowdoin Dome, Montana, from lower Phillips and upper Phillips/Mosby sandstones and Greenhorn Formation (pale grey shading). Structure contours are on top of the Second White Specks and Greenhorn formations. Lineaments (solid lines) from Anna (1986) and Kent and Christopher (1994). Dashed lineaments from this study and Ridgley et al. (2001) are approximately located. The geometry of the fault blocks has not been completely determined, and thus orientation of the inferred lineaments could be up to 90° different from that shown.

(R_o = 0.5). In this report, the focus is on southwestern Saskatchewan and adjacent areas of Montana.

Ridgley *et al.* (2001) suggested that the Belle Fourche was deposited in two distinct depositional settings. The lower part is characterized by sandstones that: a) filled in regional erosional surfaces of variable relief, and b) were affected by movement on fault-bounded basement blocks. The upper part mostly consists of prograding sandy wedges made up of parasequence sets. Both parts of the Belle Fourche were deposited during the overall Greenhorn transgression. Ridgley *et al.* (2001) subdivided the lower and upper parts of the Belle Fourche Formation into three units each. In this report, this subdivision is retained, and the upper part of the Belle Fourche is further subdivided into major parasequence sets along a transect (E-E') in southeastern Alberta and southwestern Saskatchewan. The transect ties into two previously published south-north cross sections (A-A' and D-D', Ridgley *et al.*, 2001) that extend from Montana into Canada (Figure 3).

Gas is produced from all the major sandy units in the Belle Fourche. The sandstone distribution has been affected by movement on fault-bounded basement blocks and by truncation below a regional unconformity that underlies the Second White Specks and Greenhorn Limestone (Bridge Creek time equivalent) (Gilboy, 1988; Rice *et al.*, 1990; Plint, 2000; Ridgley *et al.*, 2001). The regional distribution of producing wells in the Belle Fourche (Figure 2) is discussed more fully in Gilboy (1988) and Ridgley *et al.* (2001). Current gas-producing intervals from the upper part of the Belle Fourche in the Senate, Merryflat, and Cypress Lake pools, Saskatchewan, and

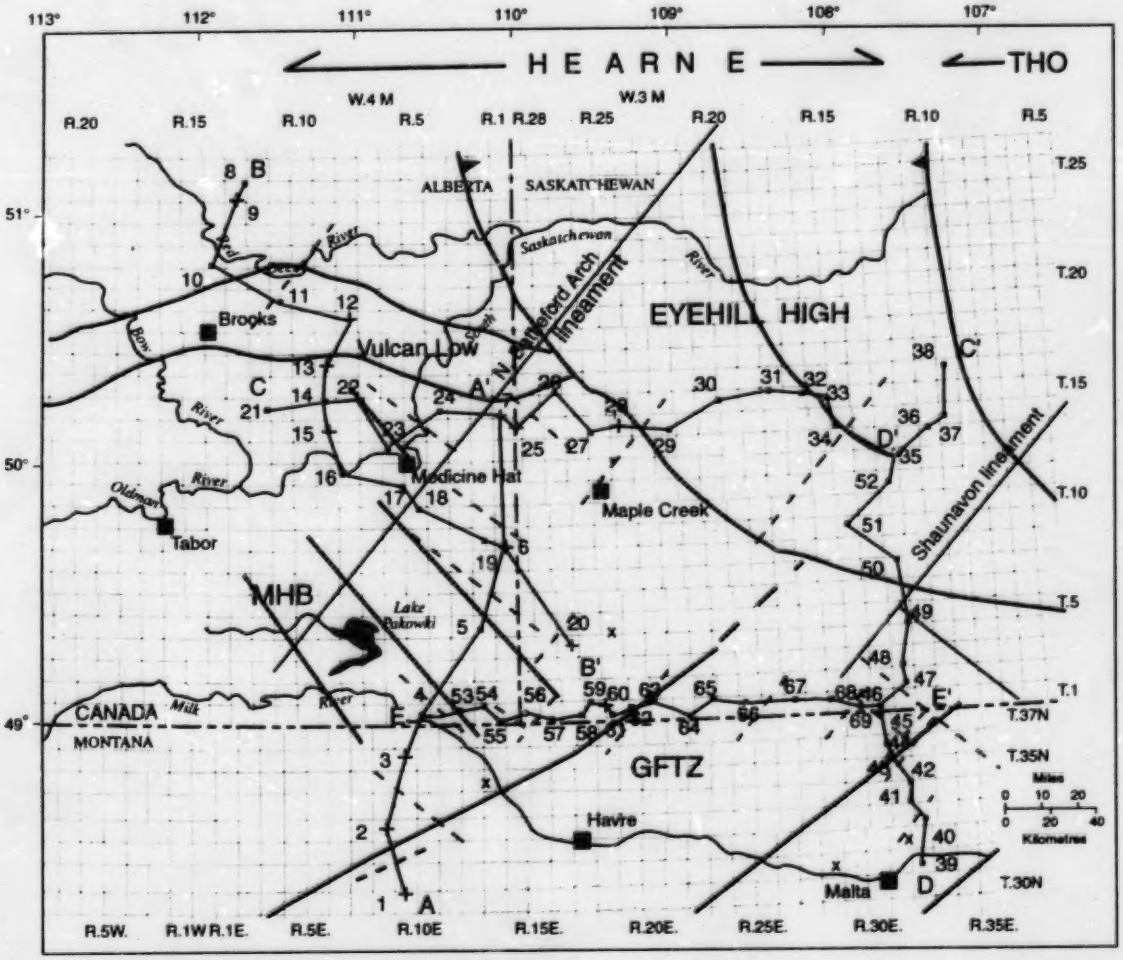

Figure 3 - Location of regional cross sections A-A', B-B', C-C', and D-D' (see Ridgley et al., 2001) and E-E' (this report). Crosses are cored sections which have been sampled for foraminiferal analysis. Dashed lineaments from this study and Ridgley et al. (2001) are approximately located. The geometry of the fault blocks has not been completely determined, and thus orientation of the inferred lineaments could be up to 90° different from that shown. Also shown are the outline of Precambrian provinces and other Precambrian structural elements (heavy black lines) as determined from magnetic anomalies (Ross, 1997; Ross et al., 2000). THO, Trans-Hudson Orogeny; MHB, Medicine Hat Block; GFTZ, Great Falls Tectonic Zone. The Eyehill High is a positive magnetic anomaly described by Ross et al. (1991). Sawteeth show the direction of thrust vergence within the Hearne Province.

from similar strata in the area around Spring Coulee Field, Montana, are placed within a proposed stratigraphic framework for the upper part of the Belle Fourche. This area has been highlighted because current production is localized in small pools of only a few wells each, located far from major sites of shallow gas production in the upper part of the Belle Fourche in Alberta and on Bowdoin Dome, Montana (Figure 2). The lithofacies in the Senate, Merryflat, Cypress Lake, and Spring Coulee areas also produce gas in the southeast Alberta Gas Field and on Bowdoin Dome.

2. Methods of Study

Subsurface interpretations of the regional geology and sedimentology are based on examination of cores from 30 wells in the Belle Fourche, Second White Specks, and Greenhorn formations and from numerous wireline logs in Alberta, Saskatchewan, and Montana, especially along the transect. Two of these cores are from wells used to construct the E-E' transect and were logged for calibration of lithologies to wireline log responses. One core was sampled for foraminiferal analysis in order to compare it to previously published stratigraphic interpretations for this well. Samples were collected to provide data to supplement sedimentologic observations, and so are not located at regularly spaced

intervals. Much of the Belle Fourche is defined by cyclic sedimentation, both 4th- and 5th-order cycles. Flooding surfaces, sandy transitional intervals, and dominantly sandy units were therefore targeted for sampling. Cross section E-E' (Figures 3 and 4) through the study area was constructed from wireline logs. The datum is the top of the Second White Specks, a regionally distinctive marker surface recognizable on wireline logs. The contact between the lower and upper parts of the Belle Fourche was used as an internal datum to ascertain the position of paleotectonic linear features and relative time of structural movement on fault-bounded basement blocks. Because of differential erosion of the upper part of the Belle Fourche below the Second White Specks and Greenhorn unconformity, the delineation of basement blocks and relative times of movement on these blocks is obscured for part of this period of deposition. Distribution of gas-producing wells in Canada is from International Datashare Corporation and is current through June 1996; cumulative production data for the Senate, Merryflat, and Cypress Lake pools are provided by Saskatchewan Energy and Mines and are current through October 2000. Locations of gas-producing wells and cumulative production data in Montana are from a database leased from IHS Energy Group. Well completion data are from publicly available files.

3. Regional Stratigraphy of the Belle Fourche Formation

The Belle Fourche, Second White Specks, and Greenhorn formations form the middle part of the Cretaceous Colorado Group. They comprise marine sandstone, shale, and limestone deposited during periods of regression and transgression in the Western Interior Seaway. Principal expansion of the seaway began in the Albian and was followed by a sea-level fall between the Albian and Cenomanian. A sea-level lowstand at the Albian-Cenomanian boundary or within the late Early Cenomanian is marked in places throughout the seaway by an incised surface (Porter *et al.*, 1993; Bloch *et al.*, 1999). In the study area, strata overlying this surface include the upper part of the Mowry Shale and upper part of the Bootlegger Member of the Blackleaf Formation in Montana (Fish Scales equivalents), and the Fish Scales Formation and Barons Sandstone in Canada (Figure 1). They are characterized by abundant fish fragments, numerous bentonite beds, and lack of foraminifera. The base of the Fish Scales and Barons is generally accepted as the boundary between the Lower and Upper Cretaceous. These units and the overlying Belle Fourche Formation are of Cenomanian age (Cobban *et al.*, 1994). Deposition of the Belle Fourche took place during an overall sea-level rise and westward expansion of the seaway. Clastic units within the Belle Fourche reflect periods of regression that resulted from increased clastic sediment input to the seaway during periods of orogenic activity to the west (Peterson, 1986). Expansion of the seaway continued throughout the Cenomanian, culminating in maximum transgression (Greenhorn) during the Early Turonian. The Second White Specks and Greenhorn formations are Late Cenomanian through Early Turonian in age (Cobban *et al.*, 1994). Following maximum transgression, the sea gradually withdrew to the east. Middle Turonian strata of the basal Carlile Shale document this regression.

Prior to the study by Bloch *et al.* (1993), strata now separately assigned to the Belle Fourche and Second White Specks Formations in Canada were referred to as the Second White Specks, Second White Speckled Shale, or Second White Specks Sandstones (Simpson, 1975; Gilboy, 1988; Glass, 1990), based on the presence of coccoliths in the calcareous shales. The redefinition of part of the Colorado Group into the Belle Fourche and Second White Specks Formations facilitates regional correlation (Figure 1) between strata to the west in the Peace River Arch area, to the east in the Manitoba escarpment area in Saskatchewan and Manitoba, and to the south in Montana. In a basinward transect, noncalcareous shales are found closer to paleoshorelines and highly calcareous shales are found in the most seaward position. Between these two facies, noncalcareous shales may be intercalated with weakly, moderately, or highly calcareous shales that reflect changing positions of water mass boundaries (Fisher *et al.*, 1994). The calcareous shales may contain sparse to abundant coccoliths. The presence of the coccoliths is not indicative of any particular formation (Belle Fourche or Second White Specks as now defined), although in the past the speckled shales were assigned to the Second White Specks. Recent summaries of the regional correlation of the Belle Fourche and age-equivalent strata can be found in Bloch *et al.* (1993), Schröder-Adams *et al.* (1996), Plint (2000), and Ridgley *et al.* (2001).

a) Lithofacies Descriptions

Subdivision of the Belle Fourche into lower and upper parts and finer lithostratigraphic units within each allows the effects of syndepositional tectonics on sediment packages to be assessed, permits more accurate modeling of the potential gas-bearing strata, and provides a detailed framework within which foraminiferal and coccolithic biozones can be placed. The lower Belle Fourche is subdivided into three units, in ascending order A, B, and C (Ridgley *et al.*, 2001). At least three principal bentonite beds are present in units B and C. The lower bentonite ("A" bentonite of Gilboy, 1988) occurs between units B and C. In many places, it has been removed by erosion prior to deposition of the overlying sandstone in unit C. The middle bentonite ("B" bentonite of Gilboy, 1988) occurs in the lower part of unit C and is a regional marker found on wireline logs. Another bentonite found near the top of unit C is also a regional marker on wireline line logs (Ridgley *et al.*, 2001). It is stratigraphically close to the boundary between the lower and upper Belle Fourche. It has been dated at 95.2 ±0.5 Ma, which places it within the late Middle Cenomanian *Plesiacanthoceras wyomingense* and *Acanthoceras amphibolum* ammonite zones (Ridgley *et al.*, 2001). The bentonites provide an excellent basis for regional correlation. As discussed below and shown on the accompanying cross section (Figure 4; Gilboy,

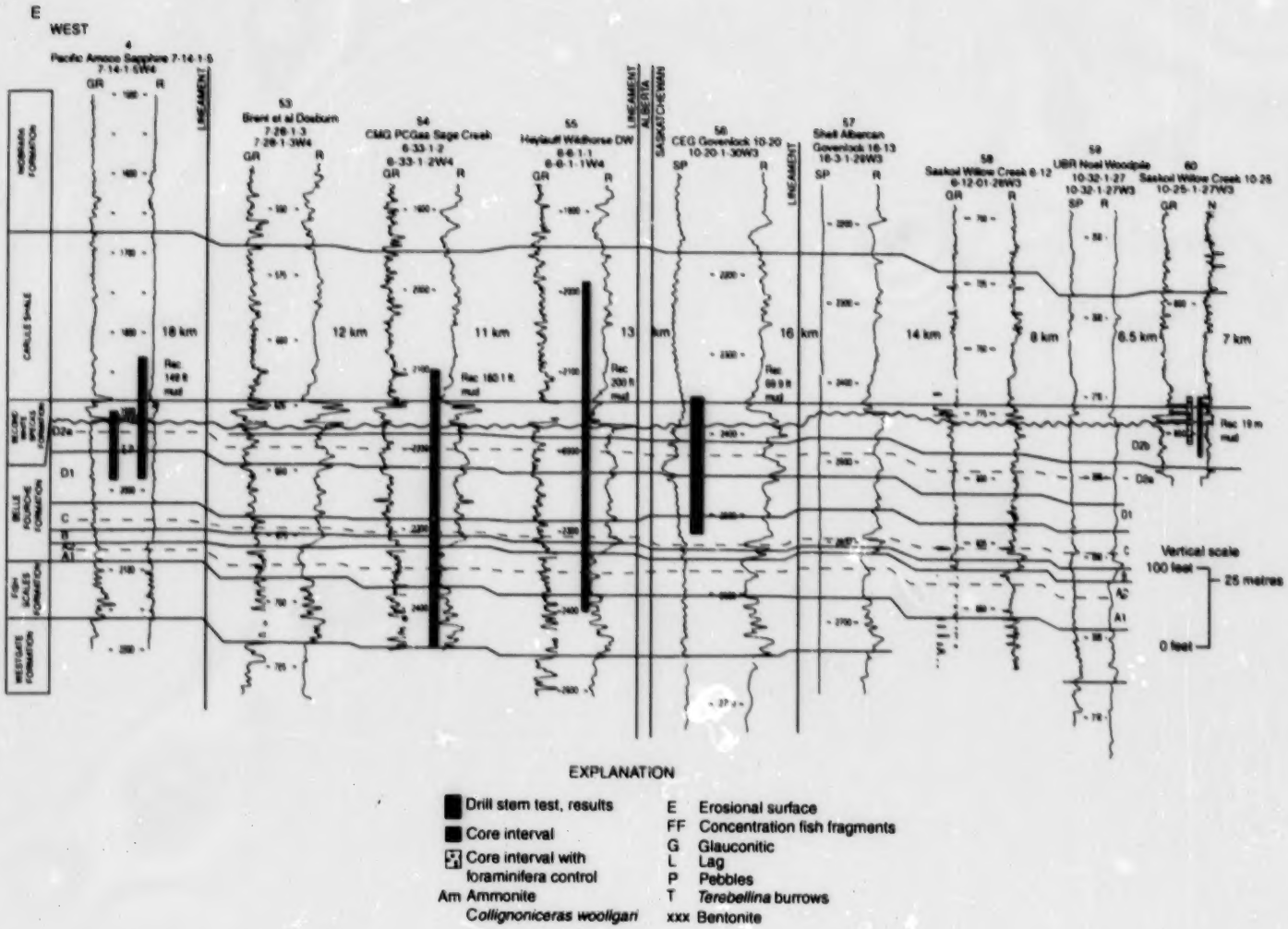

EXPLANATION

- Drill stem test, results
- Core interval
- Core interval with foraminifera control
- Am Ammonite *Collignoniceras woollgari*
- E Erosional surface
- FF Concentration fish fragments
- G Glauconitic
- L Lag
- P Pebbles
- T *Terebellina* burrows
- xxx Bentonite

Figure 4 - Log cross section E-E' showing correlation of genetic components of the Belle Fourche, Fish Scales, and Second White Specks formations, and the Carlile Shale. Depths shown for wells 4, 54 to 57, 59, and 63 to 69 are in feet and for wells 53, 58, 60 to 62, and 46 are in metres.

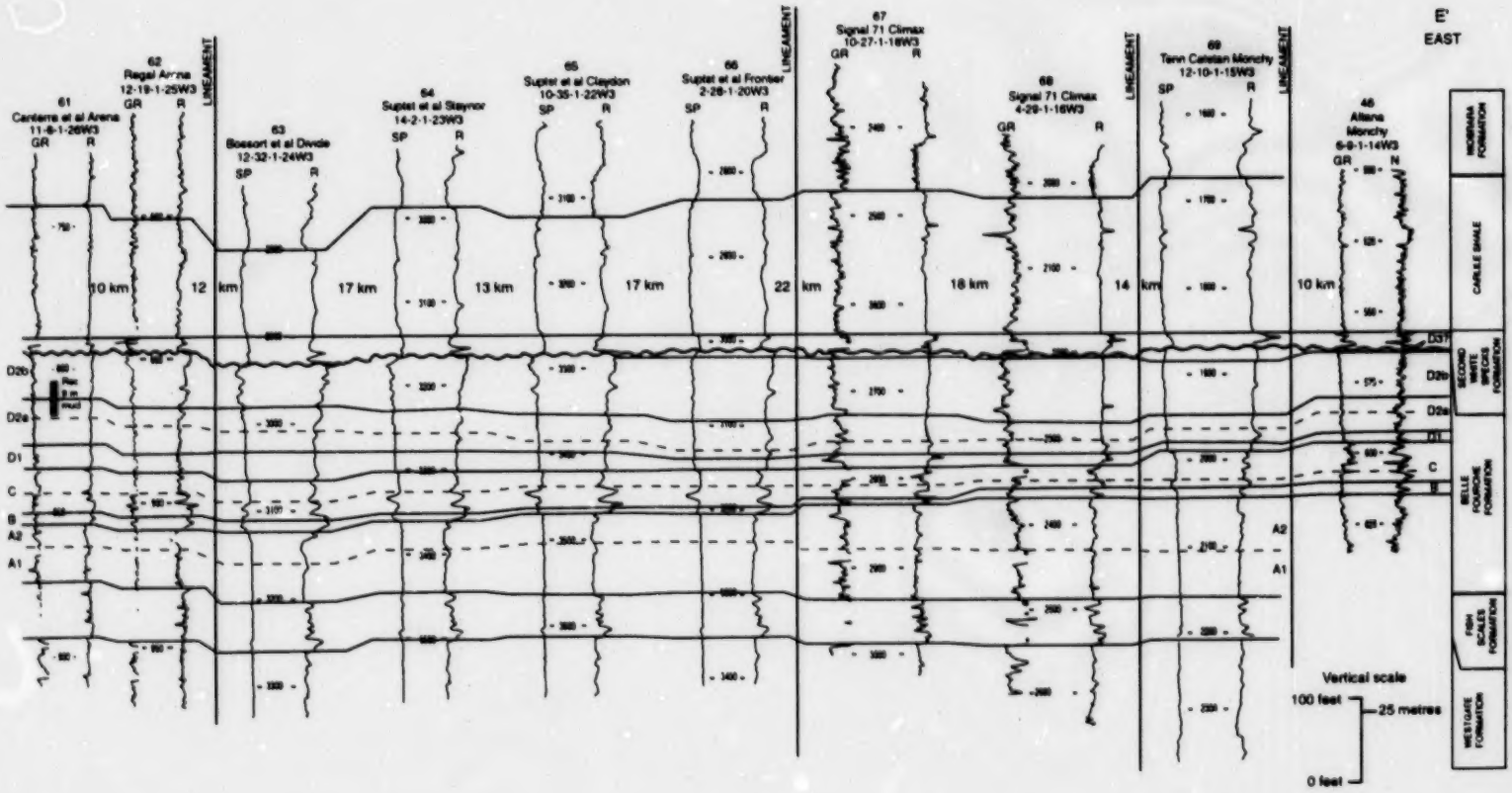

Figure 4 (continued) - Log cross section E-E' showing correlation of genetic components of the Belle Fourche, Fish Scales, and Second White Specks formations, and the Carlile Shale. Depths shown for wells 4, 54 to 57, 59, and 63 to 69 are in feet and for wells 53, 58, 60 to 62, and 46 are in metres.

1988; Ridgley *et al.*, 2001) either the middle or the upper bentonite correlates to the regional "X" bentonite which, dated at 94.93±0.53 Ma (Obradovich, 1993), separates essentially noncalcareous lower Belle Fourche shale from noncalcareous to highly calcareous shale of the upper Belle Fourche. The X bentonite occurs near the top of the *Acanthoceras amphibolum* ammonite zone and is commonly found in association with *Ostrea beloiti* beds. Because of loss or thinning of unit C, the middle and upper bentonites may occupy the same position with respect to the base of unit D. The lower and middle bentonites are in process of being dated (J.D. Obradovich, pers. comm., 2000).

On the cross section E-E' (Figure 4), unit A is subdivided into subunits A1 (older) and A2 by a prominent marker horizon. Within unit C, the B bentonite generally lies just above the basal glauconitic sandstone. These markers are useful in defining the relative effects of deposition and syndepositional tectonics on the geometry of units A, B, and C. The boundary between the upper and lower Belle Fourche is chosen just above the upper bentonite. This contact is marked by low gamma ray, spontaneous potential, and resistivity deflections on wireline logs. The silty and shaly upper part of unit C is recognizable even in the absence of the upper bentonite as it has characteristic log responses different from those of similar lithologies in the basal part of unit D.

The upper Belle Fourche, unit D, has been subdivided into three subunits, in ascending order D1, D2, D3, based on recognition of three upward-coarsening profiles observed in wireline logs from the southern end of Bowdoin Dome (Ridgley *et al.*, 2001). This tripartite subdivision has also been noted by others (Rice, 1984; Rice *et al.*, 1990). To the north, northwest, and west, the subunits are difficult to correlate because of: a) changes in facies and depositional thicknesses, and b) the differential loss of the Belle Fourche below the unconformity at the base of the Greenhorn and Second White Specks. Nevertheless, in transect E-E' (Figure 4), an attempt is made to maintain the tripartite subdivision and to further subdivide subunit D2. Subunit D3 appears generally to be absent. These subdivisions bear similarity to those of Gilboy (1988, 1996), but differ because of reinterpretations resulting from new data produced by logging additional cores, primarily in Alberta, and by ongoing foraminiferal studies done in co-operation with the Geological Survey of Canada. Summarized below are the basic sedimentological aspects of the different units of the Belle Fourche. More detailed descriptions can be found in Gilboy (1988) and Ridgley *et al.* (2001) and are directly applicable to this study.

Unit A

Unit A overlies the Fish Scales Formation or Mowry Shale equivalent, and is dominantly composed of grey noncalcareous marine shale with thin sandstone stringers in the middle and upper parts; fish scales and bone fragments are common. The proportion of sandstone to shale increases upward through the unit as does bioturbation. This unit contains an agglutinated foraminiferal assemblage characteristic of the *Verneuilinoides perplexus* zone (Ridgley *et al.*, 2001). It separates sandstones of the underlying Fish Scales or Mowry formations from the overlying sandstone of unit B. It varies in thickness and in some wells is thin or absent. In the latter case, unit B rests directly on the Fish Scales (e.g. Amoco Conrad 11-12-6-16 well in 11-12-6-16W4). Using a prominent log-defined marker horizon, Unit A has been subdivided into a lower subunit A1 overlain by subunit A2. Subunit A1 is variable in thickness throughout the study area as shown on cross section E-E' (Figure 4) and in Ridgley *et al.* (2001). It thins toward the Sweetgrass Arch in Montana and Alberta (Bow Island Arch of Tovell, 1958). Its exact nature is unknown as no core through it has been logged. Subunit A2 (Figure 4) also shows a pronounced westward thinning.

Unit B

Unit B comprises a basal sandstone and an overlying shale sequence. The basal sandstone is a regional marker bed in southeastern Alberta and southwestern Saskatchewan. It is commonly intensely bioturbated by *Terebellina* and is one of the Second White Speckled sandstones of industry usage (Gilboy, 1988). It is typically very fine grained and contains accessory biotite, glauconite, and coaly fragments. The dominant colour is tan, which contrasts with the mottled olive-green and white sandstone of the overlying unit C. Where bioturbation is most intense, primary sedimentary structures are destroyed. In several cores, bioturbation is nearly absent or restricted to certain intervals, and primary sedimentary structures such as low-inclined hummocky cross-stratification or wave-ripple laminations are preserved. Deposition of the basal sandstone was primarily in shallow shelf environments characterized by slow rates of sedimentation that permitted infauna bioturbation (Gilboy, 1988). Overlying the basal sandstone is a sequence of thin, grey, noncalcareous shale containing fish fragments interbedded with thin, sparsely bioturbated sandstone. The shale has yielded the Middle Cenomanian ammonite *Borrisiakoceras compressum* Cobban (Gilboy, 1988, 1993) in the Coseka Hatton 6-20-14-25W3 well in Saskatchewan. *B. compressum* is found in the *Conlinoceras tarrantense–Conlinoceras gilberti* ammonite zone, which separates Lower and Middle Cenomanian strata (Cobban and Scott, 1972; Cobban *et al.*, 1994). The *C. tarrantense* zone correlates with the Thatcher Limestone Member of the Graneros Shale in the central part of the Cretaceous seaway to the south (Eicher, 1965; Cobban and Scott, 1972). Unit B contains an agglutinated foraminiferal assemblage characteristic of the *Verneuilinoides perplexus* zone (Ridgley *et al.*, 2001).

In some wells, the base of unit B appears to be conformable with unit A. In other wells, small chert pebbles in the lower part of unit B suggest that the sandstone overlies a scour surface. On the regional cross sections (Figure 4; Ridgley *et al.*, 2001) the

contact can also be interpreted as being unconformable. This is especially apparent on the Sweetgrass Arch in Montana and Alberta and across some of the linear features that define fault-bounded basement blocks. The upper contact of unit B is commonly marked by an erosional surface characterized by a lag of chert pebbles, especially where unit C lies directly on the basal sandstone of unit B because of the prior removal of the intervening shale and bentonite strata. Mostly due to this loss of strata below the erosional base of unit C, the thickness of unit B is variable.

Unit C

Unit C is a sandstone, sandy shale, and shale sequence. The basal glauconitic sandstone, one of the Second White Speckled sandstones of industry usage (Gilboy, 1988), is generally fine grained with coarse-grained to, in places, pebbly layers. The pebbly layers predominantly contain black chert clasts and fish fragments, and are mainly present in the lower part of the basal sandstone, particularly on the basal surface. Overlying the basal sandstone are many vertically stacked parasequences, each beginning with black shale followed by, first, a transition of thin sandstone and shale in which the sandstone proportion increases upward, and, second, a cap of sandstone with scarce black shale partings. Many of these parasequences are incompletely developed or preserved. Benthonic foraminifera characteristic of the *Verneuilinoides perplexus* zone (Ridgley *et al.*, 2001) have been recovered from shale layers.

In contrast to unit B, burrowing is rare. Rather, the sandstones exhibit well developed hummocky cross-stratification, and ripple cross-lamination with shale drapes, suggesting migrating dunes. Flaser bedding is also present. Deposition of unit C took place in shallow shelf environments of fairly high energy and high sedimentation rate, as reflected by the lack of infauna burrowing and the dominance of hummocky cross stratification (Gilboy, 1988). The coarse-grained basal conglomerate appears to be regionally widespread, having been observed in cores in Saskatchewan, Alberta (where they are commonly coarser grained), and east-central Montana, where they have been interpreted to overlie a sequence boundary (Porter *et al.*, 1993). This sequence boundary appears to be present throughout the study area as an incised surface. Thickness of the unit varies, mostly as a result of removal of the upper part across some of the lineaments that define fault-bounded basement blocks (Figure 4; Ridgley *et al.*, 2001), but also due to infilling of the erosional surface cut into unit B. The visual representation in cross section E-E' (Figure 4; Ridgley *et al.*, 2001) suggests valley incision and the backfilling of these valleys with strata of unit C. In this study, log correlations and descriptions of logged core indicate that the basal sandstone of unit C is persistent throughout the area. This points to differential movement on basement blocks between deposition of unit C and unit D as the principal cause for the thickness variation of unit C. This interpretation is further supported by the presence of a regional marker bentonite ("B" bentonite of Gilboy, 1988) just above the basal sandstone as shown on cross section E-E' (dashed line in unit C, Figure 4). The contact with the overlying unit D is picked from its characteristic wireline-log signature. The upper bentonite in unit C was logged within this interval in the Samedan Prud Cypress 10-3-9-1 well located in 10-3-9-1W4 (Ridgley *et al.*, 2001).

Unit D

Unit D rests on an erosional surface that appears to be regionally widespread and of little relief. The base of unit D represents a major transgression and landward shift in facies, both lithologic and biologic, and the overlying strata differ in sedimentary structures, vertical stacking of lithologies, foraminiferal assemblages, and paleoenvironments. The *Verneuilinoides perplexus* zone (Ridgley *et al.*, 2001) characteristic of units A to C is absent in unit D. Regional correlation of unit D is shown in Figure 1. Rice (1984) placed all strata in central and northern Montana that are equivalent to unit D in the Mosby Sandstone Member of the Belle Fourche Shale. The Mosby is composed of three coarsening upward sequences which are especially prominent in the Bowdoin Dome area (Rice, 1984; Rice *et al.*, 1990).

Unit D is subdivided into subunits D1, D2, and D3 (oldest to youngest). These subdivisions represent three Late Cenomanian time slices, and provide a more detailed picture of the geometry of potential sandstone gas reservoirs. They also enable the effect of post-depositional tectonics on the individual units to be evaluated, and thus the time of tectonic activity to be constrained. Each of the subunits is a sandstone-capped, coarsening-upward parasequence set, each of which is composed of thinner coarsening-upward parasequences bounded by flooding surfaces (in this report, usage of parasequence follows that of Van Wagoner *et al.*, 1990).

Subunit D2 is further subdivided into subunits D2a and D2b, each of which has a characteristic reservoir geometry. Both D2a and D2b appear to be bounded by flooding surfaces of two forms. Between D1 and D2a, foraminiferal assemblages at the flooding surface contain planktonic foraminifera which are indicative of deeper water (Ridgley *et al.*, 2001). In places, the surface is marked by tan and black chert pebbles up to 4 mm in diameter, coarse quartz grains, and concentrations of shell and/or fish fragments (e.g. Amoco Sapphire 7-14-1-5 well, Figure 4), interpreted to represent a transgressive lag. The flooding surface between D2a and D2b is characterized by changes in agglutinated foraminiferal assemblages (D.H. McNeil, Geological Survey of Canada, written comm., 2000) suggesting slight shifts within the shallow-shelf environment but no major water-deepening events.

Two cores from wells along the transect, Pacific Amoco Sapphire 7-14-1-5 and Saskoil Willow Creek 10-25 (Figures 4 and 5), were examined in order to

calibrate the sedimentology to wireline log responses. Core in the Pacific Amoco Sapphire well includes strata assigned to the Second White Specks, D2a, and the upper part of D1. Core from the Saskoil Willow Creek includes strata assigned to D2b.

In the Pacific Amoco Sapphire well, the parasequences in subunit D1 are well developed and monotonous. One that immediately underlies the contact of D1 with D2a comprises about 3 m of black shale at the base overlain by 1.8 m of thinly interbedded sandstone and shale which are, in turn, overlain by about 0.3 m of sandstone. The basal black shale overlies 1.2 m of low-angle crossbedded sandstone with shale partings and layers in the lower part; the sandstone represents the top of the underlying parasequence. The transgressive lag described above marks the erosional surface at 1951.5 ft (595 m), which is the contact between subunits D1 and D2. This placement of the contact differs from that presented in Ridgley *et al.* (2001). The revised interpretation is based on preliminary foraminiferal data (D.H. McNeil, Geological Survey of Canada, written comm., 2000) from wells in Montana that permitted detailed lithostratigraphic correlation of subunits. Subunit D2a consists of stacked parasequences. The sandstones are ripple-laminated, low-angle cross-laminated, and locally burrowed. About 2.1 m of dominantly black shale separates an upper and lower sandstone. This subdivision of subunit D2a into two sandstone sequences separated by shale of variable thickness is shown on cross section E-E' (Figure 4). The lower sandstone is better developed at the west end of cross section E-E' (Figure 4) and thins and becomes siltier to the east. In contrast, the upper sandstone is less well developed, thinner, and siltier on the west end of cross section E-E' (Figure 4) and is thicker in the middle part of the cross section. It also thins and becomes siltier to the east. In this core, the Second White Specks contact with the Belle Fourche is represented by black, coccolithic shale on very fine-grained, bioturbated sandstone.

Core from the Saskoil Willow Creek 10-25 well was logged through the upper part of subunit D2b, which consists of a monotonous vertical assemblage of stacked parasequences (Figure 5). The sandstones in this core exhibit well developed hummocky cross stratification, flaser bedding and, in places, mud drapes. Bioturbation is locally present and is especially evident in the top sandstone. Near the base of the core, the sandstone is crosscut by numerous calcite-filled fractures. New foraminiferal data from this well generally agree with previously published results for the Second White Specks and Belle Fourche (compare Table 1 with data in Bloch *et al.*, 1999). Bloch *et al.* (1999)identified a flooding surface, characterized by one specimen of the planktonic foraminifera, *Praeglobotruncana delrioensis*, at 846 m. This surface occurs immediately below the last occurrence of the planktonic foraminifera *Whiteinella aprica*, the guide species for the Second White Specks and Greenhorn Limestone (McNeil and Caldwell, 1981). It was not resampled in this study. The presence of the keeled planktonic foraminifera suggests deeper water in this area. Figure 5 shows the principal planktonic and

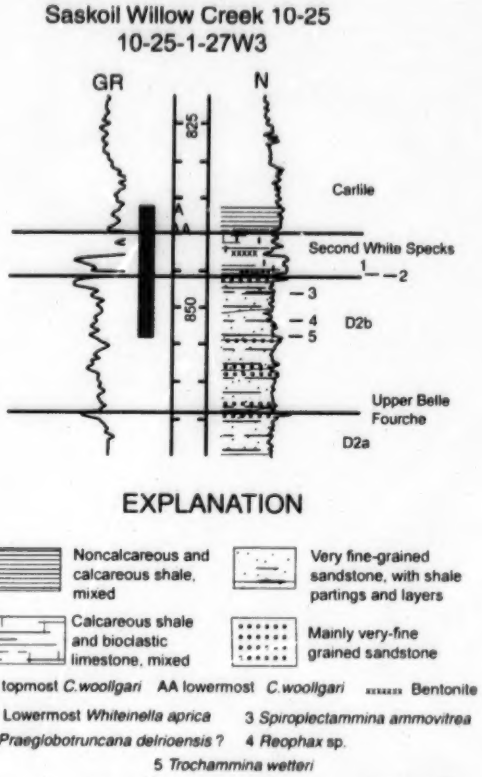

Figure 5 - Description of core from the Saskoil Willow Creek 10-25 well in 10-25-1-27W3, showing simplified lithofacies and contacts between major formations and between subunits D2a and D2b. Also shown are the positions of the major foraminifer assemblages and the first and last position of** Collignoniceras woollgari. **Depth is in metres.

agglutinated foraminiferal zones from this study and Bloch *et al.* (1999). Within D2b, agglutinated foraminiferal assemblages are dominant with sandier intervals characterized by *Reophax* sp. or *Spiroplectammina ammovitrea* and the underlying black shale layers by *Trochammina wetteri*.

A principal difference between the conclusions reached by Bloch *et al.* (1999) and those resulting from this study is the interpretation of the contact between the Second White Specks and the overlying unit. They suggested that Santonian-age rocks might rest unconformably on the Early Turonian Second White Specks, based on the presence of the coccoliths *Kamptnerius magnificus* Deflandre and *Marthasterites furcatus* (Deflandre). However, numerous specimens of *Collignoniceras woollgari* (Figure 6) are present in the shale from the top of the core down to the Second White Specks. *C. woollgari* is a Middle Turonian ammonite characteristic of the Carlile Shale (Obradovich, 1993). Its presence above the Second White Specks suggests that a major unconformity is not present in this core. Foraminiferal data from the shale interval above the Second White Specks (Table

Table 1 - Relative abundance of foraminifer species in the Saskoil Willow Creek 10-15 well in 10-25-1-27W3. The relative abundance is shown by the number of "x"s; r, rare; ?, questionable presence. Provided by D.H. McNeil, Geological Survey of Canada.

SASKOIL WILLOW CREEK 10-15 WELL

10-25-1-27W3

MICROFOSSIL DISTRIBUTION CHART

LAB MICRO # 659	Sample (metres)	FORAMINIFERA																		MISCELLANEOUS													
		Miliammina sp.	Reophax? sp.	Haplophragmoides collyra	Ammobaculites? sp.	Pseudobolivina? sp.	Trochammina rainwaterii	Hedbergella delrioensis	Hedbergella loetterlei/Whiteinella aprica?	Whiteinella aprica	Haplophragmoides spp.	Reophax?/Spiroplectammina? sp.	Saccammina lathrami	Bathysiphon sp.	Reophax sp.	Ammobaculites sp.	Ammomarginulina? sp.	Pseudobolivina? sp.	Trochammina wellleri	radiolarian (spherical)	radiolarian (discoidal)	radiolarian (discoidal with spines)	Leiosphaeridia sp. A	Leiosphaeridia sp. B	Lancettopsis sp.	calcisiltitic shale	prismatic calcite, bivalve	fish fragments	fish teeth	fine grained sandstone/calcarenitic	very fine grained sandstone	kerogen - AOM	fusain
246	836.000	x	x	xx	x	x	x																	x	x			xx		x		xxx	
247	838.000																									x	xxx					xxx	
248	840.000																			xx						x	xxx	xxx		x			
249	842.000							x												xxx	xx	xx		x			x	xxx				xxxx	
250	844.000							xxx	xx														xx			xxx	xxx	xx				xx	
251	845.796						x		x	xx	x												x			xx	xxx	xxx	x	xx		xx	
252	848.000																										x	x	x		xxx		xxx
253	850.000										?	?												xx				xx			xxx		xx
254	852.000										x		r	x	xx	x	x						x	x			xxx		x		xx		x
255	854.000												xx		x			?	xxx														

Washed Residue Descriptions (Samples are crushed, washed and sieved over a 75 micron screen)

not described

1) are also consistent with published data for the Carlile (Bloch *et al.*, 1999).

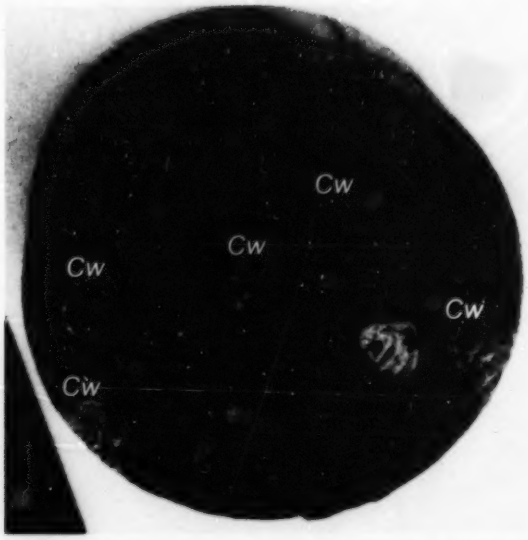

Figure 6 - Numerous small** Collignoniceras woollgari **(Cw) present in core at a depth of 838.66 m in the Saskoil Willow Creek 10-25 well in 10-25-1-27W3. Diameter of the core is approximately 10 cm.

4. Correlation and Structural Analysis

Cross section E-E' (Figure 4) shows the correlation of units and subunits in the upper and lower parts of the Belle Fourche and the nature of the contacts of the Belle Fourche with the Fish Scales below and the Second White Specks above. The line of cross section is oblique to the inferred northeast direction of depositional dip. Because the upper part of the Belle Fourche is erosionally truncated beneath the Second White Specks unconformity and because the location of the shorelines is unknown (they occur somewhere to the southwest within or beneath thrust sheets, Peterson, 1986), the true direction of depositional dip has to be inferred from the direction of probable sources. Source areas for the Belle Fourche were mainly located in southeastern British Columbia, eastern Idaho, and southwestern Montana (Ridgley *et al.*, 2001). Inferred lineaments are shown where abnormal thickening or loss of strata cannot be explained by facies changes or depositional thinning. Although the term lineament was defined to refer to surface linear features (Hobbs, 1904), others have applied it to linear features in the subsurface (Maughan and Perry, Jr., 1986; Shurr and Rice, 1986). In the subsurface, lineaments may define zones of structural weakness, fault zones, or the boundaries of basement blocks. Where lineaments represent the sides of fault-bounded basement blocks, associated movement may reverse direction in geologic time; also, periods of quiescence when no movement took place are common. Differential movement on blocks, as a whole, is more important than movement on one of the bounding faults. In this study, if the correlations indicated that movement had occurred, a

lineament was drawn between the appropriate wells. The major ones are highlighted.

On E-E', the Fish Scales Formation is generally constant in thickness over broad areas, but thins to the east. Pronounced thickness changes occur near or across inferred lineaments. As discussed earlier, unit A shows pronounced thickness changes from west to east on E-E' (Figure 4). This is especially apparent when the relative thickness of subunits A1 and A2 are examined. Some of the pronounced thickness change in A1 may be depositional as the subunit generally thins toward the Sweetgrass Arch, which may then have been tectonically active. Unit B also thins to the east but the variation in thickness is due to erosion of the upper shale strata. The basal sandstone of unit B thickens or thins as lineaments are approached or crossed. Unit C is relatively thickest in the central and eastern wells of E-E'. Within this unit, the trace of the lower bentonite marker provides a visual representation of the preservation or loss of overlying strata. The variable thickness of the glauconitic sandstone below the bentonite is attributed to infilling on an erosional surface. Overall, unit C shows pronounced thickness changes as lineaments are approached or crossed.

Subunit D1 appears to thin by deposition from west to east (from the Sweetgrass Arch to Bowdoin Dome). Subunit D2a is composed of two imbricate sandstone beds separated by mudstone. The older sandstone is more prominent in the western part of the cross section and the younger in the central and eastern part. Both sandstones thin to the east. Based on this interpretation, the contact between subunits D1 and D2a in the Altana Monchy 6-9-1-14 well (well 46 on Figure 4) has been revised from that presented in Ridgley *et al.* (2001). Subunit D2b thickens from west to east on cross section E-E' (Figure 4). This is due to preservation below the sub-Second White Specks unconformity. Very thin D3 may be present in the easternmost wells. The Second White Specks Formation shows substantial changes in thickness, especially where lineaments are approached or crossed.

In this report, variations in thicknesses of the units and subunits of the Belle Fourche and Second White Specks have been attributed to syndepositional fault movements rather than to dissolution of the Middle Devonian Prairie Evaporite Formation. However, if dissolution of the evaporite was concurrent with orogenic activity in the Cenomanian, local accommodation space would have been created, resulting in variable thickness of the Belle Fourche and Second White Specks during deposition. Detailed modeling of thickness variations in the Bell Fourche and Second White Specks in relation to preservation or loss of the Prairie Evaporite is needed to evaluate the relative effects of movement on structures and loss of evaporite.

Ridgley *et al.* (2001) suggested that the presence of inferred lineaments along three transects could be interpreted to define the boundaries of basement blocks of different sizes. The lineaments shown on E-E' support this interpretation. When observed in plan view, the boundaries of basement blocks (Figure 5) are defined by an orthogonal system of lineaments having predominantly northwest and northeast orientations. Intersection of lineaments are recorded near the west and east ends of cross section E-E' (Figure 4). The geological influence of basement blocks of a wide range of sizes has been discussed for the Rocky Mountain region and Montana by many authors (e.g. Anna, 1986; Maughan and Perry, Jr., 1986; Shurr and Rice, 1986; Shurr *et al.*, 1989; Shurr *et al.*, 1993), who deduced their existence by field mapping, isopach mapping, and Landsat imagery. The blocks range in size from the Precambrian Hearne Province and Trans-Hudson Orogen to smaller blocks within them, forming a mosaic of linear features. Superimposed on Precambrian blocks are other lineaments of younger age, primarily related to Laramide tectonics. Syndepositional or immediately post-depositional movement of basement blocks affects both original thickness and present-day geometry of Phanerozoic stratigraphic units. The younger lineaments may control fracture development and orientation. Both types of lineaments may affect gas location and production by forming compartments (Shurr *et al.*, 1993). Lineaments related to movement on basement blocks control the geometry and possible offset of reservoir units, thereby possibly creating pressure compartments if the bounding faults are sealed or if the calcareous shale of the Second White Specks is juxtaposed to sandstone of the upper Belle Fourche. Younger lineaments associated with faults (not fractures) may occur at an angle to the basement block side and thus form smaller compartments within the basement block; if these faults are sealed, smaller pressure compartments could form.

The orientation and position of some of the inferred lineaments are roughly aligned with magnetic anomalies (Ross, 1997; Ross *et al.*, 2000) and with changes across Precambrian province boundaries (Figure 3). The lineaments in the western part of the study area tend to trend northwest-southeast. They occur within the Medicine Hat Block which is characterized by pronounced northwest-southeast magnetic anomalies (Ross *et al.*, 1991; Ross, 1997). Lineaments in the eastern part of the study area tend to trend northeast-southwest, the dominant trend of magnetic anomalies in the Great Falls Tectonic Zone (Ross *et al.*, 1991; Ross, 1997). Several of these lineaments directly coincide with major magnetic anomalies in the Medicine Hat and Great Falls tectonic blocks. For example, that between wells 62 and 63 on E-E' (Figure 3) coincides with the suture zone between the Medicine Hat Block and the Great Falls Tectonic Zone, suggesting that this suture was active during the Cenomanian. The suture zone between the Medicine Hat Block, Great Falls Tectonic Zone, and Hearne Province is arcuate. The loss of sandstone in the upper Belle Fourche appears to be roughly parallel to this suture, suggesting a possible genetic link. Configuration of the geometry of this loss of upper Belle Fourche strata is in process. Also, the pronounced northeast truncation of strata below the sub-Second White Specks unconformity in

Saskatchewan is within the Hearne and Trans-Hudson blocks. These are areas in which significant deformation occurred in the Precambrian (Ross *et al.*, 2000). Regionally extensive movement between these large Precambrian blocks during the Cenomanian is possibly responsible for the truncation. How the thin lithosphere responds to tectonic loading and terrane accretion, both of which occurred in the Cenomanian (Peterson, 1986; Wu, 1991), is not fully known. Modelers of foreland basin lithospheric response to thrust loading commonly use a flexural model for defining the position of the forebulge, but do not consider what effects differential response of the basement blocks might have in defining different positions or configurations of the forebulge. More detailed studies of these relationships are needed as the definition of basement blocks and their control on sedimentation and reservoir geometries, compartments, and fluid movement are critical to understanding controls on shallow gas accumulation (Shurr *et al.*, 1993).

5. Relationship between Lithofacies and Producing Intervals

An understanding of the genetic relationship between sandstone and shale packages provides a framework within which current gas-productive intervals in the upper Belle Fourche can be examined. In southwestern Saskatchewan, isolated production takes place from the upper Belle Fourche in the Senate (Gilboy, 1988), Merryflat, and Cypress Lake pools (Figure 2). Nearby, in Montana, modest production from the upper Belle Fourche occurs in the area of the Spring Coulee Field (Figure 2). Available cumulative production for each of these pools is summarized in Table 2 which also shows the target or currently producing zone based on the subdivision of the upper Belle Fourche in this report. The significant time lag between discovery date and onset of production (except for the Cypress Lake Pool) reflects lack of infrastructure and market conditions during the early history of drilling in the area. In Montana, three of the four productive wells in the Spring Coulee Field (Figure 2) produced for only a short period of time. Most of these wells have produced from deeper strata, mainly Sawtooth, before being recompleted later in the Belle Fourche. The reason why production from the Belle Fourche ceased in these wells is not known. Although only four wells in the Spring Coulee Field have produced gas, during the late 1970s and early 1980s additional wells tested the Belle Fourche in this area (Table 3) and produced gas on stimulation and drillstem testing. Importantly, in some cases gas was not produced during drillstem testing, but was later during stimulation (Table 3). Thus, the absence of gas in a drillstem test is not conclusive for these shaly reservoirs. The wells were shut in and appear to have not been reactivated.

The current reservoirs in Saskatchewan and Montana show differences that reflect the sandstone preserved below the Second White Specks and Greenhorn unconformity (Tables 2 and 3). In Saskatchewan, most of the production appears to be from subunit D2b. Subunit D2a may also be productive in the Merryflat Pool. Units B and C of the lower Belle Fourche have also been tested in the Senate and Merryflat pools; whether or not these sandstones contribute to overall production is unknown. In Montana, gas production from the four wells has been from subunit D2a because most of subunit D2b has been removed by erosion. The gas wells that were shut in are similar: where D2b is preserved, it was the target; where it is absent or thin, the target shifted to D2a. This suggests that gas can be found in other areas where the sandy facies of subunits D2a and D2b are developed and preserved. Units B and C, not specifically addressed in this report, also warrant evaluation as they are productive in

Table 2 - Cumulative production from the upper part of the Belle Fourche Formation in the Senate, Merryflat, and Cypress Lake pools, southwestern Saskatchewan, Canada, and the area of the Spring Coulee Field, Liberty County, Montana, USA. Cumulative production data for Saskatchewan are through October 2000 and available from Saskatchewan Energy and Mines. Cumulative production data for Montana are through August 2000, and are available from IHS Energy Group. For the Saskatchewan pools, the number of wells capable of producing gas is listed first followed by the number of wells actually producing as of October 2000. Producing interval in Montana may be listed as Blackleaf, Greenhorn, or White Specks in the IHS Energy database. Conversion factors: 1 x m^3 = 35.3 ft^3; 28.3 x $10^3 m^3$ = 1 x $10^6 ft^3$; and mmcf, million cubic feet.

Pool/Field	Location	Number of Producing Wells	Discovery Date	Start Production Date	End Production Date	Cumulative Production (10^6 m^3)	Cumulative Production (mmcf)	Target Unit
Senate	T. 2 to 3, R. 28 to 29W3	12/7	1971	1986		522.5	18,444.25	D2b, C, B
Merryflat	T.6 to 7, R. 28 to 30W3	10/9	1971	1994		265.9	9,386.27	D2a, 2b, C, B
Cypress Lake	T. 5 to 6, R. 26W3	5/5	1994	1995		283.3	10,000.49	D2b
Spring Coulee		4						
Meland 1-13	13-35N-12E		1982	12/95	01/96	0.0161	0.569	D2a
Peterson 24A	24-35N-12E		1985	11/95	02/97	0.1993	7.042	D2a
Larson 19-4	19-35N-13E		1975	04/96		0.8953	31.636	D2a
Keller 1-11	11-36N-13E		1977	02/87	12/88	0.0113	0.399	D2b

Table 3 - Wells that showed the presence of gas in the Belle Fourche Formation in the area of the Spring Coulee Field, Montana. These wells were shut in and have never produced gas. IP, initial production; sgcm, slight gas cut mud; gcm, gas cut mud; pb, plugged back; and mcf, thousand cubic feet. Data are from publicly available files.

Well	Location	Completion Date	Perforation Interval/ft	IP/mcf	DST Interval/ft	DST Recovery	Target Unit
4-37-13-16 Wilmes	4-37N-13E	4/81	2242-2264				D2b
Knapp 33-37-13	33-37N-13E	4/82	2293-2303	40 est.			D2b
Knapp 3-10	3-36N-13E	1/78	2285-2318	125			D2b
NW Saddle 12-12	12-36N-13E	7/78	2493-2496 2514-2518 2524-2526 2554-2559 2569-2571	10	2540-2585	90 ft mud	D2a, D2b Well pb above D2a
Velk 24-36-1	24-36N-13E	4/81	No details				D2a, D2b, C, B?
Johnson 22-36-14	22-36N-14E	5/79	No details				D2a, D2b
State ML50 9-36	36-36N-14E	8/78	2500-2535	7	2438-2520	9mcf, 240 ft scgm	D2b
24-10 Dundas-Warren	24-35N-12E	7/77	2117-2118 2124-2136 2155-2156	18	2072-2200	18mcf; 806 ft gcm	D1, D2a
State 1-28	28-35N-13E	8/94	2190-2206				D2a

southwestern Saskatchewan and on the west side of the Kevin-Sunburst Dome (Figure 2; Ridgley *et al.*, 2001).

6. Summary

This regional study of the Belle Fourche indicates that movement of basement blocks has had a pronounced effect on preservation of stratigraphic units that comprise the formation. Detailed correlation of genetic packages in the Belle Fourche allows the magnitude and timing of movement of these blocks to be assessed. Where the upper Belle Fourche sandstones are eroded below the Second White Specks, the juxtaposition of less permeable shales of the Second White Specks to sandstone of the Belle Fourche may provide both subtle lateral and vertical seals to gas migration. Knowledge of the depositional systems of the Belle Fourche and of the structural history in the area of deposition have important consequences in the exploration for and exploitation of shallow biogenic gas in Alberta, Saskatchewan, and Montana.

7. Acknowledgments

We thank Dave McNeil of the Geological Survey of Canada for providing the foraminifera data presented herein, and Tim Hester and Curt Huffman of the U.S. Geological Survey for their critical review and suggested revisions of this manuscript.

8. References

Anna, L.O. (1986): Structural influences on Cretaceous sedimentation, Northern Great Plains; *in* Peterson, J.A. (ed.), Paleotectonics and Sedimentation in the Rocky Mountain Region, United States, Amer. Assoc. Petrol. Geol., Mem. 41, p173-191.

Bloch, J.D., Schröder-Adams, C.J., Leckie, D.A., Craig, J., and McIntyre, D.J. (1999): Sedimentology, Micropaleontology, Geochemistry, and Hydrocarbon Potential of Shale from the Cretaceous Lower Colorado Group in Western Canada; Geol. Surv. Can., Bull. 531, 185p.

Bloch, J.D., Schröder-Adams, C.J., Leckie, D.A., McIntyre, D.J., Craig, J., and Staniland, M. (1993): Revised stratigraphy of the Lower Colorado Group (Albian to Turonian), Western Canada; Bull. Can. Petrol. Geol., v41, p325-348.

Cobban, W.A. and Scott, G.R. (1972): Stratigraphy and Ammonite Fauna of the Graneros Shale and Greenhorn Limestone near Pueblo, Colorado, U.S. Geol. Surv., Prof. Pap. 645, 108p.

Cobban, W.A., Merewether, E.A., Fouch, T.D., and Obradovich, J.D. (1994): Some Cretaceous shorelines in the Western Interior of the United States; *in* Caputo, M.V., Peterson, J.A., and Franczyk, K.J. (eds.), Mesozoic Systems of the Rocky Mountain Region, U.S.A., Rocky Mtn. Sec., Soc. Econ. Paleont. Mineral., p393-413.

Eicher, D.L. (1965): Foraminifera and biostratigraphy of the Graneros Shale; J. Paleont., v39, p875-909.

Fisher, C.G., Hay, W.W., and Eicher, D.L. (1994): Oceanic front in the Greenhorn sea (late Middle though Late Cenomanian); Paleocean., v9, p879-892.

Gilboy, C.F. (1988): Geology and natural gas production of the Upper Cretaceous Second White-Speckled Shale, southwestern Saskatchewan; *in* Summary of Investigations 1988, Saskatchewan Geological Survey, Sask. Energy Mines, Misc. Rep. 88-4, p183-195.

_____ (1993): Fossil identifications from Upper Colorado Group cores, southwestern

Saskatchewan; *in* Summary of Investigations 1993, Saskatchewan Geological Survey, Sask. Energy Mines, Misc. Rep. 93-4, p200.

_____ (1996): Detailed log-based stratigraphic study of Colorado and Milk River Formation strata (Cretaceous), southwestern Saskatchewan; *in* Summary of Investigations 1996, Saskatchewan Geological Survey, Sask. Energy Mines, Misc. Rep. 96-4, p133-135.

Glass, D.J. (1990): Lexicon of Canadian Stratigraphy, Volume 4, Western Canada, including British Columbia, Alberta, Saskatchewan, and Southern Manitoba; Can. Soc. Petrol. Geol., 772p.

Hobbs, W.H. (1904): Lineaments of the Atlantic border region; Geol. Soc. Amer. Bull., v15, p483-506.

Kent, D.M. and Christopher, J.E. (1994): Geological history of the Williston Basin and Sweetgrass Arch; *in* Mossop, G.D. and Shetsen, I. (comp.), Geological Atlas of the Western Canada Sedimentary Basin, Can. Soc. Petrol. Geol./Alta. Resear. Counc., p421-424.

Maughan, E.K. and Perry, Jr., W.J. (1986): Lineaments and their tectonic implications in the Rocky Mountains and adjacent plains region; *in* Peterson, J.A. (ed.), Paleotectonics and Sedimentation in the Rocky Mountain Region, United States: Amer. Assoc. Petrol. Geol., Mem. 41, p41-53.

McNeil, D.H. and Caldwell, W.G.E. (1981): Cretaceous Rocks and their Foraminifera in the Manitoba Escarpment; Geol. Assoc. Can., Spec. Pap. 21, 439p.

Obradovich, J.D. (1993): A Cretaceous time scale; *in* Caldwell, W.G.E. and Kauffman, E.G. (eds.), Evolution of the Western Interior Basin, Geol. Assoc. Can., Spec. Pap. 39, p379-396.

Peterson, J.A. (1986): General stratigraphy and regional paleotectonics of the western Montana overthrust belt; *in* Peterson, J.A. (ed.), Paleotectonics and Sedimentation in the Rocky Mountain Region, United States: Amer. Assoc. Petrol. Geol., Mem. 41, p57-86.

Plint, A.G. (2000): Sequence stratigraphy and paleogeography of a Cenomanian deltaic complex: The Dunvegan and lower Kaskapau formations in subsurface and outcrop, Alberta and British Columbia, Canada; Bull. Can. Petrol. Geol., v48, p43-79.

Porter, K.W., Dyman, T.S., and Tysdal, R.G. (1993): Sequence boundaries and other surfaces in Lower and lower Upper Cretaceous rocks of central and southwest Montana – a preliminary report; *in* Energy and Mineral Resources of Central Montana, Mont. Geol. Soc. Guidebook, p45-59.

Rice, D.D. (1984): Widespread, shallow-marine, storm-generated sandstone units in the Upper Cretaceous Mosby Sandstone, central Montana; *in* Tillman, R.W. and Siemers, C.T. (eds.), Siliciclastic Shelf Sandstones, Soc. Econ. Paleont. Mineral., Spec. Publ. 34, p143-161.

Rice, D.D. and Claypool, G.E. (1981): Generation, accumulation, and resource potential of biogenic gas; Amer. Assoc. Petrol. Geol. Bull., v65, p5-25.

Rice, D.D., Nydegger, G.L., and Brown, C.A. (1990): Bowdoin Field – U.S.A., Bowdoin Dome, Williston Basin; *in* Structural Traps III, Tectonic Folds and Fault Traps, Treatise of Petroleum Geology, Atlas of Oil and Gas Fields, Amer. Assoc. Petrol. Geol., p337-355.

Ridgley, J.L. (1998): Gas geochemistry of Upper Cretaceous Second White Speckled Shale, southern Alberta and Saskatchewan, Canada – a regional perspective; *in* Christopher, J.E., Gilboy, C.F., Paterson, D.F., and Bend, S.L. (eds.), Eighth International Williston Basin Symposium, Sask. Geol. Soc., Spec. Publ. No. 13, p278-289.

Ridgley, J.L., McNeil, D.H., Gilboy, C.F., Fisher, C.G., Condon, S.M., Fishman, N.S., and Obradovich, J.D. (2000): Interplay of structure, facies, and unconformities on sites of biogenic gas accumulation in the Upper Cretaceous Belle Fourche and Second White Specks formations – Alberta, Saskatchewan, and Montana; Can. Soc. Petrol. Geol. Annual Meeting, abstr. #313.

Ridgley, J.L., McNeil, D.H., Gilboy, C.F., Condon, S.M., and Obradovich, J.D. (2001): Structural and stratigraphic controls on sites of shallow biogenic gas accumulations in the Upper Cretaceous Belle Fourche and Second White Specks – Greenhorn formations of southern Alberta, Saskatchewan and northern Montana; *in* Anderson, D.S., Robinson, J.W., Estes-Jackson, J.E., and Coalson E.B. (eds.), Gas in the Rockies, Rocky Mtn. Assoc. Geol., Chap. 16, 241-270p.

Ross, G.M. (1997): Assembly of the southwestern Laurentian craton; *in* Ross, G.M. (comp.), 1997 Alberta Basement Transects Workshop, LITHOPROBE Rep. 59, LITHOPROBE Secretariat, Univ. British Columbia, p23-34.

Ross, G.M., Parrish, R.R., Villeneuve, M.E., and Bowring, S.A. (1991): Geophysics and geochronology of the crystalline basement of the Alberta Basin, western Canada; Can. J. Earth Sci., v28, p512-522.

Ross, G.M., Eaton, D.W., Boerner, D.E., and Miles, W. (2000): Tectonic entrapment and its role in the evolution of continental lithosphere: An example from the Precambrian of western Canada; Tectonics, v19, p116-134.

Schröder-Adams, C.J., Leckie, D.A., Bloch, J., Craig, J., McIntyre, D.J., and Adams, P.J. (1996): Paleoenvironmental changes in the Cretaceous (Albian to Turonian) Colorado Group of western Canada: Microfossil, sedimentological and geochemical evidence; Cret. Resear., v17, p311-365.

Shurr, G.W. and Rice, D.D. (1986): Paleotectonic controls on deposition of the Niobrara Formation, Eagle Sandstone, and equivalent rocks (Upper Cretaceous), Montana and South Dakota; *in* Peterson, J.A. (ed.), Paleotectonics and Sedimentation in the Rocky Mountain Region, United States, Amer. Assoc. Petrol. Geol., Mem. 41, p193-211.

Shurr, G.W., Larson, B.S., and Watkins, I.W. (1989): The basement block mosaic beneath the mountain plains; *in* French, D.E. and Grabb, R.F. (eds.), Geological Resources of Montana, Mont. Geol. Soc., Centennial Edition Guidebook, p299-309.

Shurr, G.W., Wosick, F.D., and Rice, D.D. (1993): Regional pressure patterns as evidence for fractured reservoirs in the Bowdoin and Phillips sandstones on Bowdoin Dome, Montana; *in* Hunter, L.D.V. (ed.), Mont. Geol. Soc., 1993 Field Conference Guidebook, p117-128.

Simpson, F. (1975): Marine lithofacies and biofacies of the Colorado Group (Middle Albian to Santonian) in Saskatchewan; *in* Caldwell, W.G.E. (ed.), The Cretaceous System in the Western Interior of North America, Geol. Assoc. Can., Spec. Pap. 13, p553-588.

Tovell, W.M. (1958): The development of the Sweetgrass Arch, southern Alberta; Geol. Assoc. Can., Proceedings, v10, p19-30.

Van Wagoner, J.C., Mitchum, R.M., Campion, K.M., and Rahmanian, V.D. (1990): Siliciclastic Sequence Stratigraphy in Well Logs, Cores, and Outcrops: Concepts for High-Resolution Correlation of Time and Facies, Amer. Assoc. Petrol. Geol., Methods in Exploration Series No. 7, 55p.

Wu, P. (1991): Flexure of lithosphere beneath the Alberta Foreland Basin: Evidence of an eastward stiffening continental lithosphere; Geophys. Resear. Lett., v18, p451-454.

Stratigraphic Position of a Late Cretaceous (Cenomanian) Bonebed, East-central Saskatchewan [1]

Stephen L. Cumbaa [2] and Harold N. Bryant [3]

Cumbaa, S.L. and Bryant, H.N. (2001): Stratigraphic position of a Late Cretaceous (Cenomanian) bonebed, east-central Saskatchewan; *in* Summary of Investigations 2001, Volume 1, Saskatchewan Geological Survey, Sask. Energy Mines, Misc. Rep. 2001-4.1.

1. Introduction

Rocks exposed along river banks in the Pasquia Hills of east-central Saskatchewan record a nearly complete sequence of Middle to Late Cretaceous (Albian to Campanian) marine sedimentation (McNeil and Caldwell, 1981). These hills are the northernmost extension of the Manitoba Escarpment, which forms the eastern erosional edge of the Western Interior Basin in mid-continental North America, a relic of the Cretaceous Western Interior Seaway (WIS). The WIS was a rich and productive marine environment (Russell, 1989), and its fossil vertebrate biota has been the subject of a joint Royal Saskatchewan Museum (RSM)–Canadian Museum of Nature (CMN) study since 1991 (Cumbaa and Tokaryk, 1999).

A thin, but very concentrated vertebrate bonebed, in the form of a bioclastic conglomerate of Cenomanian age, was discovered by Mr. Dickson Hardie along the Carrot River near Arborfield, Saskatchewan some years ago, and was the subject of our initial investigations. The age, the unique bird fauna (Tokaryk *et al.*, 1997), and the diversity of this bonebed were the impetus for our team to look farther afield to see whether or not the formation of that bonebed had been more than a local phenomenon.

2. A Problematical Bonebed

a) Discovery and Context

In 1994, Tim Tokaryk (RSM), Richard Day (CMN), and Cumbaa discovered a rich bioclastic conglomerate as "float" in the bed of the Bainbridge River, 100 km northeast of the Carrot River locality, on the northeastern slope of the Pasquia Hills. The individual pieces of "float", some exceeding 100 kg in mass, contained bones and teeth of birds, vertebrae and limb elements of plesiosaurs, fragments of turtle, and hundreds of sharks' teeth, as well as teeth, vertebrae and other elements of bony fishes. These pieces of conglomeratic-looking bonebed were unlike any rock type seen in place within the stratified exposures along the river.

Determining the source and position of the bonebed fragments was important to our biostratigraphic studies. From their distribution along the river bank, a source at or near McNeil and Caldwell's (1981) "Outcrop Section 21", a 5 m outcrop of Ashville Formation, Belle Fourche Member, was indicated, but could not be confirmed.

Subsequent fieldwork in 1995 and 1997 (Cumbaa and Tokaryk, 1999; Schröder-Adams *et al.*, 1999; Collom, 2000) pinpointed the only possible location for the bonebed "float", a 20 to 25 m exposure slightly upstream from Outcrop Section 21. This exposure of the Ashville (Belle Fourche Member) and overlying Favel Formation and Morden Shale is partly slumped, but preserves a Cenomanian to Coniacian record.

The exposure was given our field number BR-3 (RSM locality number 63E09-0003). In measured sections (Schröder-Adams *et al.*, 1999; Collom, 2000), the bonebed was tentatively placed within the Belle Fourche Member of the Ashville Formation, near the base of the exposure on the basis of similarities in the section to the lithology of non-calcareous shales adhering to chunks of recently-detached bonebed "float", and micropaleontological evidence from the adhering shales.

Cumbaa *et al.* (1997) and Cumbaa and Tokaryk (1999) also suggested placement of the bonebed within the Belle Fourche Member. Their rationale was based on faunal content (primarily shark teeth of species known only from Albian and/or Cenomanian contexts), lack of any fragments of the distinctive bonebed above the Ashville-Favel contact, and the lithology of adhering shales as described above. A general description of the stratigraphy of the locality follows.

b) Stratigraphy of the Locality

Below a 2 to 3 m cap of churned and/or recently deposited sediment, the exposure at BR-3 is approximately 23 m thick, the uppermost 5 m (approximate) of which are the slightly to non-calcareous shales of the Morden Shale above the Marco Calcarenite, a regional marker bed (McNeil and Caldwell, 1981) (Figure 1).

[1] Research supported by a Canadian Museum of Nature Research Advisory Committee grant to Cumbaa and by Royal Saskatchewan Museum support to Bryant.
[2] Canadian Museum of Nature, Paleobiology, P.O. Box 3443, Station D, Ottawa, ON K1P 6P4.
[3] Royal Saskatchewan Museum, Earth Sciences, 2340 Albert Street, Regina, SK S4P 3V7.

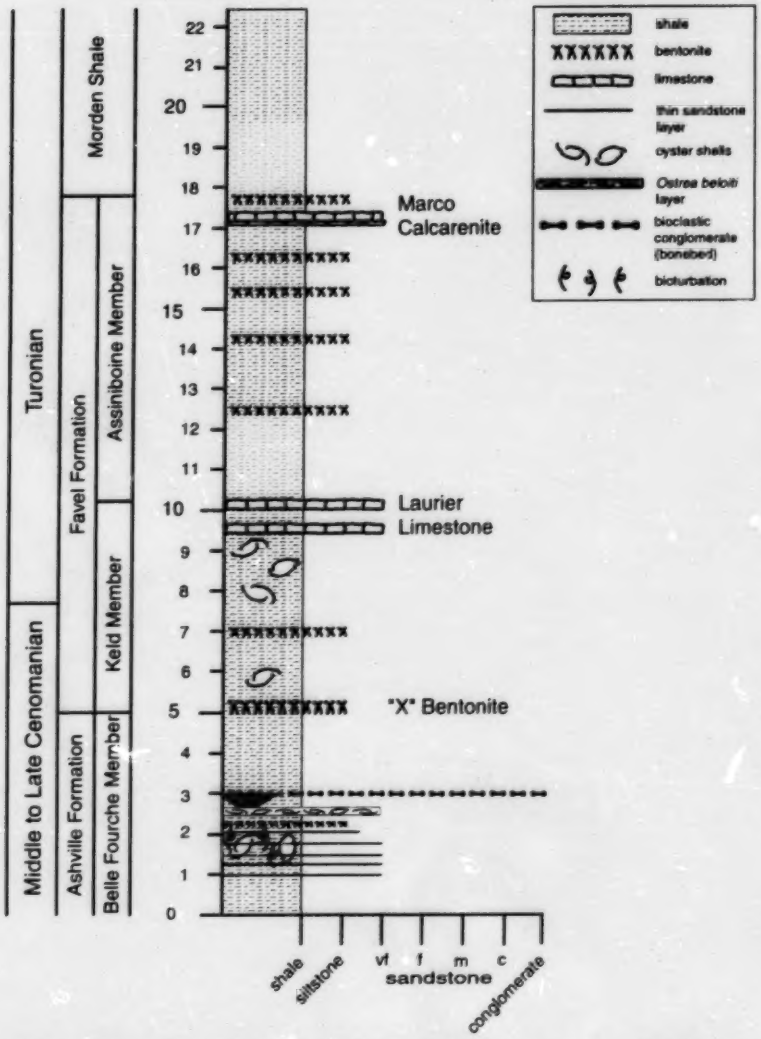

Figure 1 - Simplified stratigraphic diagram of the section at field locality BR-3, Bainbridge River, Pasquia Hills, Saskatchewan. Modified from Schröder-Adams et al. (1999). Collom (2000) notes the position of inoceramid marker species in his Figure 3, which corresponds in general terms to the stratigraphic relationships presented here.

Below the Morden Shale, most of the upper three-quarters of the exposure are relatively resistant, calcareous shales of the Favel Formation, and represent deposition during the peak of the Greenhorn Cyclothem. The Laurier Limestone, another regional marker (McNeil and Caldwell, 1981), separates the two members of the Favel Formation (Figure 1).

A 31 to 33 cm thick bentonite is clearly visible about 5 m above the base of the exposure, and is thought to represent the "X" bentonite which is widespread across the Western Interior Basin. The "X" bentonite has a $^{40}Ar/^{39}Ar$ age of 93.3 Ma (Cadrin, 1992; Obradovich, 1993). The "X" bentonite and the *Ostrea beloiti* bed below it are markers for the upper part of the Belle Fourche Member of the Ashville Formation. Thus, the base of the Favel Formation is placed at the top of the "X" bentonite (McNeil and Caldwell, 1981; Schröder-Adams *et al.*, 1999).

3. 2000 Field Season

In July 2000, Bryant and Cumbaa visited several of the Pasquia Hills localities. The Bainbridge River locality was our principal objective, in hopes that spring flooding had eroded the slumped base of the exposure enough to clear it off and reveal the bonebed layer. Fortunately, that proved to be the case and we were able to locate the bonebed *in situ* and re-measure the lower part of the section (Figure 1).

A puzzling question for the research teams over the years had been the inability to find the bonebed *in situ* on the cliff face, in that the specimens detached as "float" are common, sizeable, and among the hardest rocks in the sequence. This elusiveness, and the shape of some of the "float" pieces eventually convinced us that the "bonebed" had formed as isolated lenses. This appears to have been a reasonable inference, as can be seen in Figure 2. There were two "chunks" of bonebed in place in the lower Ashville; both were thin and lenticular and in the same stratigraphic position, but separated horizontally by several barren metres. The top of the bonebed was 2.02 m below the base of the "X" bentonite, and its base was only 5 cm above the 5 cm thick *Ostrea beloiti* lag deposit. A thin (1 cm) but persistent bentonite is exposed approximately 30 cm below the *Ostrea beloiti* lag.

4. Discussion

a) Deposition of the Bonebed

Similarities between the *Ostrea beloiti* layer and the bonebed strongly suggest their development as lag deposits in shallow water, under tidal influence. Both layers have relatively smooth, flat to undulating upper surfaces, which suggest broad wave or ripple marks. The oysters in the lower layer are closely packed, disarticulated and randomly oriented; the bonebed is more than 60% coprolites, bones, and teeth, all

Figure 2 - Lens of bioclastic conglomerate (bonebed) in situ. Note speckles of bentonite dropped down from eroding "X" bentonite 2 m above top of bonebed. The Ostrea beloiti layer is prominent underneath the bonebed at left center of photograph. Scale for reference is 5 cm. Part of the bonebed lens on the right of the photo has broken off and has been lost to erosion, as has any portion which may have extended out from the face of the exposure. The lens extended an unknown distance back into the exposure; the portion retrieved was approximately 60 cm in length.

disarticulated and randomly oriented. Both indicate tossing, winnowing, and re-mixing under sediment-starved conditions, in the absence of strong currents. Several large pieces of the *Ostrea beloiti* layer exhibit scour-filling on the bottom. Similarly, the *in situ* bonebed lenses (see Figure 2) reveal what appears to be trough filling with vertebrate debris which became the bioclastic conglomerate. Ripple-marked troughs separated by a few metres are suggestive of nearshore shallow coastal areas, which can have two or three lines of sandbars close to shore, with deeper troughs between.

Additional evidence of wave involvement in the formation of the bonebed deposit is the very common occurrence of calcite crystal-lined vugs filled with bentonite. These are interpreted as "rip-up" clasts of bentonite; chunks of compacted and degraded volcanic ash were incorporated in the bioclastic material, apparently before consolidation of the sediment, because the enclosing matrix is frequently deformed around the clast. One large, ovate vug in a piece of bonebed "float" measured approximately 30 cm by 12 cm. The source of the bentonite in these clasts is unknown, as the bonebed horizon is well below the "X" bentonite, and the closest stratigraphically is the 1 cm bentonite 30 cm below the *Ostrea* layer. Collom (2000) discusses possible origins of these bentonites.

No more than 5 cm of soft, black shale separate the *Ostrea* layer and the bonebed, but there is some evidence that deeper water conditions were briefly re-established in the interval between the shallowing cycles. A very thin, but complete inoceramid valve, approximately 15 cm in diameter, was discovered in this shale unit, near the contact with the *Ostrea beloiti* layer. It is in the process of being identified.

b) Vertebrate Fauna and Paleoenvironment

An overview of the faunal assemblage and aspects of the paleoenvironment have been presented in several preliminary papers (Cumbaa *et al.*, 1997; Cumbaa, 1999; and Cumbaa and Tokaryk, 1999).

Vertebrate Update

J.D. Stewart (Natural History Museum, Los Angeles County) and Cumbaa are preparing a paper comparing the fauna of the Bainbridge and Carrot River bonebeds with that of two Graneros Shale localities in Kansas collected by Stewart. These localities are Cenomanian and stratigraphically below the "X" bentonite. The Belle Fourche Member of the Ashville Formation " ...correlates biostratigraphically with the Graneros Shale of the standard section, although the part above the *O. beloiti* beds may equate to the lowest part of the Lincoln Limestone Member of the Greenhorn Formation" (McNeil and Caldwell, 1981, p51).

The Graneros Shale in Kansas also includes bonebeds, in both the middle and at the base of the section (Hattin, 1965). Hattin notes well-preserved ripple marks in the middle part of the formation, and suggests that bonebeds were produced by brief periods of turbulence from storms scouring the sea floor, resulting in concentration into lenses and layers of coarse organic debris that had originally been more widely scattered.

Like the Bainbridge River bonebed, the Kansas examples contain abundant coprolites as well as a rich fauna of hybodont, ptychodont, and other sharks, in addition to several rays. There is a good match between many of the chondrichthyan taxa in the bonebeds from Kansas and Saskatchewan, save for the paucity of rays in the Pasquia Hills bonebeds.

Newly identified material from the Bainbridge River bonebed includes a number of neopterygian fishes, again exhibiting similarities to the Graneros fauna. At least two genera of pycnodonts, shallow water mollusc grazers, occur in the Bainbridge deposits, as well as an amioid, probably a caturid. A new "primitive" teleost, common to both the Graneros and Ashville bonebeds, is a *Belonostomus*-like aspidorhynchid. A full description of these taxa will be presented elsewhere.

Paleoenvironmental Studies

Oxygen isotope analysis on teeth from various WIS localities was used to attempt an indirect measurement of ocean paleotemperatures (Munroe, 2000). The enamel from *Squalicorax* and *Enchodus* teeth, including samples from the Carrot River and Bainbridge River bonebeds, were processed at the Stable Isotope Mass Spectrometry Laboratory at Yale University.

The temperature values from the Pasquia Hills samples, at 31° to 42°C, are higher than would be expected of water temperatures at an approximate

paleolatitude of 45°. Present-day summer surface temperatures range from 37° to 40°C and to more than 30°C in the restricted basins of the Dead Sea and Red Sea, respectively. In the much less restricted basin of the Gulf of Mexico, summer surface temperatures along the coasts approach 32°C. Using the same methodology, samples from the Niobrara Chalk of Kansas produced temperature proxies of about 22°C, which are comparable with previous estimates (McNeil and Caldwell, 1981). However, it is important to note that the Kansas fossils are 10 million years younger than the Saskatchewan samples, and represent an open ocean paleoenvironment.

Munroe (2000) provides an interesting hypothesis for the high Pasquia Hills paleotemperature estimates. She postulates a mechanism involving the gyre concept as elaborated by Kauffman (1977), whereby influx of warm water from the south, acting in concert with a highly stratified water column in the northeastern basin of the WIS (Schröder-Adams *et al.*, in press), kept the water temperature elevated. These conditions were amplified by high salinity, shallow water, relatively low annual rainfall, little fresh water input, and high evapotranspiration rates in an overall warmer climate than the present (Munro, 2000). More isotope work is planned to further investigate these preliminary results.

5. References

Cadrin, A.A.J. (1992): Geochemistry and paleoenvironmental reconstruction of the Cretaceous Greenhorn marine cyclothem in the Western Interior Basin of Canada; unpubl. Ph.D. thesis, Univ. Saskatchewan, 191p.

Collom, C.J. (2000): High-resolution stratigraphy, regional correlation, and report of molluscan faunas: Colorado Group (Cenomanian-Coniacian interval, Late Cretaceous), east-central Saskatchewan; *in* Summary of Investigations 2000, Volume 1, Saskatchewan Geological Survey, Sask. Energy Mines, Misc. Rep. 2000-4.1, p82-97.

Cumbaa, S.L. (1999): Paleoecological implications of a marine bonebed fauna from the Late Cretaceous (Cenomanian) of Saskatchewan, Canada; J. Vert. Paleo., v19 (supp. to No. 3), p40A.

Cumbaa, S.L. and Tokaryk, T.T. (1999): Recent discoveries of Cretaceous marine vertebrates on the eastern margins of the Western Interior Seaway; *in* Summary of Investigations 1999, Volume 1, Saskatchewan Geological Survey, Sask. Energy Mines, Misc. Rep. 99-4.1, p57-63.

Cumbaa, S.L., Tokaryk, T.T., Collom, C., Stewart, J.D., Ercit, T.S., and Day, R.G. (1997): A Cenomanian bone bed of marine origin, Saskatchewan, Canada; J. Vert. Paleo., v17 (supp. to No. 3), p40A.

Hattin, D.E. (1965): Stratigraphy of the Graneros Shale (Upper Cretaceous) in central Kansas; State Geol. Surv. Kansas, Bull. 178, 83p plus accomp. map.

Kauffman, E.G. (1977): Geological and biological overview: Western Interior Cretaceous Basin; Mtn. Geol., v14, no3-4, p75-99.

McNeil, D.H. and Caldwell, W.G.E. (1981): Cretaceous rocks and their Foraminifera in the Manitoba Escarpment; Geol. Assoc. Can., Spec. Pap. 21, 439p.

Munro, L.E. (2000): $^{18}O/^{16}O$ isotopes as temperature indicators in Late Cretaceous fossil shark and bony fish teeth; unpubl. B.Sc. thesis, Carleton Univ., 38p.

Obradovich, J.D. (1993): A Cretaceous time scale; *in* Caldwell, W.G.E. and Kauffman, E.G. (eds.), Evolution of the Western Interior Basin; Geol. Assoc. Can., Spec. Pap. 39, p379-396.

Russell, D.A. (1989): An Odyssey in Time: The Dinosaurs of North America; Univ. Toronto Press (in assoc. with Nat. Mus. Natur. Sci.), 239p.

Schröder-Adams, C.J., Leckie, D.A., Craig, J., and Bloch, J. (1999): Upper Cretaceous Colorado Group in the Pasquia Hills, northeastern Saskatchewan: A multidisciplinary study in progress; *in* Summary of Investigations 1999, Volume 1, Saskatchewan Geological Survey, Sask. Energy Mines, Misc. Rep. 99-4.1, p52-56.

Schröder-Adams, C.J., Cumbaa, S.L., Bloch, J., Leckie, D.A., Craig, J., Seif El-Dein, S.A., Simons, D-J.H.A.E., and Kenig, F. (in press): Late Cretaceous (Cenomanian to Campanian) paleoenvironmental history of the eastern Canadian margin of the Western Interior Seaway: Bonebeds and anoxic events; Palaeogeog., Palaeoclim., Palaeoecol.

Tokaryk, T.T., Cumbaa, S.L., and Storer, J.E. (1997): Early Late Cretaceous birds from Saskatchewan, Canada: The oldest diverse avifauna known from North America. J. Vert. Paleo., v17, p172-176.

Timing of Gas Generation in the Cretaceous Milk River Formation, Southeastern Alberta and Southwestern Saskatchewan – Evidence from Authigenic Carbonates

Neil S. Fishman [1], Jennie L. Ridgley [1], and Donald L. Hall [2]

Fishman, N.S., Ridgley, J.L., Hall, D.L. (2001): Timing of gas generation in the Cretaceous Milk River Formation, southeastern Alberta and southwestern Saskatchewan – evidence from authigenic carbonates; *in* Summary of Investigations 2001, Volume 1, Saskatchewan Geological Survey, Sask. Energy Mines, Misc. Rep. 2001-4.1.

1. Introduction

The marine Cretaceous Milk River Formation in southeastern Alberta and southwestern Saskatchewan (Figure 1) contains abundant natural gas and contributes significantly to the >4.2 x 10^{11} m^3 (>15 trillion cubic feet) of estimated shallow gas resources in the region (Energy Resources Conservation Board, 1977). The formation is both source and reservoir rock (Ridgley *et al.*, 1999), and the contained gas is defined as a continuous-type accumulation for the purposes of exploration and resource assessments (Attanazi and Schmoker, 1997; Ridgley *et al.*, 1999). Although the unit has been previously studied, uncertainties remain concerning the timing of gas generation. During the present study, we found that the key to understanding when gas generation occurred is the recognition that the gas is biogenic. Carbon isotopic values (Figure 2) for methane in Milk River Formation-produced gas range from -66 to -75 ‰ (Fuex, 1977; Rice and Claypool, 1981; Hankel *et al.*, 1989; P. Lillis, U.S. Geological Survey, pers. comm., 2000), which is typical for primary biogenic gas generated early in the post-depositional history of marine sediments (Rice and Claypool, 1981; Whiticar *et al.*, 1986). Compositionally, the gas is dry, containing >99.45% methane (Fuex, 1977; Rice and Claypool, 1981; P. Lillis, U.S. Geological Survey, pers. comm., 2000), which is also typical of biogenic gas (Bernard *et al.*, 1976; Weber and Maximov, 1976; Rice and Claypool, 1981; Gautier, 1985).

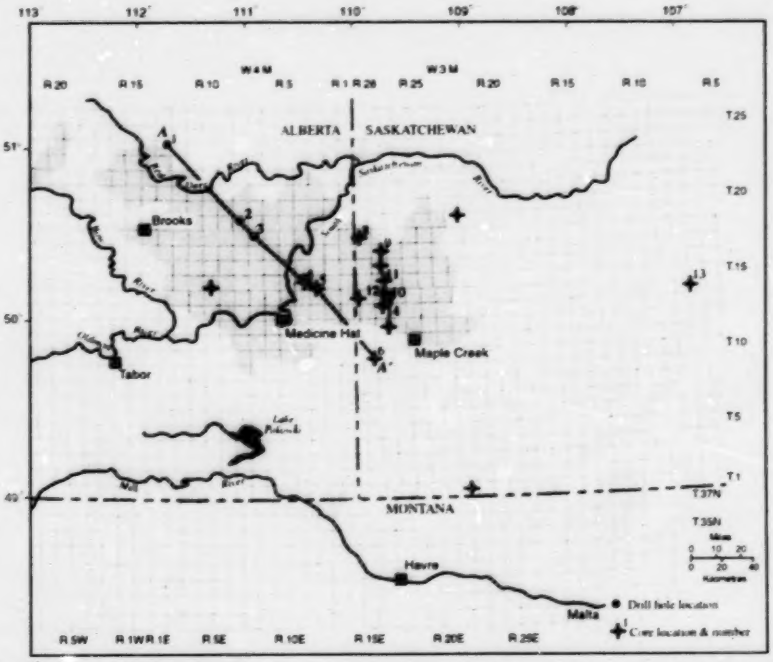

Figure 1 - Map showing locations of the study area and sampled cores. A-A' is the line of cross section in Figure 5. Grey areas indicate southeast Alberta gas fields.

The timing of gas generation in the Milk River Formation is uncertain in part because methanogenesis can occur whenever conditions in the rocks permit anaerobic bacteria, which are responsible for gas generation, to thrive (Rice and Claypool, 1981). Conditions favourable for bacterial methanogenesis include: (1) an anoxic environment; (2) appropriate temperatures (optimally 40° to 60°C, but any temperatures from 0° to 75°C are tolerable); (3) presence of organic matter; (4) low sulphate content of pore waters; and (5) sufficient permeability to allow for continuous water flow and adequate pore space for the bacteria to exist. That methanogenesis could have occurred at various times in the post-depositional history of the Milk River Formation is plausible insofar as the unit has not experienced burial

[1] U.S. Geological Survey, Central Region, Energy Resources Team, MS939, P.O. Box 25046, DFC, Denver, CO 80225-0046
[2] Fluid Inclusion Technologies, Inc., 2217 North Yellowood Avenue, Broken Arrow, OK 74012-9106

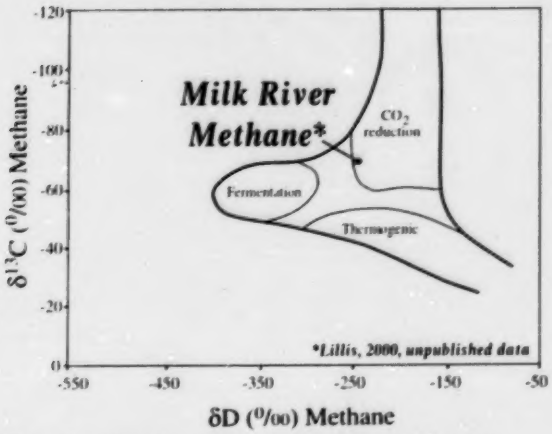

Figure 2 - Diagram on which is plotted the carbon and deuterium isotopes of natural gas, generated by different processes (modified from Whiticar et al., 1986). Analyzed samples from the Milk River Formation plot in the area of CO_2 reduction, typical of gas generated in biogenic systems.

temperatures exceeding that lethal to methanogenic bacteria. Burial reconstruction studies (Corbet and Bethke, 1992) indicate that temperatures in the unit never exceeded about 45°C (Figure 3). The shallow burial history of the Milk River Formation is consistent with the fact that Cretaceous units stratigraphically below it are thermally immature (Creaney *et al.*, 1994). Formation temperatures throughout the burial history of the Milk River Formation do not, therefore, preclude the possibility of methanogenesis having occurred at various times. However, at about 65 Ma, the Milk River Formation was buried to a maximum depth of about 1.3 km (Corbet and Bethke, 1992), slightly greater than the one kilometre depth below which primary microbial methanogenesis is generally observed to have ceased (Rice and Claypool, 1981).

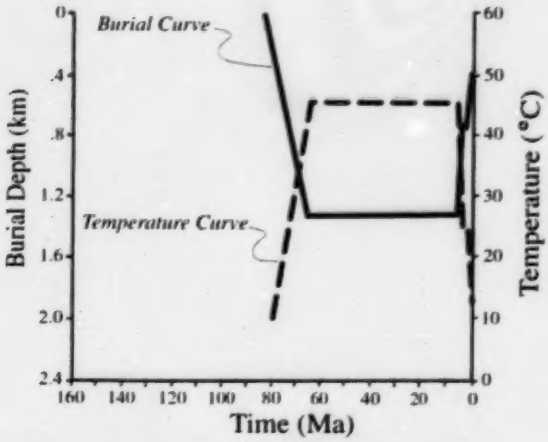

Figure 3 - Burial curve for the Milk River Formation (approximately along Township 1 in southern Alberta, after Corbet and Bethke, 1992). The Milk River Formation was buried no deeper than about 1.3 km, so maximum formation temperature was about 45°C.

Consequently, whether significant methane generation occurred when the formation was buried to depths greater than one kilometre is uncertain. As the unit was at depths of less than one kilometre for more than 15 m.y. prior to maximum burial, as well as during approximately the last seven m.y. when tectonic uplift affected the region (Figure 3), time was plentiful during which ideal microbial methanogenic conditions may have prevailed.

To address the question of timing of methane generation in the Milk River Formation, we conducted a petrologic study to determine the post-depositional alteration history of the unit, and constructed a temporal framework in which gas generation may be placed. In this paper, we present the results of petrographic, isotopic, and fluid inclusion analyses and draw preliminary conclusions.

2. Depositional History of the Milk River Formation

Although formally referenced as the Alderson Member of the Lea Park Formation (Figure 4), this stratigraphic unit is typically named the Milk River Formation by gas producers in the region, and we have chosen to use this in our study. The Milk River Formation is one of several siliciclastic units that were deposited during Late Cretaceous time in the Western Interior Seaway. Detailed examination of cores and wireline logs reveals seven distinct marine lithofacies in the formation (Ridgley, 2000) that correspond to different depositional environments (Figure 5). Interpretations of lithofacies indicate that they were deposited in delta front, coastal, shoreface, inner shelf, and outer shelf environments (Ridgley, 2000). Recently documented major erosional surfaces within the formation point to two previously unrecognized sea-level falls followed by marine transgressions (O'Connell *et al.*, 1999;

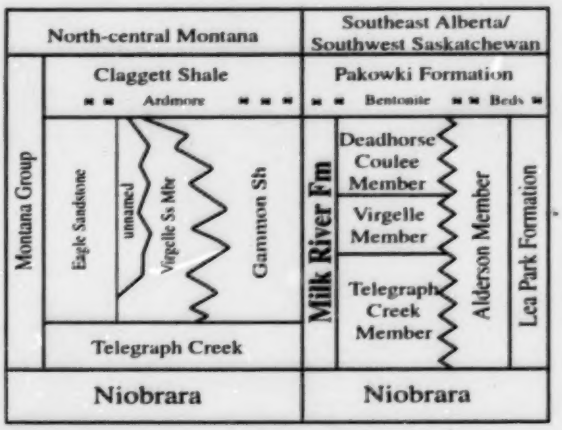

Figure 4 - Stratigraphic chart showing members of the Upper Cretaceous Milk River Formation (also referred to as the Alderson Member of the Lea Park Formation), in southern Alberta and Saskatchewan, and correlative stratigraphic units in Montana.

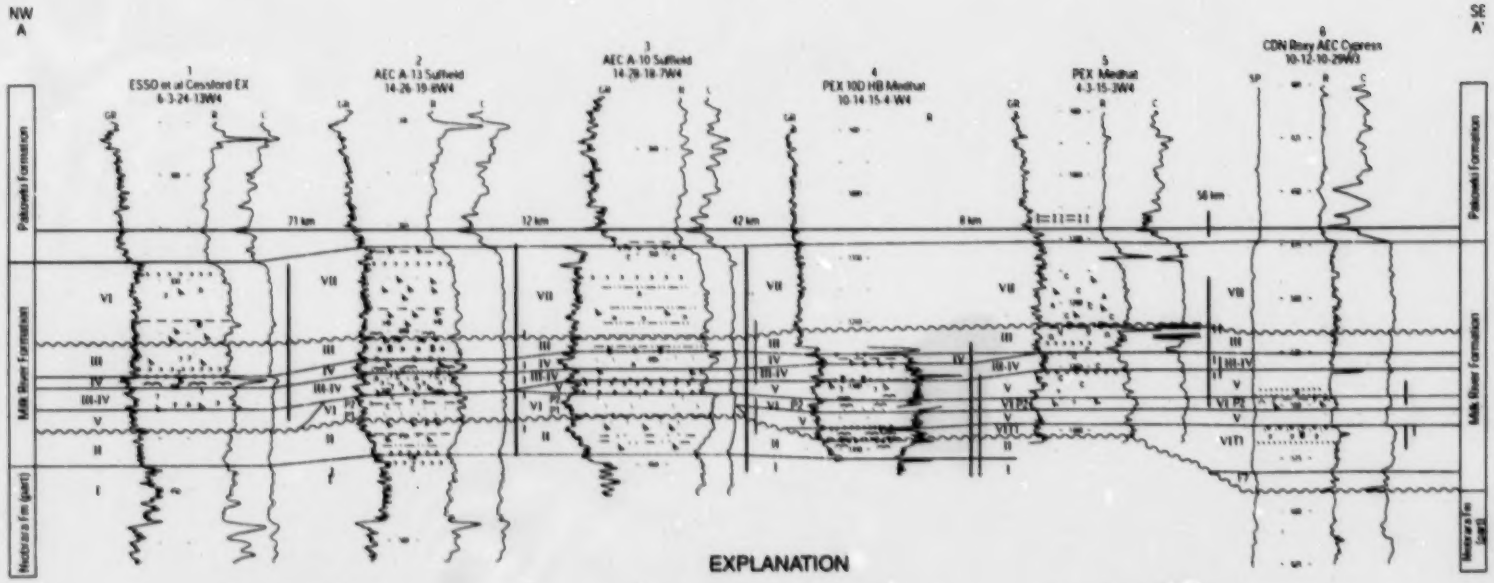

EXPLANATION

- Hummocky cross stratification
- Swaley cross stratification
- Indeterminate low angle cross stratification
- Current ripples
- Flaser bedding
- Coarse sandstone layers
- Mudstone
- Siltstone
- Coccolithic shale
- Vuggy
- Bentonite
- Siderite
- Siderite clasts or conglomerate clasts
- Intraformational siderite clasts
- Fractures
- Coiled ammonite fragments
- *Arenicolites* burrows
- *Terebellina* sp burrows
- Fish fragments
- Chert grains or coarse grit
- Biotite-rich rocks
- Carbonaceous
- Glauconite
- Cored interval
- I Offshore facies
- II Offshore-transition facies
- III Inner to outer shelf facies
- IV Shelf sandstone facies
- V Inner shelf to outer estuarine facies
- VI Coastal sandstone facies
- VII Amalgamated shoreline sandstone and mudstone facies
- Fluvial facies
- Tested interval
- P 1 Regressive shoreface sand
- T 1 Transgressive shoreface sand
- Unconformity

Figure 5 - Cross section A-A' (see Figure 1 for location), showing various lithofacies that occur in the Milk River Formation, as well as simplified sedimentary structures (modified from Ridgley, 2000). Depths for wells 1 to 3 and 6 are in metres, whereas depths for wells 4 and 5 are in feet. (Gr, gamma ray; R, resistivity; C, conductivity; and SP, spontaneous potential).

Ridgley, 2000). Although attempts have been made to determine the influence of depositional facies and unconformities on gas production, the possible control these features had on gas generation and trapping is unclear.

Lithologies of the Milk River Formation include sandstone, siltstone, mudstone, and shale. Although the different lithofacies suggest variations in wave energy in the different depositional environments, the maximum grain size in all lithologies is fine sand. Grain sizes in sandstones range from fine to very fine, and sorting from moderate to poor. Modal analyses indicate that the sandstones are lithic-rich (see Table 1). Grains typically comprise, in decreasing abundance, quartz, rock fragments, dolomite, glauconitic grains, and feldspar (Table 1). Varying amounts of organic detritus are also present (Table 1). Of the detrital constituents, only some plagioclase and chert have been partially dissolved, probably mostly in early phases of the alteration history of the formation as these dissolved areas have themselves been filled with early authigenic cement.

3. Methods

Petrographic analyses of 81 thin sections from 16 different cores were used to establish paragenetic relations of authigenic phases and other textural features that bear on the alteration history of the formation. Thin sections were made after impregnation of the rock chip with blue epoxy, then were stained with sodium cobaltinitrite to assist in identifying potassium feldspar. The thin sections were also stained with a mixture of alizarin red-S and potassium ferricyanide to determine the composition of carbonate minerals (Dickson, 1966). Point counts (typically 400 points per thin section) were conducted on selected samples for modal analysis and to determine the nature and volume of rock constituents.

Scanning electron microscopy (SEM), carbon and oxygen isotopic analyses, and fluid inclusion analyses were performed on selected samples. The SEM, equipped with an energy dispersive analyzer of X-rays (EDAX), was used to refine details of paragenetic relations and mineral composition in gold-coated samples. Polished thin sections were also coated with gold and used in the SEM to determine the composition and distribution of elements of some authigenic phases. Semi-quantitative analyses were performed using the combined SEM-EDAX system to obtain approximate elemental composition of authigenic carbonates.

Carbon and oxygen isotope compositions were determined on 18 samples containing authigenic carbonates. The samples selected contained a single or dominant authigenic carbonate species, identified through careful petrographic and X-ray diffraction analyses. Isotopic measurements were made on CO_2 that was produced by reaction of phosphoric acid on calcite-bearing samples for six hours at 25°C. Samples containing siderite were heated to 150°C to obtain CO_2 for isotopic analysis. The oxygen isotope fractionation factor between the acid-extracted CO_2 and siderite at 150°C is 1.00771 (Rosenbaum and Sheppard, 1986). In this paper, we report isotopic data as $\delta^{13}C$ and $\delta^{18}O$, which represent the permil difference in the ratio of $^{13}C/^{12}C$ or $^{18}O/^{16}O$ in the sample to that of the PDB standard (*Belemnitella americana* from the Cretaceous Peedee Formation in South Carolina). The reported oxygen isotope values can be converted to values relative to standard mean ocean water (SMOW) using the relationship $\delta_{SMOW} = (\delta_{PDB} + 29.94)/0.97006$.

The nature of the gases (organic and inorganic) contained in fluid inclusions was assessed by the new technique of fluid inclusion stratigraphy (FIS). This technique was used because most of the samples contain authigenic carbonate phases that were either too small (<10 μm) or the inclusions were too small to

Table 1 - Modal analyses (in percent) for selected sandstone samples, Milk River Formation. Qtz, quartz; Dol; dolomite; Feld, feldspar, dominantly potassium feldspar; RF, rock fragments, dominantly sedimentary including chert, shale, and mudstone; Glauc, glauconitic grains; Corg, organic detritus; IGV, intergranular volume (sum of all cements and primary porosity). Clay percentages include both smectite and kaolinite. Core #, see Figure 1 for core location. Sample number includes well identification/location followed by sample depth (*, depth in metres; **, depth in feet).

		Percent Detrital Grains						Percent Cements and Porosity						
Sample Number	Core #	Qtz	Dol	Feld	RF	Glauc	Corg	Siderite	Calcite	Clay	Pyrite	Primary Porosity	Secondary Porosity	Percent IGV
4-25-14-28W3 423*	10	52.5	4.3	0	14.0	2.5	1.0	6.5	13.8	1.8	2.0	0	1.8	24.1
4-25-14-28W3 425.4*	10	54.8	5.5	0.3	11.8	1.8	1.0	2.8	15.5	3.3	3.5	0	0	25.1
6-22-17-28W3 457.7*	9	39.8	14.0	0.5	13.5	0.5	0.5	1.5	27.5	1.3	0.8	0.3	0	31.4
6-22-17-28W3 444.13*	9	43.3	2.8	0.8	23.8	1.0	4.3	0	0.3	2.8	3.0	18.0	0.3	24.1
6-22-17-28W3 460.25*	9	56.0	7.8	0	12.8	0.8	2.0	1.3	15.5	2.3	1.3	0	0.5	10.4
4-1-15-3W4 1288**	5	42.0	4.3	2.3	25.3	0.8	5.8	0.8	0	2.5	1.0	14.0	1.5	18.3
4-25-14-28W3 1403**	10	42.0	2.8	2.0	28.0	0.3	3.3	0	0	2.8	2.3	15.3	1.5	20.4
3-24-15-28W3 442*	11	37.3	4.7	2.3	26.0	1.0	4.3	0.7	2.7	3.0	0	16.0	2.0	22.4
10-12-10-29W3 562.3*	6	40.3	6.7	2.3	32.0	1.3	4.7	0	0	2.0	2.0	7.3	1.3	11.3
10-12-10-29W3 566.2*	6	45.5	6.3	0.8	26.0	1.5	2.8	0.8	1.3	1.5	1.8	11.0	1.0	16.4
10-23-14-30W3 1567.5**	12	35.7	5.2	1.7	21.7	0	1.7	0	28.7	0.9	1.7	0.9	1.7	32.2

successfully obtain analyses by a more conventional optical-based system using polished thin sections. Also, FIS analysis allows detection of species, both organic and inorganic, that cannot be evaluated with optical-based methods. Nine samples were carefully selected for fluid inclusion studies, based on detailed petrography, isotopic analyses, and X-ray diffraction analyses. In seven samples, siderite was the only or dominant carbonate phase present whereas the other two contained abundant calcite with little or no siderite. The selected samples were first washed to ensure that surfaces were free of volatile contaminants, then placed along with standards, in a vacuum chamber that was pumped (10^{-5} bars) to reduce water and hydrocarbon contents to acceptable levels. Bulk fluid-inclusion volatiles were liberated by mechanical crushing of the samples, and were pumped through four quadrupole mass spectrometers for ionization and separation according to their mass-to-charge ratio. Petroleum species with as many as 13 carbon atoms, as well as inorganic gases, were measured, and compounds with an abundance range of six orders of magnitude were detected and processed.

The volatiles analyzed by the FIS technique represent a composite of all inclusions in the sample and are not from individual inclusions as would be the case using an optical-based system. This technique provides important information because the samples were carefully selected to ensure that they were dominated by the authigenic phase of interest. Hence, indications of hydrocarbons and/or bacterially derived volatile compounds suggest that the processes that formed them occurred during or after precipitation of the host mineral phase. At least three replicates of each sample were run for quality control and to determine the variability of the volatile content of fluid inclusions.

4. Post-depositional Alteration History

Post-depositional alterations in the Milk River Formation include dissolution of detrital constituents, precipitation of authigenic minerals, and compaction. The nature and relative timing of these events are summarized in Figure 6, which is a compilation of data from core, including sandstone, siltstone, and mudstone, from across the study area. Although all the events shown were not generally found in any individual sample, several were consistently present in many samples and were used to establish an overall paragenetic sequence of alterations for the formation.

a) Authigenic Minerals

Milk River authigenic cements include silicates, sulphides, and carbonates (Figure 6). Most cement types that formed throughout the alteration history of the unit occur in relatively minor amounts and do not appear to have any relation to methanogenesis. Thus, these cements, principally the silicates and sulphides, will be only briefly discussed. Emphasis has instead been placed on authigenic carbonate minerals because

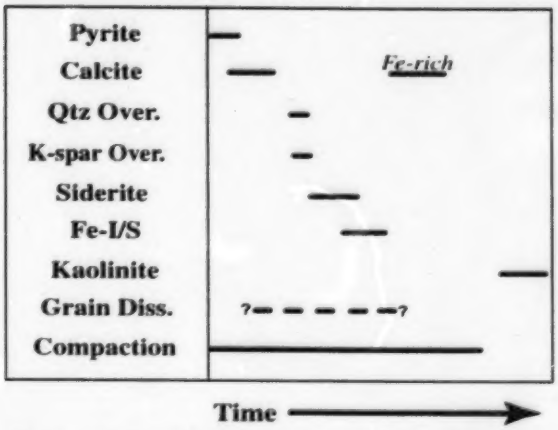

Figure 6 - Diagram showing nature and relative timing of alterations in the Milk River Formation. Diagenetic events represent precipitation of minerals unless otherwise noted. (Qtz, quartz; Over., overgrowth; K-spar, potassium feldspar; Fe-I/S, iron-rich smectite; Fe, iron; and Diss., dissolution).

they are either volumetrically significant or can be linked to methanogenesis.

Silicates

Authigenic silicate cements in sandstones and siltstones include small quartz and potassium feldspar overgrowths, iron-rich smectite, and kaolinite. SEM observations reveal that the overgrowths are typically <10 μm across, and modal analyses indicate that they comprise less than 1% of the rock volume. Iron-rich smectite appears to have developed relatively early (Figure 6), whereas kaolinite was the last to form. Smectite coats detrital grain surfaces or previously formed authigenic minerals. This relationship helps to establish the position of smectite in the paragenetic sequence (Figure 6). Kaolinite is present as relatively large (>20 μm in length) worm-like masses and occurs on all earlier authigenic minerals. Both clay types are best developed in sandstone, although they are also present in other lithologies.

Pyrite

Pyrite occurs as framboids ≤20 μm across and as masses (>50 μm across) of pyrite crystallites (each crystallite ≤2 μm across). Pyrite is ubiquitous but volumetrically most significant in mudstone and siltstone. In sandstones, pyrite typically comprises <4% of the rock volume (Table 1), although locally as much as 11%. Pyrite was observed to be cemented by later siderite and calcite (Figure 6), which is the same sequence of authigenesis observed in rocks of similar age and depositional setting in the Western Interior of the United States (Gautier, 1982) and in marine sediments in general (Nissenbaum *et al.*, 1972; Claypool *et al.*, 1973; Claypool and Kaplan, 1974; Irwin *et al.*, 1977).

Siderite

Authigenic siderite was observed in all lithologies in the Milk River Formation and formed relatively early (Figure 6). It is present in interstices in sandstone and siltstone as rhombic crystals <10 µm across (Figure 7A) and as overgrowths (up to 50 µm) on detrital dolomite grains (Figure 7B). Both forms of siderite typically occupy only 7% or less of the rock volume (Table 1). The siderite in these clastic rocks contains (by weight) as much as 16% MgO and/or as much as 16% CaO with the remainder being FeO. This amount of impurity is diagnostic of authigenic siderite that forms from marine waters in which Mg^{2+} and Ca^{2+} are abundant. In contrast, siderite that forms from meteoric water in continental environments is typically pure $FeCO_3$ (Mozley, 1989; Mozley and Carothers, 1992).

Siderite also occurs in large (maximum height about 15 cm, with horizontal dimensions limited by the diameter of core) concretionary masses that typically formed at lithofacies boundaries (Figure 5). In addition to the mosaic of interlocking 5 to 7 µm-diameter rhombic siderite microcrystals (Figure 7C), the concretions contain clay and minor amounts of authigenic pyrite and quartz or detritus of quartz, pelloids, glauconitic grains, organic material, and fossil fragments. Concretionary siderite is compositionally similar to siderite cement and overgrowths, indicating that all authigenic siderite studied in the Milk River Formation formed contemporaneously and from waters of similar chemical composition. That the siderite formed early in the post-depositional history of the formation is also indicated by the condition of ductile grains in concretions; little or no deformation was observed for grains such as glauconite, delicate pelloids, organic detritus, or rare fossil fragments. Deformation of these delicate grains would likely have begun during shallow burial if little or no siderite had formed early to create a competent preservative framework.

Carbon isotopic values ($\delta^{13}C$) for authigenic siderite in concretions range from -1.99 to -14.23 ‰ and oxygen ($\delta^{18}O$) from -10.87 to -19.41 ‰ (Figure 8). These ranges are consistent with an origin from marine waters (Mozley and Wersin, 1992). The $\delta^{13}C$ values also fall in the range with those of siderite formed during methanogenesis (Claypool and Kaplan, 1974; Gautier,

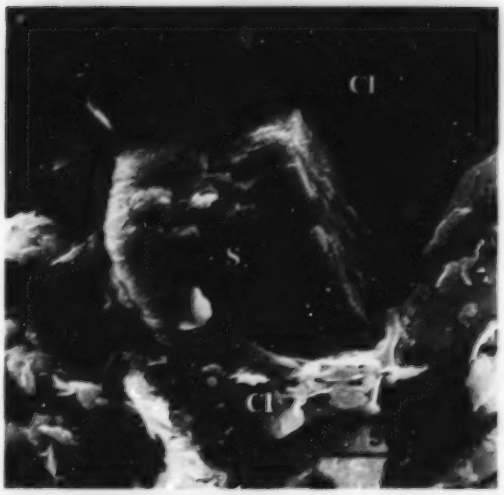

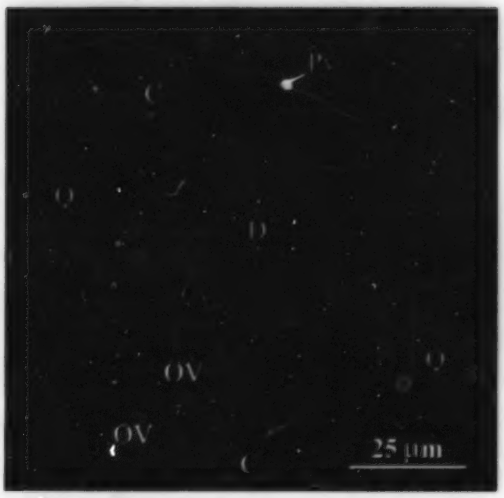

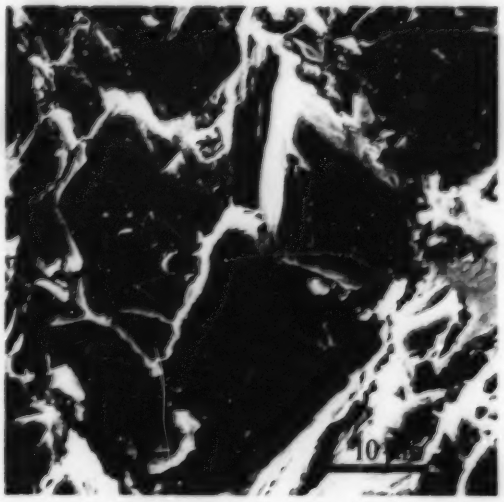

Figure 7 - Scanning electron photographs of siderite in the Milk River Formation. See Figure 1 for all sample locations.
A) Early siderite (S) overlain by or possibly intergrown with iron-rich smectite clay (Cl). Sample (number 6-22-17-28W3, 455.4 m) is from core 9.
B) Back-scattered electron image of siderite overgrowth (OV) on detrital dolomite (D). Euhedral shape of detrital quartz (Q) results from the presence of small quartz overgrowths. Later calcite (C) cements both siderite and quartz overgrowths. Pyrite (Py) is enclosed by siderite overgrowth at top of photograph. Sample (number 6-22-17-28W3, 457.7 m) is from core 9.
C) Mosaic of siderite crystallites in a concretionary mass. Sample (number 11-8T-18-29W3, 1541 ft) is from core 8.

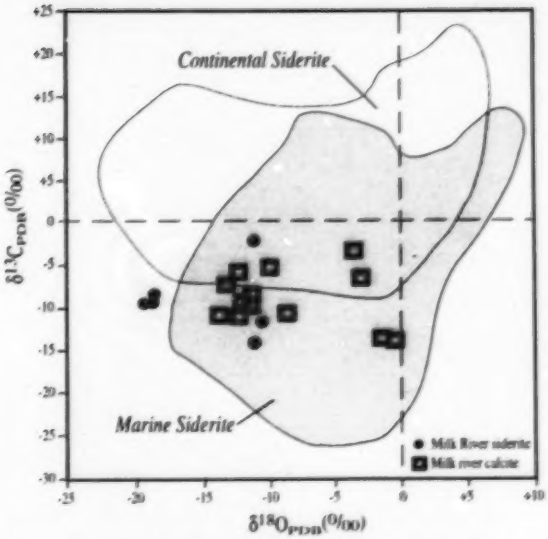

Figure 8 - Plot of $\delta^{13}C$ and $\delta^{18}O$ values for siderite and calcite in the Milk River Formation. Fields for marine and continental siderites taken from Mozley and Wersin (1992). Note that many Milk River Formation samples fall within the field for marine siderite. (Siderite samples are largely from concretions or concretionary masses in mudstone, whereas calcite samples are from sandstone).

1981, 1985). The variable oxygen isotopic values (Figure 8) may be the result of precipitation from waters that were compositionally modified by ongoing water/rock interactions as has been suggested for similar findings elsewhere (Mozley and Wersin, 1992). The fact that several alteration events preceded siderite formation (Figure 6) indicates the occurrence of earlier water/rock interactions which possibly served to shift the oxygen isotopic value of the pore fluids in the Milk River Formation from which the siderite was precipitated. Alternatively, ^{18}O-enriched seawaters may have resided, at least periodically, in the Western Interior Seaway as a result of higher than normal input of freshwater into the Cretaceous sea (Tourtelot and Rye, 1969; Kaufmann and Scholle, 1977; Pratt, 1985; Arthur *et al.*, 1985; Pratt *et al.*, 1993; Pagani and Arthur, 1998). If so, pore waters in the Upper Cretaceous marine sediments may also have been enriched in ^{18}O. The possibility that an almost 9 ‰ variability in $\delta^{18}O$ values was caused by the effects of temperature is unlikely because the Milk River Formation was not buried deeply enough. Moreover, all the siderite in the Milk River Formation occurs in the same paragenetic position, which indicates that all formed at approximately the same time and thus probably under similar temperature conditions.

Fluid inclusion studies indicate that siderite formed during methanogenesis. All seven sideritic concretionary samples analyzed for fluid inclusions contained methane (Figure 9) as well as other volatile compounds usually associated with bacterial processes (for example, acetic acid ±COS, CS_2, and H_2S). Given that the samples were evacuated prior to analysis to remove any possible traces of hydrocarbons that might have been in the pores, the analyses point to inclusions in the siderite as the source of methane and other bacterially mediated compounds. We believe that the fluid inclusions in the siderite are primary for the following two reasons: (1) siderite is stable and does not typically recrystallize during diagenesis (Curtis *et al.*, 1975; Gould and Smith, 1979; Matsumoto and

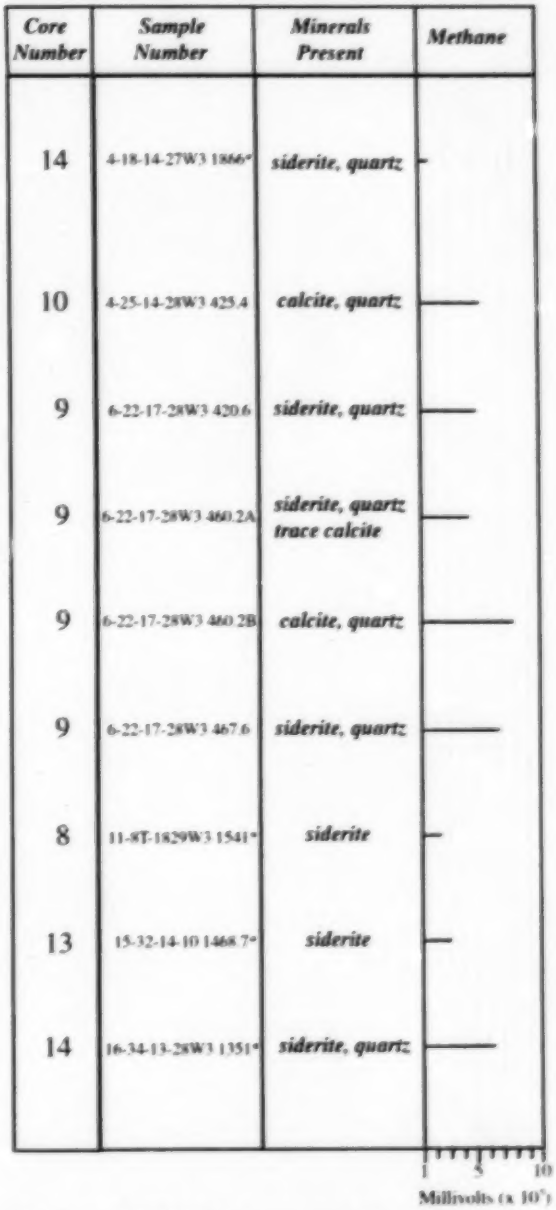

Figure 9 - Fluid inclusion–mass spectrometric analyses for methane in samples from the Milk River Formation. Also shown are the core and sample numbers (*, depth in feet; other depths are in metres), and the minerals present as indicated by X-ray diffraction analysis.

Iijima, 1981; Gautier, 1982; Curtis and Coleman, 1986); and (2) analytical or other evidence of post-siderite alteration such as compositional variations or fractures are lacking within the samples studied. Although trace amounts of higher hydrocarbons (>C_1) were also detected from the fluid-inclusion analyses, their presence is not surprising because they are known to occur even in biogenic gas systems in recent sediments (Weber and Maximov, 1976; Claypool and Kvenvolden, 1983).

Calcite

Authigenic calcite formed both before and after precipitation of siderite (Figure 6); however, the composition of these two generations of calcite differs.

Early-formed calcite is highly calcic, as indicated from the staining of thin sections. This calcite occurs as an interstitial cement in sand-filled burrows, but such occurrences are areally and volumetrically insignificant compared to the amount of calcite precipitated after siderite in the Milk River Formation (see Figure 7B).

The later generation of calcite is a poikilotopic cement in sandstone and siltstone in volumes ranging from <1% to as much as 28.7% (Table 1). It is variable in composition, as determined from stained thin sections. Overall, the iron content decreases toward the centre of interstitial pores indicating that pore waters responsible for calcite formation evolved from a more iron-rich to iron-depleted state. The $\delta^{13}C$ composition of the calcite ranges from -3.68 to -14.02 ‰ and the $\delta^{18}O$ composition from -0.63 to -13.16 ‰ (Figure 8). Because these isotopic values represent bulk sample analysis, it is unclear whether the variability in $\delta^{13}C$ and $\delta^{18}O$ corresponds to changes in the iron content of the calcite. Nevertheless, significant overlap of calcite and siderite isotopic values is evident (Figure 8). As such, the isotopic signature of the calcite is consistent with its formation from marine waters. In addition, the $\delta^{13}C$ values also fall within the range of values expected for minerals that formed during methanogenesis (Claypool and Kaplan, 1974; Gautier, 1981; Claypool and Kvenvolden, 1983; Gautier, 1985). As with siderite, the variability of $\delta^{18}O$ values for the calcite indicates that it may have formed from marine waters that had evolved isotopically due to water/rock interactions or from ^{18}O-enriched marine waters, or from a combination of both.

Fluid inclusion studies also suggest that the calcite formed during methanogenesis. Although only two samples containing abundant calcite cement were analyzed, both contained methane in submicroscopic fluid inclusions (Figure 9) as well as other volatile compounds usually associated with bacterial processes (for example acetic acid ± COS, CS_2, and H_2S). The interpretation that methane and other bacterially generated compounds liberated during fluid inclusion analysis is in the authigenic calcite and not the detrital quartz is supported by petrographic observations, which indicate that the quartz grains were derived largely from igneous and metamorphic source rocks. Although methane can occur in fluid inclusions in quartz from metamorphic or igneous rocks, the presence of bacterially mediated compounds cannot. As with siderite, trace amounts of other hydrocarbons were also detected during fluid inclusion analyses of the calcite; this can be expected for carbonates that form in biogenic gas systems (Weber and Maximov, 1976).

b) Compaction

Sandstone beds in the Milk River Formation display textural features that indicate they have undergone varying degrees of compaction. Intergranular volumes (IGV; volume of the rock that is primary pore space plus authigenic cement; see Houseknecht, 1987) in sandstone beds range from 11.3 to 32.2% (Table 1), whereas the original porosity of these sandstone beds is postulated to have been about 35% (original porosity estimated from information in Beard and Weyl (1973) and Carozzi, (1993)). Based on the relation between the observed IGV and the estimated original porosity, a sandstone bed with an IGV of 32% has experienced about a 9% reduction in porosity ((35% to 32%)/35% = 9%), whereas an IGV of 11.3% indicates a 65% reduction in porosity. The IGV of sandstone beds completely cemented with calcite ranges from about 20 to 32% (Table 1). This range suggests that calcite cementation began when the IGV of sandstone beds was about 32% and continued until the IGV had dropped to about 20% (a 43% reduction in porosity) due to burial compaction. Sandstone beds lacking calcite cement have IGV values ranging from about 11 to 24% (Table 1). These generally lower values imply that compaction was greater in these beds than in calcite-cemented beds, which in turn suggests that calcite cementation ended before burial compaction had concluded in the Milk River Formation. Compaction was most significant in beds containing little or no calcite.

Textural features corroborate the timing of calcite cementation relative to maximum burial. Petrographic observations show that sandstone beds lacking calcite cement display more ductile grain (sedimentary rock fragments and glauconitic grains) deformation than sandstone beds with abundant calcite. Moreover, sandstone beds with little or no calcite cement and abundant ductile grains have experienced the greatest volume of porosity loss due to compaction (up to 65%). Thus calcite cementation must have ended prior to maximum burial of the Milk River Formation.

5. Timing of Gas Generation

The detailed petrologic studies of the Milk River Formation have been useful in establishing the nature and timing of authigenic siderite and calcite formation and in linking the timing of methane generation to that of siderite and calcite precipitation. Several lines of reasoning point to early formation of siderite in both a relative and absolute sense in the post-depositional history of the Milk River Formation. First, the elemental and isotopic composition of siderite is

indicative of a carbonate that formed from marine waters. Thus, siderite precipitation had to occur when sufficient marine waters were still present in the sediments, which is likely to be shortly after deposition but before extensive dewatering from compaction. Secondly, siderite is present as large overgrowths on detrital dolomite in sandstone and siltstone (Figure 7B); large overgrowths require large empty pore spaces in which to grow and such large pores would not have survived much cementation and compaction. Thirdly, ductile and fragile grains in concretions show little or no evidence of deformation, indicating that they were encased within a rigid authigenic siderite framework early in the post-depositional history of the rock, which allowed for preservation of their delicate textures and shapes. Deformation of ductile grains would have begun after minimal lithostatic pressure due to shallow burial, and would have become more intense with increasing burial depth.

The link between siderite formation and methanogenesis, indicated by the presence of methane-bearing inclusions within the siderite, helps to corroborate an early timing for methanogenesis in the Milk River Formation. Although the carbon isotopic composition of siderite is indicative of a methanogenic source for carbon, the presence of methane in presumed primary fluid inclusions provides a temporal link between methanogenesis and siderite formation. The presence of methane during siderite formation is consistent with observations from ocean-drilling projects that have found authigenic siderite in the zone of methanogenesis (Claypool and Kaplan, 1974; Rodriguez *et al.*, 2000).

A temporal link between methanogenesis and post-sideritic alterations is further supported by petrologic data. The presence of methane in fluid inclusions in the later generation of calcite cement implies that methanogenesis continued at least through the time of calcite precipitation. Thus, methane generation appears to have spanned a significant amount of time during the post-depositional alteration of the Milk River Formation.

The minimum duration of methane generation can be broadly bracketed by combining petrographic observations from the sample suite used in this study with results of studies on marine sediments obtained through ocean-drilling projects. Methane generation probably began in the Milk River Formation shortly after deposition (t_1 on Figure 10), after sulphate in the pore waters was largely consumed in the formation of early pyrite (see Figure 6). Methane generation can only occur after virtually all sulphate is removed from the pore waters because small amounts of sulphate can inhibit the growth of methanogens, the bacteria responsible for methane generation (Claypool and Kaplan, 1974; Gautier, 1985). Depletion of sulphate and the associated ending of pyrite precipitation then allows for an increase in the Fe^{2+} activity, which favours precipitation of siderite. Siderite formation also probably began slightly after the start of methane generation.

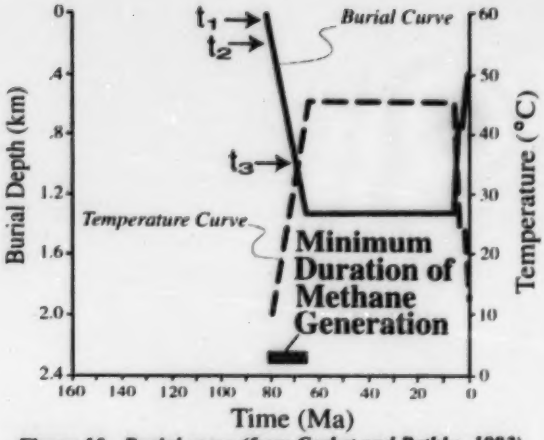

Figure 10 - Burial curve (from Corbet and Bethke, 1992) for the Milk River Formation along an east-west line in southern Alberta, at a latitude that approximately parallels Township 1 N, with times t_1, t_2, and t_3 (see text for explanation of the significance of t_1, t_2, and t_3). The minimum duration of principal gas generation, times t_1 to t_3, was determined in the present study to approximately bracket the timing of methanogenesis in the Milk River Formation.

After the end of siderite precipitation, probably owing to depletion of available iron from pore fluids, methanogenesis continued as indicated by methanic inclusions in the later calcite. The later calcite cementation, however, did not commence until there was at least a 9% reduction in porosity of Milk River Formation sandstone beds due to burial compaction (see earlier discussion). A reduction in porosity of about 9% is estimated (estimations, made following results of experimental studies of compaction by Pittman and Larese (1991), are based on grain size, sorting, and volume of ductile grains) to have occurred after the Milk River Formation was buried to about 200 m (t_2, Figure 10). Calcite in sandstone beds continued to form contemporaneously with methane generation until a porosity reduction of up to 43% was reached (see Table 1).

The fact that sandstone beds lacking calcite cement compacted more than 43% indicates that calcite cementation ceased prior to maximum burial. Although primary methanogenesis is not observed today in marine sediments below burial depths of about 1 kilometre (Rice and Claypool, 1981), microbial communities have been discovered in more deeply buried rocks (Scott *et al.*, 1994; Martini *et al.*, 1998), allowing for speculation that biogenic gas can be generated at greater depths.

These observations broadly indicate that methanogenesis continued at least until the Milk River Formation had been buried to about one kilometre (t_3, Figure 10) and possibly to the maximum burial depth of 1.3 kilometres. Methane generation in the Milk River Formation appears to have spanned at least 15 m.y. from time of sediment deposition until about 65 Ma. If methanogenesis continued after the strata

were buried only slightly deeper than one kilometre, its duration would lengthen significantly (see Figure 10). Although methanogenesis occurred early in the post-depositional history of the formation, the gas appears to have remained in the formation, perhaps in pore fluids, because of very low permeability, which is in part a function of methane-related diagenesis. The gas probably remained in solution until rapid uplift in the region, which began about 7 to 8 Ma (see Figure 3), when a significant reduction in hydrostatic and lithostatic pressures resulted in its exsolution. Nevertheless, the isotopic composition of the exsolved gas in the Milk River Formation, along with the constraints placed on the timing of generation, indicate that the gas is primary and biogenic, not a younger generation of biogenic gas that was generated after uplift and flushing with fresh water as proposed by Martini *et al.* (1998) for biogenic gas in the Antrim Shale in the Michigan Basin.

6. Conclusions

Based on petrologic, isotopic, and fluid inclusion studies of the Cretaceous Milk River Formation in southeastern Alberta and southwestern Saskatchewan, the timing of biogenic methane generation can be estimated and the duration of methanogenesis broadly bracketed. Siderite, an authigenic cement, was precipitated during methanogenesis as indicated by the presence of methanic fluid inclusions. The carbon and oxygen isotopic signature of siderite is a further indication that it formed during methane generation. Authigenic calcite cementation followed precipitation of siderite, but isotopic similarities between the two minerals indicate that they formed from pore fluids of similar isotopic composition. The presence of methane in fluid inclusions in the calcite provides additional evidence that methanogenesis spanned the interval of both siderite and calcite formation. A consideration of: 1) the textural features of Milk River sandstone beds, 2) their burial history, and 3) the observed relations of methanogenesis in modern marine sediments, indicates that methane generation started soon after deposition of the Milk River Formation and continued for at least 15 m.y. and perhaps longer. Further work will include: 1) additional analyses on the authigenic carbonate minerals, and 2) dating of the waters co-produced with methane to determine their age and whether or not they are in equilibrium with the methane. Results from these future efforts will further constrain models for gas accumulation and trapping in the Milk River Formation.

7. Acknowledgments

This manuscript was greatly improved by the technical reviews of George Claypool and Mitch Henry and editorial review of Richard Keefer. We are also appreciative of the many helpful conversations we had about this work with George Claypool, Don Gautier, and Marty Parris. Clay-mineral analyses were kindly performed by Dennis Eberl, and we thank him for his assistance. This work was funded by the Energy Resources Program of the U.S. Geological Survey.

8. References

Arthur, M.A., Dean, W.E., Pollastro, R.M., Scholle, P.A., and Claypool, G.E. (1985): A comparative geochemical study of two transgressive pelagic limestone units, Cretaceous western interior basin, U.S.; *in* Pratt, L.M., Kauffman, E.G., and Zelt, F.B. (eds.), Fine-grained deposits and biofacies of the Cretaceous Western Interior Seaway–evidence of cyclic sedimentary processes; Soc. Econ. Paleont. Mineral., 1985 Midyear Mtg., Field Trip Guidebook 4, p16-27.

Attanazi, E.D. and Schmoker, J.W. (1997): Long-term implications of new U.S. gas estimates; Nonrenew. Resour., v6, p53-62.

Beard, D. and Weyl, P. (1973): Influence of texture on porosity and permeability of unconsolidated sand; Amer. Assoc. Petrol. Geol. Bull., v57, p349-369.

Bernard, B.B., Brooks, J.M., and Sackett, W.M. (1976): Natural gas seepage in the Gulf of Mexico; Earth Planet. Sci. Lett., v31, p45-54.

Carozzi, A.V. (1993): Sedimentary Petrography; Prentice Hall, Englewood Cliffs, 263p.

Claypool, G.E. and Kaplan, I.R. (1974): The origin and distribution of methane in marine sediments; *in* Kaplan, I.R. (ed.), Natural Gases in Marine Sediments; Plenum Press, New York, p99-139.

Claypool, G.E. and Kvenvolden, K.A. (1983): Methane and other hydrocarbon gases in marine sediment; Ann. Rev. Earth Planet. Sci., v11, p299-327.

Claypool, G.E., Presley, B.J., and Kaplan, I.R. (1973): Gas analyses in sediment samples from Legs 10, 11, 13, 14, 15, 18, and 19; Initial Report, Deep Sea Drilling Project, v19, p879-884.

Corbet, T.F. and Bethke, C.M. (1992): Disequilibrium fluid pressures and groundwater flow in the western Canada sedimentary basin; J. Geophys. Resear., v97, noB5, p7203-7217.

Creaney, S., Allen, J., Cole, K.S., Fowler, M.G., Brooks, P.W., Osadetz, K.G., Macqueen, R.W., Snowden, L.R., and Riediger, C.L. (1994): Petroleum generation and migration in the Western Canada Sedimentary Basin; *in* Mossop, G.D. and Shetsen, I., (comp.), Geological Atlas of the Western Canada Sedimentary Basin; Can. Soc. Petrol. Geol./Alta. Resear. Counc., p455-468.

Curtis, C.D. and Coleman, M.L. (1986): Controls on the precipitation of early diagenetic calcite, dolomite, and siderite concretions in complex depositional sequences; *in* Gautier, D.L. (ed.), Roles of organic matter in sediment diagenesis,

Soc. Econ. Paleont. Mineral., Spec. Publ. 38, p23-33.

Curtis, C.D., Pearson, M.J., and Somogyi, V.A. (1975): Mineralogy, chemistry, and origin of a concretionary siderite sheet (clay-ironstone band) in the Westphalian of Yorkshire; Mineral. Mag., v40, p385-393.

Dickson, J.A.D. (1966): Carbonate identification and genesis as revealed by staining; J. Sed. Petrol., v36, p491-505.

Energy Resources Conservation Board (1977): Alberta's reserves of crude oil, gas, natural gas liquids, and sulphur at 31 December 1977; Energy Resour. Conserv. Board, Rep. 78-18, 308p.

Fuex, A.N. (1977): The use of stable carbon isotopes in hydrocarbon exploration; J. Geochem. Expl., v7, p155-188.

Gautier, D.L. (1981): Relationship of organic matter and mineral diagenesis–report of the 1983 Society of Economic Paleontologists and Mineralogists Research Conference; J. Sed. Petrol., v54, p1028-1032.

_____ (1982): Siderite concretions–indicators of early diagenesis in the Gammon Shale (Cretaceous); J. Sed. Petrol., v52, p859-871.

_____ (1985): Interpretation of early diagenesis in ancient marine sediments; Relationship of Organic Matter and Mineral Diagenesis, Soc. Econ. Paleont. Mineral., Short Course 17, p6-72.

Gould, K.W. and Smith, J.W. (1979): The genesis and isotopic composition of carbonates associated with some Permian Australian coals; Chem. Geol., v24, p137-150.

Hankel, R.C., Davies, G.R., and Krouse, H.R. (1989): Eastern Medicine Hat gas field–a shallow, Upper Cretaceous, bacteriogenic gas reservoir of southeastern Alberta; Bull. Can. Petrol. Geol., v37, p98-112.

Houseknecht, D.W. (1987): Assessing the relative importance of compaction processes and cementation to reduction of porosity in sandstones; Amer. Assoc. Petrol. Geol. Bull., v71, p633-642.

Irwin, H., Curtis, C.D., and Coleman, M. (1977): Isotopic evidence for source of diagenetic carbonates formed during burial of organic-rich sediments; Nature, v269, p209-213.

Kauffman, E.G. and Scholle, P.A. (1977): Abrupt biotic and environmental changes during peak Cretaceous transgressions in Euramerican; *in* North American Paleontology Convention II, Abstracts, J. Paleont., v51, p16.

Martini, A.M., Water, L.M., Budai, J.M., Ku, T.C.W., Kaiser, C.J., and Schoell, M. (1998): Genetic and temporal relations between formation waters and biogenic methane–Upper Devonian Antrim Shale, Michigan Basin, USA; Geochim. Cosmochim. Acta, v62, p1699-1720.

Matsumoto, R. and Iijima, A. (1981): Origin and diagenetic evolution of Ca-Mg-Fe carbonates in some coalfields of Japan; Sediment., v28, p239-259.

Mozley, P.S. (1989): Relation between depositional environment and the elemental composition of early diagenetic siderite; Geol., v17, p704-706.

Mozley, P.S. and Carothers, W.W. (1992): Elemental and isotopic composition of siderite in the Kuparuk Formation, Alaska–effect of microbial activity and water/sediment interaction of early pore-water chemistry; J. Sed. Petrol., v62, p681-692.

Mozley, P.S. and Wersin, P. (1992): Isotopic composition of siderite as an indicator of depositional environment; Geol., v20, p817-820.

Nissenbaum, A., Presley, B.J., and Kaplan, I.R. (1972): Early diagenesis in a reducing fjord, Saanich Inlet, British Columbia–I, Chemical and isotopic changes in major components of interstitial water; Geochim. Cosmochim. Acta, v36, p1007-1027.

O'Connell, S., Campbell, R., and Bhattacharya, J. (1999): The stratigraphy, sedimentology, and reservoir geology of the giant Milk River gas field in southeastern Alberta and Saskatchewan; Can. Soc. Petrol. Geol., Ann. Meeting, Abst., p99-83-O.

Pagani, M. and Arthur, M.A. (1998): Stable isotopic studies of Cenomanian-Turonian proximal marine fauna from the U.S. Western Interior Seaway; *in* Dean, W.E. and Arthur, MA. (eds.), Stratigraphy and paleoenvironments of the Cretaceous Western Interior Seaway, USA, Soc. Econ. Paleont. Mineral. Conc. Sediment. Paleont. v6, p201-225.

Pittman, E.D. and Larese, R.E. (1991): Compaction of lithic sands–experimental results and applications; Amer. Assoc. Petrol. Geol. Bull., v75, p1279-1299.

Pratt, L.M. (1985): Isotopic studies of organic matter and carbonate in rocks of the Greenhorn marine cycle; *in* Pratt, L.M., Kauffman, E.G., and Zelt, F.B. (eds.), Fine-grained deposits and biofacies of the Cretaceous Western Interior Seaway–evidence of cyclic sedimentary processes; Soc. Econ. Paleont. Mineral., Midyear Meeting, Field Trip Guidebook 4, p38-48.

Pratt, L.M., Arthur, M.A., Dean, W.E., and Scholle, P.A. (1993): Paleo-oceanographic cycles and events during the Late Cretaceous in the Western Interior Seaway of North America; *in* Caldwell,

W.G.E. and Kauffman, E.G. (eds.), Evolution of the Western Interior Basin, Geol. Assoc. Can., Spec. Pap. 39, p333-353.

Rice, D.D. and Claypool, G.E. (1981): Generation, accumulation, and resource potential of biogenic gas; Amer. Assoc. Petrol. Geol. Bull., v65, p5-25.

Ridgley, J.L. (2000): Lithofacies architecture of the Milk River Formation (Alderson Member of the Lea Park Formation), southwestern Saskatchewan and southeastern Alberta–its relation to gas accumulation; *in* Summary of Investigations 2000, Volume 1, Saskatchewan Geological Survey, Sask. Energy Mines, Misc. Rep. 2000-4.1, p106-120.

Ridgley, J.L., Hester, T.C., Condon, S.M., Anna, L.O., Rowan, E.L., Cook, T., and Lillis, P.G. (1999): Reevaluation of the shallow biogenic gas accumulation, northern Great Plains, USA–is the similar gas accumulation in southeastern Alberta and southwestern Saskatchewan a good analog?; *in* Summary of Investigations 1999, Volume 1, Saskatchewan Geological Survey, Sask. Energy Mines, Misc. Rep. 99-4.1, p64-78.

Rodriguez, N.M., Paull, C.K., and Borowski, W.S. (2000): Zonation of authigenic carbonates within gas hydrate-bearing sedimentary sections on the Blake Ridge–offshore southeastern North America; *in* Paull, C.K., Matsumoto, R., Wallace, P.J., and Dillon, W.P. (eds.), Proceedings of ODP Science Results, 164, College Station, Texas (Ocean Drilling Program), p301-312.

Rosenbaum, J. and Sheppard, S.M.F. (1986): An isotopic study of siderites, dolomites and ankerite at high temperature; Geochim. Cosmochim. Acta v50, p147-1150.

Scott, A.R., Kaiser, W.R., and Auers, W.B., Jr. (1994): Thermogenic and secondary biogenic gases, San Juan basin, Colorado and New Mexico–implications for coalbed gas producibility; Amer. Assoc. Petrol. Geol. Bull., v78, p1186-1209.

Tourtelot, H.A. and Rye, R.O. (1969): Distribution of oxygen and carbon isotopes in fossils of Late Cretaceous age, Western Interior region of North American; Amer. Assoc. Petrol. Geol. Bull., v80, p1903-1922.

Weber, V.V. and Maximov, S.P. (1976): Early diagenetic generation of hydrocarbon gases and their variations dependent on initial organic composition; Amer. Assoc. Petrol. Geol. Bull., v60, p287-293.

Whiticar, M.J., Faber, E., and Schoell, M. (1986): Biogenic methane formation in marine and freshwater environments–CO_2 reduction vs. acetate fermentation-isotopic evidence; Geochim. Cosmochim. Acta, v50, p693-709.

B. Appendices

Acknowledgments

The scientific and production editors are grateful for the peer editing provided by Jim Christopher, Fran Haidl, and Kim Kreis, who greatly assisted in the smooth and relatively "glitch-free" production of the volume. The editors also thank the authors who took the time to document the progress of their research and for their co-operation in helping out with the inevitable last minute details.

We deeply appreciate the assistance given in the editing and production process by Erik Nickel and Laura Smith of Saskatchewan Energy and Mines and all the industry authors' production staff who used their skills to visible effect in creating the graphics and in resolving an assortment of graphics-related problems.

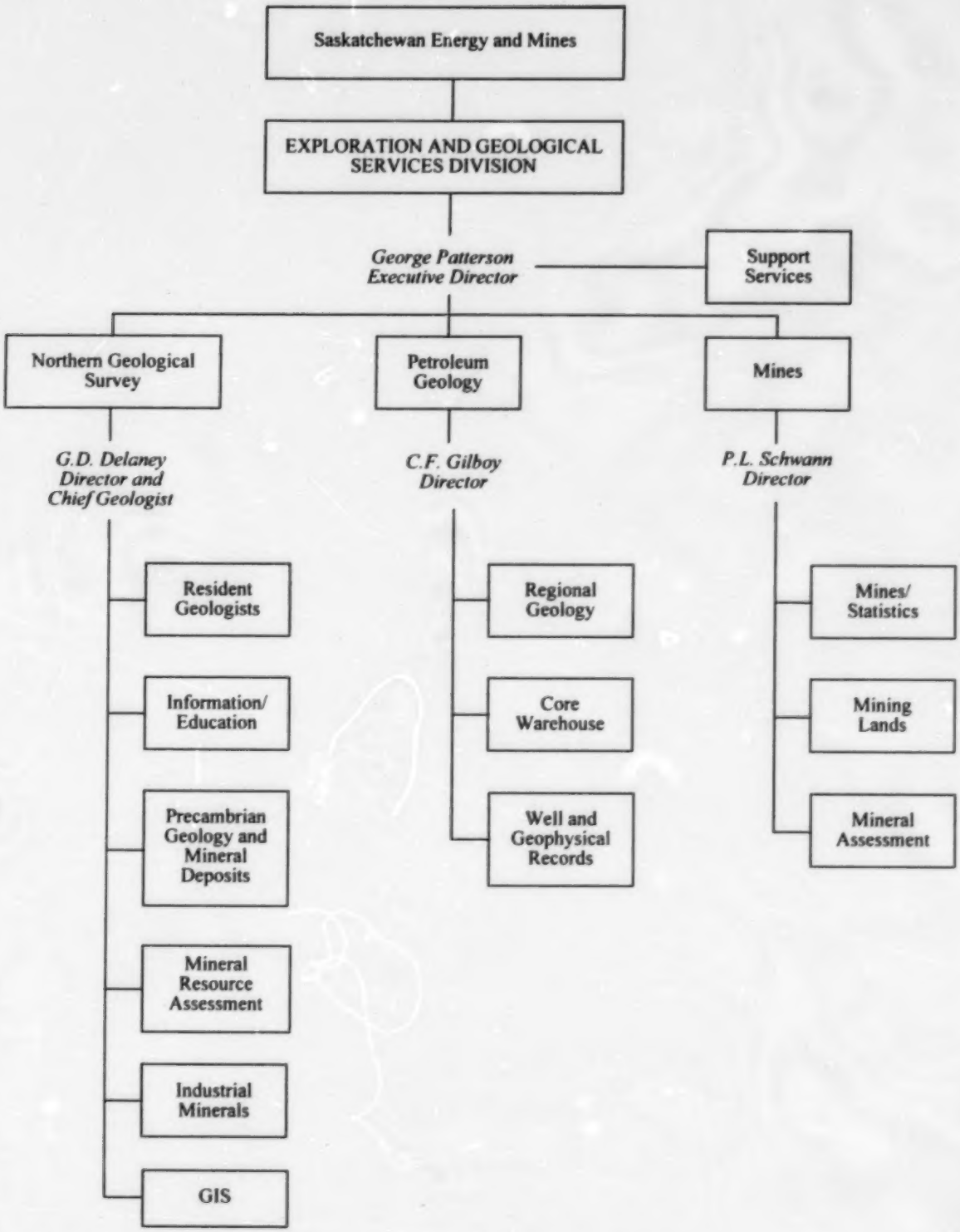

The Saskatchewan Geological Survey comprises the geoscience activities of the Northern Geological Survey and Petroleum Geology.

Staff as of April 1, 2001

Exploration and Geological Services Division
Administration

2101 Scarth Street, Regina, SK S4P 3V7

Executive Director George Patterson, *Ph.D., P.Geo.* (787-2560)
E-mail: gpatterson@sem.gov.sk.ca

Secretary ..... J. Adams (787-2476)

Northern Geological Survey Branch

2101 Scarth Street, Regina, SK S4P 3V7
FAX: 787-1284

Director and Chief Geologist ..... G.D. Delaney, *Ph.D., P.Geo.* (787-1160)
E-mail: gdelaney@sem.gov.sk.ca

Precambrian Geology:
Project Geologists ..... K.E. Ashton, *Ph.D., P.Geo.* (787-1909)
E-mail: kashton@sem.gov.sk.ca
Jurgen Kraus, *Ph.D., G.I.T.* (787-3931)
E-mail: jkraus@sem.gov.sk.ca
R. Maxeiner, *M.Sc., P.Geo.* (787-2553)
E-mail: rmaxeiner@sem.gov.sk.ca
G. Yeo, *Ph.D., P.Geo.* (787-2568)
E-mail: gyeo@sem.gov.sk.ca

Scientific Editor/Project
Geologist ..... C.T. Harper, *Ph.D., P.Eng., P.Geo.* (787-2578)
E-mail: charper@sem.gov.sk.ca

Industrial Minerals:
Geologist ..... Lynn Kelley, *M.Sc., P.Geo.* (787-2646)
E-mail: lkelley@sem.gov.sk.ca
Shawn Harvey, *B.Sc.* (787-2506)
E-mail: sharvey@sem.gov.sk.ca

GIS Geologist ..... W.L. Slimmon, *M.Sc., P.Geo.* (787-9181)
E-mail: bslimmon@sem.gov.sk.ca

GIS Technician ..... Ken Tong, *B.Sc.* (787-2436)
E-mail: ktong@sem.gov.sk.ca

Geological Information/Education:
Geologist ..... D.G. MacDougall, *B.Sc.(Hons.), P.Geo.* (787-2579)
E-mail: dmacdougall@sem.gov.sk.ca

Mineral Resource Assessment:
Geologist ..... M. Rogers, *M.Sc., P.Geo.* (787-1932)
E-mail: mrogers@sem.gov.sk.ca
Technician ..... Ryan Bayne, *B.Sc. (Hons.)* (787-7284)
E-mail: rbayne@sem.gov.sk.ca

Secretary ..... J. Bilkhu (787-2585)
E-mail: jbilkhu@sem.gov.sk.ca

Warehouse Operator (part-time) ..... I.P. Gaw (787-2491)

Mineral Assessment/Mineral Deposits Index:
FAX: 787-2488
Geologist ..... R.W. Bennett, *B.Sc.(Hons.), P.Eng., P.Geo.* (787-2569)
E-mail: rbennett@sem.gov.sk.ca
Clerk ..... L. Smith, *B.Sc.* (787-2582)
E-mail: lsmith@sem.gov.sk.ca

Resident Geologist Offices:

La Ronge:
P.O. Box 5000, La Ronge, SK S0J 1L0
FAX 425-4471

Geologists ..... A.J. Gracie, *Ph.D., P.Eng., P.Geo.* (425-4499)
E-mail: agracie@sem.gov.sk.ca
Ghislain Tourigny, *Ph.D.* (425-4564)
E-mail: gtourigny@sem.gov.sk.ca
Clerk ..... T. Beck (425-4498)

Creighton:
P.O. Box 70, Creighton, SK S0P 0A0
688-8800

Support Services Section

2101 Scarth Street, Regina, SK S4P 3V7
FAX: 787-1284

Production Editor ..... C.L. Brown, *B.Sc.(Hons.)* (787-2590)
E-mail: cbrown@sem.gov.sk.ca

Petroleum Geology Branch

201 Dewdney Avenue East, Regina, SK S4N 4G3
FAX: 787-4608

Director ..... C.F. Gilboy, *Ph.D., P.Eng., P.Geo.* (787-2573)
E-mail: cgilboy@sem.gov.sk.ca

Regional Geology:
Geologists ..... F.M. Haidl, *M.Sc., P.Geo.* (787-6116)
E-mail: fhaidl@sem.gov.sk.ca
I.K. Kreis, *M.Sc., P.Geo.* (787-2620)
E-mail: kkreis@sem.gov.sk.ca
E. Nickel, *B.Sc., G.I.T.* (787-0169)
E-mail: enickel@sem.gov.sk.ca
Part-time Geologists ..... D. Harvey, *B.Sc., G.I.T.* (787-2621)
A. Nimegeers, *B.Sc. (Hons.), G.I.T.* (787-2621)

Warehouse:
Supervisor ..... M. Mongrain (787-2622)
Staff ..... D. Gallant (787-2622)
T. Mounstephen (787-2622)
Part-time Staff ..... K. Desjarlais (787-2622)
R. Sawa (787-2622)
Secretaries ..... C. Boyle (787-1393)
R. Lavigne (787-2621)

2101 Scarth Street, Regina, SK S4P 3V7
FAX: 787-2488

Well and Geophysical Records:
Geologist ..... D.R. Troyer, *M.Sc., P.Eng., P.Geo.* (787-2562)
E-mail: btroyer@sem.gov.sk.ca
Engineer ..... T. Badger, *P.Eng.* (787-2492)
E-mail: tbadger@sem.gov.sk.ca
Horizontal Well Coding Clerk ..... R. Ferner (787-2550)
E-mail: rferner@sem.gov.sk.ca
Well File Clerks ..... L. Mikenas (787-3804)
B. Russell (787-7416)
G. Schick (787-1363)
L. Siapno (787-7373)
Coding Clerks ..... N. Bhasin (787-7420)
A. Landry (787-7412)
R. McCall (787-7413)
P. McMillen (787-7421)
D. Read (787-2443)
C. Syrota (787-2398)
J. Tanouye (787-2757)
E-mail: geodata@sem.gov.sk.ca
Geophysical Clerk ..... L. Merkel (787-2558)
E-mail: geophysical@sem.gov.sk.ca

Mines Branch

2101 Scarth Street, Regina, SK S4P 3V7
FAX: 787-1284

Director ..... P.L. Schwann, *M.Sc., P.Geo.* (787-2584)
E-mail: pschwann@sem.gov.sk.ca
Administrator ..... L. Troesch (787-2537)
E-mail: ltroesch@sem.gov.sk.ca
Mining Recorder ..... K. Klyne (787-2538)
E-mail: kklyne@sem.gov.sk.ca
District Mineral Officer (La Ronge) ..... M. O'Brien (425-4600)
E-mail: mo'brien@sem.gov.sk.ca
Clerk ..... S. Bond (787-8247)
Industrial Minerals Clerks ..... D. Buckshaw/M. Zaron (787-2539)
Assessment Geologist ..... H. Stolz, *B.Sc., P.Eng.* (787-2564)
E-mail: hstolz@sem.gov.sk.ca
Mining Engineer ..... G. Lopez, *B.Sc., P.Eng., P. Admin.* (787-2559)
E-mail: glopez@sem.gov.sk.ca
Clerk ..... V. Bohn (787-7631)
E-mail: minestats@sem.gov.sk.ca
Data Processing Geologist ..... N. Lee, *B.Sc., P.Eng.* (787-2574)
E-mail: nlee@sem.gov.sk.ca